Hollow fibre bioreactors for bone tissue engineering

Shearer, Holly

Award date:
2007

Awarding institution:
University of Bath

HOLLOW FIBRE BIOREACTORS FOR BONE TISSUE ENGINEERING

Holly Shearer

A thesis submitted for the degree of Doctor of Philosophy

University of Bath

Department of Chemical Engineering

October 2007

ProQuest LLC
789 East Eisenhower Parkway
P.O. Box 1346
Ann Arbor, MI 48106-1346

ABSTRACT

Bone tissue engineering offers the potential to create tissue for the repair of bone defects. The aim of this thesis was to optimize the biodegradable polymer fibres used in a hollow fibre bioreactor for bone tissue engineering. Combining the high surface area and efficient mass transfer properties of hollow fibres with biodegradable polymers should allow the development of a construct that will eventually resemble natural bone. PLGA hollow fibres were prepared by wet spinning through a double orifice spinneret. The membrane structure was found to be altered by traditional sterilization techniques leading to the development of a method using antibiotics to sanitize the fibres without undue alterations to the membrane. Media perfusion through the fibre wall was improved through sodium hydroxide surface treatment; this was found to remove the membrane skin revealing the underlying porous structure. The interior structure of the hollow fibres after a two week culture period suggested confined regions were undergoing accelerated degradation due to autocatalysis, however the unique structure of the fibre wall prevented the formation of a large single void. Production of the fibres was investigated to identify parameters that could control the surface pore size of the membranes. An air gap between 0 – 10 cm was found to alter the surface pores sizes from 0.2 – 0.3 μm, with water and polymer flow rates in the range 170 – 220 cm^3h^{-1} controlling surface porosity between 30 – 50%. Introduction of solvent into the bore fluid was found to deteriorate the fibre structure. Shear stresses on the polymer solution as it passed through the spinneret were not found to influence the surface pore size of the hollow fibres. This work has developed a better understanding of the novel use of biodegradable fibres in a bone tissue bioreactor.

ACKNOWLEDGEMENTS

My time as a post-graduate at the University of Bath has been hugely rewarding and surpassed all my expectations. The following people have had a significant role in making it so.

I would like to thank Professor Julian Chaudhuri whose guidance and supervision, while allowing me to explore my interests, has been invaluable to this project. Without his knowledge and experience this work would not have been possible and without his patience and flexibility in the direction of the research I would not have enjoyed it so much.

I would also like to thank Dr Semali Perera for providing expertise in the field of membranes and spinning; ensuring the membrane work was robust and the biological components well explained.

I thank Dr Marianne Ellis, whose own thesis is frequently cited in this work, who helped me get underway and ensured there was always someone there to answer my questions.

Dr Chin Chih Tai was a careful and precise tutor in the knacks and skills of spinning hollow fibres; whose patience with my initial spinning attempts was enormous and very much appreciated.

The other members who have passed through the Tissue Engineering group while I have been here have all provided advice along the way. In particular Ben Ainsworth provided guidance and questioning in equal measure.

The support I had from technicians saved me a lot of time in learning new techniques, in particular thanks to Hugh Perrott, Ursula Potter and Anne O'Reilly in the Centre for Electron Optical Studies and Chris Arnold in the Dept of Mechanical Engineering.

Other members of the chemical engineering post-graduate community have made a huge difference to my time here; providing support, encouragement and a lot of laughs along the way. Thank you to you all.

I gratefully acknowledge the University of Bath for the financial support that has made this work possible.

I thank my family for their support and encouragement to pursue my ambitions. They have provided both advice and a place of refuge for when a break was needed; and have an uncanny ability to identify which is required.

Thanks to Chris who has listened, advised, and motivated.

TABLE OF CONTENTS

TABLE OF FIGURES

TABLE OF TABLES

NOMENCLATURE

1	Related to sample group 1 (typically the control group)	
2	Related to sample group 2 (typically the test group)	
50:50	PLGA comprising 50% lactic acid 50% glycolic acid	
65:35	PLGA comprising 65% lactic acid 35% glycolic acid	
75:25	PLGA comprising 75% lactic acid 25% glycolic acid	
85:15	PLGA comprising 85% lactic acid 15% glycolic acid	
a_f	Void space finally	(L^3)
a_i	Void space initially	(L^3)
A	Annulus area	(L^2)
A_f	Cross-sectional area finally	(L^2)
A_i	Cross-sectional area initially	(L^2)
A_m	Membrane area	(L^2)
A_p	Total pore area	(L^2)
ANCOVA	Analysis of co-variance	
ANOVA	Analysis of variance	
b	Polymer volume	(L^3)
b_f	Polymer volume finally	(L^3)
b_i	Polymer volume initially	(L^3)
B	Value of blue channel	(-)
B	Bore fluid composition	(-)
BSA	Bovine serum albumen	
C	Solution composition	(-)
C	Concentration	(-/L^{-3}N/ L^{-3}M)
COA	Certificate of analysis	
d	Diameter of cell	(L)
$\bar{d}_e$	Average effective pore diameter	(L)
d_e	Effective pore diameter	(L)
d_{ei}	Internal effective pore diameter	(L)
d_{eo}	External effective pore diameter	(L)
d_h	Hydraulic diameter	(L)
d_t	Distance between diffusion front and edge of scaffold at time = t	(L)

d/D	Ratio of orifice diameter to pipe diameter	(-)
d.f.	Degrees of freedom	
D	Density	($L^{-3}M$)
DMEM	Dulbecco's modified eagle's medium	
DMSO	Dimethyl sulfoxide	
E	Young's modulus	($LM^{-1}T^{-2}$)
ECM	Extra cellular matrix	
EDTA	Ethylenediaminetetraacetic acid	
f	Friction factor	(-)
$_f$	Refers to fluid	
FCS	Foetal calf serum	
FDA	Food and Drug Administration	
FS	Flat sheet	
g	Acceleration due to gravity	(LT^{-2})
g	Greyscale value	(-)
G	Air gap for spinning	(L)
G	Glycolic acid content	(-)
G	Green channel value	(-)
HCl	Hydrochloric acid	
$HClO_4$	Hyperchloric acid	
HF	Hollow fibre	
HFB	Hollow fibre bioreactor	
ID	Identity	
ID	Inner diameter	
IV	Intrinsic viscosity	
K	Mark-Houwink constant	(-)
$L_{critical}$	Critical length	(L)
Lsd	Least significant difference	
L	Lactic acid content	(-)
L:G	Lactic acid to glycolic acid ratio	
m	Percentage mass of scaffold remaining	(-)
m_f	Mass finally	(M)
m_i	Mass initially	(M)

$\dot{m}_w$	Mass flow rate of water through the membrane	(MT^{-1})
M	Lactic acid content of membrane	(-)
M	Molarity	$(L^{-3}N)$
M_n	Number average molecular weight	(-)
M_v	Viscosity average molecular weight	(-)
M_w	Molecular weight	(-)
MG63	Cell type	
MWCO	Molecular weight cut-off	
n	Sample size	(-)
n_p	Number of pores	(-)
N	Total number of samples in all groups	(-)
N_c	Number of cells	(-)
N_i	Number of molecules	(-)
NaOH	Sodium hydroxide	
NEAA	Non-essential amino acids	
NMP	1-methyl-2-pyrrolidinone	
OD	Outer diameter	(L)
p	Porosity	(-)
p	Porosity of scaffold initially	(-)
P	Percentage assay	(-)
P	Trans-membrane pressure difference	$(L^{-1}MT^{-2})$
P_f	Porosity finally	(-)
P_i	Porosity initially	(-)
P_r	Percentage porosity of scaffold remaining	(-)
PBS	Phosphate buffered saline	
PEG	Poly(ethylene glycol)	
PLGA	Poly(lactic-co-glycolic acid)	
PTFE	Poly(tetrafluoroethylene)	
Q	Volumetric flow rate	(L^3T^{-1})
Q-Q Plot	Quantile-quantile plot	
r	Radius	(L)
$r_{sa:v}$	Surface area to volume ratio	(L^{-1})
R	Fibre concentricity factor	(-)

R	Molar gas constant	$(L^2MT^{-2}\Theta^{-1}N^{-1})$
R	Value of red channel	(-)
R_1	Spinneret inner radius	(L)
R_2	Spinneret outer radius	(L)
Re	Reynolds number	(-)
rpm	Revolutions per minute	(T^{-1})
s	Refers to cell	
SD	Standard deviation	
S.D.	Significant difference	
SE	Standard error	
SEM	Scanning electron microscope	
SP	Sodium pyruvate	
SS	Stainless steel	
t	Treatment duration	(T)
t	t-test statistic	
t_{min}	Minimum fibre wall thickness	(L)
t_{max}	Maximum fibre wall thickness	(L)
T	Temperature	(Θ)
TE	200 mM Tris-HCl, 20 mM EDTA (buffer for PicoGreen assay)	
u	Number of groups	(-)
u_i	Instantaneous velocity	(LT^{-1})
UV	Ultraviolet light	
U_z	Velocity	(LT^{-1})
v	Percentage volume of scaffold remaining	(-)
v_f	Volume finally	(L^{-3})
v_i	Volume initially	(L^{-3})
v_p	Flow rate of polymer	$(L^{-3}T^{-1})$
v_w	Flow rate of water	$(L^{-3}T^{-1})$
v/v	Volume by volume solution	
V	Volume	(L^3)
w/w	Weight by weight solution	
x	Cell number	(-)
x	Sample result	

$\bar{x}$	Sample mean	
x_0	Initial cell number	(-)
α	Mark-Houwink constant	(-)
γ	Shear rate	(T^{-1})
ΔP	% increase in porosity	(-)
Δm	% loss of mass	(-)
θ	Angle	(-)
μ	Specific growth rate	(T^{-1})
μ	Viscosity	($L^{-1}MT^{-1}$)
$[\mu]$	Intrinsic viscosity	(L^3M^{-1})
μ_s	Viscosity of solvent	($L^{-1}MT^{-1}$)
μ_o	Zero shear viscosity	($L^{-1}MT^{-1}$)
ν	Number of samples	(-)
ρ	Density	($L^{-3}M$)
σ	Breaking stress	($L^{-1}MT^{-2}$)
σ	Standard deviation	
σ_d^2	Variance of difference of mean	
τ	Shear stress	($L^{-1}MT^{-1}$)
τ_p	Relaxation time	(T)
ω	Angular velocity	(-)

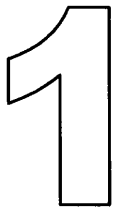

CHAPTER ONE - INTRODUCTION

1.1 The Need for Tissue Engineering

Bone tissue is unique, among human tissues, in its capacity for self renewal; throughout life bone is continually remodelling, this means that following an injury bone can repair itself and then naturally remodel to completely recover without scarring.

This mechanism only breaks-down when the extent of damage to the bone is such that there is a significant loss of material and the ends of the broken bones are no longer in contact. In these cases medical intervention is required to bring the broken bones back together and replace the lost material. The present gold-standard solution to this problem is to harvest bone from another part of the body to provide the replacement material. This is called an autograft. Material suitable for this procedure is severely limited and a second surgical site is required in addition to the original injury; this increases the financial cost of the operation and increases pain for the patient. An alternative to autograft is allograft, where the replacement material is provided by a donor. This material is also in limited supply and must be treated before transplantation to prevent the transmission of disease. The third option is to use an artificial bone substitute. This is available in unlimited supply and its production is far less costly both in financial terms and patient pain. The reason this option isn't widely used is the reduced quality of the repair. The synthetic substitute can't be resorbed and remodelled meaning the bone can never return to its pre-injured state. Differences in mechanical properties between bone and the substitute can lead to wear at the joint which can cause failure of the implant.

Engineering bone in the laboratory offers the potential to provide the benefit of synthetic bone replacement while maintaining the unique remodelling capacity of bone.

Tissue engineering has gradually evolved from techniques used for cell culture by the addition of three-dimensional scaffolds to support cells. The term *Tissue Engineering* is reputed to have been first used in this context in 1988 at a National Science Foundation Conference; however there are arguments that tissue engineering, or techniques that lead directly on to what we think of as tissue engineering today, have been taking place for much longer.

Tissue engineering involves the combination of cells, a supporting scaffold and nutrients in an environment suitable for cell growth. The cells are allowed to proliferate and lay down their own extra cellular matrix. This process is illustrated in Figure 1.1. The scaffold provides a surface for the cells to adhere to, it provides architecture for the overall shape of the scaffold and provides channels through which to deliver the nutrients to the cells.

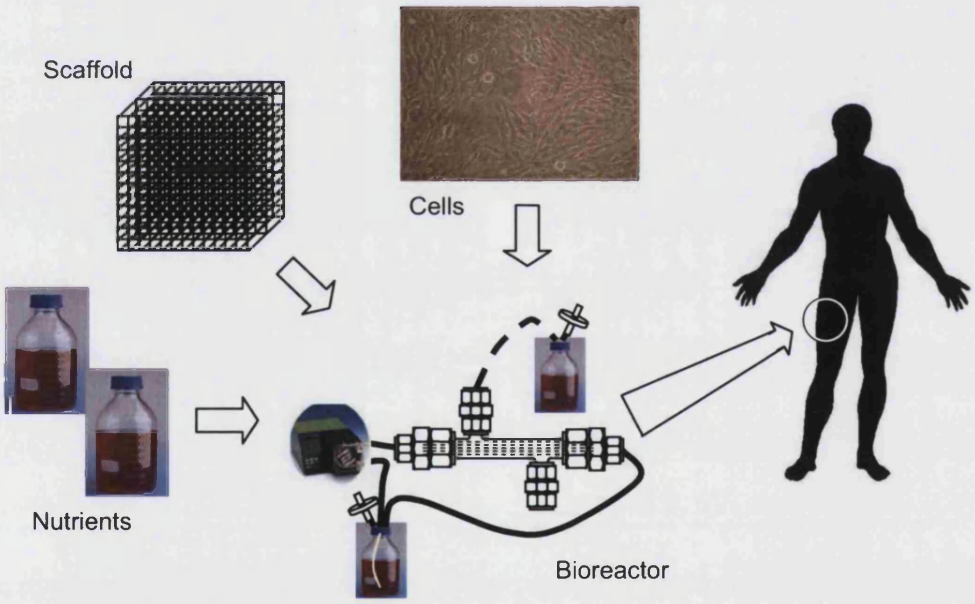

Figure 1.1 Schematic of tissue engineering.

To tissue engineer bone cells are combined with a supporting scaffold and nutrients in an environment suitable for cell growth. Once a tissue is formed it may be implanted into the patient.

Successful tissue generation *in vitro* requires highly specialized scaffolds. Mass transfer, topography, surface chemistry, (Curtis *et al.* 2004; Jansen *et al.* 2005) mechanical properties and degradation rates (Hutmacher 2000) are just some of the

factors that influence the ability of cells to colonize a scaffold and form an organized tissue construct. Implantation *in vivo* requires the scaffold to be biocompatible, integrate with the surrounding natural tissue, and over a favourable time scale to be completely eliminated from the host via biodegradation. This thesis investigates the use of biodegradable hollow fibres in a custom designed bioreactor to grow bone tissue suitable for grafting in the laboratory.

1.2 Purpose of this work

The purpose of this work is to realize the potential of the hollow fibre bone tissue bioreactor proposed by Ellis (2005). Hollow fibre membrane configurations are well known for providing large surface areas and efficient mass transfer. The use of hollow fibres as a scaffold around which tissue-like cell densities could be cultured was identified at least 35 years ago (Knazek *et al.* 1972), initially these systems were exploited as an efficient system for growing cells and harvesting cell products. By combing the hollow fibre bioreactor with degradable polymers the potential for this system in the field of tissue engineering has recently been recognized (Ellis 2005; Ye *et al.* 2006; Wen and Tresco 2006). The fibre degrades as the tissue develops resulting in a construct consisting entirely of natural tissue. The incorporation of a degradable scaffold introduces a new gradient into the tissue growing process; not only is the nascent tissue growing around the fibre, but the fibre itself is degrading. This makes the system very complex.

This work concentrates on the hollow fibres used in the bioreactor. The process by which the fibres are formed is investigated alongside post-production processing to optimise the fibres for use in the hollow fibre bioreactor for bone tissue engineering. The degradation of the fibres is also investigated.

1.3 Thesis outline

This thesis is divided into chapters which outline experimental investigations. Chapter Two reviews present knowledge in the field of bone tissue engineering and hollow fibre production and hollow fibre bioreactors; detailed literature relevant to the experimental studies is presented in the introduction to the experimental chapters. Chapter Three gives details of the experimental methods and materials used and the statistical methods

used to determine significance in the results. Chapters Four to Eight cover the experimental work carried out. Chapter Four is an investigation into suitable methods to sterilize the bioreactor, considering the sensitivity of the degradable polymer to present sterilization methods and the unique sensitivity of hollow fibre form. Chapter Five and Chapter Six investigate the use of surface treatment agents to improve the porosity of the membrane surfaces on flat sheet membranes and hollow fibre membranes respectively. Chapter Seven investigates how the hollow fibre form and associated scaffold interior architecture, as well as the hollow fibre bioreactor environment influence the degradation profile of the polymer. Chapter Eight investigates the influence operating conditions during spinning have on the final scaffold structure. Chapter Nine provides the overall conclusions for the work and outlines the future work that is required both in the short term and longer term.

CHAPTER TWO – BONE TISSUE ENGINEERING

Bones, fibres and bioreactors

This chapter gives an introduction the main topics covered in this work: bone, hollow fibres and hollow fibre bioreactors. Further literature reviews relevant to the experimental studies are presented in the introduction to the experimental chapters.

2.1 Bone

There are 206 bones in the adult human body providing; internal support, protection, and levers for movement. Bone is a specialised connective tissue composed of cells supported by a natural scaffold known as the extra cellular matrix or ECM. The ECM is comprised of macromolecules such as collagen that are secreted by cells, allowing the formation of ECM as it is required. ECM is important in providing a support onto which cells may attach and allowing cells to communicate through signalling molecules contained within the ECM. The ECM of bone is mineralized, providing rigidity and strength; collagen fibres in the matrix infer tensile strength. Bone and bone marrow are also involved in mineral homeostasis in the body (Bilezikan *et al.* 1996).

2.1.1 Bone type and structure

There are two types of bone categorised by their morphology. These are: cortical bone also known as compact bone and cancellous or trabecular bone.

Cortical bone is found in the diaphysis (shafts) of long bones, surrounding the marrow cavity, it also forms the outer walls of all bones. Approximately 80% (Bilezikan *et al.* 1996) of the skeletal mass of an adult human is cortical bone. Cortical bone surrounds

cancellous bone providing a protective layer; it achieves this through a structure consisting of tightly packed collagen fibrils forming concentric lamellae (Figure 2.1).

Figure 2.1 Light micrograph of mature human cortical bone (from a digit) (Davies and Hosseini 2000)

Showing lamellar osteons (Haversian systems) outlined by cement-line boundaries

Cortical bone is roughly distinguished from cancellous bone by possessing a volume fraction of pores less than about 30% and a density up to about 2 gcm^{-3} (Keller *et al.* 1990), however there is no precise distinction. Cancellous bone is found in the epiphysis (ends) of long bones and in flat bones and vertebrae. Cancellous bone is made up of a porous matrix with fine partitions enclosing bone marrow containing cavities.

Bone is supplied with nutrients by blood vessels that run through a network of channels known as Haversian and Volkman's canals. Haversian canals also contain nerve fibres and are linked with each other, and bone marrow, by Volkman's canals.

The hollow fibre is well suited to replicating the structure of cortical bone. By supplying the nascent bone with nutrients through the lumen of the hollow fibres a system very similar to the natural supply of nutrients to bone through the Haversian

canals is created. Haversian canals have diameters a few micrometers across (Rho *et al.* 1998), while this is much smaller than hollow fibres which are typically a few hundred micrometers across it is anticipated cells will grow in layers surrounding their nutrient supply. The elements of the structure making up bone are shown in Figure 2.2.

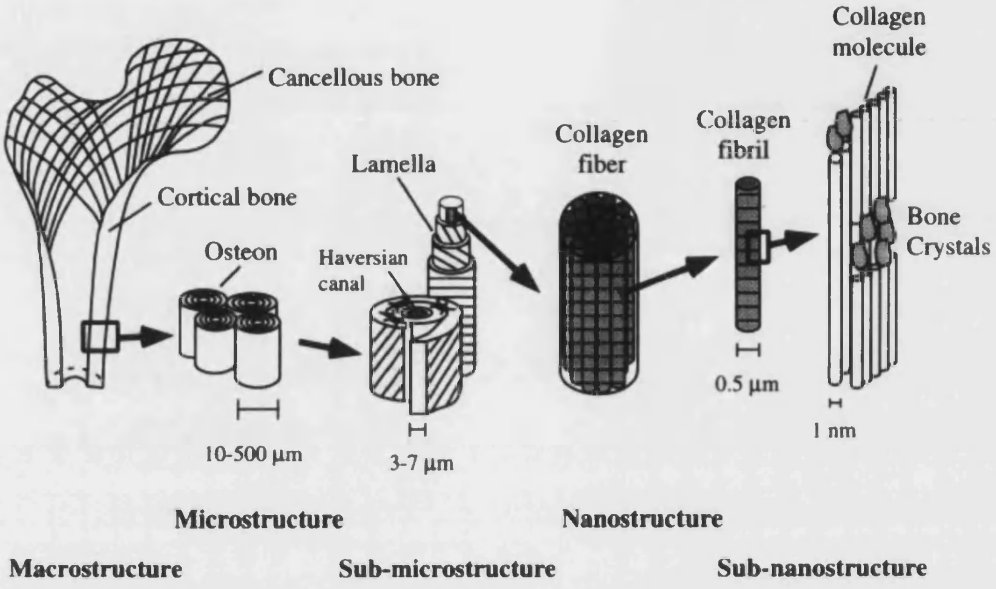

Figure 2.2 Hierarchical structural organisation of bone

Far left: *cortical and cancellous bone;* ***Left:*** *osteons with Haversian systems;* ***Middle:*** *lamellae;* ***Right:*** *collagen fibre assemblies of collagen fibrils;* ***Far right:*** *bone mineral crystals, collagen molecules, and non-collagenous proteins (Rho et al. 1998)*

2.1.2 Bone cells

There are four different cell types involved in bone (Figure 2.3): osteoblasts, osteoclast, bone lining and osteocytes (Bilezikan *et al.* 1996).

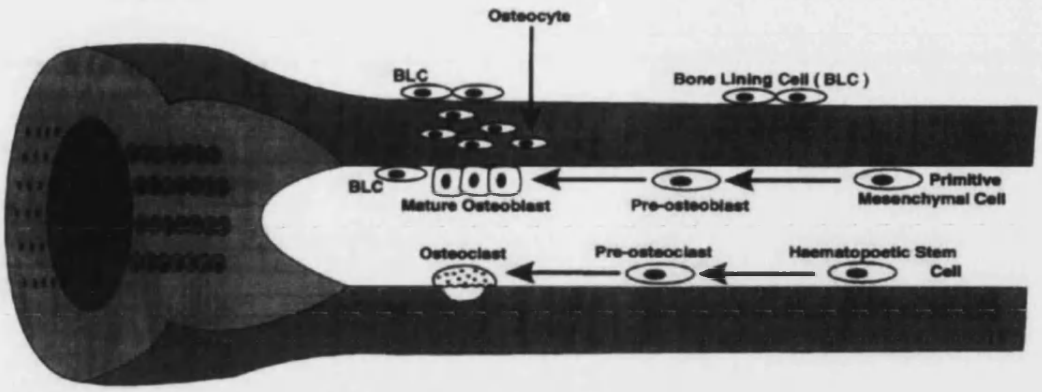

Figure 2.3 Representation of bone cells involved in long bone growth

Osteoblasts produce bone matrix, osteoclasts, resorb bone, bone lining cells both resorb and produce bone on the bone surface, osteocytes monitor the mechanical stresses on bone and tissue damage. (Orthoteers 2001)

Osteoblasts are fully differentiated cells present on the surface of bone, their function is to produce bone matrix. This involves: the synthesis of macromolecules including collagen and non-collagenous proteins; organisation of the architecture of the matrix; and control of the mineralization.

Osteoclasts are also present on the surface of bone, however while osteoblasts synthesise bone matrix, osteoclasts are specialised to resorb bone. This is achieved by dissolution of the mineral components and enzymatic digestion of organic macromolecules. Osteoclasts are large multinucleated cells; they have two specialised features allowing them to resorb bone: an area of highly in-folded plasma membrane, known as the ruffled border, where bone resorption takes place; and a clear zone consisting of a microfilament-rich, organelle-free area of plasma membrane providing an area for attachment to the bone matrix. Both osteoblasts and osteoclasts are temporary cells which do not migrate far and have relatively short life spans controlled by apoptosis.

Bone lining cells originate from local osteoprogenitor cells; they are flat and elongated in appearance and are present on the surface of bone. They participate in both bone

formation and resorption. Bone-lining cells identify sites for resorption and recruit osteoclast precursors; they also help to prepare the bone surface for resorption.

Osteocytes are present in the interior of bone; they have minimal involvement in bone synthesis, carrying out remodelling of their local environment. Osteocytes are contained within lacunae and communicate via cell processes which travel through the canaliculi in bone. Osteocytes are believed to be involved in a sensory network to monitor mechanical load and tissue damage, triggering the appropriate bone formation or resorption responses (Majeska 2001).

2.1.3 Bone repair and remodelling

Bone tissue is unique in its ability to regenerate after injury without the development of scar tissue. Inflammation occurs directly after injury and usually lasts a few days, a haematoma forms to limit loss of blood from damaged blood vessels and platelets release vasoactive mediators and growth factors. Inflammatory cells arrive at the site and remove necrotic tissue. Inflammation is followed by repair; a fracture callus of osteoblasts, cartilaginous matrix and woven bone is formed; this provides the raw material required for remodelling. Remodelling through resorption and deposition takes place following stimulation from local mechanical stresses; highly organised lamellar bone results. Each of the three biological stages takes an increasing duration to occur; durations depend on the location and nature of the fracture.

The stages outlined above return bone to its original state following a fracture, however, the size of fracture that may be repaired in this way is limited. Typical treatments for large bone defects are autogenous trabecular bone graft. This is bone taken from elsewhere on the patient, which is in limited supply and creates a second surgical site. If suitable bone can be grown in the hollow fibre bone bioreactor this harvesting of bone will not be required; achieving the high performance of autologous bone transplantation while eliminating the disadvantages of this procedure.

Wound repair following transplantation undergoes a very similar mechanism to that without transplantation; damage to local blood vessels trigger clotting, which attracts inflammatory cells and osteoblasts. Cellular elements of the graft largely undergo necrosis and remaining cells have a minimal contribution to osteogenesis. Integration

of the graft initiates with revascularization, followed by migration of osteoblasts into the graft; mechanical strength of the graft is transiently increased through deposition of new bone onto the existing grafted bone. Ultimately bone is remodelled and exhibits properties of uninjured bone (Yaszemski *et al.* 1996). Grafting provides a link between bone tissues on either side of the defect; the graft material is resorbed and remodelled to suit the requirements of its new location. Using bone tissue to bridge the gap ensures the structural properties are well suited for vascularization and cell proliferation.

The remodelling ability of bone makes it particularly suitable as a target for tissue engineering. Remodelling of the graft once it has been implanted greatly reduces the need to exactly match the newly generated tissue to the old tissue. Once implanted the tissue engineered bone will be remodelled naturally to reproduce the lost tissue. Tissue engineering aims to produce bone tissue suitable for grafting by replicating the natural cellular environment *in vitro*; to allow cells to grow and interact in exactly the same way as they do in natural bone.

2.2 Hollow fibre bioreactors for bone tissue engineering

Hollow fibre bioreactors have been used in a variety of medical engineering applications; including the isolation of cells for use as a temporary artificial organ, such as the liver or kidneys, and the production of biochemicals. They have also been shown to support cell growth at densities approaching those *in vivo* (Wei and Russ 1977). Uniquely the hollow fibre bioreactor provides a physical barrier between the nutrient flow and cells; nutrients are fed through the opposite side of the hollow fibre membrane to the cells and diffuse through the semi-permeable membrane. This allows the flow rate of nutrients past the cells to be optimised without creating adverse shear stresses and shields cells from sudden changes in media composition (Wei and Russ 1977). Cells may be located either on the shell, or tube side of the bioreactor, for the production of biochemicals cells would typically be isolated on the tube side; allowing easy recovery of products on the shell side. By locating cells on the outside of the fibres, for tissue engineering, the *in vivo* capillary system is simulated; providing a physiological environment for cultured cells in terms of nutrient supply and waste removal (Kumar *et al.* 2004) and a continuity of tissue is achieved. The hollow fibre bioreactor offers a variety of configurations for operations, most of which have been

attempted and reported in literature (Table 2.1). Each configuration offers a different approach to achieving effective and uniform distribution of nutrients to cells.

Table 2.1 Possible modes of operation for hollow fibre bioreactors.

The hollow fibre bioreactor offers many possible modes of operation, which have different benefits to the cells within the reactor.

Flow arrangement	Description	References
Luminal feed open shell (Ultra filtration)	Medium enters the lumen and permeates through the fibres and exits continuously through a shell port; retentate exits the downstream side of the tube	Tharakan and Chau 1986
Luminal feed closed shell (Recycle)	Medium enters the lumen, there is no effluent from the shell, and waste products either diffuse back into the lumen or are periodically drained.	Tharakan and Chau 1986
Ablumen cross flow (Back flush)	Medium enters the ablumen uniformly along the length of the fibre it permeates through the fibre wall to exit via the lumen.	Tharakan and Chau 1986
Counter current flow	Media is flowed through both the lumen and the ablumen in opposite directions	
Co-current flow	Media is flowed through both the lumen and the ablumen in the same direction	
Dual fibre (one inside other)	A highly permeable silicon tube passing through the lumen of the fibre provides O_2 and CO_2. Nutrients flow through the annular space and cells are supported on the exterior of the fibre.	Chresand *et al.* 1988
Twin fibre (source and sink)	Fibres at higher pressure and concentration than the ECS act as a source of nutrients, fibres at lower pressure and concentration that the ECS act as a sink for waste products.	Cracauer *et al.* 1987
Separate gas and nutrient delivery	A central core provides nutrient delivery, hollow fibres are used to distribute gaseous nutrients and remove waste products.	Tharakan and Chau 1985
Dual operation	Flow oscillates between lumen to ECS and ECS to lumen	Chresand *et al.* 1988

A typical hollow fibre bioreactor set up with axial feed and a closed shell is described by Knazek *et al.* (1990); hollow fibres support cells on the exterior of the fibres, and liquid nutrients pass through the lumen. Nutrients are recycled after re-oxygenation and pH adjustment; mimicking *in vivo* homeostasis. Flow is directed out of the lumen at the upstream end of the reactor and back into the lumen on the downstream end of the reactor. This closely replicates the *in vivo* capillary network with nutrients diffusing out of the arterial end of the capillary and waste products diffusing back into the venule end of the capillary and is known as Starling flow.

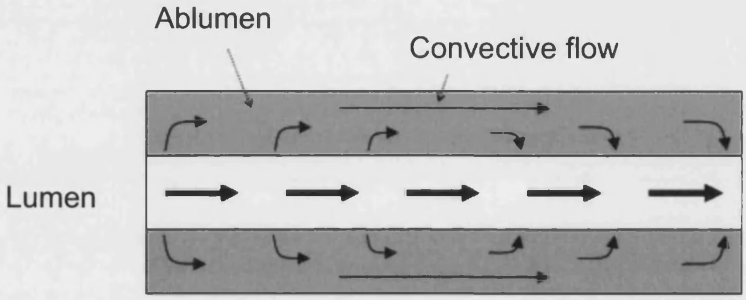

Figure 2.4 Schematic of convective flux around a fibre or capillary.
Media in the lumen at the upstream end is at higher hydrostatic pressure than that in the ablumen, this causes media to perfuse out to the abluminal space. At the downstream end the hydrostatic pressure differential is reversed causing perfusion in the opposite direction. This induced flow in the abluminal space is known as Starling flow.

Starling flow can generate co-current convective flow in the ablumen of a bioreactor at about 2% of the lumen flow rate (Wei and Russ 1977), this can lead to undesirable spatial variations in nutrient concentrations; cells in the upstream end of the bioreactor experience fresh media whereas cells in the latter half of the reactor only experience media that has already been used by cells in the first half of the reactor. Cells will also tend to aggregate in the downstream end of the reactor where they will become compressed onto the fibres (Tharakan and Chau 1986). Knazek *et al.* (1990) use periodical reversal of lumen flow direction to minimize axial variations in nutrient distribution. In a similar reactor configuration Piret and Cooney (1990) found the distribution of cells was improved and the total number of cells present went up by a factor of three for a reactor with flow reversing every 5 min compared to single direction flow. The time period for flow reversal reported in literature varies in the region of 5 to 10 min (Knazek *et al.* 1990; Piret and Cooney 1990) however no

justification for the time period has been given other than to mention it is preferential to reverse flow direction before complete polarisation of nutrients occurs (Piret and Cooney 1990). The optimal cycle of flow reverse will depend on the geometry and flow rates of the system in question. Other methods for uniform distribution of nutrients, such as using gravity to counteract the effects of one-way flow in a vertically orientated reactor were described as unsuccessful by Piret and Cooney (1990). However in the horizontal reactor gravity was found to increase spatial variations in nutrient distribution with increased protein concentrations from abluminal fluid sampled from a downward facing port in comparison with samples taken from an upward facing port (Piret and Cooney 1990).

The synonymy of hollow fibre bioreactors to the *in vivo* capillary system extends to the mass transfer models used to describe and predict the transfer of nutrients from the lumen to, and into, the cell mass surrounding the fibre. Mathematical models primarily developed for transport phenomena associated with capillaries may be applied, with minor modifications, to the hollow fibre bioreactor.

While all practical applications of hollow fibre bioreactors will contain multiple fibres useful models have been developed based around single fibres. Starling first described the transfer of fluid between the capillary and surrounding tissue in terms of hydrodynamic and osmotic driving forces with the Starling equation (cited by Fournier 1999).

$$\frac{J}{L_P S} = \left[\left(P_C - P_{IF}\right) - \left(\pi_C - \pi_{IF}\right)\right] = \overline{\Delta P} \qquad \textbf{Equation 2.1}$$

J = Volumetric fluid transfer rate (L^3T^{-1})

L_P = Hydraulic conductance of capillary membrane ($L^2 M^{-1}T$)

S = Total circumferential surface area of capillary wall (L^2)

P_C = Hydrodynamic pressure in the capillary ($L^{-1}MT^{-2}$)

P_{IF} = Hydrodynamic pressure of the interstitial fluid ($L^{-1}MT^{-2}$)

π_C = Osmotic pressure in the capillary ($L^{-1}MT^{-2}$)

π_{IF} = Osmotic pressure in the interstitial fluid ($L^{-1}MT^{-2}$)

π_P = Effective pressure ($L^{-1}MT^{-2}$)

If the effective pressure is positive there will be a net flow of fluid from the capillary into the surrounding tissue, which is the case at the arterial end of the capillary or upstream end of the bioreactor. At the venous end of the capillary or downstream end of the reactor the effective pressure is negative meaning there is a net flow of fluid back into the capillary or fibre. *In vivo* average values along the lengths of capillaries result in a small positive value for effective pressure of 0.3 mm Hg (≡ 0.04 kPa) which results in about 10% of the fluid leaving the capillary remaining in the tissue. *In vivo* this fluid enters the lymphatic system, it may be replicated *in vitro* by an open shell side or periodic draining of the abluminal fluid.

The Krogh model (Figure 2.5) also describes capillary transfer phenomena and can be used to calculate how far into a tissue nutrients will diffuse before they are used up, the model is based on Fick's law of diffusion and rate equations for the uptake or nutrients (Fournier 1999).

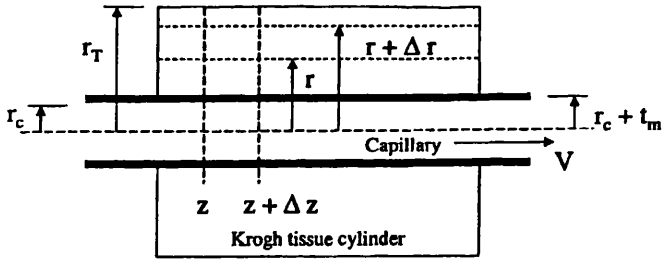

Figure 2.5 Geometry of Krogh tissue cylinder (Fournier 1999).

Krogh describes a cylinder of tissue surrounding the nutrient supply to which the nutrients will diffuse before being used up.

In its simplest application the hollow fibre membrane is designed to support cells on the exterior of the fibre while allowing free passage of nutrients through the fibre wall. Pores too small for the passage of cells allow the much smaller media components to pass through. While it is possible to exclude a component based on size, it is not possible to ensure the passage of smaller nutrients though the membrane without some degree of filtering. Electrostatic, hydrophobic and Van der Waals interactions can act to either repel components from the entrance of pores, or attract components to the pore walls, decreasing the pore diameter and preventing the transfer of components across the membrane (Wei and Russ 1977).

Two methods of transport from capillaries occur *in vivo* depending on both the molecule being transported and the permeability of the tissue. Small molecules, such as oxygen, diffuse through impermeable tissues but as the permeability of the membrane and the size of the molecule increase convection takes over (Wei and Russ 1977).

Ensuring the cells receive an adequate supply of all the required nutrients will require that both the operating conditions and the permeability of the fibres are suited to this task.

2.3 Hollow fibres as scaffolds

The hollow fibres give form as well as name to the hollow fibre bioreactor. The fibres provide the key elements of structural support and nutrient delivery to the nascent tissue. The characteristics of the fibres are equally dependent on the polymer they are made from and the system used to make them. This section is therefore divided between the polymer in Section 2.3.1 and the spinning process in Section 2.3.2. More on the spinning process is given in the introduction to Chapter Eight.

2.3.1 Polymer

Biodegradable polymers are useful in medicine as they can eliminate the need to surgically remove a non-degradable material; as a scaffold for bone tissue engineering biodegradable polymers also have a number of specific benefits. The engineered implant will eventually resemble natural bone tissue with all traces of the polymer eliminated. The load experienced by bone will alter its architecture, and ultimately, mechanical properties; this process is known as Wolff's law. Polymer degradation allows a gradual transfer of load bearing properties onto the developing bone allowing the bone to remodel accordingly. A non-degradable implant results in a sudden transfer of load on the removal of the implant, at which point the surrounding bone, having been shielded from stress by the implant, may not be sufficiently developed to support the load. A degradable scaffold also allows the developing tissue more space as the scaffold degrades.

Vert *et al.* (1992) give convenient definitions of different methods of removal of the scaffold *in vivo*:

- *Biodegradable* describes the break down due to macromolecular degradation with dispersion *in vivo* but no proof of elimination from the body.
- *Bioresorbable* applies to materials which bulk degrade and are resorbed *in vivo* and eliminated, with no side effects, through natural pathways such as; filtration of degradation by-products, or after metabolism.
- *Bioerodible* refers to surface degradation and leads to total elimination.
- *Bioabsorbable* scaffolds dissolve in body fluids without any polymer chain cleavage or molecular mass decrease.

While biodegradation is commonly used to describe the break down and removal of the polymer from the body, using the definitions above, bioresorption or bioerosion, leading to the ultimate elimination from the body, are more accurate. For convenience, the term biodegradable will be assumed to imply break down and removal from the body.

Degradation of polymers typically takes place through hydrolysis of the polymer backbone. This occurs in two phases (Middleton and Tipton 2000): first the water penetrates the bulk of the device and attacks the chemical bonds in the amorphous phase, resulting in the cleavage of long polymer chains and a reduction in molecular weight; in the second phase fragments are metabolised by enzymes resulting in a rapid loss of polymer mass. Physical properties are maintained by the crystalline phase until the device starts to fragment. Polymer degradation is associated with a decrease in the local pH, due to the release of acidic products which acts to autocatalyse the degradation process (Middleton and Tipton 2000). On the surface of the scaffold acidic degradation products may be removed from the vicinity, however, in the interior of the device an acidic local environment develops. An acidic environment increases the rate of hydrolytic attack. This mechanism of degradation can result in the faster degradation of low porosity structures than those with higher porosity; due to the inability of the acidic products to diffuse from the interior of low porosity structures. Degradation rates *in vivo* may therefore be controlled by both the structure and composition of the polymers.

Degradation rates of polymers must compliment the development of the nascent tissue. Polymers that degrade via hydrolysis, as described above, may go through a relatively

long period where polymer backbones are being hydrolysed but very little change in structure or mechanical integrity is apparent. This may be followed by a large decrease in structural integrity over a relatively short time period associated with the number of bonds broken exceeding a critical value and the polymer scaffold fragmenting. A degradation process of this type could have the implication that during initial stages of culture or implantation, there is little space for the expanding tissue to grow. Upon scaffold failure there will be a large transfer of load onto tissue that may have been largely shielded up to that point, and not developed sufficient load-bearing properties; this degradation profile is only slightly better than that achieved through surgical removal of non-degradable scaffolds. Surface hydrolysing polymers that undergo controllable mass loss throughout degradation and allow a gradual transfer of load onto the newly formed tissue are favourable.

Poly(α-hydroxy acids), PLA, PGA and PLGA, are the most widely used synthetic polymeric materials in bone tissue engineering. Their history of FDA approval as sutures makes them favourable as a tissue engineering scaffold by reducing the need to prove biocompatibility (Liu and Ma 2004).

Both lactic acid and glycolic acid are formed into intermediate cyclic dimers, which are then purified and polymerised. These dimers are termed lactide or poly(lactide), and glycolide or poly(glycolide) respectively. PLGA is typically described with a composition ratio such as 75:25 or 50:50, with the first number indicating the molar percentage of lactic acid and the second number the molar percentage of glycolic acid (Middleton and Tipton 2000).

Poly(lactide) exists in two stereo isomers, signified by D for dexoratory or L for levortary, L-lactide is the naturally occurring isomer. Polymers of pure lactic acid and poly(lactic-co-glycolic acid) may contain a single isomer or a combination of both isomers, ratios of D:L isomers are quoted as molar percentages.

Degradation of Poly(α-hydroxy acids) occurs via bulk hydrolysis of the ester bond, the highly crystalline structure of poly(L-lactide) results in a long degradation period of up to two years. This may be reduced by the addition of poly(glycolide) or poly(D,L-lactide) to disrupt the crystalline structure. Figure 2.6 shows how differing ratios of

PLA and PGA in the copolymer vary the half-life of the polymer from a few weeks for copolymers up to years for homopolymers. Decreased degradation rates associated with increased lactide content may be explained by the presence of a methyl group on the repeating lactide unit reducing the chemical reactivity of the ester groups through steric hindrance (Coombes and Meikle 1994). The increased resistance of pure PGA to degradation is a result of the semi-crystalline structure which restricts water ingress reducing hydrolysis (Coombes and Meikle 1994). Polymers with higher molecular weights are also known to degrade slower than those with lower molecular weights. The degree of crystallinity of both co-polymers and homopolymers may be affected by polymer processing and will also affect the rate of degradation, with more crystalline polymers resulting in a longer degradation period. Further discussion on the degradation of PLGA is given in the introduction to Chapters 5 and 6.

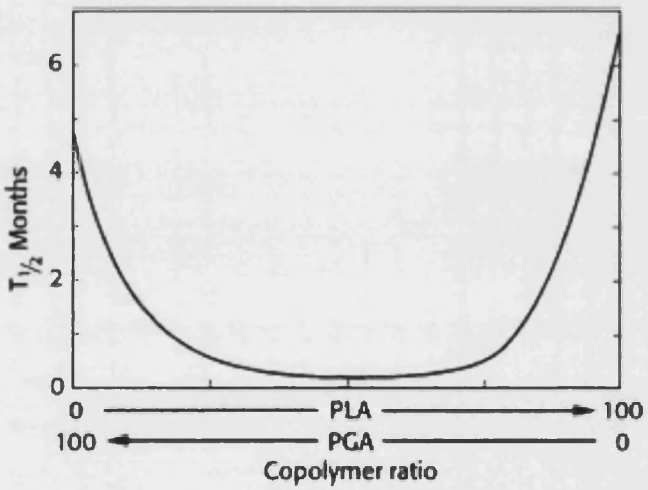

Figure 2.6 Half-Life of PLA and PGA homopolymers and copolymers.
Data from polymers implanted in rat tissue (Middleton and Tipton 2000).

2.3.2 Spinning hollow fibres

A scaffold provides many functions for developing tissue: large surface area for cell anchorage, appropriate three-dimensional shape, space for cells to migrate and proliferate, and mechanical support. Highly interconnected pores allow the passage of nutrients into, and waste products out of the structure. Hollow fibres, combined with a suitable bioreactor, are well suited to these tasks. They provide a large surface area that may be efficiently provided with nutrients by a network that will not become blocked by cell growth.

A huge variety of methods are available for the processing of polymers spanning their use in everyday objects to highly specialised materials. Processing techniques employed for the production of tissue engineering scaffolds may be selected on their ability to produce the required scaffold architecture, their suitability for use with the desired polymers, their ability to incorporate any necessary modifications or biological molecules and the absence of detrimental effects on the scaffold such as residual solvents. Processing techniques must allow a high degree of reproducibility in scaffold architecture; variations in shape down to scales of 5 nm can influence cell adhesion, morphology, and expression (Curtis *et al.* 2004). In addition, the molecular weight of the polymer must not be adversely affected during processing; hydrolysis of the ester bond in the polymer backbone will give the polymer a tendency to reduce in molecular weight during processing.

Hollow fibres are formed from polymer solutions through a process known as spinning; polymer solution is concurrently extruded through a double orifice spinneret with a non-solvent into a bath of non-solvent. The non-solvent diffuses into the polymer solution from both the external coagulation tank and the bore fluid; causing the polymer to precipitate in the shape of a hollow fibre. This topic is discussed in more detail in the introduction to Chapter Eight.

2.4 Conclusions

The number and variety of published papers in the field of tissue engineering and in particular on bone tissue engineering show the diversity in tissue engineering. At present there are no single answers to the problems of which scaffold material to use, what scaffold architecture to use and how to produce it, and which bioreactor to use. Even once these basic questions have been answered further work will be required to optimize the processes involved from production of bioreactors and scaffolds; to sourcing cells and seeding them into the bioreactor; operation during culture; and harvesting and implantation *in vivo*. One explanation for the variety of approaches is the variety of clinical needs; this is combined with a balance between increased process costs and increased performance. It is difficult to undertake an economic assessment of the potential benefit to patients, in terms of reduced pain and quicker recovery, that a more expensive process may, or may not, provide.

This work is focussed on the potential the hollow fibre bioreactor has to offer the field of tissue engineering. While neither hollow fibres in themselves nor their application in cell culture are particularly novel, the combination of these techniques with biodegradable polymers allowing their use in tissue engineering is a recently emerging prospect. Hollow fibre bioreactors have been used for cell culture allowing the isolation of cell products for easy recovery but their potential as a replica of the *in vivo* capillary system is now being realised. An annulus of bone developing around a nutrient supplying hollow fibre is synonymous to the *in vivo* lacunae structure of cortical bone (Davies and Hosseini 2000).

The formation of fibres with appropriate characteristics is critical to the success of the hollow fibre bone tissue bioreactor. This work aims to optimise the hollow fibres for their role as a tissue engineering scaffold and delivery network. The newly found combination of hollow fibres, biodegradable polymers and bone tissue bioreactor is showing good potential as a solution to the problem of bone tissue engineering. However the component parts are far from optimized to their new use. Assumptions about the degradation profile are being made from work on three-dimensional porous scaffolds; even though the structure of the scaffold is known to influence the degradation profile. Fibres are formed by methods traditionally used to make hollow fibre gas separation membranes which need totally different specifications than the fibres required for the bioreactor. This work aims to further develop the hollow fibre bioreactor for bone tissue engineering by ensuring the main feature of the bioreactor is optimized for its new role.

2.5 Aim and Objectives

The aim of this thesis is to optimize the production of biodegradable polymer hollow fibres for use in a bone tissue bioreactor, considering both the initial characteristics of the fibre and the profile of the characteristics during use in the bioreactor.

Specifically the objectives of this thesis are:

- To develop a reproducible spun hollow fibre with the optimised specifications for bone tissue culture *in vitro*.
- To analyse the hollow fibre for characteristics important to its role as a bone tissue engineering scaffold and nutrient delivery network.

- To develop a protocol to effectively sterilize the hollow fibres without adversely affecting their characteristics.
- To evaluate surface treatment as a post-production method for improving the surface of the fibres for tissue engineering.
- To evaluate the degradation profile of the fibres and how it is influenced by the scaffold shape and polymer type.
- To investigate the potential to influence the fibre properties through control of the operating parameters during spinning.

CHAPTER THREE - MATERIALS AND METHODS

3.1 Introduction

Details of all the experimental procedures used along with an alphabetical list of all the materials used are provided here. For clarity, the materials used are divided into three tables: polymers, cells and cell culture medium, and other materials.

3.2 Materials Used In Experimental Work

3.2.1 Polymers

Four ratios of PLGA with a variety of intrinsic viscosities were sourced from four different suppliers. Details are in Table 3.1.

Table 3.1 List of polymers used with supplier and product details.

ID = identity of polymer, IV = intrinsic viscosity.

ID	Polymer	Product no.	Lot no.	Lactide content	IV ($dL\ g^{-1}$)	Synthesis date	Supplier
D5050	PLGA (50:50)	50DG105 0.95-1.2 IV	A06-021a	52	1.12	19/04/2006	DURECT corporation, Pelham, USA
D7525	PLGA (75:25)	75DG065 0.55-0.75 IV	A06-077	76	0.67	14/12/2006	DURECT corporation, Pelham, USA
LS5050	PLGA (50:50)	50:50 DL HIGH IV	LP-178	53	0.77	01/03/2006	Alkermes Inc, Ohio, U.S.
LS6535	PLGA (65:15)	65:35DL HIGH IV	LX00004-94	65	0.7	02/02/2006	Alkermes Inc, Ohio, U.S.
LS7525	PLGA (75:25)	75:25DL HIGH IV	LX00004-74	75	0.56	12/08/2005	Alkermes Inc, Ohio, U.S.
LS8515	PLGA (85:15)	85:15DL HIGH IV	4133-657	86	0.72	05/12/2004	Alkermes Inc, Ohio, U.S.
PS5050	PLGA (50:50)	23987 0.66-0.8 IV	470599	54	0.72	Pre-1997	Polysciences Europe, GmbH, Eppelheim, Germany
RG503	PLGA (50:50)	RG 503 0.32-0.44 IV	1002249	51	0.42	11/05/2001	Boehringer Ingelheim GmbH, Ingelheim, Germany
RG504	PLGA (50:50)	RG 504 0.45- 0.6 IV	0515	51	0.56	12/04/2006	Boehringer Ingelheim GmbH, Ingelheim, Germany
RG752	PLGA (75:25)	RG 752 S 0.16 – 0.24 IV	RES-0478	76	0.2	22/06/2005	Boehringer Ingelheim GmbH, Ingelheim, Germany
RG755	PLGA (75:25)	RG 755 S 0.5-0.7 IV	1021286	75	0.68	14/10/2005	Boehringer Ingelheim GmbH, Ingelheim, Germany
RG756	PLGA (75:25)	RG 756 S 0.71 -1.0 IV	RES-0365	75	0.8	12/05/2004	Boehringer Ingelheim GmbH, Ingelheim, Germany

3.2.2 Cells and media composition

MG63 are an osteoblast-like osteosarcoma cell line, they are used as an indicator for *in vivo* or *in vitro* cellular response to scaffold and reactor combinations. MG63 cells were kindly donated by Dr Marianne Ellis. Details of the media used are given in Table 3.2.

Table 3.2 Alphabetical list of MG63 media composition with supplier details.

Component	*% (v/v)*	*Description*	*Product no.*	*Address*
Antibiotic solution	Optional 1	Penicillin G, streptomycin sulphate, and amphotericin B	A5955	Sigma-Aldrich Company Ltd., Dorset, UK
DMEM	87/88*	Dulbecco's modified eagles media with high glucose, basal media	32430-027	Invitrogen Ltd, Paisley, UK,
FCS	10	Foetal calf serum, media additive	F7524	Sigma-Aldrich Company Ltd., Dorset, UK
NEAA	1	Non-essential amino acids, media additive	M7145	Sigma-Aldrich Company Ltd., Dorset, UK
Sodium pyruvate	1	Media additive	11360-039	Invitrogen Ltd, Paisley, UK,

*** 87% if antibiotic solution is added, 88% if not.**

3.2.3 General materials

Details of materials, other than the polymers or cell culture medium, used in the experimental work are listed alphabetically in Table 3.3.

Table 3.3 Alphabetical list of the materials used and their source.

Material	*Description*	*Product no*	*Address*
Antibiotic solution	Penicillin G, streptomycin sulphate, and amphotericin B	A5955	Sigma-Aldrich Company Ltd., Dorset, UK
BSA	Bovine Serum Albumin, adhesion protein	A3059	Sigma-Aldrich Company Ltd., Dorset, UK
Compressed air	Compressed air	-	BOC Gases, Surrey, UK
Distilled water	From water purification unit	-	ELGA lab water, Bucks, UK
DMSO	Dimethyl sulfoxide, cryoprotective agent	D2650	Sigma-Aldrich Company Ltd., Dorset, UK
Ethanol	96% (v/v), disinfectant	E/0555DF/25	Fisher Scientific UK Ltd, Loughborough, UK
Hydrochloric acid	37% analytical grade	H/1200/PB17	Fisher Scientific UK Ltd, Loughborough, UK
Lambda DNA standard	DNA standards	P7589	Invitrogen Ltd, Paisley, UK,
Molecular grade water	Molecular grade water	5171	CLP Ltd, Northampton, ENGLAND
Nitrogen	Compressed Nitrogen	-	BOC Gases, Surrey, UK
NMP	1-methyl-2-pyrrolidinone 99%, solvent	12763-0025	Fisher Scientific UK Ltd, Loughborough, UK
PBS	Phosphate buffered saline solution	D8537	Sigma-Aldrich Company Ltd., Dorset, UK
Peracetic acid	Peracetic acid solution, sterilization agent.	77240	Sigma-Aldrich Company Ltd., Dorset, UK
Perchloric acid	70% acid	P/1280/PB08	Fisher Scientific UK Ltd, Loughborough, UK

Continued

Table 3.3 Continued

Material	*Description*	*Product no*	*Address*
PicoGreen® dsDNA Quantitation Kit	Assay for determining cell number by DNA concentration	P7589	Invitrogen Ltd, Paisley, UK,
Potassium hydroxide	Potassium hydroxide pellets 85%	10210	BDH Chemicals, Poole, Dorset, UK
Quant-iT™ PicoGreen® dsDNA reagent	Pico green in DMSO	P7589	Invitrogen Ltd, Paisley, UK,
Sigmacote	Prevents cells from adhering to glass surfaces	SL2	Sigma-Aldrich Company Ltd., Dorset, UK
Sodium Hydroxide	1 M NaOH >99%	71689	Fluka Biochemica, Sigma-Aldrich Company Ltd., Dorset, UK
TE	200 mM Tris-HCl, 20 mM EDTA	P7589	Invitrogen Ltd, Paisley, UK,
Trypan blue	Cell stain (stains dead cells)	15250-061	Neubauer
Trypsin-EDTA	Cell dissociation enzyme	T4174	Sigma-Aldrich Company Ltd., Dorset, UK

3.3 Experimental Methods

3.3.1 Preparation of Polymer Scaffolds

3.3.1.1 Polymer solutions

Polymer solutions were prepared with 1-methyl-2-pyrrolidinone (NMP). Initially a 20% (w/w) solution was made; the concentration was then adjusted depending on the viscosity of the solution required. Details of the polymers used are given in Table 3.1. The solution was left on a roller mixer (SRT9D, Bibby-Stuart, UK) under ambient conditions (8-20°C) for at least 24 h or until the polymer had completely dissolved.

3.3.1.2 Formation of flat sheet membranes

Flat sheet scaffolds were formed by solvent exchange with distilled water. 3-5 cm^3 of polymer solution was spread onto a 15 cm by 25 cm glass support, using 100 μm or 250 μm wire guides to control thickness; this was immersed in distilled water at 10-15°C. After two to three minutes the polymer precipitate was lifted off the glass

support. The polymer was soaked in water for 24 h for solvent removal. The scaffolds were then removed from the water tank and dried in ambient conditions (8-20°C) for at least 24 h.

Figure 3.1 Photographs of the apparatus used to make flat sheet membranes.

***Top left**: polymer solution, glass rod for spreading polymer and glass support; **Bottom left**: close up of wires used to control the thickness of the membrane; **Right**: two membranes cast into the water bath just prior to lifting off the glass support.*

3.3.1.3 Spinning hollow fibre membranes

Polymer solutions were extruded through a double-orifice spinneret (Figure 3.2), to form hollow fibre membranes, in a process known as wet-spinning. Polymer solution flows through the spinneret outer annulus (OD 1.0 mm, ID 0.7 mm), concurrently water flows through the inner orifice. The spinneret is positioned on the surface of a water bath so the polymer solution contacts the bore fluid and external water bath at the same time. The polymer precipitates on contact with the water forming a hollow fibre. The process was carried out under ambient conditions; the room temperature was in the range 18 ± 2°C and the water bath which was filled with cold tap water (the volume required prevented the use of distilled water) was 14 ± 1°C.

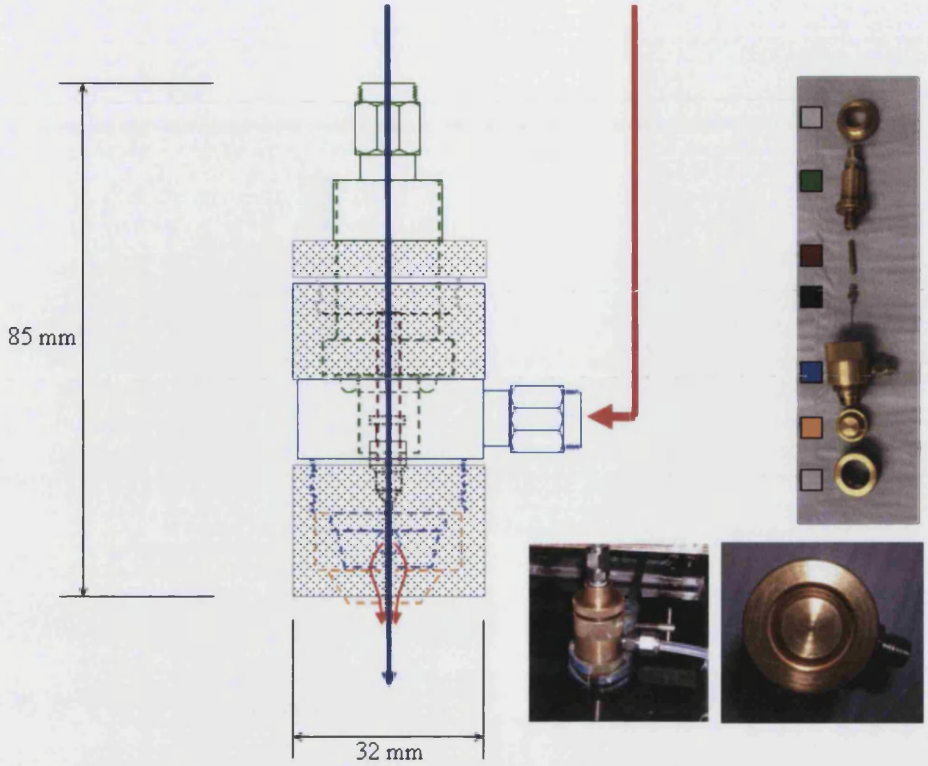

Figure 3.2 Double orifice spinneret.

Blue arrow indicates flow of water, red arrow indicates flow of polymer.

Two methods were employed for extrusion of polymer solution through the spinneret. Before either the polymer solution was de-gassed, this was carried out by placing the polymer solution in its original bottle with the lid loosened in a vacuum (E2M2, BOC Edwards, UK) for 5 – 10 minutes or until no bubbles could be seen in the polymer solution.

Method A – Nitrogen pressurization

This method is shown in Figure 3.3; polymer was placed in a stainless steel reservoir and connected to the spinneret via PTFE tube containing a ball valve. The polymer reservoir was pressurized to ~ 2×10^2 kPa gauge with nitrogen to expel the polymer solution; the flow rate of the polymer into the spinneret was controlled using the ball valve. Distilled water was filtered (40 μm), and pumped (gear pump, Reglo-Z, Ismatec, Switzerland) concurrently through the inner orifice (ID 0.4 mm) at a rate of 3.5 – 7.0 cm^3min^{-1}.

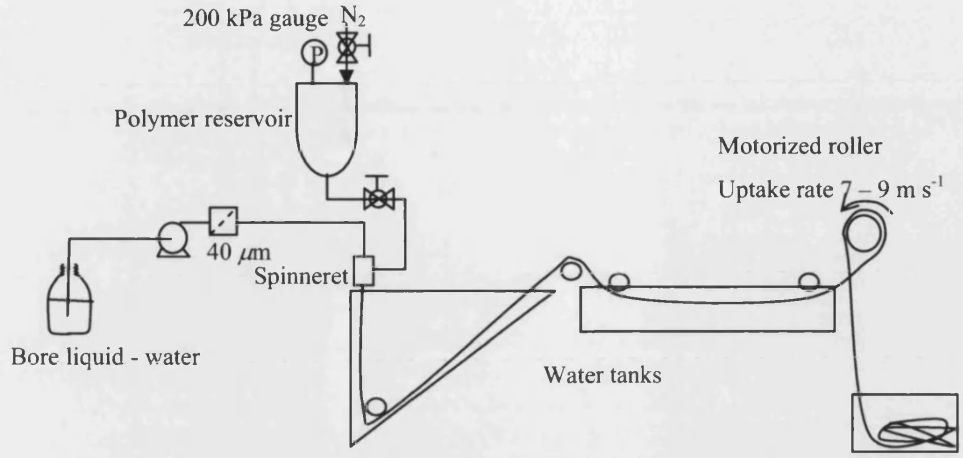

Figure 3.3 Schematic diagram of the spinning apparatus used in Method A.

Polymer was expelled from the reservoir tank using 200 kPa gauge nitrogen.

Method B – Syringe pumps

This method is shown in Figure 3.4; two syringe pumps (PHD 22/2000, Harvard Apparatus, Massachusetts, US) were used to accurately and independently control the flow rate of the polymer and bore fluid entering the spinneret. Flow rates in the range of $5.0 – 6.0 \times 10^{-2}$ cm^3 s^{-1} were used for both the polymer and bore fluid. Changes were made to the flow rate based on visual assessment of the fibre diameter and wall thickness, this was necessary due to small variations in the polymer solution viscosity and the ambient laboratory temperature which could not be controlled. 60 cm^3 syringes were used to hold both the polymer solution and bore fluid; flexible tubing was used to connect the syringes to the spinneret.

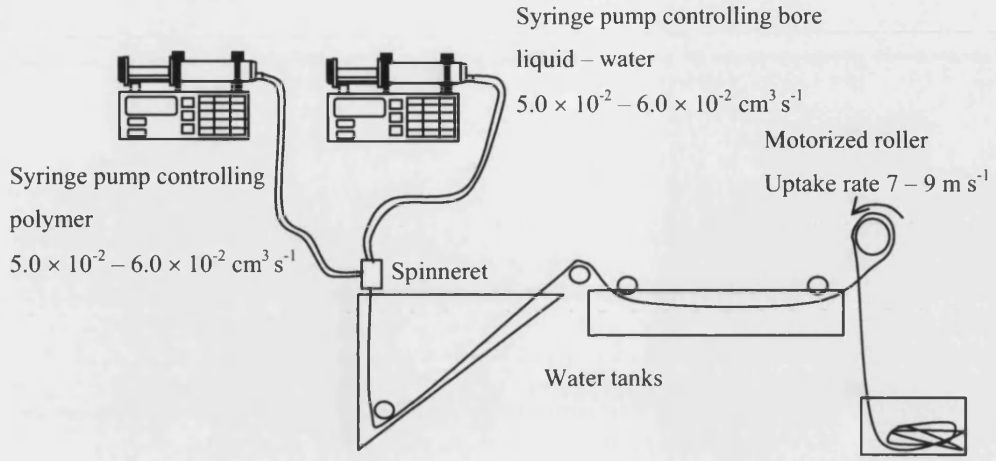

Figure 3.4 Schematic diagram of the spinning apparatus used in Method B.
Syringe pumps were used to extrude both the polymer and water through the spinneret giving a greater degree of control over flow rates.

For either method of delivery of solutions to the spinneret the nascent fibre passed through two water tanks, of 1.2×10^{-1} m^3 and 3.6×10^{-2} m^3 volume respectively, and a motorized roller (Roller: AM63MT4, AEG, Nuremburg, Germany; Controller: Fara Moscon-E5, Samsung, Surrey, UK) guided it at a rate of 7 – 9 m s^{-1} into a final water tank. After 2-3 h the water the fibres were in was changed, this time replaced with distilled water (14 ± 1°C) and they were left for 24 h to ensure solvent removal before drying in ambient conditions (8-20°C).

3.3.1.4 Formation of polymer beads

Spherical polymer beads were created by dispensing polymer solution drop-wise from a syringe with a 25 gauge needle. The polymer solution was dispensed at a rate of 3.0×10^{-3} cm^3 s^{-1} from a height of 20 cm using a syringe pump (PHD 22/2000, Harvard Apparatus, Massachusetts, US). The drops, which tended to be spherical due to surface tension, landed in a 150 cm^3 beaker of distilled water stirred with a magnetic stirrer such that the vortex was about 2 cm from the bottom of the beaker, the water was 14 ± 1°C. The beads were left in water for 48 h with continual stirring; they were then removed and allowed to dry in ambient conditions (8-20°C).

3.3.2 Sterilization and disinfection study

Flat sheets were clipped into circular 13 mm (OD) membrane supports; excess scaffold was removed with a scalpel. Hollow fibres were cut into 10 mm lengths. One flat sheet or two hollow fibre sections were sterilized in individual cells in a 24 well-plate. Both flat sheet and hollow fibre samples had a mass of 4 ± 0.6 mg (mean ± SD; n = 12) prior to treatment.

3.3.2.1 Ethanol treatment

1 cm^3 70% (v/v) ethanol solution (diluted from 96% (v/v) ethanol with distilled water) was added to each well. Samples were treated for 15 min, 30 min, 1 h, 2 h, 5 h and 24 h, and subsequently rinsed five times with 1 cm^3 phosphate buffered saline (PBS).

3.3.2.2 UV treatment

Samples were irradiated with a 12 W, UV lamp at a wavelength of 254 nm at a distance of 15 cm for a total time of 30 min, 1 h, 2 h, and 5 h and were turned over halfway through the treatment to irradiate the top and bottom surfaces. Flat sheet samples were also prepared without turning.

3.3.2.3 Antibiotic treatment

Polymer samples were placed in a solution of 1% (v/v) antibiotic antimycotic solution (penicillin/streptomycin, P/S) in PBS and incubated at 4°C for 6 h, 15 h, 24 h and 31 h. Samples were rinsed three times with PBS before use.

3.3.2.4 Peracetic acid treatment

Peracetic acid treatment was carried out for the same durations as ethanol treatment with a volume by volume solution of 0.1% peracetic acid (peracetic acid solution 39% in acetic acid), 4% ethanol 95.9% distilled water. Samples were rinsed in 1 cm^3 PBS for 1 h, three times.

3.3.2.5 Preparation of controls

Control flat sheet samples were prepared as for antibiotic treatment, replacing antibiotic solution with PBS or distilled water. No rinsing was carried out post-treatment. Untreated control scaffolds were also tested.

3.3.3 Surface treatment of polymer membranes

Alkali solutions were prepared to the required concentration by the addition of solid pellets to water. Acid solutions were prepared by diluting concentrated acid solutions with distilled water to the desired concentration.

1 cm^3 solution per 1 cm^2 membrane was added to each sample in a suitably sized well plate and left for the required duration at room temperature (19°C ± 2°C). Following treatment samples were thoroughly rinsed with distilled water.

3.3.4 Degradation studies

Degradation studies were carried out on all three scaffold forms, *viz.* flat sheet, hollow fibre and spherical bead. Scaffold samples, 2 cm × 4 cm flat sheet membranes, hollow fibres 5 cm in length and 10 spherical beads, were placed inside T25 cell culture flasks. These were then sterilized in a 5 cm^3 solution of 1% (v/v) antibiotic antimycotic solution (penicillin/streptomycin, P/S) in PBS at 4°C for 24 h. Scaffolds were rinsed with PBS. 5 cm^3 FCS was added to the flask and the flask placed in conditions according to its future degradation conditions for 24 h. The samples were rinsed thoroughly in appropriate degradation fluid and set up for degradation studies. 5 cm^3 degradation liquid, either complete cell culture media or distilled water, was added. The flasks were placed in the appropriate environment, either an incubator at 37°C 5% CO_2, or ambient laboratory conditions (20 ± 3°C) on a rotational mixer (STR4, Barlow world Scientific, Staffordshire, UK) and rotated at the lowest speed to prevent the scaffolds floating (the mixing maintained a layer of liquid on the top surface of the scaffolds).

Scaffolds degraded under flow conditions were set up in the hollow fibre bioreactor (refer to section 3.4) and if necessary seeded with MG63 cells according to section 3.4.2. Luminal, abluminal and dual flow arrangements were utilized with all flow rates 20 cm^3min^{-1}.

3.4 Design of the hollow fibre bioreactor

A custom designed bioreactor (Figure 3.5) was used for hollow fibre experiments; a 100 mm long 12 mm outer diameter (OD), 7 mm inner diameter (ID) borosilicate glass tube formed the body of the reactor with two 6 mm OD side ports with PTFE ferules and stainless steel (SS) fittings (Figure 3.6). The glass bioreactors were treated with

sigmacote to prevent cells adhering to the glass surfaces. Five or ten fibres were placed in the bioreactor; the fibres were sealed into the reactor with epoxy resin (Araldite Rapid). Fluid was circulated through the lumen by means of a peristaltic pump (503U Watson-Marlow Bredel, Falmouth, UK).

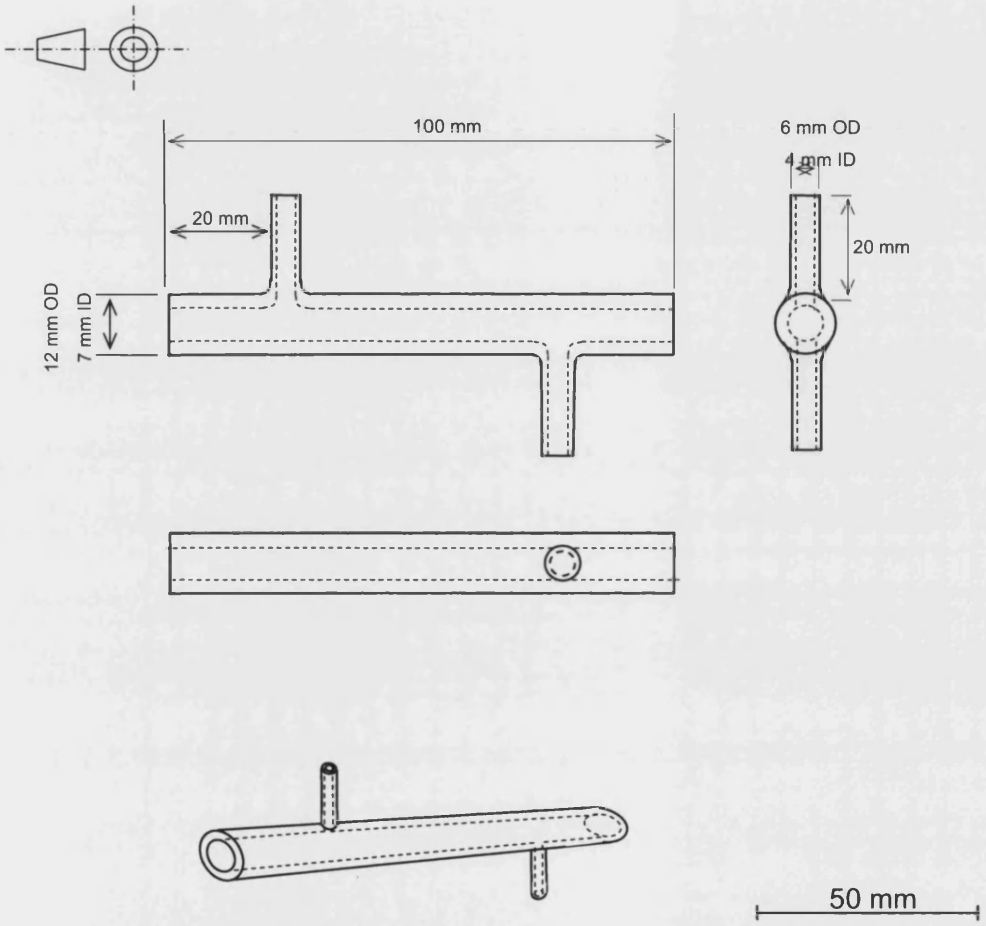

Figure 3.5 Diagrams of the glass hollow fibre bioreactor.

Top: First angle projection of the glass bioreactor with dimensions. Bottom: Linear perspective of the glass bioreactor. Scale 1:1.3

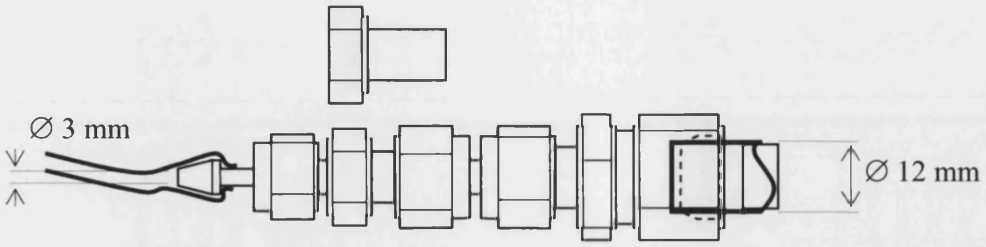

Figure 3.6 Hollow fibre bioreactor end fittings.

From left to right: 3 mm port connector, 3 mm to 6 mm expansion, 6 mm port connector, 6 mm to 12 mm expansion. All fittings stainless steel except 12 mm PTFE ferrule (dotted) for seal to glass bioreactor. Scale 1:1

Figure 3.7 shows the bioreactor circuit for lumen flow with abluminal media perfusing to waste. A number of other configurations are also possible and are listed below (Table 3.4); details of the flow regime used for specific studies are given in the later chapters.

Table 3.4 Flow configurations for the hollow fibre bioreactor

	Flow configuration
1	Luminal flow
2	Luminal flow with removal of permeate through the side port
3	Abluminal flow
4	Abluminal flow with permeate removal through the fibres
5	Co-current flow through the lumen and ablumen
6	Counter-current flow through the lumen and ablumen

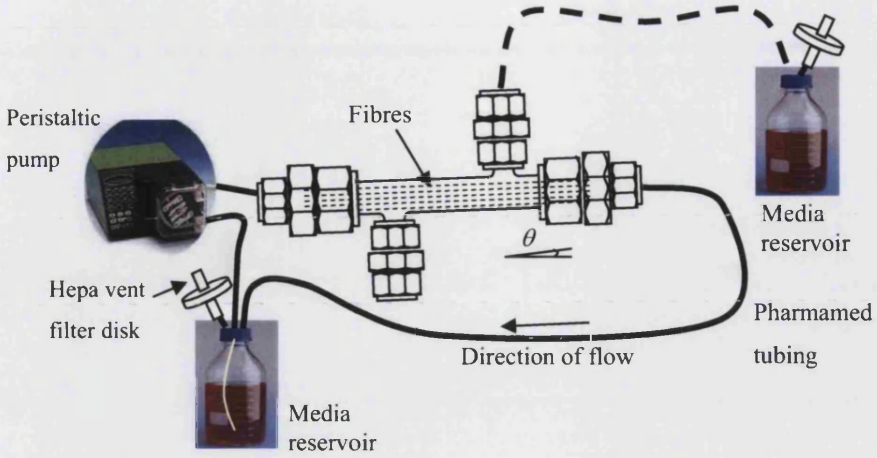

Figure 3.7 Hollow fibre bioreactor circuit.

The dotted line indicates the optional permeate removal line. The bioreactor is positioned on a slight incline ($\theta = 5 - 10^{o}$), with the media exiting from the higher end, to prevent the formation of air pockets.

3.4.1 Sterilizing the bioreactor

All components for the bioreactor rig, except the bioreactor itself, were autoclaved at 121°C and 103 kPa for 15 min prior to use. The bioreactor containing the fibres, which would be damaged by autoclaving, was sterilized by charging the reactor with antibiotic solution diluted 100× in PBS. The lumen was charged by adding the sterilizing fluid to the media reservoir bottle and running the pump until the circuit was seen to be fully charged. Using a needle syringe approximately 4 cm^3 of the sterilizing solution was withdrawn from the media reservoir and charged to the ablumen of the bioreactor via a side port. The bioreactor was then incubated at 4°C for 24 h.

3.4.2 Seeding the bioreactor

Following sterilization with antibiotic solution the bioreactor was flushed for at least an hour with DMEM and then complete media supplemented with 1% antibiotic solution. Flushing was carried out by draining the circuit and then charging the media bottle with the required fluid and circulating the fluid through the lumen of the fibres; the ablumen was filled through a side port. During flushing the entire rig was placed within the incubator at 37°C and 5% CO_2.

The bioreactor was seeded by draining the ablumen of media and charging with approximately 2 cm^3 of cell suspension containing 20,000 cells per cm^2 of hollow fibre surface area. The ablumen was then topped up with complete media. The entire rig was placed back in the incubator. The rig was turned 180° every hour for six hours to improve cell distribution within the bioreactor. After six hours the rig was set up with the required flow conditions.

3.5 Cell Culture Techniques

Cell culture was carried out according to good cell culture practice, under aseptic conditions and within a category II laminar flow containment hood (Kendro Laboratory Products Plc, Hertfordshire, UK). All reagents were pre-warmed to 37°C prior to contact with cells.

3.5.1 MG63 cell type and maintenance of cell line

MG63's were maintained in T75 or T150 cell culture flasks and incubated at 37°C and 5% CO_2. Cells were fed by removing the old media and replacing with 15 cm^3 fresh media every 2 – 3 days, or as required indicated by a yellowing of the media. Media composition is given in Table 3.2. On reaching confluence cells were passaged, this was typically 4 – 5 days. Cells were rinsed with 3 times with PBS. Trypsin-EDTA was used to release the cells from the surface, the cells suspension was then centrifuged at 1200 rpm, 20°C for 5 min the supernatant was discarded and the cells suspended in cell culture media and seeded into new cell culture flasks.

3.5.2 Seeding flat sheet membranes

Cell culture was carried out on polymer flat sheets in a custom polycarbonate culture chamber designed to support the flat membranes with a known surface area exposed to culture (Figure 3.8). The chamber was sterilized by autoclave (15 min at 123°C) prior to use, the membrane was inserted and sterilized with 5 ml of antibiotic solution for 24 h at 4°C. The membranes were then rinsed once with DMEM and soaked in DMEM for 1 h followed by soaking in complete media for 1 h prior to seeding. Membranes were seeded with 6.9×10^4 cells suspended in 3.5 ml complete media supplemented with 1% antibiotic solution. Hepa filters were used to close the seeding port and the whole chamber was placed in the incubator at 37°C and 5% CO_2.

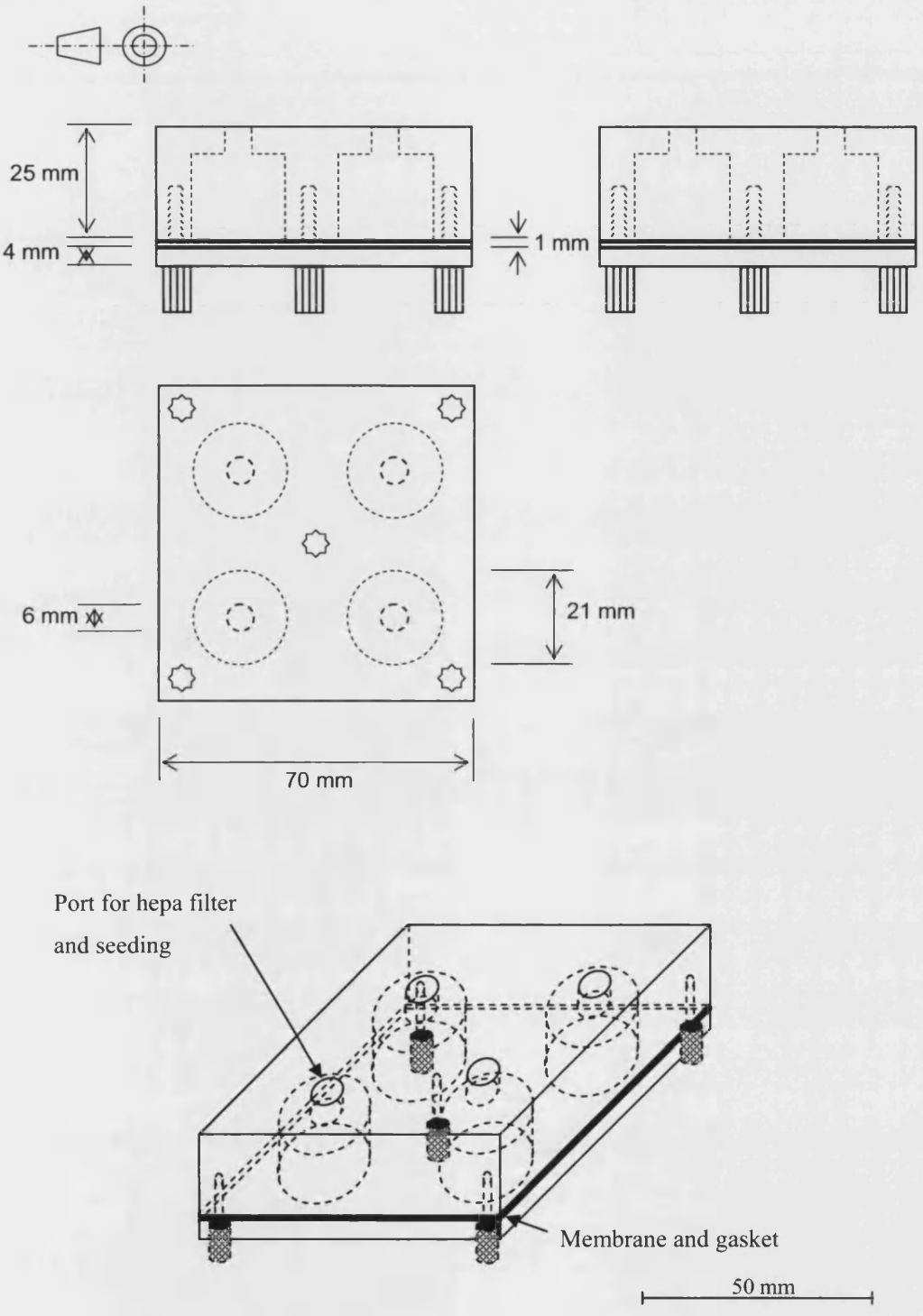

Figure 3.8 Diagrams of the flat sheet chamber.

***Top**: First angle projection with dimensions, **Bottom**: isometric projection. Scale 1:1.4*

3.6 Analytical Methods

3.6.1 Cell number

Two methods were used to determine cell number. Method A allowed a distinction between live and dead cells, while Method B was less labour intensive allowing larger numbers of samples to be analysed.

Method A – Trypan blue staining and live dead count

Cells were suspended in a known volume of DMEM, 10% trypan blue was added to the cell sample. Live (unstained) and dead (stained blue) cells were counted using a haemocytometer.

Method B – PicoGreen®

A PicoGreen® dsDNA Quantitation Assay Kit was used to determine the number of cells present in a sample. Cells were lysed by the addition of TE buffer and freeze/thawed (-80°C/37°C), this also allowed samples to be stored at -80°C until analysis. For analysis 100 μL of each sample was added to wells in a 96 well plate, three repeats were carried out for each sample. In addition DNA calibration was carried out for each analysis session using known concentrations of DNA in the range 0 – 2 μg cm^{-3}. 30 μL of the PicoGreen® solution diluted 200× in TE buffer was added to each well and sample fluorescence at 480 nm excitation and 520 nm emission was read immediately.

3.6.2 Analysis of polymer and solutions used to make scaffolds

3.6.2.1 Viscosity

Viscosity of polymer solutions was determined using a plate and cone controlled stress rheometer (Bohlin BR-CS-50, Malvern Instruments Ltd, Worcester, UK) at a constant temperature of 20°C. Initial tests indicated solutions showed very good Newtonian fluid behaviour so a single sweep of increasing shear stress was used to determine viscosity. Viscosities above 0.5 Pa s were measured using a 4 cm diameter / 4° cone over a range of shear stresses from 5.9×10^{-2} to 1.1×10^{2} Pa. Viscosities below 0.5 Pa s were measured using a 6 cm diameter / 1° cone over a range of shear stresses from 5.9×10^{-2} to 7.2×10^{1} Pa. Intrinsic viscosity was determined from a series of low concentration solutions.

3.6.2.2 Diffusion of water into polymer

The propagation of the diffusion front into an element of a solid fibre was monitored using a custom designed chamber. A drop of polymer was held between two glass slides with spacers at either end (Figure 3.9). This was submerged in water, allowing water to rapidly surround the polymer droplet. The diffusion front was defined as the change in of the polymer from a translucent liquid to an opaque solid. This was photographed at 10 s intervals with a scale bar and stop watch in view. Allowing the subsequent image analysis to plot the distance the diffusion front had moved against time.

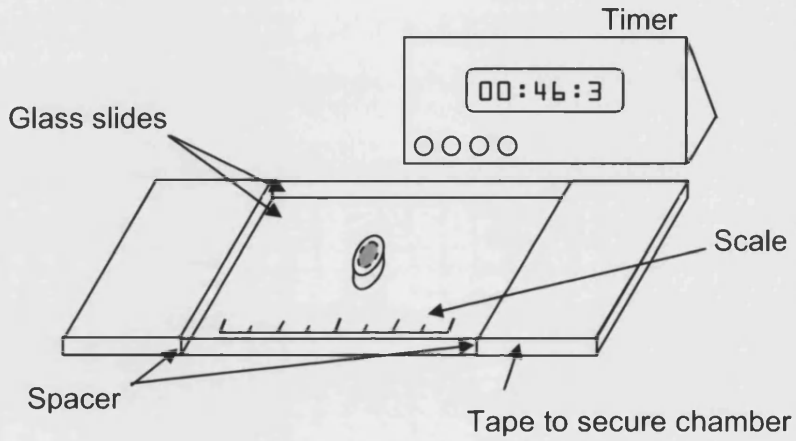

Figure 3.9 Diagram of the diffusion chamber.

A droplet of polymer solution was trapped between two glass slides; spacers at either end separated the glass slides by a known distance. Tape secured the slides together. The whole chamber was submerged in a water bath to monitor the progression of the diffusion front into the polymer droplet. The initially translucent polymer solution became opaque as water diffused in and caused the polymer to precipitate. Isometric projection, scale bar approximately 2 cm.

3.6.2.3 Colour of polymer

The colour of the raw polymers were recorded and quantified by taking a digital photograph of each of the raw polymers under the same lighting conditions. The values of the red, green and blue channels were identified using the image analysis software ImageJ (Rasband 1997-2006). These were combined into a single grey-scale value using Equation 3.1.

$$g = 0.3R + 0.59G + 0.11B \qquad \textbf{Equation 3.1}$$

g = Greyscale value (-)

R = Value of red channel (-)

G = Value of green channel (-)

B = Value of blue channel (-)

This formula is commonly used in digital imagery to manipulate colour images into greyscale images and allows for the sensitivity of the human eye to different colours. The single greyscale value allows the colour of the polymer to be compared to other quantitative data.

3.6.3 Analysis of scaffolds

3.6.3.1 Sterility treatment

Samples were incubated for 48 h at 37°C and 5% CO_2 in 1 cm^3 cell culture media (Table 3.2) and checked periodically for signs of infection, indicated by yellowing of the media (DMEM contains the indicator phenol red) and increased media opacity. Unsterilized scaffolds were used as a positive control and media with no scaffold as a negative control.

3.6.3.2 Pore size and porosity

Two methods were employed to gauge the surface porosity and surface pore size of the membranes.

Method A - Scanning Electron Microscopy (SEM)

Samples were prepared with a scalpel to reveal all the surfaces, liquid nitrogen was used as required to freeze the polymer and prevent structural damage. Samples were mounted on a sample tray, using double-sided sticky carbon discs, and sputtered with gold (5150B, BOC EDWARDS, Sussex, UK) before viewing with the scanning electron microscope (JEOL JSM6310, JEOL (U.K.) LTD., Herts, UK).

SEM images were viewed qualitatively to determine the appearance of the scaffolds. The programme ImageJ (Rasband 1997-2006) was used to determine the average pore size and surface porosity of scaffolds. In order to determine pore characteristics the

contrast and brightness of the image was manually adjusted to enhance the contrast between dark pores and the lighter surface of the scaffold. Scale calibration was performed through the *Spatial Calibration* plug-in based on the scale bar on the SEM images. Pore regions were then selected based on colour using the *Threshold* function; where possible the automatic function was used to do this to prevent user bias. These regions were then set to black with all other regions set to white. The *Particle Analysis* function was then used to measure the area and number of pores. Other measurements were taken from the image using the line tool to measure the distance between points. Random pores were selected to determine inter-pore distances using a random number generator to generate x and y co-ordinates to select a particular pore to measure the inter-pore distances from.

Method B - Gas permeation

The membrane characterization technique of gas permeation was used to determine pore diameter. 120 mm hollow fibre samples were glued using epoxy resin (Araldite rapid) into 100 mm long 6 mm diameter stainless-steel (SS) tubes and excess length was trimmed, at one end the tube-side was sealed at the other end the shell-side was sealed (Figure 3.10). Nitrogen permeation through the fibre walls was measured for inlet pressures between 1×10^2 kPa gauge and membrane failure (typically $5 - 6 \times 10^2$ kPa gauge). Pore sizes were calculated based on the assumption of Poiseuille flow through porous media, details of the calculation are given in Appendix A

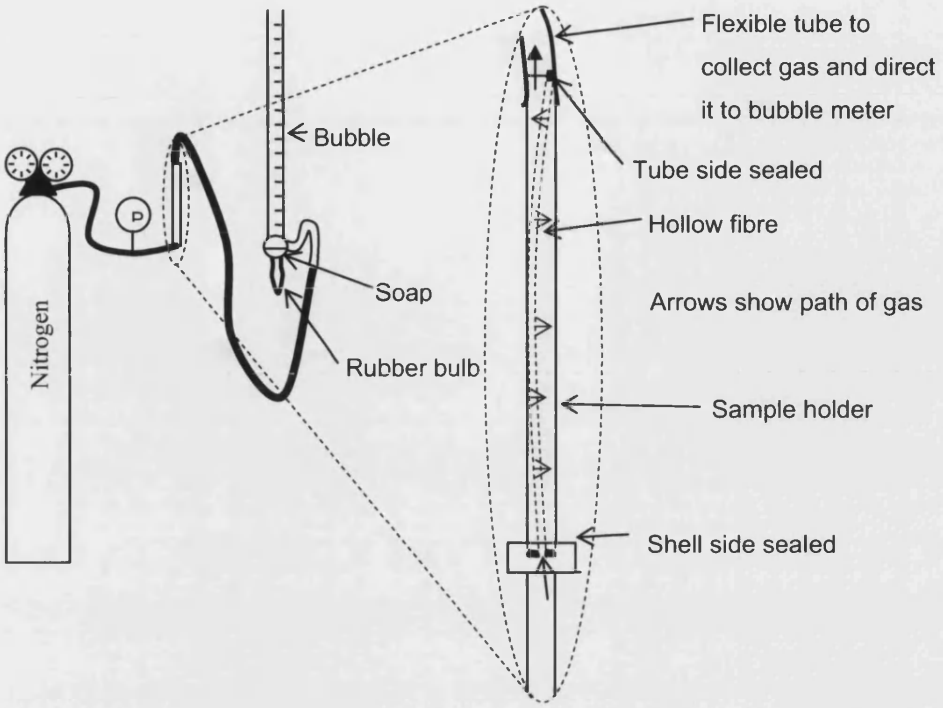

Figure 3.10 Schematic of the gas permeation rig.
Gas flows into the bottom end of the fibre, the top of the fibre is sealed so any gas collected in the bubble-meter has perfused through the fibre wall.

3.6.3.3 Water flux

Hollow fibres were prepared as for the gas permeation tests and fitted into the bioreactor (Figure 3.11). Water was circulated through the lumen of the fibres at a range of pressures ($0 - 2 \times 10^2$ kPa gauge trans-membrane pressure difference) and inlet, outlet and permeate flow rates were measured. Trans-membrane pressures were achieved by a combination of increased pump speed and throttling with a control valve. Membranes underwent a wetting period of up to two days to ensure the membrane was completely wet and permeation rate had reached equilibrium for constant conditions. Blue food dye was used to identify any possible leaks through the membrane potting or obvious defects in the membrane and to illustrate the flow pattern within the reactor; this was thoroughly rinsed out before quantitative permeation data was collected.

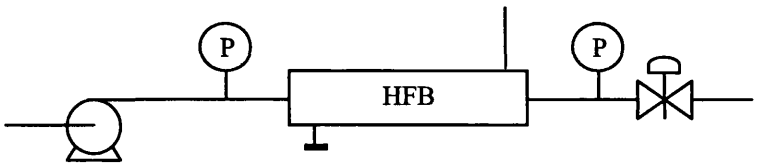

Figure 3.11 Hollow fibre bioreactor circuit for testing water flux.

Water is pumped through the fibre lumen, permeate is collected via a side port. Pressure gauges on the inlet and outlet allow the determination of the average trans-membrane pressure drop.

3.6.3.4 Mechanical testing

Hollow fibres were tested to breaking tension (INSTRON 1122, Instron, Norwood, Massachusetts) with a full scale load of 500 g and a cross-head speed of 20 mm min^{-1}. Samples were tested dry or kept in distilled water after sterilization and tested within 30 min. Samples which were not already wet were soaked in distilled water for 2 h before testing. Breaking stress (σ) and Young's modulus (E) were calculated, details of the calculation are given in Appendix A

3.6.3.5 Mass

Mass below 125 g was measured using 125A Precisa scales to an accuracy of $\pm 10^{-4}$ g. Mass above 125 g was determined using PM30000 Mettler Toledo Ltd. Scales to an accuracy of ± 0.1 g. Measurements of mass of hollow fibres coming from the bioreactor were made per unit length, to allow the removal of the ends of the fibres where they were potted into the reactor.

The percentage mass remaining of the scaffolds was used as a standardised quantitative measurement for the mass change of the scaffolds; as described by Equation 3.2.

$$m = \frac{m_f}{m_i} \times 100 \qquad \textbf{Equation 3.2}$$

m = Percentage mass remaining (-)

m_f = Final mass of scaffold (M)

m_i = Initial mass of scaffold (M)

3.6.3.6 Size

Size of the scaffolds was determined by digitally photographing (Coolpix 3200, Nikon UK Limited, Surrey, UK) the white scaffolds against a matt black background with a scale bar. Measurements were taken from the image using the programme ImageJ (Rasband 1997-2006). The volume was determined from photographs taken of each dimension of the scaffold.

The percentage volume remaining of the scaffolds was used as a standardised quantitative measurement for the volume change of the scaffolds; as described by Equation 3.3.

$$v = \frac{v_f}{v_i} \times 100 \qquad \textbf{Equation 3.3}$$

v = Percentage volume remaining (-)
v_f = Final volume of scaffold (L^3)
v_i = Initial volume of scaffold (L^3)

To standardise and quantify the cross-sectional area of the scaffolds the percentage cross-sectional area remaining was used, as defined by Equation 3.4

$$A = \frac{A_f}{A_i} \times 100 \qquad \textbf{Equation 3.4}$$

A = Percentage cross-sectional area remaining (-)
A_f = Final cross-sectional area of scaffold (L^2)
A_i = Initial cross-sectional area of scaffold (L^2)

The porosity of the scaffold was determined from the mass of the scaffold and the bulk volume for the scaffold, the scaffold mass was converted into volume using the density provided by the manufacturers of the polymer.

$$P = \frac{1 - \frac{m}{\rho}}{V} \times 100 \qquad \textbf{Equation 3.5}$$

P = Porosity of scaffold (-)

m = Mass of scaffold (M)

ρ = Density of polymer ($L^{-3}M$)

V = Volume of scaffold (L^3)

The percentage porosity remaining of the scaffolds was used as a standardised quantitative measurement for the porosity change of the scaffolds; as described by Equation 3.6.

$$P_r = \frac{P_f}{P_i} \times 100$$ **Equation 3.6**

P_r = Percentage porosity remaining (-)

P_f = Final porosity of scaffold (%)

P_i = Initial porosity of scaffold (%)

3.7 Statistical Methods

Statistical methods have been employed to determine whether test results indicate a reason to reject the null hypothesis. In all cases the null hypothesis assumes the sample mean does not differ from the control sample mean. The following two subsections describe the methods used to graphically represent the data and quantitatively analyse the data. Full details of all the methods used and explanations may be found in Crawley (2005).

3.7.1 Graphical Representation

Scatter plots typically show all data points. Regression lines and confidence intervals as calculated by least squares linear regression are also shown where necessary. Box and whisker plots show the spread of the data with the box representing the inter-quartile range, the bar the median and the whiskers showing minima and maxima. Outliers, points further than 1.5 times the inter-quartile range above or below the quartiles are shown as points. Bar charts show mean with error bars indicating least significant difference. This is to allow simple visual identification of significant differences between samples, overlapping error bars indicate no significant difference and non-overlapping error bars indicate significant difference.

3.7.2 Statistical analysis

Statistical analysis was carried out using R: A Language and Environment for Statistical Computing (R 2007). Analysis of variance (ANOVA) was used to test significant differences between samples (except in the case of only two samples where a *t*-test was used instead). As ANOVA will only signify significant difference between samples and does not identify which samples are different from one another, following ANOVA *a priori* contrasts were set and Tukey's honest significant difference (Tukey's HSD) method was used to determine where the significant differences lay. Single or multiple linear regressions were used to determine relationships between two or more continuous variables. Analysis of covariance (ANCOVA) was used to determine significant differences when there were both continuous and categorical explanatory variables. Samples were considered to be significantly different when p fell below 0.05.

Statistical correlations were developed considering all possible explanatory variables; variables which did not significantly add to the explanatory power of the correlation (as determined by ANOVA between the more complex and simplified correlations) were removed in the order of least significance (on the principle of parsimony) until all remaining terms were significant in explaining the response of the dependant variable. Correlations were checked for heteroscedasticity on a residuals versus fitted values plot, and Normality (the population of the data fits a Normal distribution) on a quantile-quantile plot (Q-Q plot) against a normal distribution, Normal data will lie on the $y = x$ line). Where data did not fit a normal distribution with good heteroscedasticity transformations were trialled to improve the correlation.

Count data (eg. number of cells) was analysed using a poisson or quasipoisson distribution with a generalized linear model to account for all the data being positive, the variance of this type of data being likely to increase with the mean, and the errors not being normally distributed.

Percentage data (eg. porosity of the surface of membranes) was transformed using the arc-sin transformation prior to Normal analysis to set boundaries for the correlation at 0 and 100%.

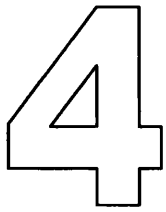

CHAPTER FOUR – STERILIZATION AND DISINFECTION

An investigation into the affects of two methods of sterilization and two methods of disinfection on flat sheet and hollow fibre scaffolds made from 50:50, 65:35 and 85:15 PLGA[1]

4.1 Introduction

Materials and production methods for suitable polymer scaffolds attract extensive research interest; however the effects of subsequent sterilization on these scaffolds are often overlooked. Low polymer melting points, complex architectures and hydrolytic degradation mechanisms result in scaffolds that may be easily damaged by harsh sterilization protocols. Typical medical or cell culture sterilization methods may prove unsuitable for polymer scaffolds. Standard techniques include autoclaving, ethylene oxide treatment or gamma irradiation; these have already been shown to be unsuitable for polymer scaffolds due to deformation from elevated temperatures, lengthy degassing and deterioration due to decreased molecular weights (Athanasiou *et al.* 1996).

This study investigates four methods of disinfecting flat sheet and hollow fibre scaffolds made from 50:50, 65:35 and 85:15 PLGA; 70% ethanol treatment, ultraviolet (UV) irradiation, peracetic acid treatment and antibiotic treatment with penicillin G, streptomycin sulphate and amphotericin B with the objective of effective decontamination of the scaffold with minimal or no structural damage. Ethanol and

[1] Published as:

Shearer, H., Ellis, M. J., Perera, S. P. and Chaudhuri, J. B., 2006. Sterilization of flat sheet and hollow fibre plga tissue engineering scaffolds. *Tissue Engineering,* 12 (10), 2717-27.

antibiotic treatments will not kill all possible contaminants and are therefore considered to be disinfection of the membrane while UV and peracetic acid treatment are known to result in sterilization. Changes to the surface morphology of the scaffold, which may affect the ability of cells to adhere to the scaffold, were determined by scanning electron microscopy. Gas permeation and water flux were measured to calculate the effects of sterilization method on the pore diameter and to quantify mass transfer parameters, respectively. The mechanical properties of the fibre were determined by measuring the breaking stress and strain.

4.2 Results

Flat sheet and hollow fibre scaffolds were successfully fabricated from 20% (w/w) PLGA in NMP solution. SEM revealed flat sheets had an asymmetric cross-section; a dense skin, 1-2 μm thick, was present on the top, below which a region of parallel pores ran perpendicular to the surface, the bottom of the sheet exhibited a random pore network with large macro-pores (Figure 4.1). Hollow fibre cross-sections showed skin-layers of approximately 8-10 μm on the interior and exterior of the fibre (Figure 4.1). Parallel pores extended about halfway across the fibre wall from both the interior and exterior of the fibre.

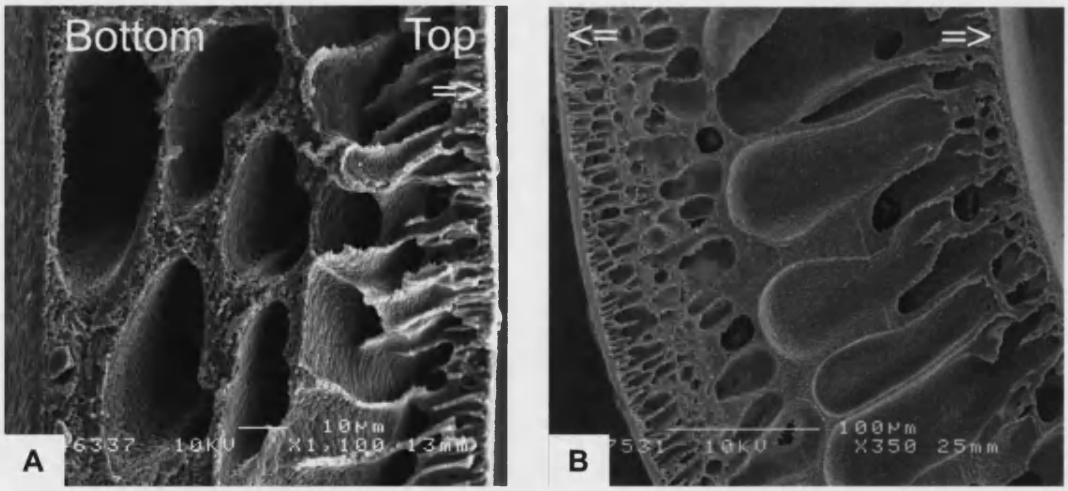

Figure 4.1 Electron micrograph cross section views of PLGA flat sheet and hollow fibre scaffolds. *There is a skin on the top of the flat sheet and both interior and exterior of the hollow fibres.* ***A:*** *Flat sheet with 1-2 μm skin on the top surface. Scale bar 10 μm.* ***B:*** *Hollow fibre with 8-10 μm skin on both surfaces. Scale bar 100μm.*

Decontamination effectiveness was determined qualitatively by the absence of signs of infection after a 48 h culture period; infection was indicated by a change of indicator colour and opacity of culture medium. Only the 50:50 polymer composition was tested for decontamination effectiveness because no difference in the ability of the treatments on different PLGA rations was anticipated. Two hollow fibre and two flat sheet samples were tested for each combination of treatment and duration. Untreated controls all showed infection and all control media (*i.e.* no scaffold) remained free of infection for the time period. All the samples tested indicated successful decontamination in equal to, or less than, the durations quoted in literature (Table 4.1, Karp *et al.* 2003; Fischbach *et al.* 2001; McFetridge 2002; Rose 2005). These results indicate the suitability of the techniques to the particular scaffolds. While the full treatment duration suggested in literature was not always found to be required, it is assumed that the low stringency of this assay could not justify a reduction in treatment duration. Treatment duration for decontamination was therefore assumed to be 30 min for ethanol, 2 h for UV and peracetic acid and 24 h for antibiotic antimycotic treatment.

Table 4.1 Comparison of treatment method and duration required for decontamination of flat sheet and hollow fibre PLGA scaffolds.

Two hollow fibre and two flat sheet samples were tested for each combination of treatment and duration. Untreated controls all showed signs of infection in the time period, all control media (no scaffold) remained without signs of infection for the time period. √ *= no visible infection after 48 h of culture in media at 37°C 5% CO_2,* × *= infection indicated in some or all samples, (media changed form pink to yellow and became opaque),* - *= treatment/ duration combination not tested,* ■ *= equal to, or longer than duration required for decontamination quoted in literature (Ellis and Chaudhuri 2005; Karp et al. 2003; Fischbach et al. 2001; Holy et al. 2001).*

Treatment	0	¼ h	½ h	1 h	2 h	5 h	6 h	15 h	24 h	31 h
Negative control (no sample)	√	-	-	-	-	-	-	-	-	-
Positive control (not sterilized)	×	-	-	-	-	-	-	-	-	-
Ethanol	×	×	√	√	√	-	-	-	√	-
UV (turned)	×	-	×	√	√	√	-	-	-	-
UV (not turned)	×	-	×	√	√	√	-	-	-	-
Peracetic acid	×	√	√	√	√	-	-	-	√	-
Antibiotics	×	-	-	-	-	-	√	√	√	√

4.2.1 Effect of treatment on scaffold structure

Changes to the structure of the scaffolds were found over the complete treatment range; in all cases increasing treatment duration lead to an increased effect on the structure. Table 4.2 gives details of the scanning electron microscopy images of all the scaffolds both before and after sterilization, along with estimates of porosity and pore size from ImageJ (Rasband 1997-2006)

Table 4.2 Summary table.

Comparison of effect of four methods of disinfection on 3 polymer compositions and two scaffold forms.

Scaffold		Control	30 min Ethanol	2 h UV	2 h Peracetic acid	24 h Antibiotics
50:50 PLGA flat sheet	*Top*	Slightly wrinkled with an even distribution of pores. Porosity ~ 10% pore diameter ~ 0.5 μm	Surface shows increased wrinkling. Porosity ~ 1% pore diameter ~ 0.4 μm	Pores slightly smaller and rounder than control. Porosity ~ 9% pore diameter ~ 0.4 μm	Large variation in pore size. Cracks in surface. Porosity ~ 8% pore diameter ~ 0.4 μm	Wrinkled surface. Decreased porosity and pore size.
	Bottom	Smooth with some irregular patches about 50 – 100 μm diameter showing increased porosity, very few pores outside these regions. Pores much larger than top surface.	Very patchy with all pores within porous regions ~ 50 – 100 μm in diameter. Pores are larger than upper surface.	Porous patches with reduced number of larger pores.	Lots of porous regions with large pores.	More porous regions with larger pores than control.
65:35 PLGA flat sheet	*Top*	Smooth with well defined pores. Porosity 7% pore diameter 0.4 μm	Wrinkled with very few pores. Porosity ~ 0% pore diameter 0.4 μm	Increased porosity. Porosity ~12% pore diameter ~ 0.5μm	Wrinkled with cracks along troughs. Pore diameter ~ 0.4 μm.	Smooth with large pores. Porosity ~ 17% pore diameter ~ 0.6 μm
	Bottom	Regions showing increased porosity and cracking are elongated, ~25 μm wide and 100-150 μm long. Surface wrinkling present.	Circular patches < 50 μm diameter showing increased porosity.	Circular patches ~ 25μm of increased porosity.	Surface is wrinkled with porous regions.	Smooth with even distribution of pores.

85:15 PLGA flat sheet	*Top*	Smooth with even distribution of pores. Porosity ~ 11% pore diameter ~ 0.4 μm	Very few pores, surface wrinkling. Porosity ~ 4% pore diameter ~ 0.4 μm	Slightly wrinkled with evenly distributed pores. Porosity ~ 11% pore diameter ~ 0.4 μm	Wrinkled surface, large range of pore sizes with some cracks. Pore diameter ~ 0.2 μm	Large pores showing regions of increased porosity. Porosity 13% pore diameter 0.7 μm
	Bottom	Larger pores with some irregular regions showing increased porosity.	Patches of increased porosity.	Large range of pore sizes, patches with larger pores, small pores all over surface.	Regions of increased porosity.	Large pores and cracks visible in surface.
50:50 Hollow fibre	*Inside*	Large variation in pore size.	Highly porous.	Pores aligned along length of fibre.	Large cracks.	Very porous and uneven surface.
	Outside	Even distribution of pores, groves aligned with fibre.	Few pores	Fewer pores than inside; aligned along length of fibre.	Small pores and surface wrinkling along length of fibre.	Small pores and irregular surface wrinkling.

SEM images of the untreated 50:50 flat sheet and hollow fibres samples (Figure 4.2) showed homogeneity across the surfaces, both surfaces of the flat sheets showed similar distribution of pores, the top surface exhibited a higher degree of surface roughness. Pores appeared larger on the hollow fibres than the flat surfaces and the exterior of the fibre appeared rougher than the interior, with wrinkles and lines of pores following the length of the fibre.

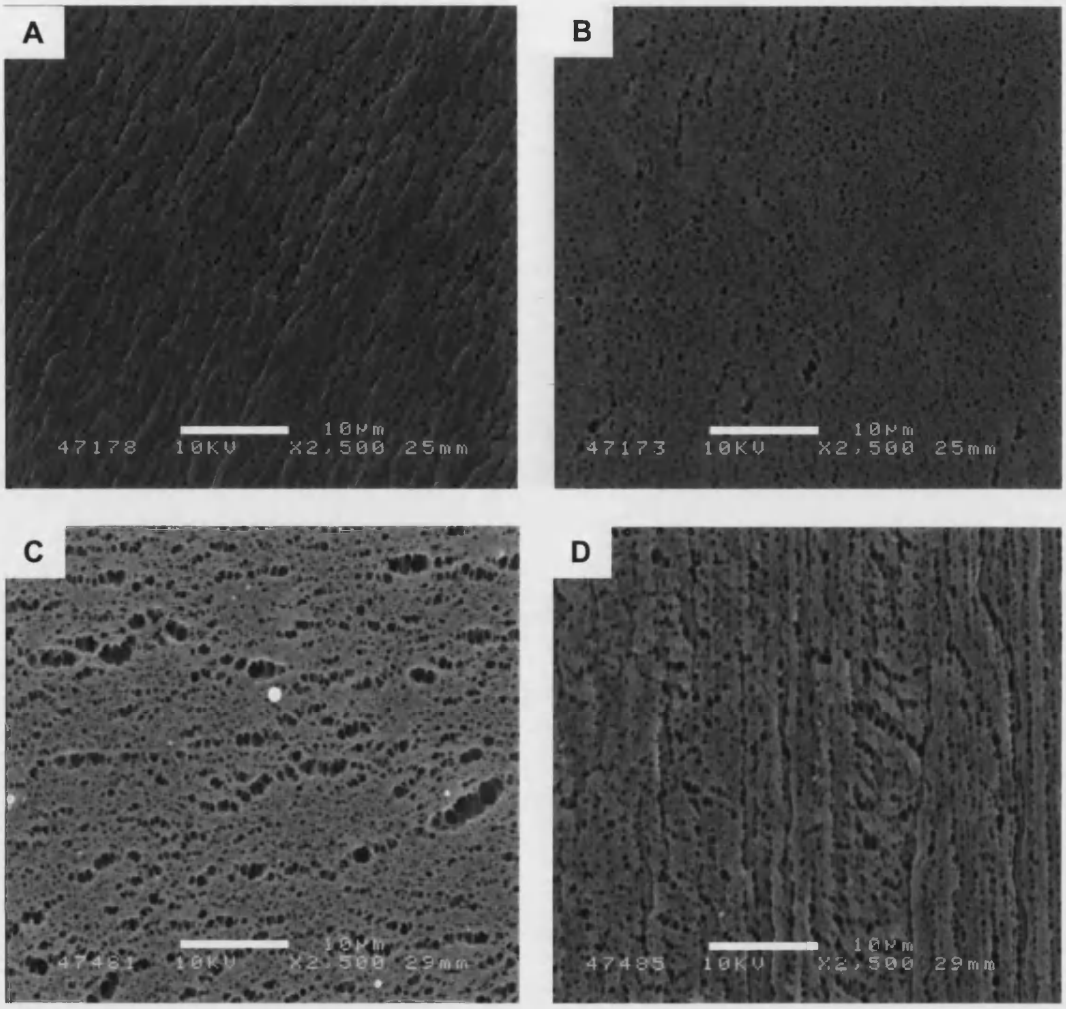

Figure 4.2 Electron micrographs of surfaces of untreated PLGA flat sheet and hollow fibre.
A: *Top of flat sheet (as formed).* ***B:*** *Bottom of flat sheet (as formed).* ***C:*** *Interior of hollow fibre.*
D: *Exterior of hollow fibre. Scale bar: 10 μm.*

Increases in pore numbers and sizes were apparent on the top and bottom of the flat sheets following treatment with ethanol. Damage to the top of the flat sheets appeared uniformly across the surface, whereas damage to the bottom surface appeared as patches of localized increased porosity (Figure 4.3). Hollow fibres exhibited larger pores on the interior of the fibre (Figure 4.5) while the exterior of the fibre showed very few pores after treatment. After less than 10 min in ethanol 120 mm hollow fibres deformed and fused together (Figure 4.4). The membranes treated with ethanol for longer periods were more fragile under the SEM; magnifications above ×2500 resulted in damage to the sample within seconds.

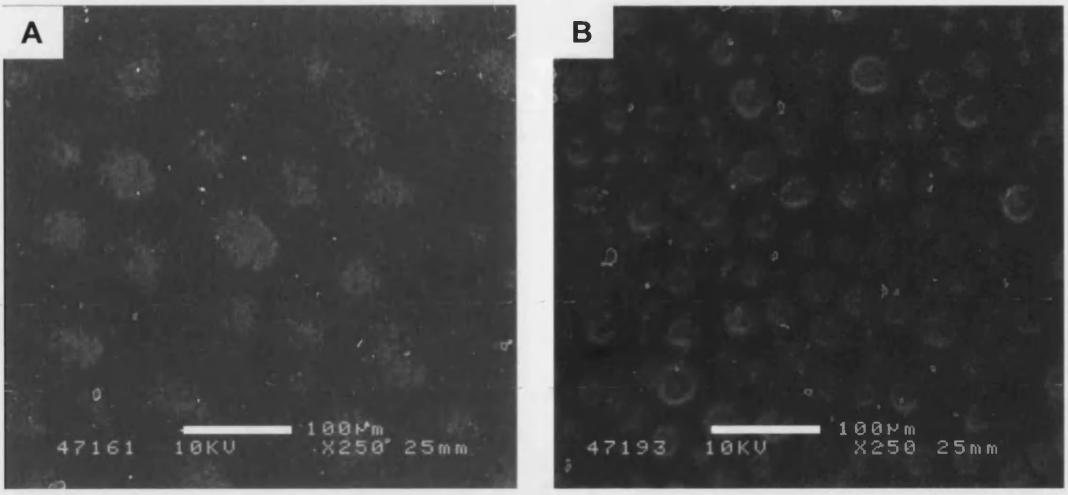

Figure 4.3 Electron micrograph of ethanol treated flat sheets.

Bottom surface (as formed and treated) of PLGA flat sheet following treatment with 70% v/v ethanol. ***A:*** *Treated for 30 min.* ***B:*** *Treated for 2 h. Scale bar 100 µm.*

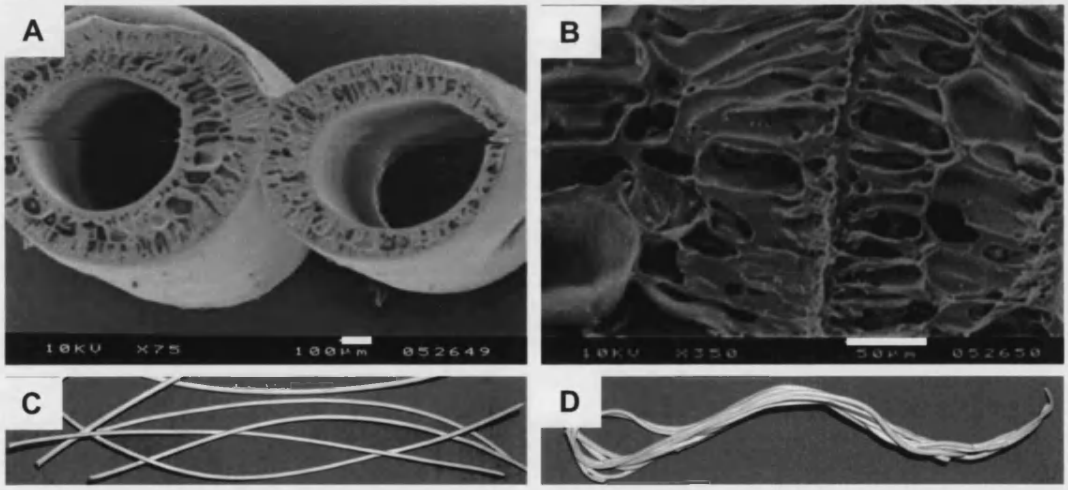

Figure 4.4 Electron micrographs and photographs of ethanol treated fibres.

Top: *SEM of fibres fused together.* ***A:*** *75x Scale bar: 100 µm.* ***B:*** *350x Scale bar: 50 µm.* ***C:*** *120 mm long fibres prior to ethanol treatment.* ***D:*** *120 mm long fibres fused together after ethanol treatment for 30 min.*

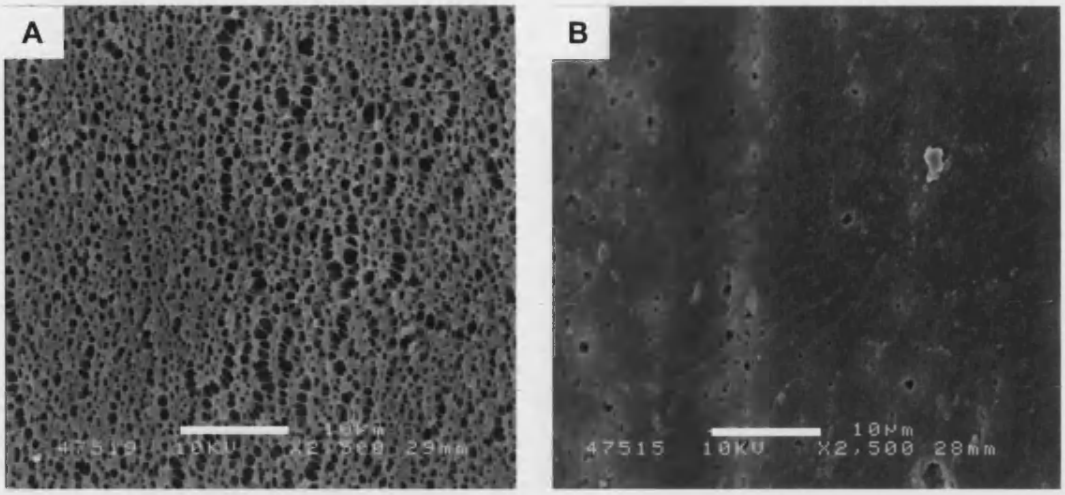

Figure 4.5 Electron micrographs of surfaces of ethanol treated fibres.

Surfaces of PLGA hollow fibre following treatment with 70% (v/v) ethanol for 30 min. ***A:*** *Interior.* ***B:*** *Exterior. Scale bar: 10 μm.*

UV treated scaffolds showed little change in porosity. The exterior of the fibres showed smoothing of the surface and smaller pores (Figure 4.6). The interior of hollow fibres were not directly exposed to UV light and consequently showed very little change in appearance.

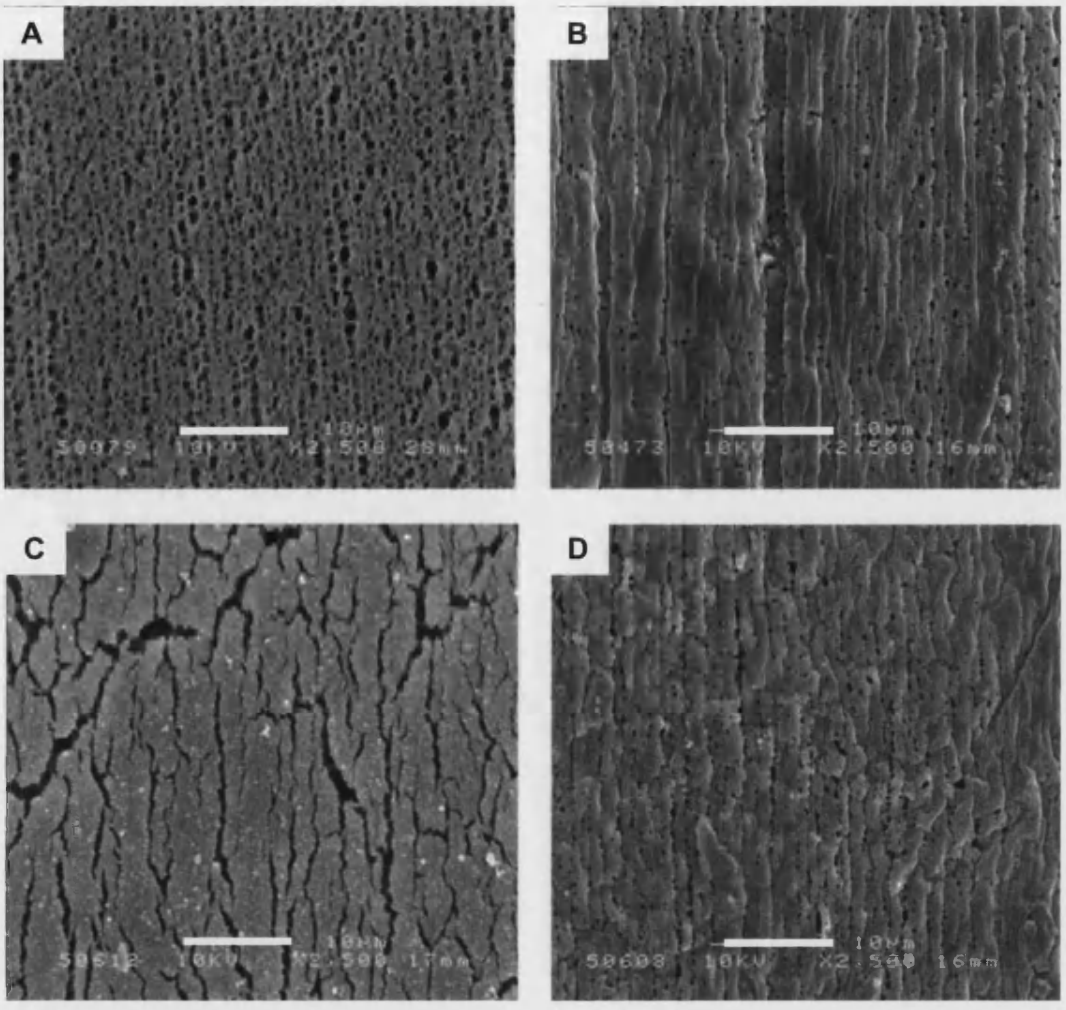

Figure 4.6. Electron micrographs of surfaces of treated PLGA hollow fibres.
Top: *UV light for 2 h.* ***A:*** *Interior.* ***B:*** *Exterior.* ***Bottom:*** *Peracetic acid solution for 2 h* ***C:*** *Interior.* ***D:*** *Exterior Scale bar: 10 μm.*

Peracetic acid had a large impact on the surface of the scaffolds. Cracks were visible and salt crystals were present, which may have been a result of interactions between the acid and PBS used to rinse the scaffolds. PBS was used to rinse other samples with no adverse effects (Figure 4.6).

A high degree of damage was associated with antibiotic treatment. Increased surface wrinkling was present on all surfaces with a high density of small pores on the top of the flat sheets. The bottom of the flat sheets showed much fewer, larger pores (Figure 4.7). At lower magnification (Figure 4.8) a fractal-like pattern could be seen on the top of the flat sheets. The pattern was depicted by regions covered by a smooth skin layer

in contrast to the more porous surface underneath. The skin layer appeared to have completely dissolved on the interior of the hollow fibres. The outer surface of the fibres showed increased wrinkling with fewer pores (Figure 4.7).

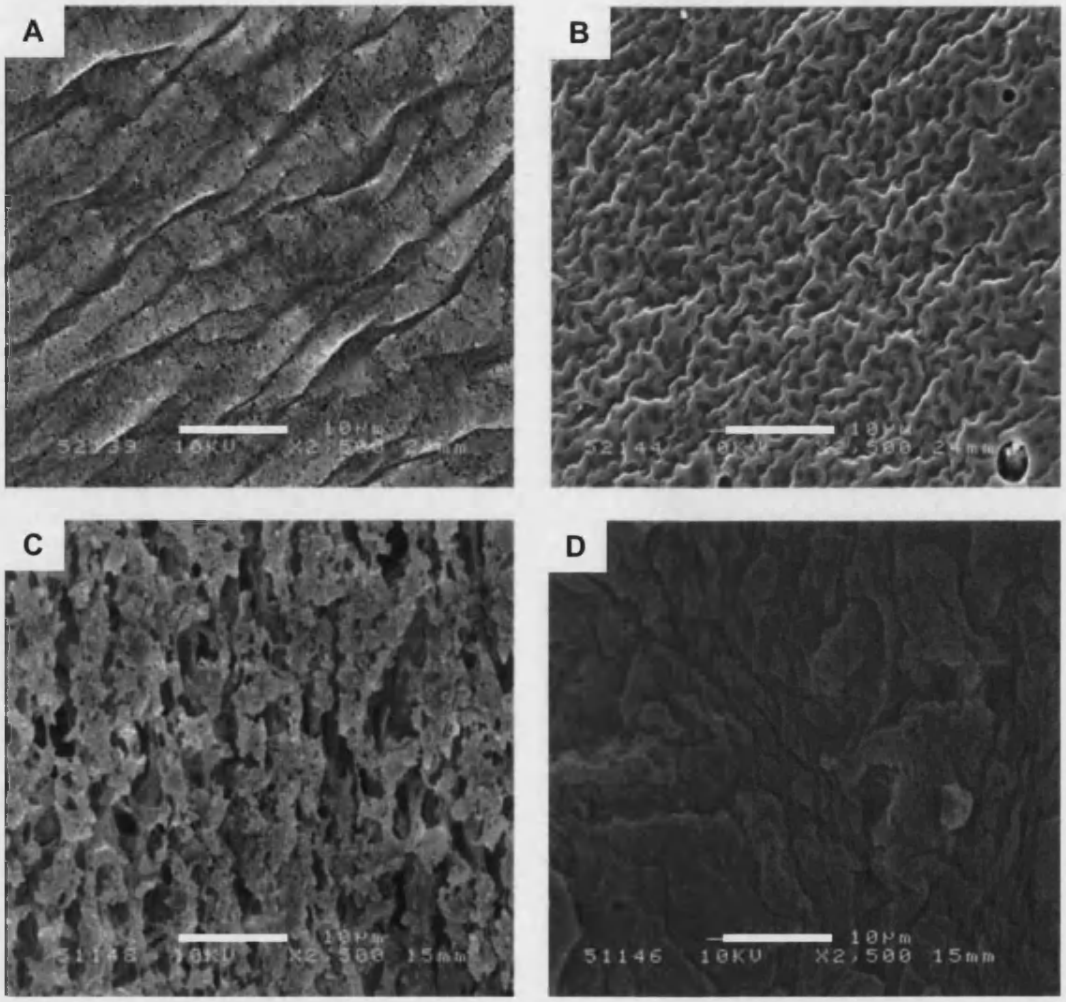

Figure 4.7. Electron micrographs of antibiotic treated PLGA flat sheet and hollow fibre.
Surfaces of flat sheets and fibres following treatment with antibiotic/antimycotic solution for 24 h. ***A:*** *Top of flat sheet (as formed and treated).* ***B:*** *Bottom (as formed and treated).* ***C:*** *Interior of hollow fibre.* ***D:*** *Exterior of hollow fibre. Scale bar: 10 μm.*

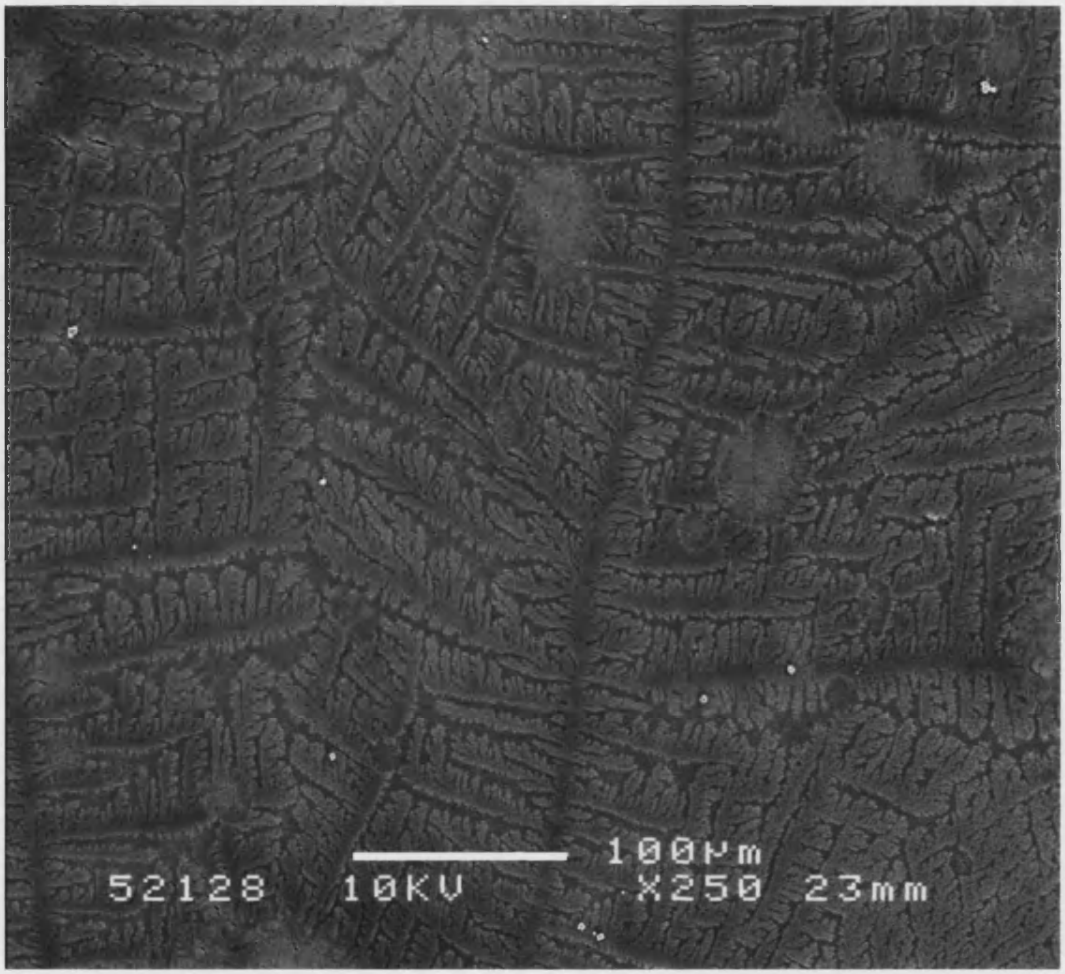

Figure 4.8. Electron micrograph of surface of PLGA flat sheet treated with antibiotic/antimycotic solution.

Top surface (as formed and treated) of PLGA flat sheet following treatment with antibiotic/antimycotic solution for 24 h. Scale bar: 100 μm.

Some change in polymer structure was observed for control samples treated with water or PBS, but this was much less than the sterilized samples. The sample treated with PBS for 24 h showed indications of a similar pattern to that found on the antibiotic samples.

SEM images revealed that all three polymer compositions responded to the treatments in a similar manner. Further tests on gas permeation, water flux and mechanical testing were therefore only carried out on the 50:50 polymer ratio.

4.2.2 Characterization of treated scaffolds by gas permeation, water flux, and mechanical stress measurements

All treatments resulted in an increased external skin pore diameter as shown by gas permeation. The largest difference was for the peracetic acid sample with a pore diameter more than double the control sample; all other samples were within 25% of the control (Figure 4.9) however no statistically significant difference was revealed.

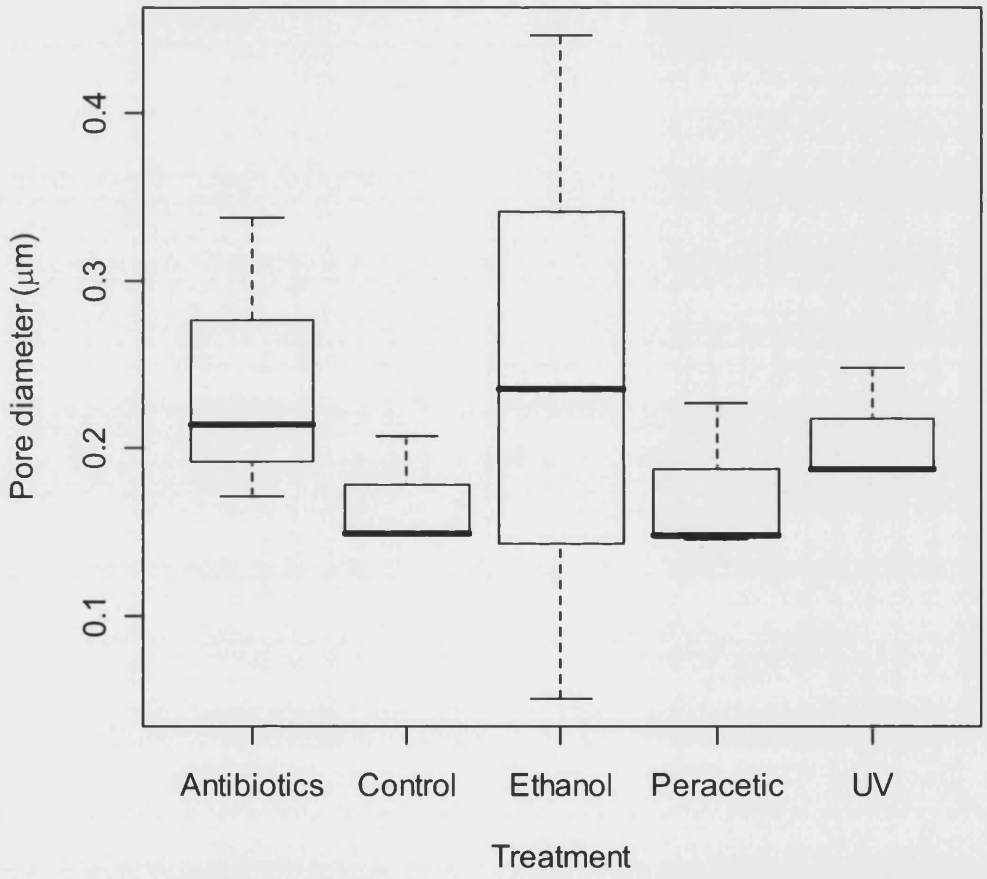

Figure 4.9 Box and whisker plot of average pore diameter of hollow fibres (μm) following sterilization treatment.

Boxes show inter-quartile range, bold lines show median and whiskers show minima and maxima n = 3. The ethanol and antibiotic treated samples show a much greater variation in pore size than the control. No statistically significant difference was found between samples.

The ethanol treatment exhibited a large variance; this is thought to be due to the extent of the damage caused by ethanol treatment and irregularities in the fibre resulting from

the spinning process as is illustrated in Figure 4.10. Material removed from the outer wall of an asymmetric fibre may or may not reveal the finger-like pore region of the fibre; leading to large variation in surface pore size.

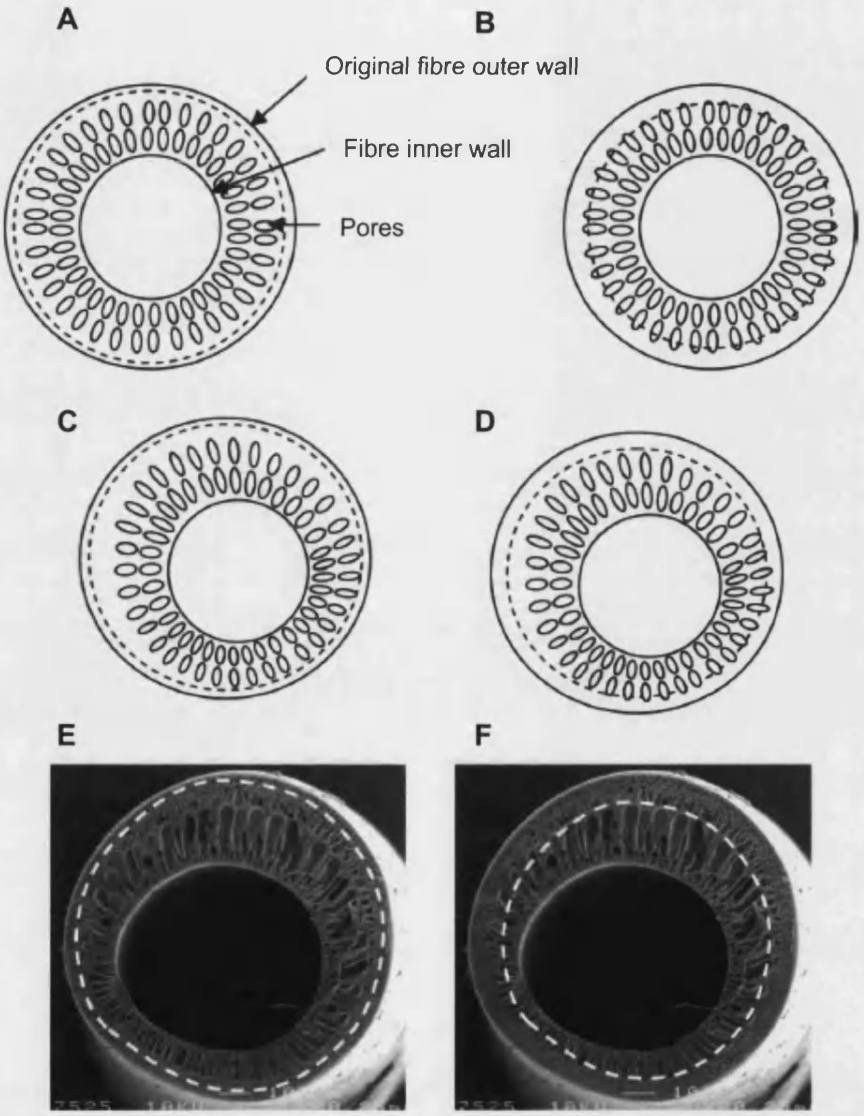

Figure 4.10 Influence of scaffold structure on treatment effects.

*Dotted lines show outer circumference of fibre following treatment. (**A**) Treatment does not completely remove skin layer; therefore surface porosity changes little. (**B**) A small increase in extent of damage by treatment results in complete removal of skin layer and large increase in surface porosity. (**C** and **E**) even with irregular fibres; a small degree of damage by treatment will not penetrate the skin region of the fibre. (**D** and **F**) If the fibre is asymmetric as the extent of damage increases, some areas of the porous interior of the fibre will be exposed and some will not, leading to a greater degree of variation in the properties exhibited by the fibre.*

All treated samples also exhibited significantly higher water fluxes than the control (Figure 4.11). The largest water flux, found for the ethanol sample, was nearly two orders of magnitude higher than the control. Due to the deformation of fibres when treated with ethanol the fibres were treated in the bioreactor. The whole bioreactor was submerged in the sterilising solution for 30 min, and then rinsed thoroughly with deionized water.

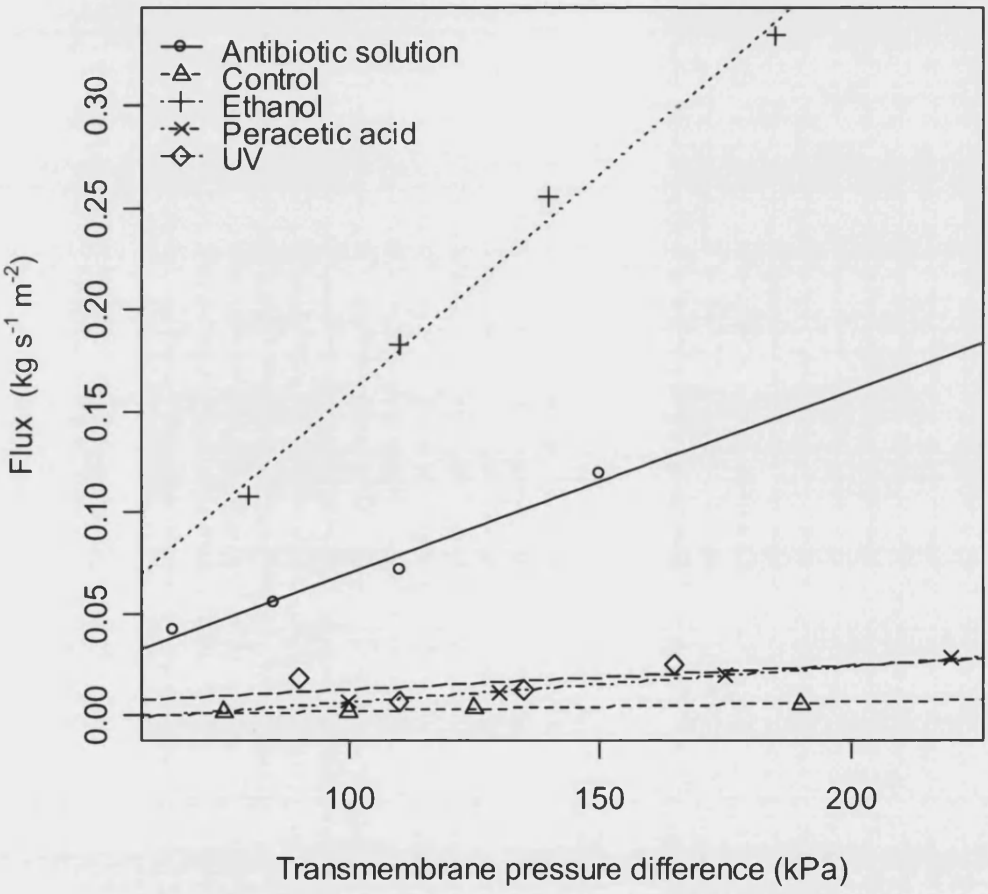

Figure 4.11 Average water flux through fibre against trans-membrane pressure.
▲ = *Ethanol*, □ = *Peracetic acid*, ○ = *Control*, Δ = *Antibiotics*, ■ = *UV. Each sample showed a significantly different linear correlation between flux and transmembrane pressure difference.*

Mechanical testing revealed no significant statistical differences via Tukey's honest significant difference test. However the wet samples exhibited a higher breaking stress than the equivalent dry sample in all samples other than the ethanol treated sample

(Figure 4.12). Young's modulus also exhibited no significant differences but again the wet value generally exceeded the dry value (Figure 4.13).

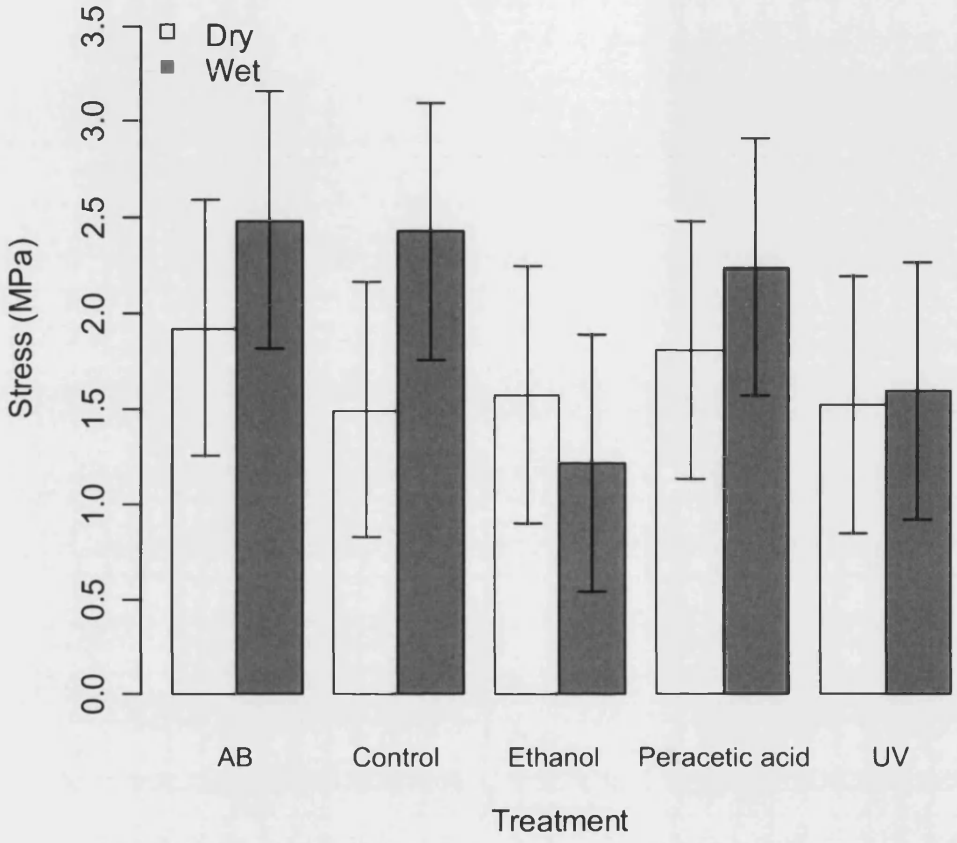

Figure 4.12 Average hollow fibre breaking stress (MPa).

500 g full scale load, cross head speed 20 mm min^{-1} (n = 3, mean ± lsd). No significant differences are found by Tukey's Honest Significant Difference test.

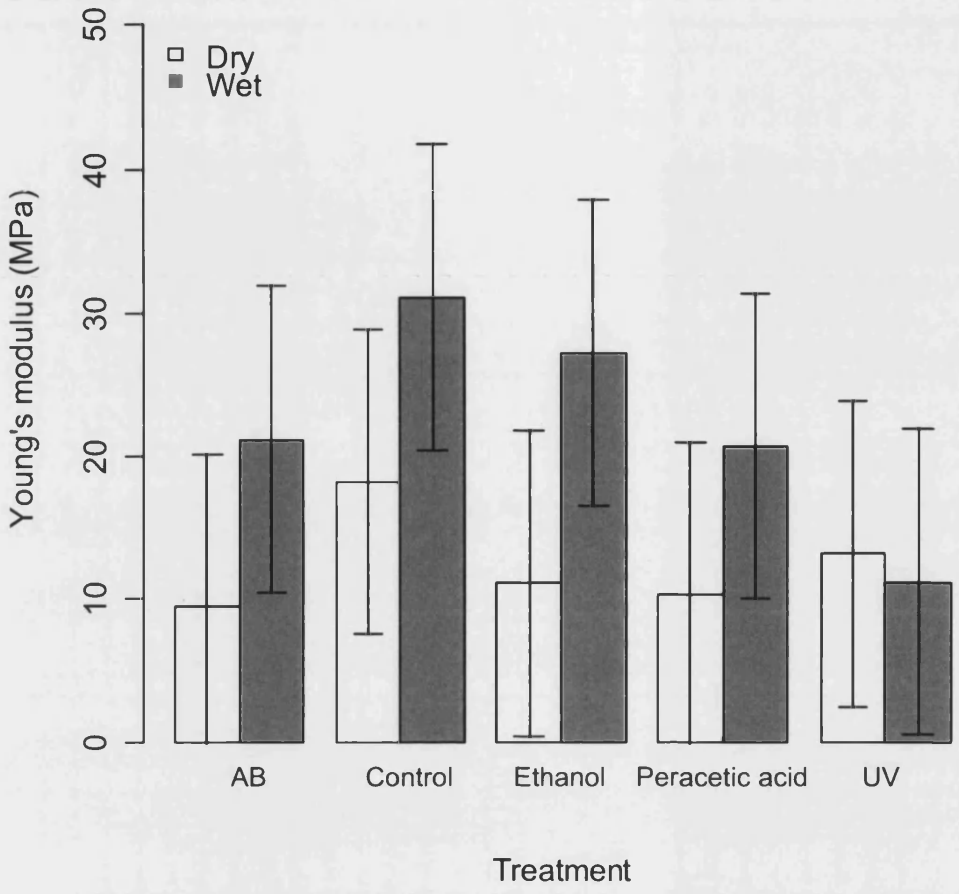

Figure 4.13 Average hollow fibre Young's Modulus (MPa).
500 g full scale load, cross-head speed 20 mm min^{-1} (n = 3, mean ± lsd). No significant differences are found by Tukey's Honest Significant Difference test.

4.3 Discussion

Disinfection treatments were investigated in order to find an effective method to decontaminate PLGA structures for use as *in vitro* scaffolds for tissue engineering without damaging the scaffold. All treatments reduced the chances of the sample becoming infected under culture conditions; however structural damage could not be avoided. While the assay employed to determine decontamination can not be considered conclusive with the possibility of incomplete sterilization not being indicated over the 48 h culture period the results are be supported by other studies (Fischbach *et al.* 2001; Holy *et al.* 2001; Huang *et al.* 2004).

Ethanol at concentrations of 60-80% (v/v) is classified as a disinfectant, rather that a sterilization agent, due to its inability to destroy hydrophilic viruses or bacterial spores (Holy *et al.* 2001), however ease of use and apparent effectiveness makes ethanol a favourable, and widely used, tool for *in vitro* studies.

This study found that UV sterilization was achieved within 1-2 h. This is supported in the literature that treatment for 2 h results in complete sterilization of the sample. A concern with the use of UV sterilization is its ability to sterilize larger three-dimensional scaffolds throughout, for example the porous hollow fibres. However, it was found there was no need to turn either scaffold form in order to achieve sterilization; suggesting UV radiation, with sufficient intensity for sterilization, is able to pass through thin polymer membranes. Use of this method for larger, thicker scaffolds would need to be assessed separately.

Peracetic acid has approval for use by the US Food and Drug Administration (FDA) for sterilizing tissues such as skin or bone (Huang *et al.* 2004). The results suggest that treatment of just 15 min was sufficient to sterilize, however protocols in literature use a duration of 2-3 h (McFetridge 2002; Huang *et al.* 2004).

No mention is found in published literature on pre-treatment with antibiotics for sterilization. Antibiotic treatments were therefore performed over a wide range of treatment durations. The results indicate decontamination was achieved after the shortest test duration of 6 h. However due to the low stringency of the assay recommendations of 24 h treatment were adhered to (Rose 2005).

While all polymer surfaces showed structural variation, resulting from production and handling, trends of increasing damage with increasing sterilization duration give a clear indication to the specific treatment causing the damage. Scaffold surfaces were categorized into three groups based on their surface structure: flat sheet upper surface with a thin skin-layer (1-2 μm) above a section of parallel pores perpendicular to the surface; flat sheet lower surface with macro pores, and surfaces of the hollow fibres with thicker skin layers (8-10 μm) and parallel pores perpendicular to the surface. Rapid exchange of solvent with water at the edges of the scaffold during fabrication

leads to fast contraction of the polymer chains forming dense skins (Chung and Hu 1997b). SEM consistently revealed greater damage by sterilization to the bottom of the flat sheets suggesting the skin acts to protect the scaffold from the harmful effects of sterilization. Patches of increased porosity on the bottom of ethanol and peracetic acid treated flat sheets would be consistent with removal of a thin layer of scaffold revealing large macro voids. Similar removal of polymer on the other membrane surfaces wouldn't break through the skin, resulting in little change to the appearance of the scaffold.

Damage caused by ethanol treatment was unexpected, reports of similar processes in literature make no comment of structural damage (Karp *et al.* 2003) and ethanol has been reported elsewhere to result in no morphological or chemical damage to polyester scaffolds (Holy *et al.* 2001). The form of the hollow fibre scaffolds is thought to have highlighted this problem which may not have been apparent for other scaffold structures. The only indication of ethanol damage on flat sheets was patches of increased local porosity. The membrane support maintained the shape of the flat sheet scaffolds during treatment, whereas the hollow fibres were unsupported revealing the deformation caused. The cross-discipline application of membrane characterization techniques to tissue engineering scaffolds revealed the massive increase in water flux. This reduction in mass transport resistance suggests an opening of internal channels and together with the morphological changes, this suggests partial dissolution of polymer in ethanol; subsequent deposition of polymer, driven by high polymer concentrations at the solid-liquid interface, may have caused fusion of fibres treated together.

UV treatment had the least impact on the scaffold appearance, all the samples except the 85:15 flat sheet showed a slight decrease in surface roughness and Young's modulus. A similar investigation into the effects of UV sterilization on poly(D,L-lactic acid)-poly(ethylene glycol)-monomethyl ether (Me.PEG-PLA) (Fischbach *et al.* 2001) also found a decrease in surface roughness and polymer molecular weight, however this was reported to be a result of removal of PEG from the scaffold surface. While this cannot be the reason for the increased smoothness of PLGA, energy provided by UV light may provide activation energy for similar photo-oxidative reactions and cleavage of ester bonds.

Treatment with antibiotics resulted in the formation of a pattern on the polymer surface, which was also indicated on PBS control samples. This may primarily result from interactions with the salt solution (PBS is used to dilute the antibiotic antimycotic solution); however some other component of the antibiotic solution must serve to magnify this effect, possibly the citric acid buffer.

Changes caused to the scaffold are not necessarily detrimental; increased pore diameter and water flux increase nutrient transfer across the membrane. Pore diameters for the treated samples were found to be in the range 0.45 to 0.80 μm with 0.37 μm for the control, which relate to a molecular weight cut off (MWCO) of approximately 4500 – 8000 kDa for the treated samples and 3700 kDa for the control (Planchamp *et al.* 2003) which is above the MWCO of other hollow fibre bioreactors (Kumar *et al.* 2004), indicating pores are large enough for the transport of nutrients across the membrane, yet small enough to prevent the ingress of cells into pore entrances (Beresford 2002). Increased water flux exhibited by the ethanol and antibiotic samples of up to 3.34 and 1.19 kg m^{-2} s^{-1} respectively over the control value of 0.01 kg m^{-2} s^{-1} may also improve delivery of nutrients to cells.

4.4 Conclusions

This sterilization study has shown the significance of the effects of sterilization on PLGA scaffolds. All sterilization techniques successfully reduced the chance of the sample becoming infected. Pore size and water flux were found to increase following all the sterilization treatments and visible changes to the surfaces were detected via SEM in all cases.

This study has shown that one of the most common sterilization techniques (soaking in 70% ethanol) causes substantial damage to PLGA scaffolds. While the changes caused by UV light are unlikely to have any detrimental effects on the performance of the scaffolds with respect to tissue engineering the ability of UV light to sterilize larger, 3D scaffolds remains unclear. In addition, the UV sterilization process requires the scaffolds to be treated in sterile environment before being placed in the bioreactor. A liquid sterilization process eliminates the need to handle the fibres between sterilization and use. Peracetic acid treatment resulted in less structural damage to the scaffold, but

the increased irregularity to the surface caused by the presence of cracks may prove detrimental to cell adhesion. Antibiotic treatment shows increased pore size, water flux and surface roughness over the control.

The objective of this study was to determine the most suitable sterilization technique for PLGA hollow fibre scaffolds. While the results show that none of the sterilization methods are ideal in terms of sterilizing the sample without causing structural changes, it is thought the antibiotic treatment will provide a convenient, effective sterilization method with which to sterilize PLGA hollow fibres for use as a tissue-engineering scaffold.

CHAPTER FIVE - SURFACE TREATMENT OF FLAT SHEETS

Modification of flat sheet membranes to improve wetting, cell adhesion and hydraulic permeation

5.1 Introduction

The purpose of the membrane in tissue engineering is to provide a structural support, through which cells may be provided with nutrients. The asymmetry of membranes formed through immersion-precipitation phase-inversion (more details of which can be found in Chapter Eight) has two influences on the mass transfer through the membrane: the large finger-like pore structure provides channels for convective transport with low resistance to mass transfer (Figure 5.1); the dense skin layer provides resistance to mass transfer. Removal of the skin layer has the potential to increase mass transport through the membrane.

While the preparation of hollow fibre membranes requires relatively large quantities of expensive polymer and a lengthy set-up process, flat sheets can be made efficiently on a much smaller scale. Flat sheet membranes exhibit one surface (in direct contact with water during fabrication) very similar to the surface of the hollow fibres, while the other surface (the one in contact with the glass during fabrication) has no skin layer and a more heterogeneous surface pore distribution (Figure 5.1). This chapter exploits the similarity of the top surface of flat sheet membranes to hollow fibres, to investigate surface treatment of flat sheet membranes as a model for hollow fibres; utilizing the lower temporal costs, better economy and higher consistency in membrane structure afforded by the flat sheet membranes. The difference in the two membrane surfaces

offered by the flat sheets also allows the effects of the dense skin on the surface treatment process to be analysed.

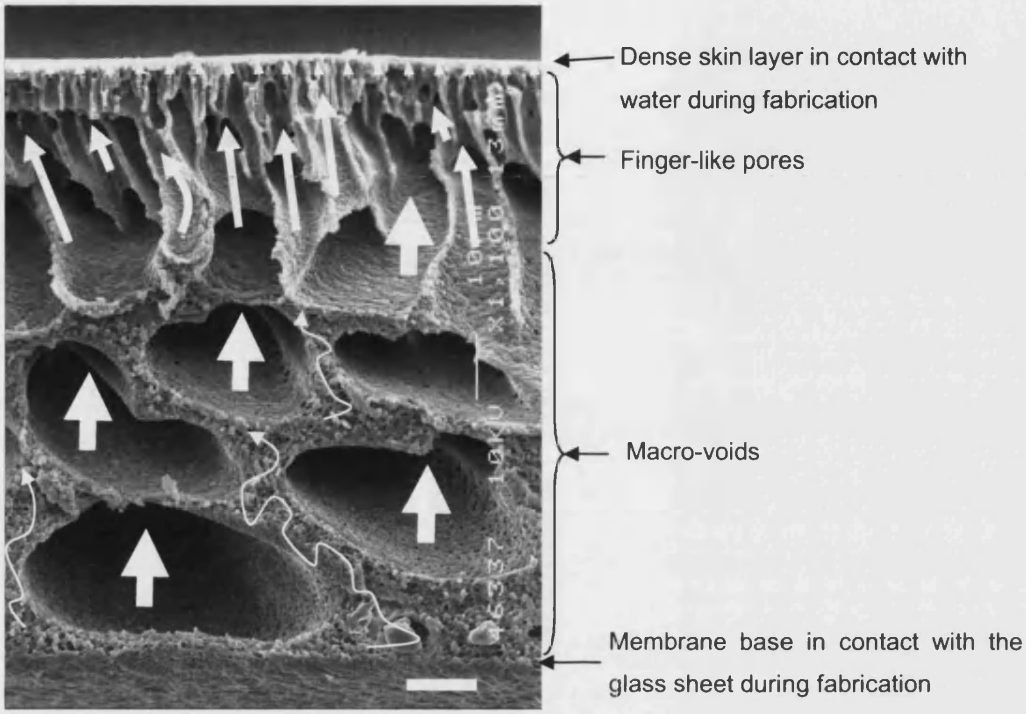

Figure 5.1 Schematic representation of an asymmetric flat sheet membrane and effect of pores on mass transfer.

The top of this membrane is the surface that is exposed to the water directly on fabrication – leading to a surface very similar to that found in hollow fibres. The bottom shows a surface with no skin layer and a heterogeneous surface pore distribution. Scale bar 10 μm.

PLGA degrades in an aqueous environment by hydrolysis of the ester bond. If the hydrolysis reaction is faster than the diffusion of water molecules into the membrane the water molecules will be used up by hydrolysis at the surface of the scaffold, however, if the hydrolysis reaction is slower than diffusion water will diffuse into the scaffold and bulk degradation will take place. Burkersroda *et al.* (Burkersroda *et al.* 2002) define a critical dimension, $L_{critical,}$ which may be used to predict the mechanism of degradation; matrices with dimensions smaller than $L_{critical}$ undergo bulk degradation while matrices with dimensions larger than $L_{critical}$ undergo surface erosion. Burkersroda *et al.* report a general figure for $L_{critical}$ for poly(α-hydroxy-esters), such as PLGA, in water as 7.4 cm. They do not define the PLGA internal structure used in their study. As the diffusion of

water into the matrix will depend on the structure, the significance of this figure is reduced. However, as membranes for tissue engineering are likely to be, in at least one dimension, substantially less than 7.4 cm it is likely that bulk erosion taking place. Changing the mechanism of degradation requires the ratio of rate of hydrolysis to rate of diffusion into the scaffold to be augmented.

Khang *et al.* (2002) carried out a study of physicochemically treated evaporation-cast flat sheets of PLGA. In this study they investigated the effects of surface treatment with chloric acid, sulphuric acid and sodium hydroxide on the flat sheets in terms of hydrophilicity and cell attachment. The reported results indicate that all the treatments increased hydrophilicity and improved cell attachment in terms of both cell number and morphology; however no details were given of either the initial or the modified membrane structure.

Another study was carried out at a similar time (Kay *et al.* 2002) investigating the effects of sodium hydroxide on evaporation cast PLGA film (1 x 1 x 0.5 cm). In this study three membrane classifications are identified: untreated "conventional" PLGA, "sub-micron" PLGA treated with 1 mol dm^{-3} sodium hydroxide for 30 min, and "nano-phase" PLGA treated with 10 mol dm^{-3} sodium hydroxide for 1 h. Reportedly the surface features of the membranes have fibre diameters of 10 μm, 500 nm and 50 nm, and lengths of 1000 μm, 100 μm, and 10 μm respectively. The results indicated an increase in cell adhesion with decrease in surface fibre dimensions, however this is not found to be significantly different. Possible explanations for this increase in cell adhesion are given as increased surface area; which may directly allow a larger area for cell attachment, or indirectly increase protein adhesion to the surface. Alternatively the sodium hydroxide treatment results in increased numbers of exposed –OH and –COOH groups for the cells to adhere to.

Of key importance to the hollow fibre bioreactor is the porous membrane structure, therefore not only will surface treatment increase surface area through pitting of the surface, it will also unveil the porous interior, leading to a much more significant increase in surface area.

While the result of the reaction and the type of reaction are the same for both acidic and alkaline degradation the mechanism is different depending on whether the degradation environment is acidic or alkaline.

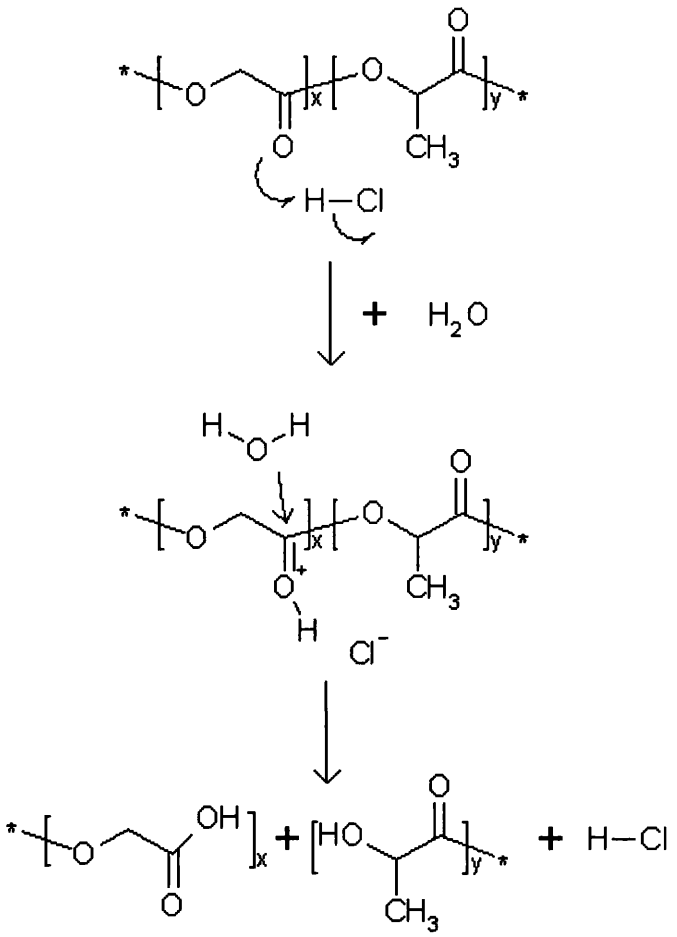

Figure 5.2 Schematic of hydrolytic degradation of PLGA in an acidic environment.
First the acid protonates the carbonyl group which activates it towards nucleophilic attack by the water molecule. The molecule is then cleaved releasing the proton.

Figure 5.2 shows the reaction scheme of the hydrolytic degradation of PLGA in an acidic environment; first the acid protonates the carbonyl group which activates it towards a nucleophilic attack from water, the molecule is cleaved releasing the proton.

In an alkaline environment (Figure 5.3) the molecule is first cleaved to form a salt which is then acidified in the presence of water.

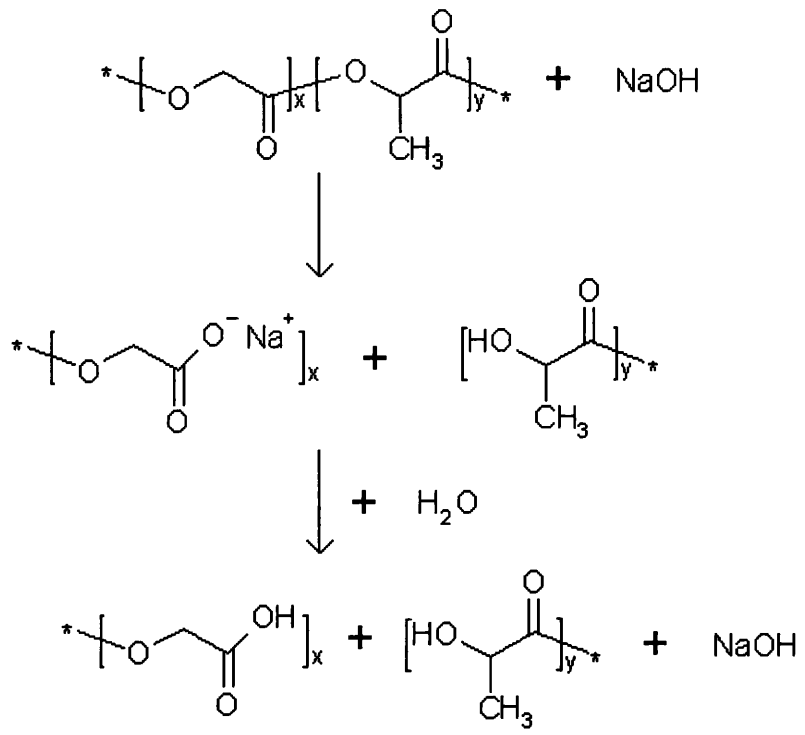

Figure 5.3 Schematic of hydrolytic degradation of PLGA in an alkaline environment.
The polymer is cleaved to form a salt which is then acidified in the presence of water.

Figure 5.3 illustrates the reaction of PLGA in an alkaline environment; here it can be seen one that OH^- ion is required to break one ester bond in PLGA.

In this study two acid and two alkali solutions are used to catalyse the hydrolytic degradation of the polymer ester bond in order to tip the ratio of rate of absorption of water to rate of hydrolysis in the favour of surface erosion and away from bulk degradation. This will allow the removal of the skin layer of the membrane without unduly affecting its mechanical properties and degradation rate of the interior scaffold. If this step is carried out *in situ* in the bioreactor this has the added advantage that the porous internal structure of the membrane is protected from damage during handling by the membrane skin, it is also likely that an *in situ* stringent treatment with acid or alkali will also aid the sterilization of the membrane.

5.1.1 Assessing surface treatment

This chapter reports an investigation into both concentration and treatment duration for the catalysis of surface erosion by hydrolysis using acid and alkali solutions.

Hydrochloric and perchloric acid and sodium and potassium hydroxides were used to treat flat sheet membranes as a model for the surface treatment of hollow fibres. The effects are reported in terms of scaffold structure (pore size and porosity), hydrophilicity (water contact angle and water adsorption), bioaffinity (cell adhesion), membrane hydraulic permeability, and polymer molecular weight (determined from intrinsic viscosity). Details of the materials and methods used can be found in Chapter Three.

5.2 Results

5.2.1 Acid and alkali treatments of flat sheets

5.2.1.1 Surface morphology

SEM images for all treatments show a change in scaffold surface morphology compared to the control (Figure 5.4 to Figure 5.8); this is more pronounced following longer treatment. The control membranes show patchy regions of pores on the bottom of the membranes with a much more homogeneous pore spatial distribution on the top of the membranes. The pores on the bottom of the membrane are found to be slightly larger than those on the top and are grouped into pore regions of approximately 10 μm diameter roughly circular regions. The pores on the top of the membrane are smaller and evenly distributed over the surface of the membrane.

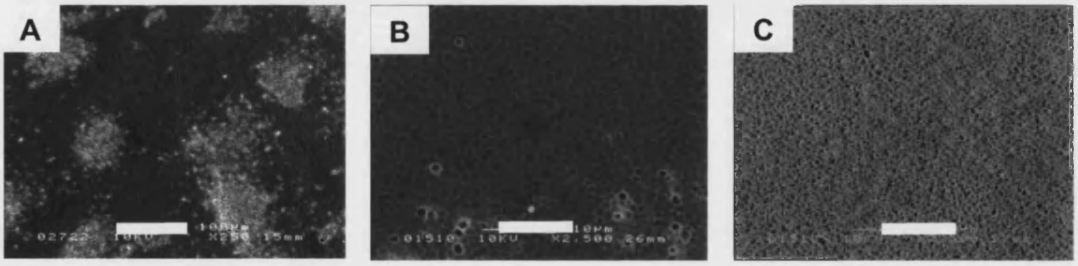

Figure 5.4 Electron micrographs of the surfaces of control, untreated, flat sheet membranes.
Exterior surfaces of flat sheet membranes formed by immersion-precipitation phase-inversion. ***A:*** *shows bottom surface with a scale bar of 100 μm,* ***B:*** *shows bottom surface with a scale bar of 10 μm and* ***C:*** *shows top surface with a scale bar of 10 μm*

The membranes treated with alkaline solutions (Figure 5.7 and Figure 5.8) consistently show a greater level of degradation than the equivalent time and concentration of treatment with acid, however there appears to be no difference in the nature of the degradation. All membranes show an increase in surface porosity with increased

treatment duration until the point where the entire skin layer has been removed to reveal the underlying structure.

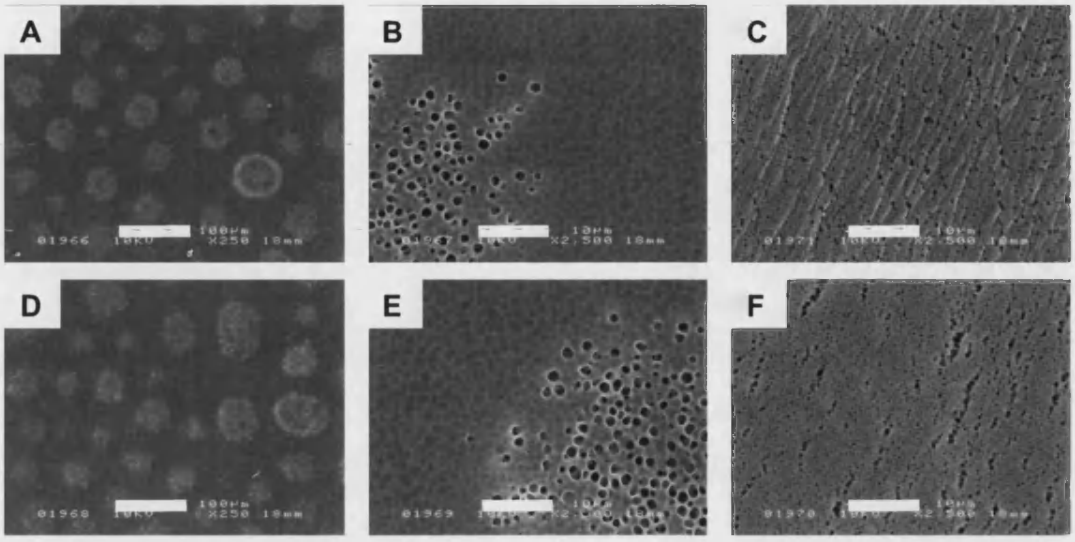

Figure 5.5 Electron micrographs of flat sheet membranes treated with 0.1 mol dm^{-3} HCl for 15 min (A - C) and 30 min (D - F).

A and C *show the bottom of the membranes at a low magnification showing patchy pore regions, scale bar 100 μm.* ***B and E*** *show the bottom of the membranes at a higher magnification showing detail of pores, scale bar 10 μm.* ***C and F*** *show the top surface of membranes showing more spatial homogeneity to the pore distribution and pore size increasing with treatment duration, scale bar 10 μm. This treatment has resulted in a small change compared to the control membranes.*

With treatment the patches of pores on the bottom of the membranes become increasingly prominent. In the case of alkaline treatment large voids are revealed; this is consistent with removal of the surface of the membrane revealing the large macro-voids found in the bottom layer of the asymmetric membrane.

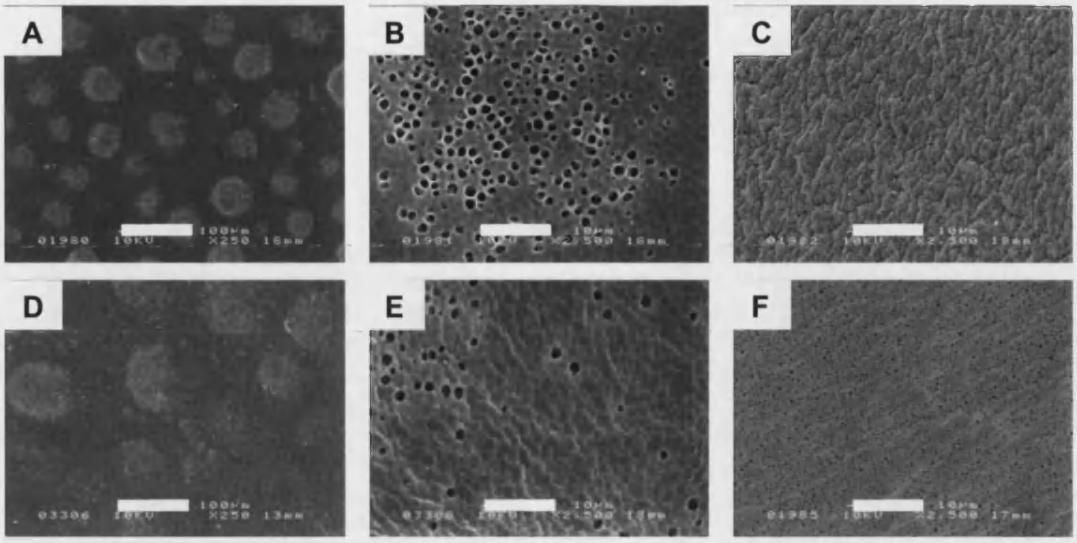

Figure 5.6 Electron micrographs of flat sheet membranes treated with 0.1 mol dm^{-3} $HClO_4$ for 15 min (A - C) and 30 min (D - F).

A and D: *Bottom of the membranes at a low magnification showing patchy pore regions, scale bar 100 μm.* ***B and E:*** *Bottom of the membranes at a higher magnification showing detail of pores, scale bar 10 μm.* ***C and F:*** *Top surface of membranes showing more spatial homogeneity to the pore distribution and pore size increasing with treatment duration, scale bar 10 μm.*

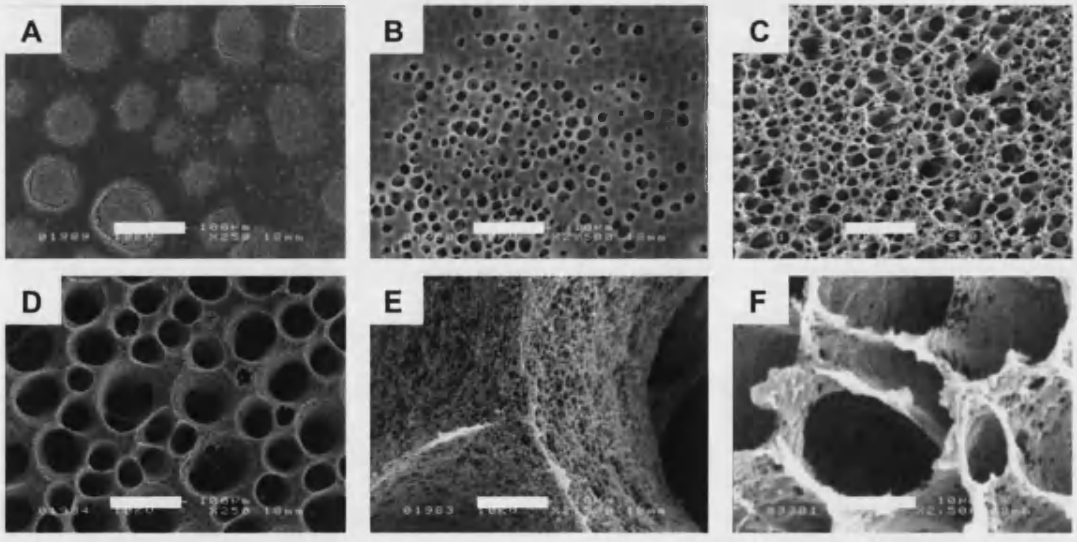

Figure 5.7 Electron micrographs of flat sheet membranes treated with 0.1 mol dm^{-3} KOH for 15 min (A - C) and 30 min (D - F).

A and D *show the bottom of the membranes at a low magnification showing patchy pore regions, scale bar 100 μm.* ***B and E*** *show the bottom of the membranes at a higher magnification showing detail of pores, scale bar 10 μm.* ***C and F*** *show top surface of membranes showing more spatial homogeneity to the pore distribution and pore size increasing with treatment duration, scale bar 10 μm.*

Both the top and the bottom of the membranes show an increase in pore size over the control, however once the skin of the membrane has been removed the top and bottoms of the membranes show very different underlying structures.

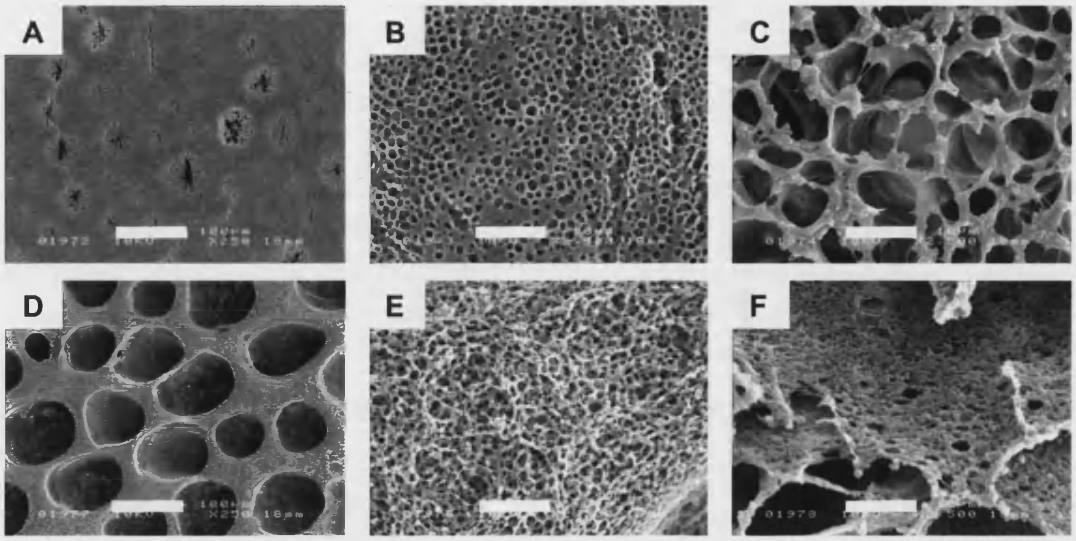

Figure 5.8 Electron micrographs of flat sheet membranes treated with 0.1 mol dm^{-3} NaOH for 15 min (A - C) and 30 min (D - F).

A and D *show the bottom of the membranes at a low magnification showing patchy pore regions, scale bar 100 μm.* ***B and E*** *show the bottom of the membranes at a higher magnification showing detail of pores, scale bar 10 μm.* ***C and F*** *show top surface of membranes showing more spatial homogeneity to the pore distribution and pore size increasing with treatment duration, scale bar 10 μm.*

5.2.1.2 Pore size and surface porosity

Measuring the pore size and surface porosity allows the changes occurring to the membranes to be assessed quantitatively as well as qualitatively. Pore sizes were evaluated using image analysis software (ImageJ, Rasband 1997-2006) to detect the area of the surface occupied by pores (selected on basis of colour). Pore diameters were calculated by dividing the total pore area by the number of pores and assuming circular pores.

$$d_e = 2\sqrt{\frac{A_p}{\pi n_p}}$$

Equation 5.1

d_e = Effective pore diameter (L)

A_p = Total pore area (L^2)

n_p = Number of pores (-)

Figure 5.9 shows the pore distributions for the different treatment types and durations (the control is the 0 min treatment for each treatment type). The median is shown by a thick bar, the inter-quartile range is shown by the box with the whiskers showing the minima and maxima, outliers (values more than 1.5 times the inter-quartile range above or below the quartiles) are shown by points. The width of the boxes is proportional to the number of pores present. The whole scale is shown (left) as well as a magnification of the low end of the range (right). The data for the acid treatments reveal little change compared to the control, with some movement from the ends of the inter-quartile range into the outliers, increasing the range of pore sizes. The alkaline treatments show a much bigger change in pore size compared to the control. The treatment clearly increases pore size with loss in numbers of pores (as would be expected as these measurements are taken over a fixed membrane area). Increasing treatment duration also increases the pore size further.

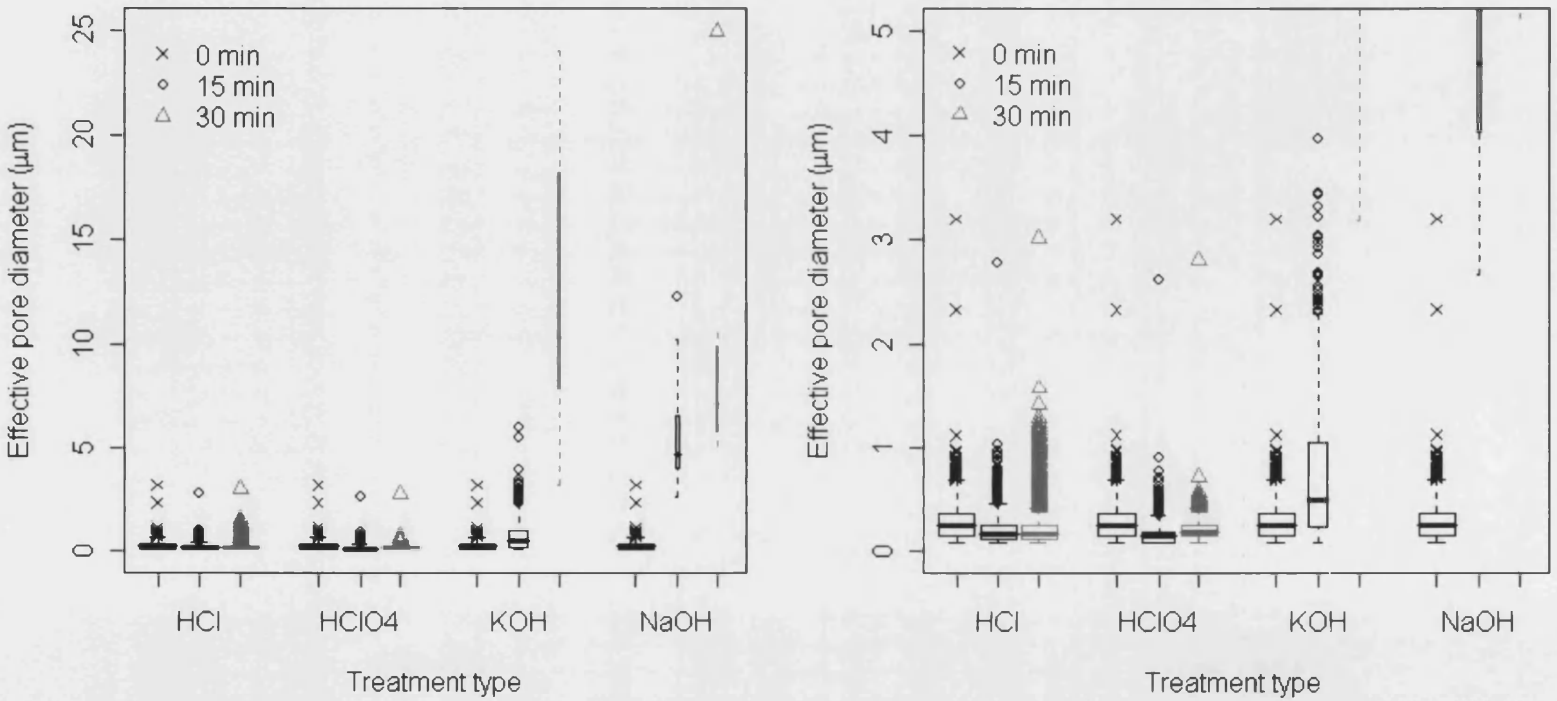

Figure 5.9 Box and whisker plot of effective pore diameters from the top surface of flat sheet membranes following treatment with two acids and two alkalis at 0.1 mol dm^{-3}.

***Left**: Whole scale, **Right**: Focus on pore diameter < 5µm. Data is presented for all pores visible on an 1823 µm2 section of membrane. Boxes show the inter-quartile range, the thick bar shows the median; whiskers show minima and maxima. Outliers (data more than 1.5 times the inter-quartile range above or below the quartiles) are shown as points. The width of the boxes is proportional to the square root of the number of pores.*

Geometric means (Equation 5.2) were used to analyse the data due to the large ranges involved. Table 5.1 shows a summary of the pore size data from the treated membranes, the geometric mean falls more in line with the median and is less affected by outlying data.

$$\bar{d}_e = \left(\prod_{i=1}^{n} d_{e_i} \right)^{1/n} \qquad \textbf{Equation 5.2}$$

$\bar{d}_e$ = Average effective pore diameter (L)

Analysis of co-variance (ANCOVA) suggested there was no significant increase in explanatory power of the correlation by treating the four treatments separately, so by the principle of parsimony they were grouped into acids and alkalis. Significant ($p < 0.01$) linear correlation was found between treatment duration and average effective pore diameter for the alkali samples but not for the acid samples, these are shown in Figure 5.10 and the expression is given in Equation 5.3.

Table 5.1 Summary of pore size data.

Membranes treated with different 0.1 mol dm^{-3} solutions for different durations. Geometric mean (Geo. mean) is closer to the median and less affected by outlying data than the arithmetic mean (Mean), this is especially true when the range is large. Data is presented for an 1823μm^2 membrane area.

	Effective pore diameter (μm)					
	0 min treatment		15 min treatment		30 min treatment	
HCl	Mean	0.28	Mean	0.21	Mean	0.20
	Median	0.24	Median	0.17	Median	0.17
	Geo. Mean	0.24	Geo. mean	0.18	Geo. mean	0.17
	Min.	0.09	Min.	0.09	Min.	0.09
	Max.	3.20	Max.	2.78	Max.	3.01
$HClO_4$	Mean	0.28	Mean	0.17	Mean	0.20
	Median	0.24	Median	0.15	Median	0.19
	Geo. Mean	0.24	Geo. mean	0.15	Geo. mean	0.18
	Min.	0.09	Min.	0.09	Min.	0.09
	Max.	3.20	Max.	2.62	Max.	2.81
KOH	Mean	0.28	Mean	0.72	Mean	12.49
	Median	0.24	Median	0.50	Median	10.27
	Geo. Mean	0.24	Geo. mean	0.48	Geo. mean	10.61
	Min.	0.09	Min.	0.09	Min.	3.18
	Max.	3.20	Max.	5.97	Max.	24.03
NaOH	Mean	0.28	Mean	5.50	Mean	9.46
	Median	0.24	Median	4.68	Median	7.12
	Geo. Mean	0.24	Geo. mean	5.13	Geo. mean	8.20
	Min.	0.09	Min.	2.66	Min.	5.11
	Max.	3.20	Max.	12.29	Max.	24.98

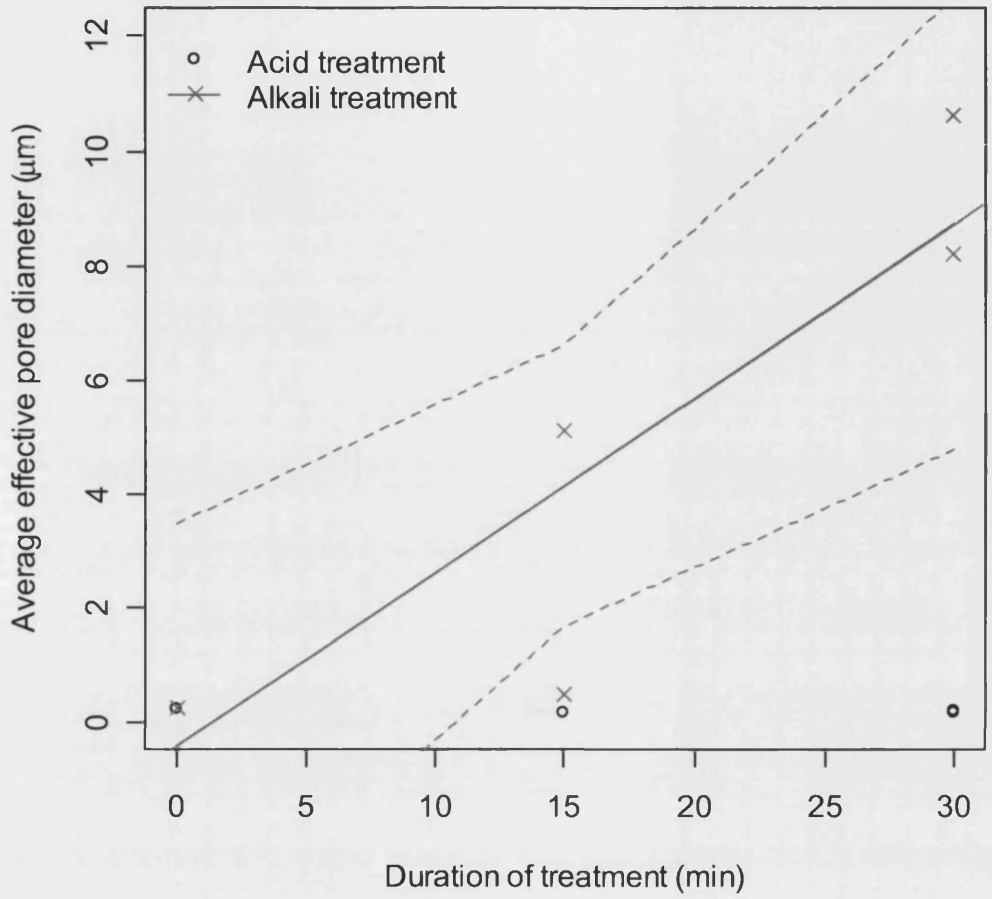

Figure 5.10 Scatter plot showing average effective pore diameter against treatment duration.
*Flat sheet membranes were treated with 0.1 mol dm-3 acid and alkali solution (HCl and NaOH). Single data points are presented along with the significant linear correlation ($p < 0.01$) between treatment duration and average effective pore diameter for the alkali samples; regression line (**solid**) and 95% confidence interval (**dashed**) are shown. No significant correlation was found between treatment duration and average effective pore diameter for the acid samples.*

$$\bar{d}_e = -0.44 \pm 1.4 + 0.31 \pm 0.07t \qquad \textbf{Equation 5.3}$$

$\bar{d}_e$ = Average effective pore diameter (L; μm)

t = Treatment duration (T; min)

The porosity of the membranes was calculated by determining the entire pore area as above and dividing by the total area of the membrane.

$$p = \frac{A_p}{A_m} \times 100$$ **Equation 5.4**

p = Porosity (-)

A_p = Total area of pores (L^2)

A_m = Area of membrane (L^2)

The porosity data is given as a percentage of the membrane covered by pores. As such the errors are not normally distributed, the variance is not constant and the data is bounded; because of this the arc-sine transformation (Equation 5.5) was performed before the data was analysed as Normal.

$$x = \sin^{-1}\left(\sqrt{0.01p}\right)$$ **Equation 5.5**

Again there was no statistical justification not to group the two acid and two alkali treatments. As above significant correlation was found by ANCOVA for the alkali samples but not the acid samples. Figure 5.11 shows the data with the significant ($p < 0.001$) trend line for the alkali treated samples.

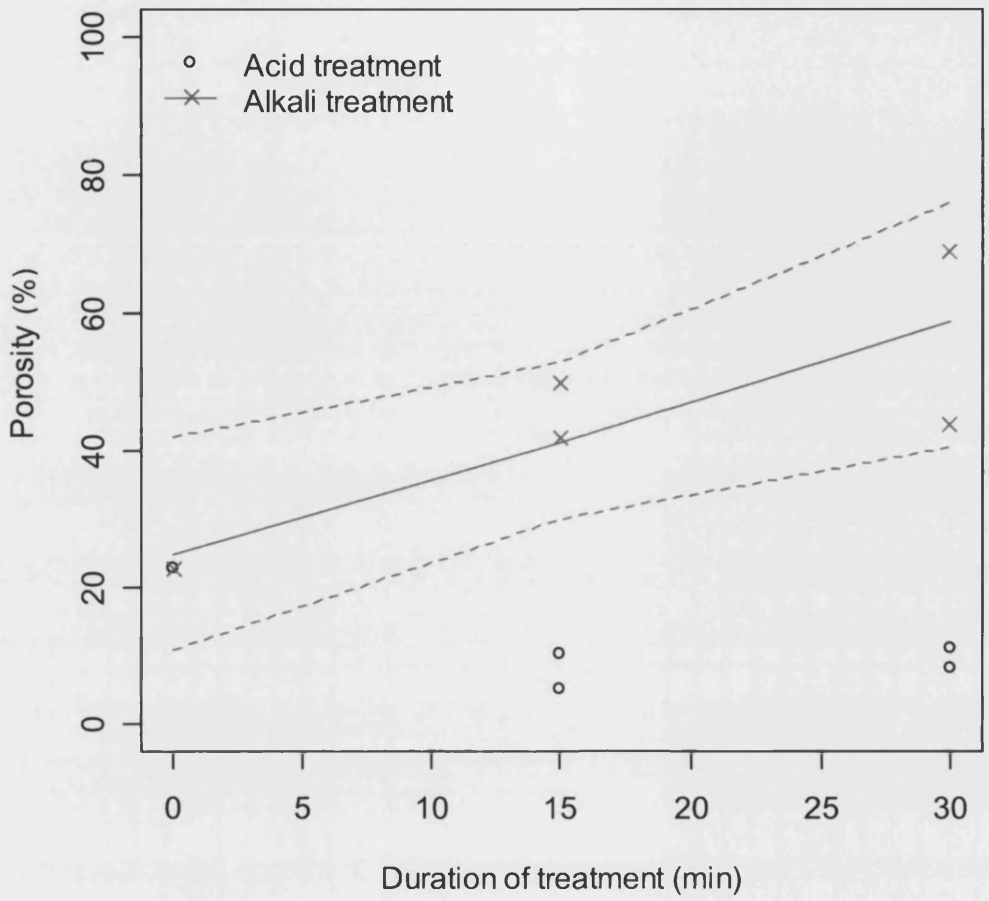

Figure 5.11 Scatter plot showing average surface porosity of flat sheet membranes following 0.1 mol dm^{-3} acid or alkali treatment.

*Alkali treatment showed a significant ($p < 0.01$) correlation with treatment duration; regression line (**solid**) and 95% confidence interval (**dashed**) are shown. Acid treatment showed no significant correlation between porosity and treatment duration. Points represent single samples.*

5.2.1.3 Cell adhesion

All the treated samples showed a significant ($p < 0.01$) increase in the number of cells adhered after 6 h over the control sample (Figure 5.12) as determined by ANOVA. However there was no significant difference between the numbers of cells adhered to the treated samples. In addition there appeared to be no correlation between numbers of cells adhered and pore size or porosity with hydrochloric acid and perchloric acid, which both have similar pore sizes and porosities, showing the largest and smallest numbers of adhered cells respectively of all the treated samples and the sodium

hydroxide and potassium hydroxide, both with much lager pore sizes and higher porosities, showing very little difference in numbers of cells adhered.

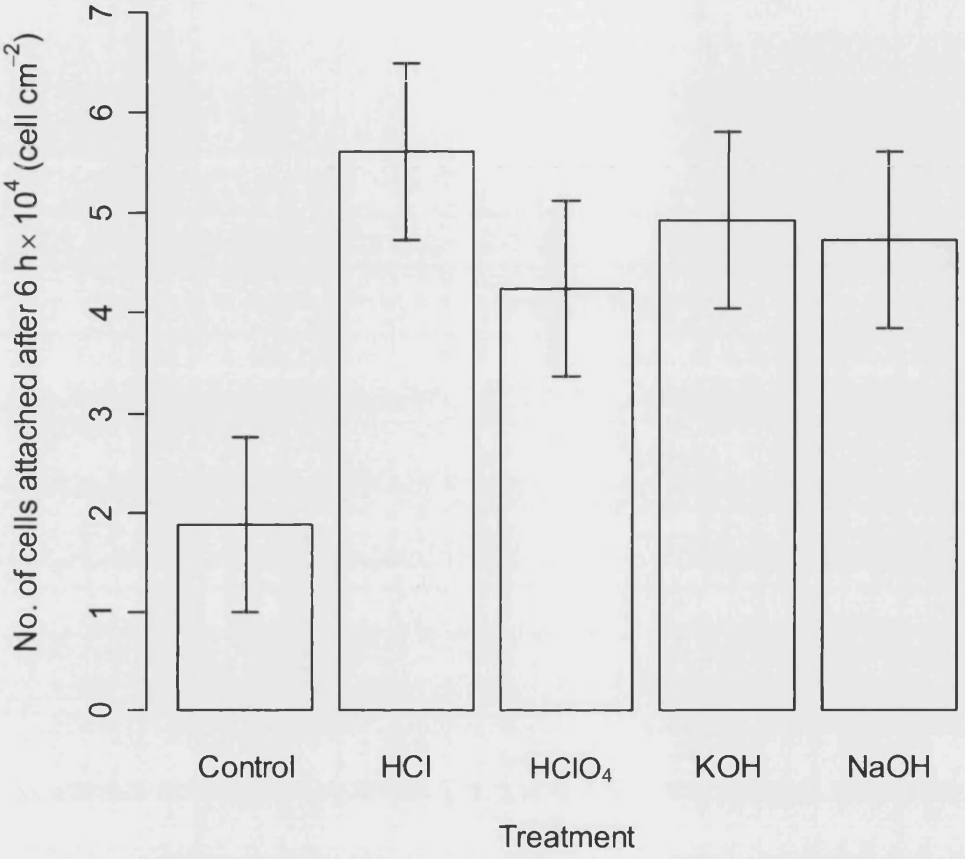

Figure 5.12 Bar plot showing number of cells attached to membrane surface following treatment. *Membranes were treated with 0.1 mol dm^{-3} acid or alkali for 15 min prior to seeding. Cell number determined by Picogreen assay. Error bars show least significant difference (lsd), no-overlap means there is significant difference between the samples at $p < 0.01$, overlap means there is no significant difference between the samples (mean ± lsd; $n = 4$). All the treated samples show a significant increase in number of cells attached over the control, however there is no significant difference between the different treatments.*

5.2.2 Varying the concentration of acid and alkali treatment

Varying the concentration of the treatment solution for both acid (hydrochloric acid) and alkali (sodium hydroxide) showed a similar trend to increasing the duration of the treatment.

5.2.2.1 Surface morphology of acid and alkali treated samples

The samples treated with different concentration hydrochloric acid solutions showed little change over the range of concentrations (0.01 - 0.2 mol dm^{-3}), with pores only appearing very slightly larger on membranes treated with more concentrated solutions. Figure 5.13 shows electron micrographs of the surfaces of the membranes with increasing treatment concentration with distance down the page.

A large change in the appearance of the membrane is visible in the electron micrographs of membranes treated with different concentration sodium hydroxide solutions (0.01 - 0.2 mol dm^{-3}). Initially an increase in the surface pore size is seen, however with treatment concentrations above 0.1 mol dm^{-3} the interior of the membrane is revealed making the measurement of surface properties difficult as the "surface" has been removed. Figure 5.14 shows the electron micrographs of treated membranes with treatment concentration increasing further down the page.

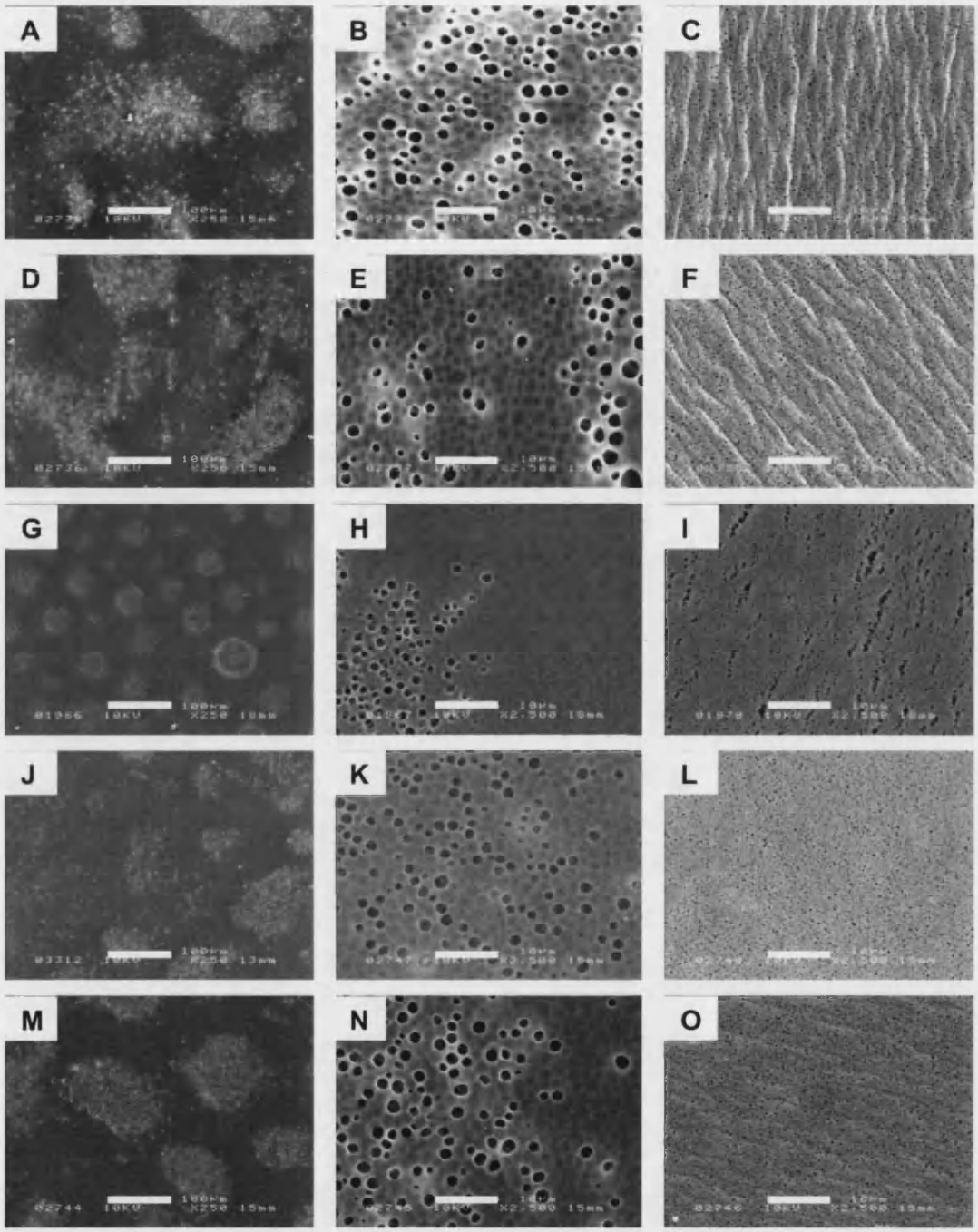

Figure 5.13 Series of electron micrographs showing the effects of treatment of increasing concentrations of HCl on PLGA flat sheet membranes for 15 min.

*Different rows show different treatment concentrations **A – C** are 0.01 mol dm^{-3} HCl solution, **D – F** are 0.05 mol dm^{-3} solution, **G – I** are a repeat of the top row of Figure 5.5 showing membranes treated with 0.10 mol dm^{-3} solution, **J – L** are 0.15 mol dm^{-3} solution and **M – O** are 0.20 mol dm^{-3} solution. **A, D, J and M** show low magnification images of the bottom of the scaffolds, scale bar 100 μm. **B, E, H, K and N** show higher magnification images of the bottom surface of the membranes, scale bar 10 μm. **C,F, I, L and O** show the top surface of the treated membranes, scale bar 10 μm.*

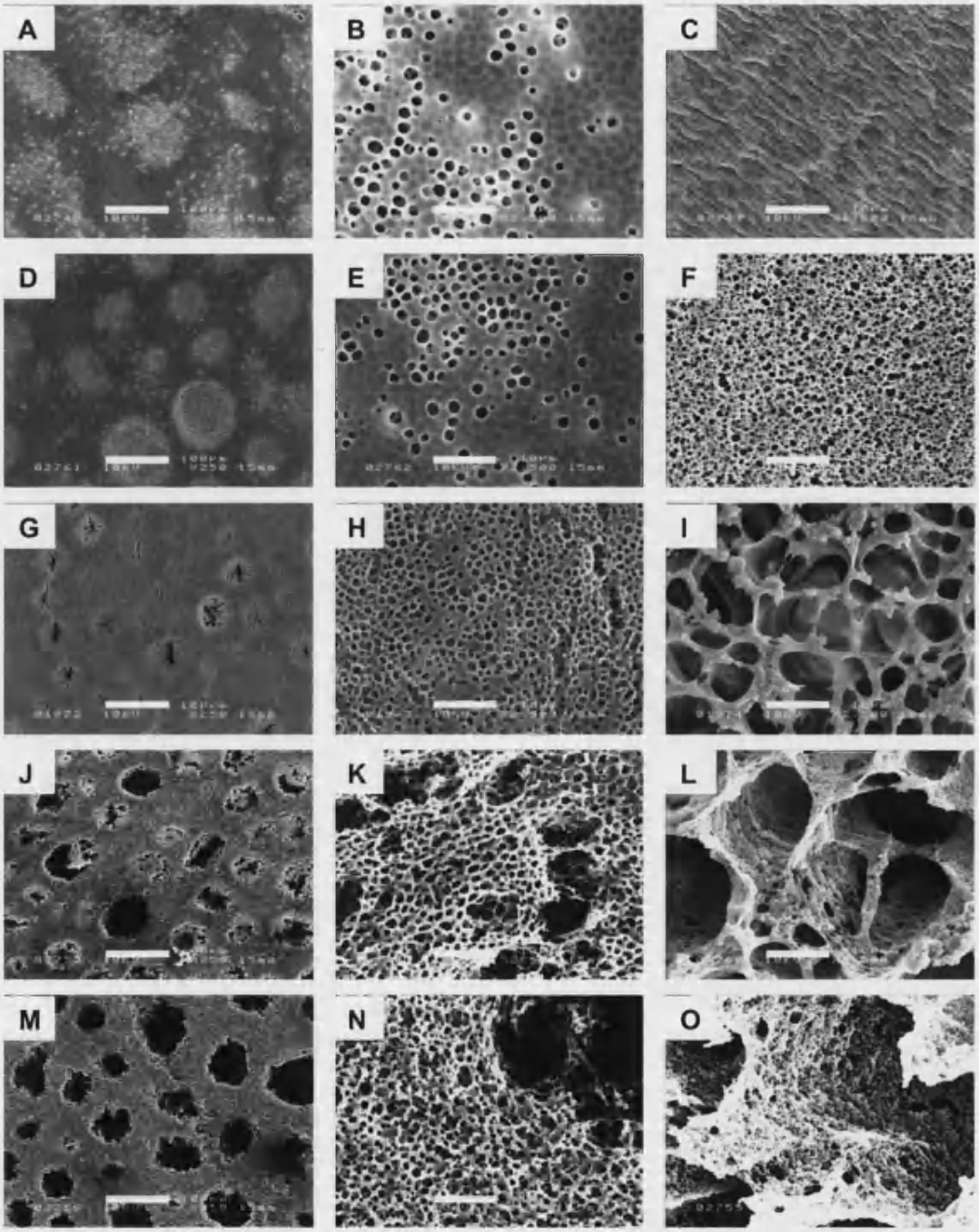

Figure 5.14 Series of electron micrographs showing the effects of treatment of increasing concentrations of NaOH on PLGA flat sheet membranes for 15 min.

*Different rows show different treatment concentrations **A – C** are 0.01 mol dm^{-3} HCl solution, **D – F** are 0.05 mol dm^{-3} solution, **G – I** are a repeat of the top row of Figure 5.8 showing membranes treated with 0.10 mol dm^{-3} solution, **J – L** are 0.15 mol dm^{-3} solution and **M – O** are 0.20 mol dm^{-3} solution. **A, D, J and M** show low magnification images of the bottom of the scaffolds, scale bar 100 μm. **B, E, H, K and N** show higher magnification images of the bottom surface of the membranes, scale bar 10 μm. **C,F, I, L and O** show the top surface of the treated membranes, scale bar 10 μm..*

5.2.2.2 Pore size and surface porosity

Figure 5.15 shows an increase in pore size for the samples treated with higher concentrations of sodium hydroxide solution, with little change for the samples treated with increasing concentration of hydrochloric acid solution. For the sodium hydroxide treated samples there is significant linear correlation ($p < 0.001$) between the treatment concentration and pore size.

$$\bar{d}_e = 48.4 \pm 6.3C - 0.36 \pm 0.7 \qquad \textbf{Equation 5.6}$$

$\bar{d}_e$ = Average effective pore diameter (L; μm)

C = Concentration of solution (NL^{-3}; mol dm^{-3})

The equation shows the parameter estimate as determined by analysis of co-variance (ANCOVA) plus the standard error of the estimate.

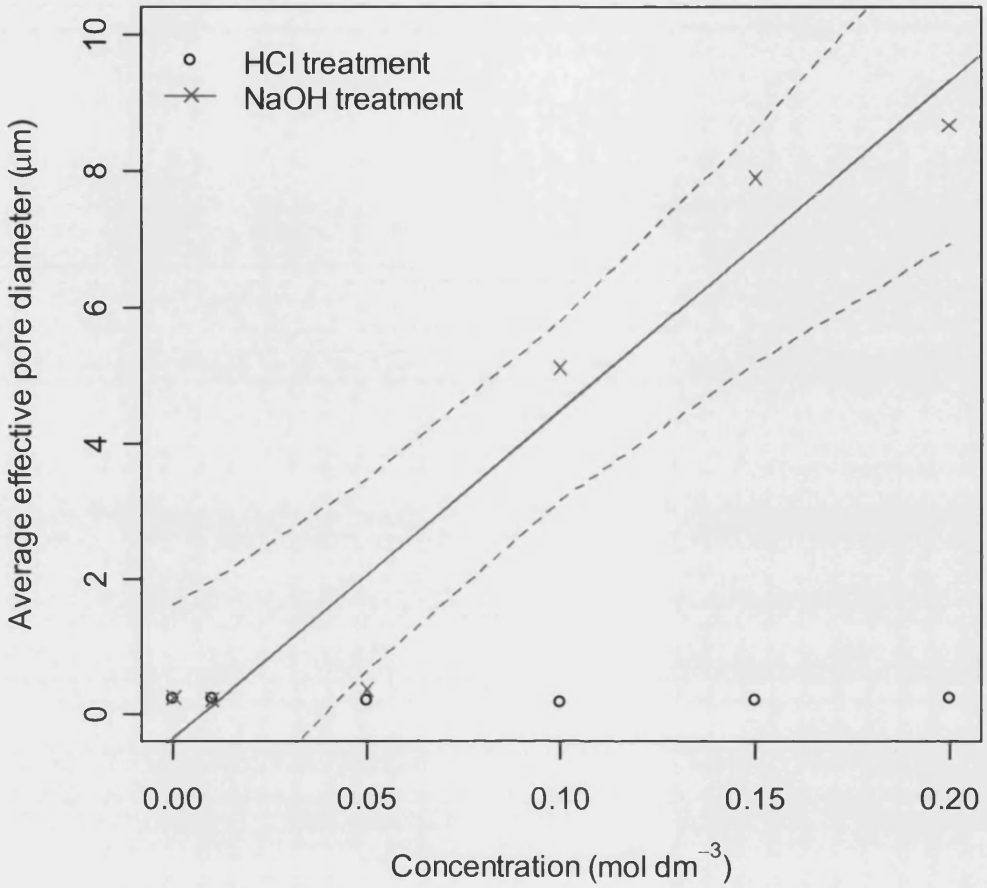

Figure 5.15 Scatter plot showing average pore diameter of the top surface of flat sheet membranes following acid or alkali treatment for 15 min at varying concentrations.

Single data points are shown. ANCOVA revealed a significant ($p < 0.001$) linear correlation for sodium hydroxide samples and no significant correlation for hydrochloric acid samples. The linear regression line (solid) and 95% confidence interval (dashed) are shown.

Figure 5.16 shows a very similar response for the porosity of the membranes treated with increasing concentrations of acid and alkaline solutions as for the pore size of these membranes. Porosity data was again transformed by the arc-sin transformation (Equation 5.5) before analysing with ANCOVA. The equation is given by Equation 5.7 (estimate □ standard error).

$$p = \left(\sin\left(0.41 \pm 0.08 + 3.1 \pm 0.67C\right)\right)^2 \times 100 \qquad \textbf{Equation 5.7}$$

p = Percentage surface porosity of polymer (-; %)

C = Concentration of solution (NL^{-3}; mol dm^{-3})

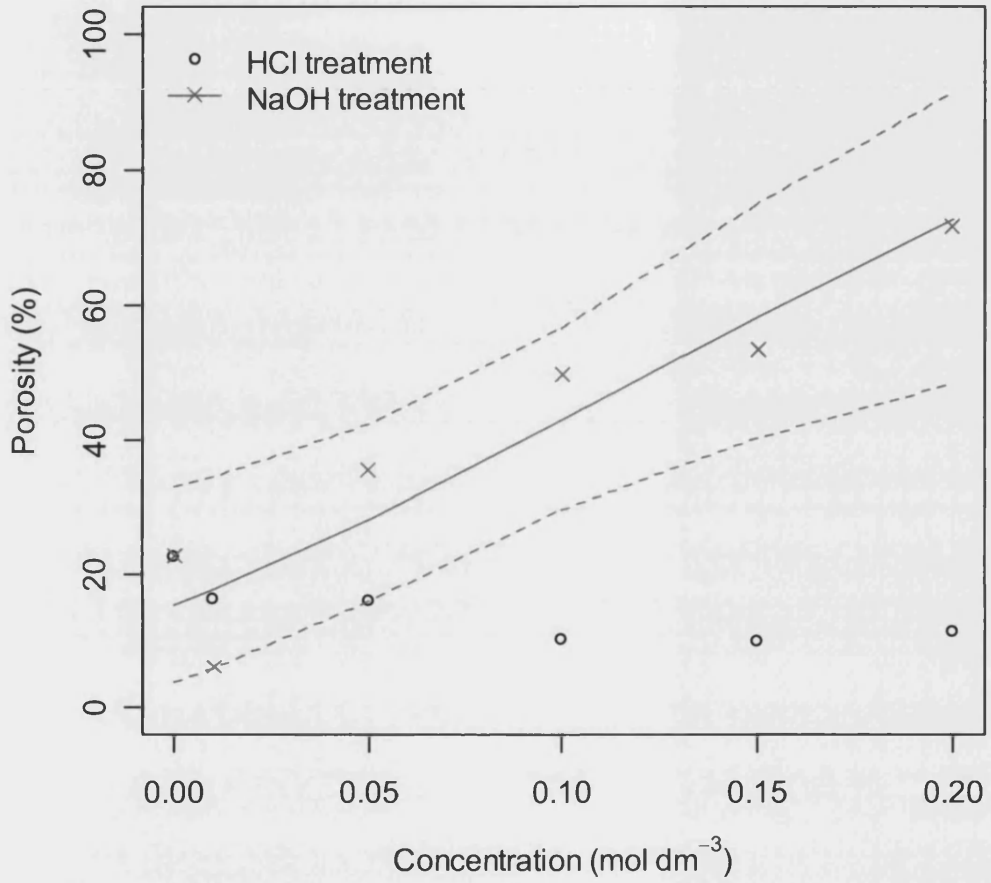

Figure 5.16 Scatter plot showing surface porosity of flat sheet membranes following acid or alkali treatment for 15 min at varying concentrations.

Single data points are shown. Alkali treatment shows significant correlation ($p < 0.01$), acid treatment shows no correlation. Regression line (solid) and 95% confidence interval (dashed) are shown.

5.2.2.3 Cell adhesion

Figure 5.17 shows the numbers of cells adhered to the membranes treated with different concentration solutions. The data was in the form of count data (number of whole cells per membrane area) with large variances, as such a generalized linear model with quasipoisson errors was used and revealed a significant ($p < 0.01$) logistic correlation between cell number and treatment concentration of the samples treated with sodium

hydroxide the equation with standard errors of the estimates of the parameters is given in Equation 5.8. There is no significant correlation between increasing treatment concentration and increasing adhered cell number for the hydrochloric acid treated samples.

$$N_c = \log(11.3 \pm 0.3 + 7.9 \pm 2.2C) \qquad \textbf{Equation 5.8}$$

N_c = Number of cells (-)

C = Concentration of solution (NL^{-3}; mol dm^{-3})

If the cell number data is combined with pore size a relationship is found between the numbers of cells adhered and the pore size of the membrane, this is seen in Figure 5.18. The equation with standard error of the estimates is given in Equation 5.9.

$$N_c = \log(12.0 \pm 0.1 + (8.3 \pm 2.1) \times 10^{-2} d_e) \qquad \textbf{Equation 5.9}$$

d_e = Effective pore diameter (L; μm)

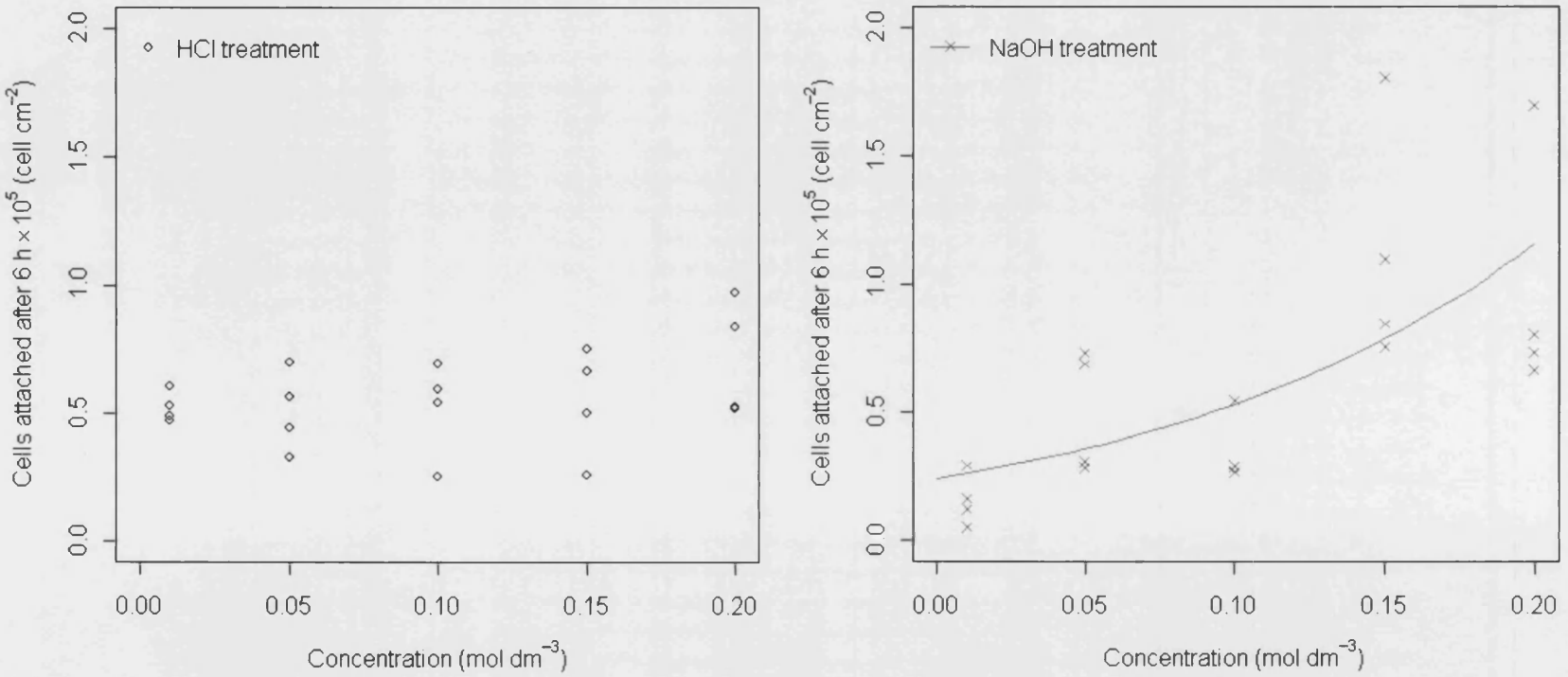

Figure 5.17 Scatter plots showing the number of cells attached after 6 hours to membrane surfaces treated with varying concentration solution for 15 min.

Membranes were treated with acid (right) or alkali (left) for 15 min prior to seeding. Cell number was determined by Picogreen assay. Single data points are shown. A significant ($p < 0.01$) correlation (solid line) was found for the sodium hydroxide treated samples with no correlation for the hydrochloric acid treated samples.

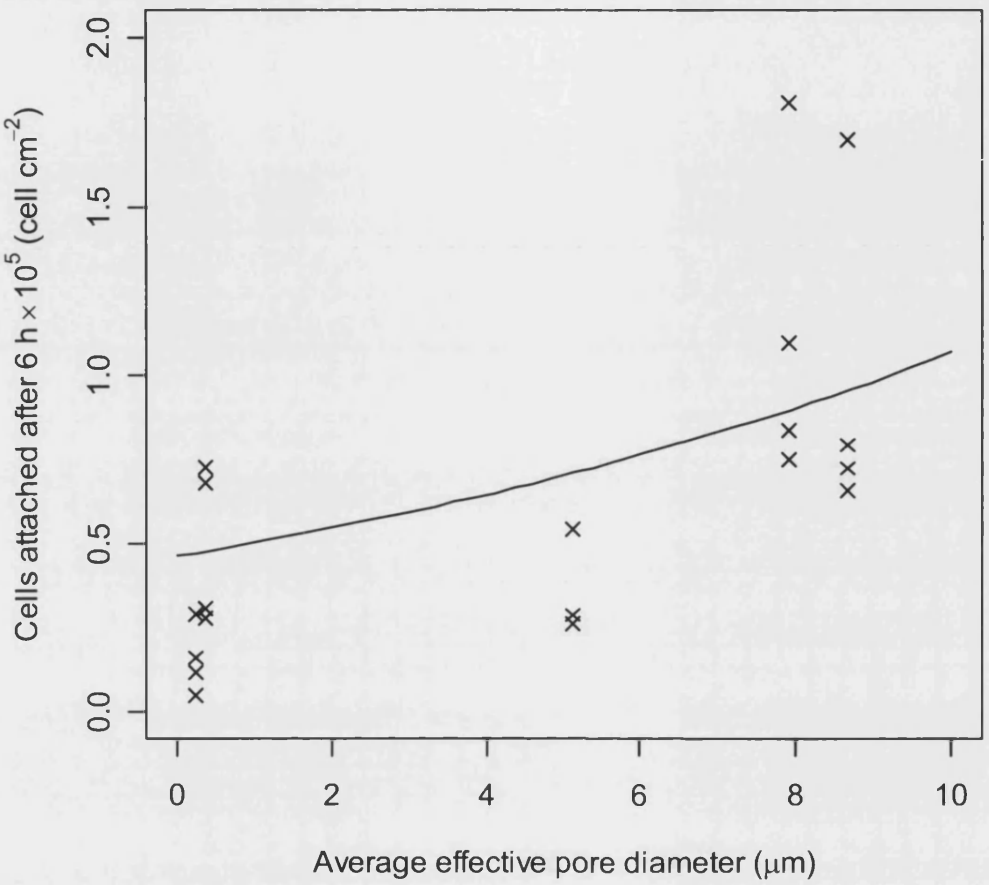

Figure 5.18 Scatter plot showing the relationship between cell attachment and membrane effective pore diameter.

Membranes were treated with acid or alkali solutions with concentrations 0.01 - 0.2 mol dm-3 for 15 min prior to seeding to augment the pore diameter. Cell number was determined by Picogreen assay. Single data points are shown. A significant ($p < 0.01$) logistic relationship is found between cell number and average pore diameter and shown with a ***solid line****.*

5.2.3 Alkali treatment of 50:50, 65:35 and 85:15 polymer flat sheets

5.2.3.1 Pore size

Results of the treatment of three different membrane compositions with sodium hydroxide solutions at two different concentrations and for two different durations are presented in Figure 5.19. The regression line was generated following an iterative simplification procedure from the most complicated correlation available, where all three of membrane composition, treatment concentration and treatment duration were

given as explanatory variables, and all possible interactions between the three were included in the correlation. The correlation also included quadratic terms for each explanatory variable as initial scatter plots indicated curved responses. The correlation was simplified by an iterative process: removing the least significant term (as indicated by ANOVA) from the correlation until all terms remaining were significant in explaining the behaviour of the response variable. A residuals versus fitted data plot showed good heteroscedasticity and a Q-Q plot (quantile-quantile plot; compares the ranked data from ranked data taken from the normal distribution) indicated the data was well modelled by the Normal distribution. The equation of the regression line is given by Equation 5.10 and details of the correlation are given in Table 5.2.

$$\bar{d}_e = 7.14 - 1.9\times10^{-1}M + 1.6\times10^{-1}t - 1.4\times10^{-3}t^2 + 1.3\times10^{-3}M^2 - 2.0\times10^{-3}Mt + 6.3\times10^{-3}tMC \qquad \textbf{Equation 5.10}$$

$\bar{d}_e$ = Average effective pore diameter (L; μm)

M = Percentage lactic acid in membrane (-; %)

t = Treatment duration (T; min)

C = Concentration of solution (NL^{-3}; mol dm^{-3})

Table 5.2 Regression correlation for pore size for different membrane compositions, treatment concentrations and treatment durations.

Values of the coefficients from the regression correlation for the response of the average effective pore diameter to changes in the membrane composition (Type; % lactide content), treatment duration (Time; min) and treatment concentration (Conc; mol dm^{-3}).

	Estimate	Std. Error	t	p	Sig.
Intercept	7.14E+00	2.08E+00	3.43E+00	1.22E-03	*
Type	-1.94E-01	6.27E-02	-3.09E+00	3.23E-03	*
Time	1.64E-01	3.25E-02	5.05E+00	6.21E-06	***
$(Time)^2$	-1.37E-03	6.15E-04	-2.22E+00	3.08E-02	.
$(Type)^2$	1.32E-03	4.60E-04	2.87E+00	6.02E-03	*
Type:Time	-2.01E-03	4.23E-04	-4.76E+00	1.71E-05	***
Type:Time:Conc	6.32E-03	9.85E-04	6.41E+00	4.95E-08	***

Significance codes: * = 0.0001, ** = 0.001, * = 0.01, .= 0.05**

The correlation indicated the membrane composition and treatment duration and concentration all significantly affected the average effective pore diameter. It can be seen from the graph (Figure 5.19) that as the treatment concentration and duration increase so does the average effective pore diameter, with the exception of the 0.1 mol dm^{-3} treatment of the 85:15 membrane. As the lactic acid content of the membrane increases the effective pore diameter decreases (shown across the three graphs).

There were quadratic correlations between membrane composition and time and interactions between all three independent variables. This is shown in the tree diagram in Figure 5.20, the length of the branches indicate the degree of deviance explained. In this correlation the duration of treatment (Time) is the most important factor in explaining the change in pore diameter, for times of less than 7.5 min there is no difference in the membranes or the treatments (which is to be expected as with a treatment duration of 0 min there was no treatment). For the treated samples the concentration of the treatment was only significant for the membranes with a lactic acid content of greater than 57.5 (65:35 and 85:15).

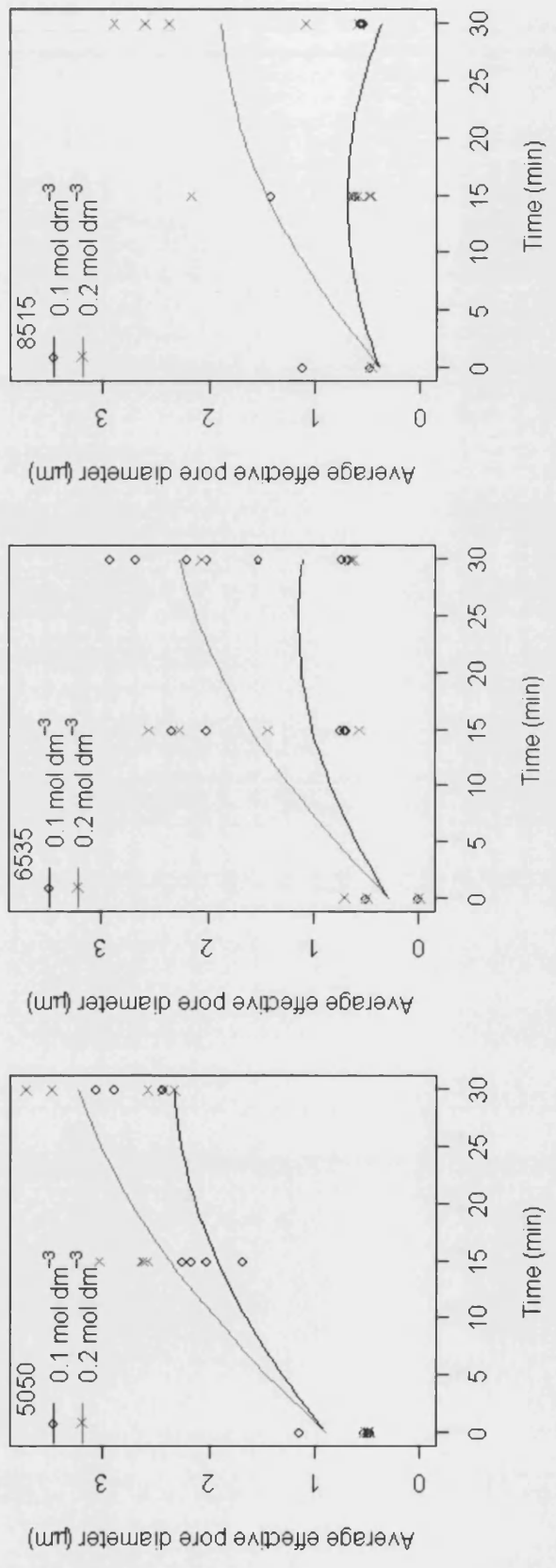

Figure 5.19 Series of scatter plots showing the effect of different treatment concentrations and times on effective pore diameter of different membrane compositions. ***Left**: 50:50 PLGA, **Middle**: 65:35 PLGA, **Right**: 85:15 PLGA. Single data points and regression lines are shown.*

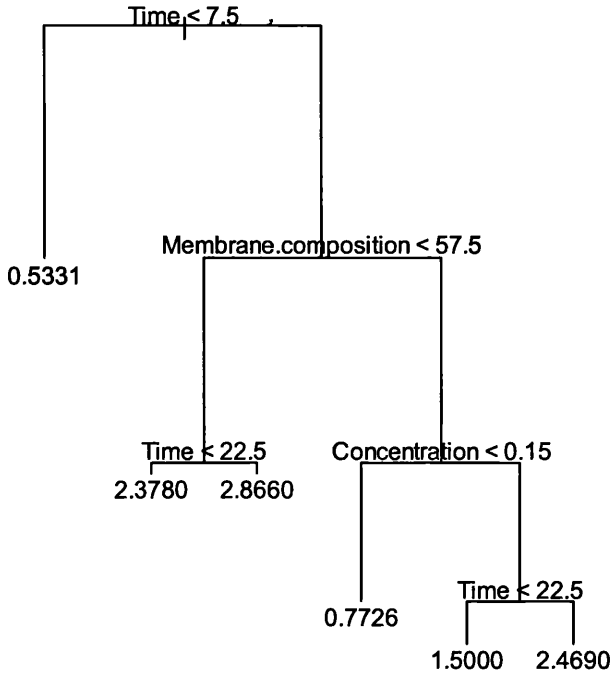

Figure 5.20 Tree diagram showing the interactions between the independent variables correlating with the average effective pore diameter.

The length of the branches is proportional to the amount of deviance explained. The numbers at the end of the branches are the mean effective pore diameters (μm).

5.2.3.2 Hydrophilicity

The water contact angle of the membranes before and after treatment was measured as an indicator of the hydrophilicity of the membrane: the higher the water contact angle the more hydrophilic the membrane. Membrane composition, concentration and duration of treatment were all found to lead to significant differences in the water contact angle; there were also significant interactions between treatment duration and concentration and treatment duration and membrane composition as well as an interaction between all three.

Table 5.3 Regression correlation for the water contact angle for different membrane compositions, treatment concentrations and treatment durations.

Values of the coefficients from the regression correlation for the response of the water contact angle to changes in the membrane composition (Type; %), treatment duration (Time; min) and treatment concentration (Conc; mol dm^{-3}).

	Estimate	***Std. Error***	***t***	***P***	***Sig.***
Intercept	60.6	1.22	49.8	$< 2 \times 10^{-16}$	***
Time	3.01	5.59×10^{-1}	5.4	1.71×10^{-6}	***
Time:Type	-3.09×10^{-3}	8.07×10^{-3}	-3.8	3.51×10^{-4}	**
Time:Conc	-14.1	3.62	-3.9	2.75×10^{-4}	**
Time:Type:Conc	1.50×10^{-1}	5.33×10^{-2}	2.8	6.80×10^{-3}	*

Significance codes: * = 0.0001, ** = 0.001, * = 0.01, .= 0.05**

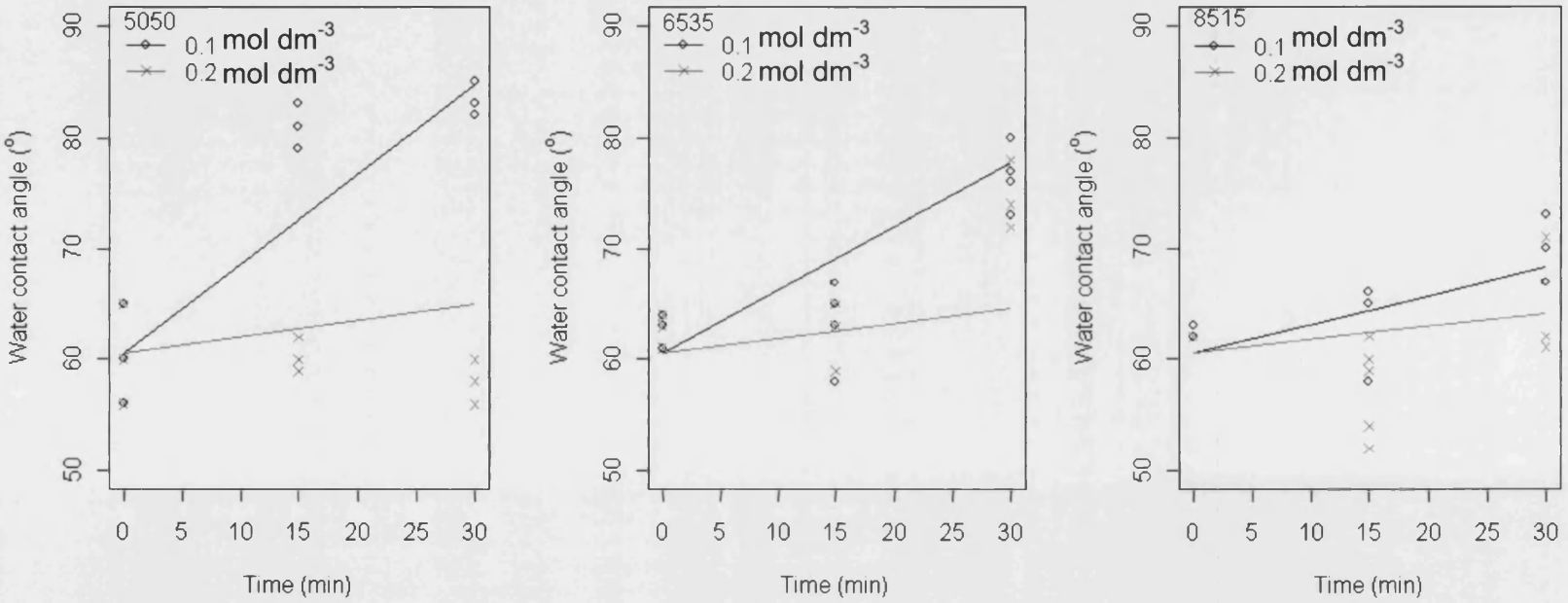

Figure 5.21 Series of scatter plots showing the effect of different treatment concentrations and times on the water contact angle of different membrane compositions.

***Left**: 50:50 PLGA, **Middle**: 65:35 PLGA, **Right**: 85:15 PLGA. Single data points and regression lines are shown.*

5.2.4 Mass loss of samples treated with sodium hydroxide

All treated samples showed a reduction in mass following treatment with 0.1 mol dm^{-3} sodium hydroxide (Figure 5.22). Percentage mass remaining data was transformed with the arc-sin transformation and analysed by least squares linear regression. A significant (p <0.001) relationship between mass loss and treatment duration was found.

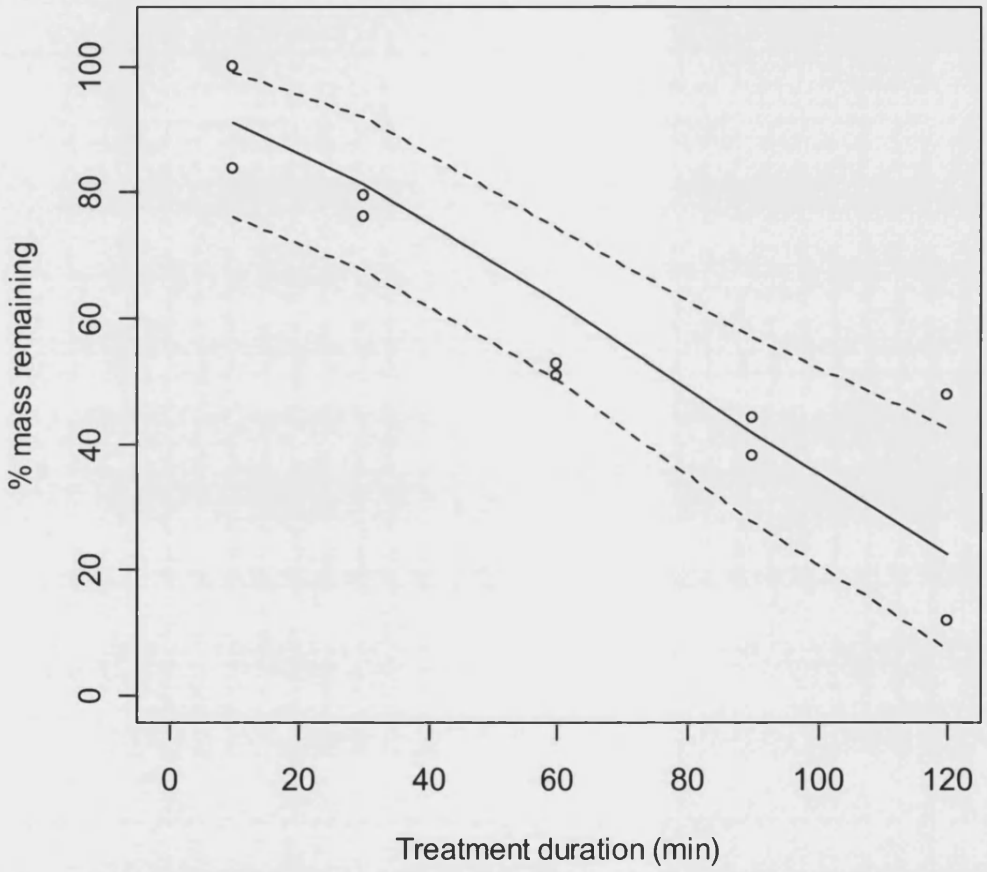

Figure 5.22 Scatter plot showing percentage mass loss by 50:50 PLGA flat sheets treated with 0.1 mol dm^{-3} sodium hydroxide for different durations.

*Initial polymer weight of $4.8 \times 10^{-3} \pm 6.4 \times 10^{-4}$ g. Single data points, regression line (**solid**) and 95% confidence limits (**dashed**) are shown.*

No significant trend was found between the rate at which the polymer was losing mass and the treatment duration, suggesting the reaction rate was constant throughout the 2 hour maximum treatment duration (Figure 5.23).

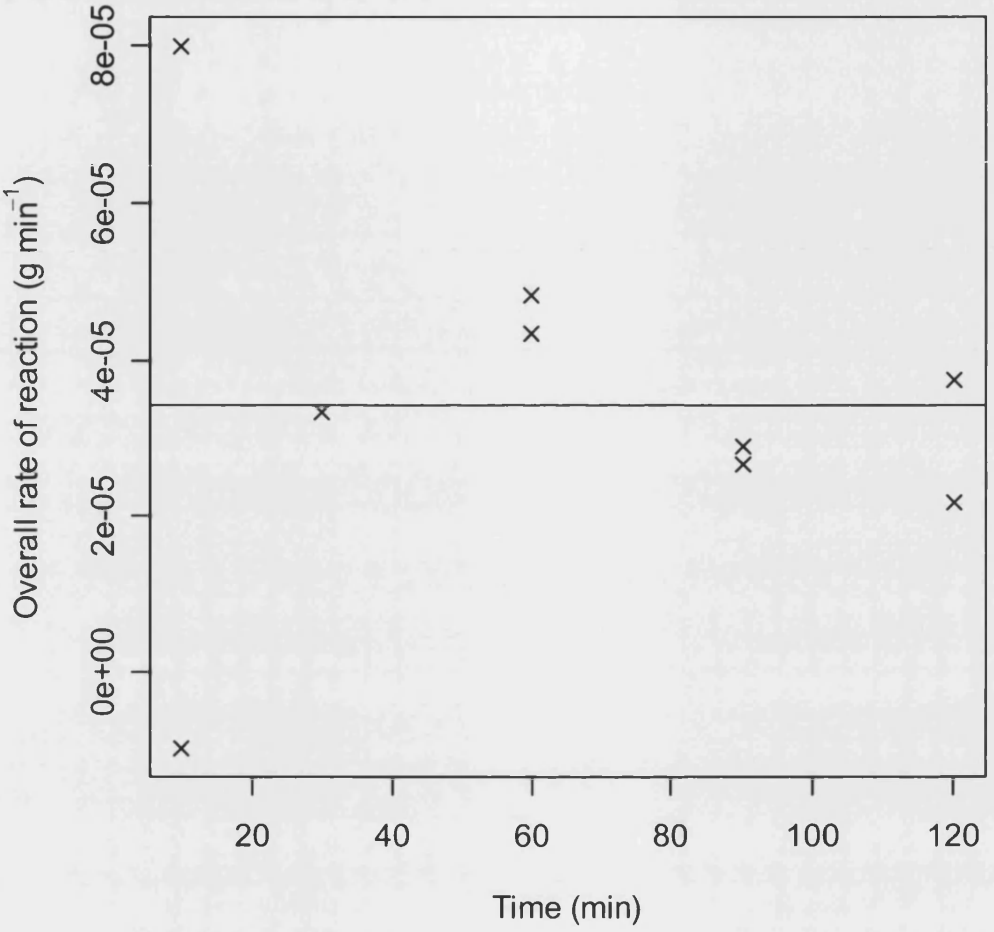

Figure 5.23 Scatter plot showing the rate of reaction for the different duration of reactions.
No significant trend is found therefore the null hypothesis that the rate of reaction is constant with time must be adhered to. ***Line*** *shows the average rate of reaction, single data points are presented.*

5.3 Discussion

5.3.1 Acid versus alkali treatment

All four treatments resulted in changes to the surface of the membranes compared to the controls. Consistently the alkali treatments resulted in larger changes from the control membranes than the acid treatments.

All the treatments have high dissociation constants (Table 5.4) leading to almost complete dissociation in an aqueous environment. Therefore the same concentration of ions are released by all of the treatments. Both reaction mechanisms (Figure 5.2 and Figure 5.3) show a single ion is responsible for one bond cleavage. With the same concentration solution there is the same probability that the ion will contact the bond for either acid or alkali treatments. However, the reaction mechanism is different for the acid and alkali treatment. This suggests that within the acid treatments the same concentration of protons is attacking the membrane surface and within the alkali treatment the same concentration of hydroxide ions are attacking the membrane surface; but the effect of the proton and hydroxide ion attacks are different. Further discussion on the differences between the acid and alkali treatments is given in Section 5.3.3.

Table 5.4 Dissociation constants for the treatment chemicals.

Species	$K_{a/b}$*
HCl	10^{8}
$HClO_4$	10^{10}
KOH	$10^{2.29}$
NaOH	$10^{2.43}$

*** a = acid, b = base**

K_a = Acid dissociation constant (-)

K_b = Base dissociation constant (-)

The minimal changes associated with acid treatment agree with the findings of Burkersroda *et al.* (2002) who found that the degradation of PLGA at pH 2 was not changed compared to neutral degradation (pH 7.4). This was purported to be because the environment at pH 2 was equivalent to the localized drop in pH seen due to autocatalysis in neutral degradation conditions.

Increasing alkaline treatment duration and concentration significantly increased the average effective pore diameter; this was not found for the acid treated samples.

5.3.2 Membrane composition

Increasing lactide content in the membrane reduced pore diameter on both the controls and the treated samples (Figure 5.19). It is known that the hydrolytic degradation rate PLGA with compositions other than 50:50 are slower than the equal mix. The ester bond is the same between any combination of lactide and glycolide monomers which would suggest that the difference occurs due to ingress of the aqueous media into the scaffold. Any movement away from 50:50 PLGA increases the crystallinity of the polymer; this reduces the diffusion of water into the solid and reduces the degradation rate (Middleton and Tipton 2000).

The untreated membranes of different compositions also exhibited different pore sizes making it likely that the lactide content acts to alter the initial membrane formation as well as the hydrolytic degradation leading to increased pore diameter.

Tamada and Langer (1993) found that following hydrolytic degradation of 50:50 PLGA 90% of the initial GA monomer was found in the degradation solution but only about 50% of the initial LA was found. They concluded the balance of the LA must remain in the LA enriched scaffold. This would suggest that bonds between glycolide monomers are easier to break; suggesting scaffolds with higher ratios of glycolic to lactic acid would result in increased degradation. This is consistent with the results of this study where the membranes with increased lactide content exhibited smaller changes in pore size. While the composition of the remaining scaffold was not analysed to see if the composition of the membrane changed following treatment it was noticed the fragility of the membrane increased following treatment. This appeared to be associated with a more crystalline structure to the membrane. This would be consistent with the hypothesis that the glycolic acid component had become depleted; leaving a membrane enriched with the more crystalline lactic acid.

5.3.3 Bulk or surface degradation

Burkersroda *et al.* (2002) found alkaline degradation markedly changed the degradation from bulk erosion to surface erosion; the complete degradation process was reduced from a matter of weeks to hours. This agrees with the results found in this study where noticeable degradation occurred over periods of less than an hour.

Croll *et al.* (2004) suggest an explanation of why the alkaline degradation is surface erosion while acidic degradation tends towards bulk degradation. Two factors apply: the first is that the hydroxyl group is bulkier than the single proton in acidic degradation, which reduces the rate at which is diffuses into the bulk of the mechanism; the second is the negatively charged carboxyl groups generated during the degradation act to repel the solvated hydroxide ion.

The increased changes to the surface of the membrane for alkali treatment over acid treatment found in this study may be a result of the alkali treatment selectively attacking the membrane surface while the acid treatment results in a more homogenous bulk degradation.

No mention in the literature, or result of this study, is found to indicate any cancellation of the effects of the alkaline treatment by acidic degradation products. However as the presence of acidic degradation products are widely accepted to build up in the interior of a low porosity scaffold during degradation this may also explain why alkaline degradation is surface based. In the interior the small volumes of fluid would lead to the degradation products making a significant difference to the localized pH, however in the bulk fluid the small release of acidic degradation products is unlikely to result in a significant change in pH.

5.3.4 Mechanism of pore size increase

There are two methods by which the pore size may increase as a result of surface treatment, the first is to assume the pores already exist within the membrane and increasing treatment concentration results in removal of the skin layer revealing the underlying pore structure (Scenario A, Figure 5.24). The second is that new pores are being formed by the treatment (Scenario B Figure 5.24); once a nucleation point develops a hemi-spherical pore forms around it.

In the first the amount of material lost will effectively be a two-dimensional area of skin, which is assumed to be of the same thickness in all cases, therefore the amount of material lost will be proportional to the square of the pore radius. In the latter case the problem is three-dimensional, therefore the amount of material lost will be proportional to the pore radius cubed.

There are a number of assumptions that apply to either of these cases. In the first situation it is assumed that the skin layer is two-dimensional. If the ends of the pores are close to hemi-spherical, which is likely due to the significance of surface tensions during their formation, and the radius of the pore is much larger than the skin thickness then this is a reasonable assumption. In the latter case the assumption is harder to justify. The quantity of material lost is calculated from the volume of a sphere. For this to hold true it requires the assumption that there are no pores already present in the membrane to complicate the geometry. As has been illustrated by the cross-sectional SEM images this is not true. It would not take much loss of material for the new pore to bump into an existing pore. However in the condition of high treatment concentrations and times, the final pore size is many times larger than that of the initial membrane. Therefore the presence of existing pores has to be assumed to be negligible.

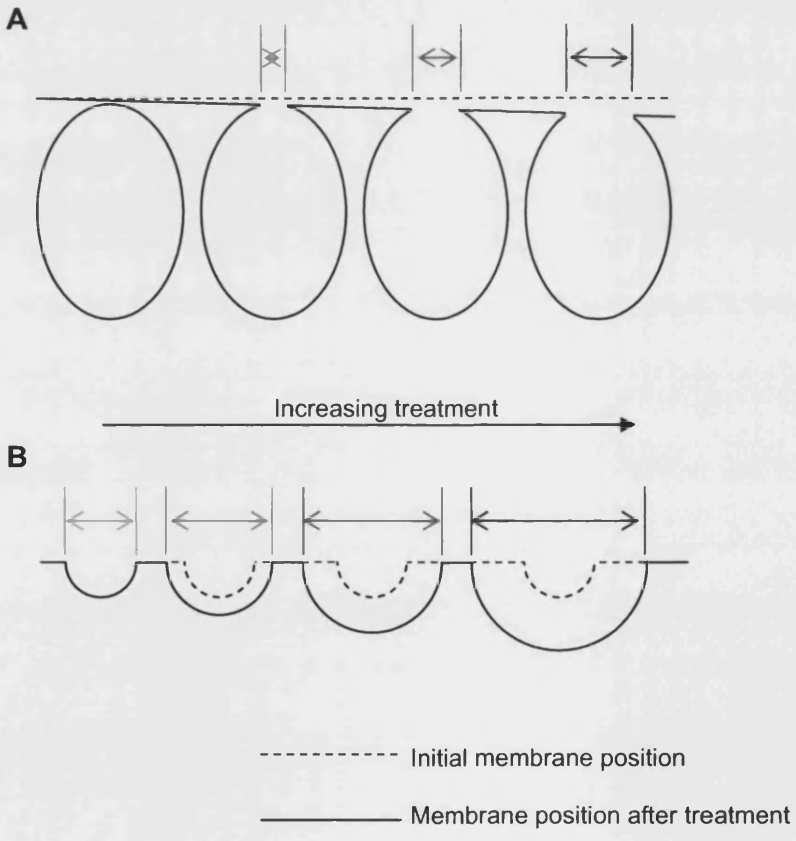

Figure 5.24 Representation of different effects of surface treatment.

***A**: Pores already exist in membrane and are revealed by removal of skin layer. **B**: Pores are formed by surface treatment.*

Figure 5.25 was plotted using change in pore size data, gathered from SEM via ImageJ (Rasband 1997-2006). For Scenario A: the change in the surface area between pores was used as an indication of reaction rate. The duration of reaction was the same in all cases so extent of reaction is synonymous with reaction rate. For Scenario B: the change in volume of what were assumed to be hemi-spherical pores, based on pore diameter, was used as an indicator for reaction rate. In Scenario A a significant linear correlation ($p < 0.01$) is found (Figure 5.25; Left) suggesting that in Case A the reaction is of first order with respect to sodium hydroxide. Scenario B fits a quadratic correlation (Figure 5.25; Right) suggesting that if the reaction is progressing by scenario B the reaction is second order with respect to sodium hydroxide.

As the PLGA is a solid the concentration of molecules available to react is defined by its exposed surface area. It is evident from Figure 5.23 the rate of mass loss with time shows no correlation between rate of reaction and duration of reaction. The exposed surface area of the membranes increases with treatment due to the opening up of the internal porous structure; therefore the lack of increase in reaction rate with increased exposed surface area suggests either the reaction is zero order with respect to PLGA, or PLGA is in excess and the sodium hydroxide is the limiting reactant. This second possibility is in agreement with the increased degradation seen with higher sodium hydroxide concentrations.

Croll *et al.* (2004) and Kirby (1972) report for lower aliphatic esters: hydrolysis in an alkaline environment is first order with respect to the hydroxide ions. This provides support for the first order reaction undergoing scenario A in Figure 5.24.

Flom and Elving (1953) report that the alkaline hydrolysis of ethyl acetate is a second order reaction overall. Combined with the conclusions from Croll *et al.* (2004) and Kirby (1972) this may be strong evidence to suppose that the alkaline hydrolysis of PLGA is also second order overall and first order with respect to either component. This suggests the membrane surface pore sizes are increasing by Scenario A in Figure 5.24; a layer of skin is being removed revealing a larger pore diameters just below the surface of the membrane.

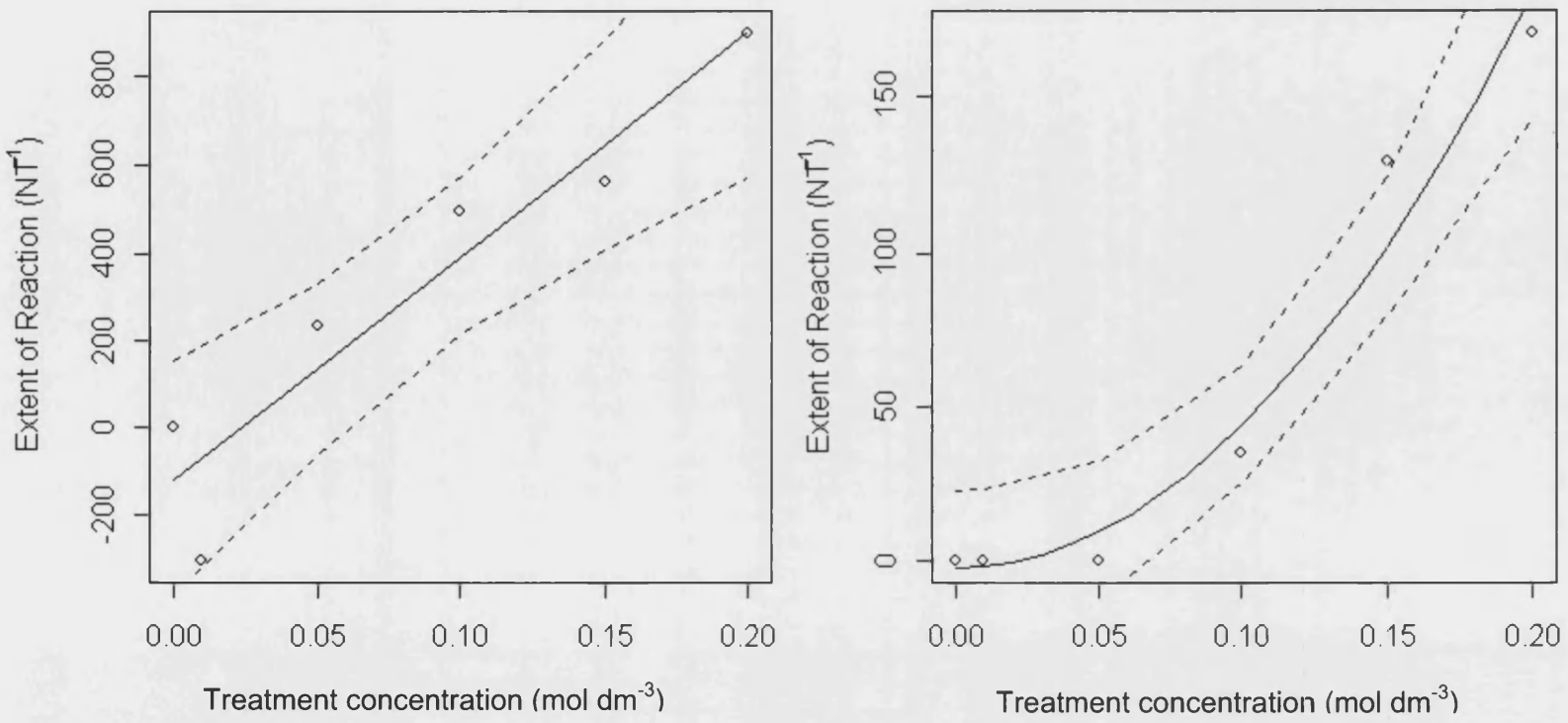

Figure 5.25 Two scatter plots showing the relationship between the extent of reaction and the concentration of the treating solution following two different proposed methodologies for the increase in pore size of the membranes.

Right *show the linear correlation between the extent of reaction and treatment concentration assuming a skin layer is removed revealing larger pores.* ***Left*** *shows the quadratic correlation between extent of reaction and treatment concentration assuming new hemi-spherical pores are created by the treatment. Points show the data gathered from treatment with Sodium hydroxide solution for 15 min. 95% confidence intervals (**dashed**) for the regression lines (**solid**) are also shown.*

5.3.5 Cell adhesion

All treatments were found to increase the adhesion of cells to the membrane. No difference was found between acid and alkali treatment; despite large differences in pore size and porosity. Increasing alkaline treatment duration and concentration was found to significantly increase cell adhesion; this correlated with increased pore size. These two factors suggest there are at least two effects resulting in increased cell adhesion.

It is possible that, although the changes in pore size and porosity were very different for the alkali and acid treatments, the changes to the surface on a much smaller scale were very similar. Zinger *et al.* (2005) find that MG63 cell attachment depends on sub-micron scale roughness. In their study adhered cell number was increased by acid etching the surface of titanium, which reportedly increases sub-micron scale roughness from 60 nm to 700 nm. The increased cell adhesion exhibited by all samples may due to microscopic changes making the surface preferable for cell adhesion.

The further increase in cell adhesion with alkaline treatment concentration may be due to an increased exposed surface area. As the surface pore size increases the diameter exceeds that of the cells allowing the cells to ingress into the porous scaffold interior.

A significant logarithmic correlation is presented for the pore size versus cell adhesion data (Figure 5.18). This correlation was fitted on the principle of parsimony; without further knowledge the simplest adequate correlation is the best. If the data is re-fitted with a correlation allowing for a critical pore diameter around which the surface area undergoes a massive expansion due to the availability of the interior surface area to cells a different conclusion may be drawn. Without further data on the exposed surface area, and the minimum diameter (or bottle-neck) leading to it, these arguments are difficult to resolve.

In the literature Lee *et al.* (2004) show MG63 cells grown on polycarbonate membrane surfaces with uniform cylindrical pores. Cell adhesion is found to be better with pore sizes of 0.2 μm and decreases with pore size increasing to 8 μm. These pores are of the same range encountered with the sodium hydroxide treatment, however increasing pore size with sodium hydroxide treatment resulted in increased cell adhesion. The finding

by Lee *et al.* (2004) means that the increased surface area associated with increased pore diameter is not the only factor influencing cell adhesion, otherwise cell adhesion would increase with pore diameter. Equally the statistical significance of cell adhesion increasing over the same range of pore sizes on the PLGA membranes provides a convincing argument that increased surface area does increase cell adhesion. The simplest explanation for this discrepancy is that the internal structure of the PLGA membrane is revealed making a much larger difference in surface area.

While Lee *et al.* (2004) found that cell adhesion was highest with pore diameters of 0.2 μm, the functionality of the cells (as shown by alkaline phosphatase and other assays) was highest on the surfaces with pore diameters in the region of 4-5 μm. This was also found by Zinger *et al.* (2005).

While increased cell adhesion is beneficial to the initiation of tissue formation if this is at the cost of the channels required to pass nutrients through the membrane this will be detrimental to the success of the bioreactor. Therefore while it is beneficial to increase cell adhesion cells must not be allowed to ingress into the scaffold interior where they will block the pathway of nutrients to cells on the exterior of the membrane.

The improved cell adhesion for the treated membranes may also be due to increased hydrophilicity of the treated membranes. The water contact angle of the membranes was seen to decrease with treatment. This indicates the hydrophilicity of the membrane increased during treatment. Increased hydrophilicity was found to correlate with treatment duration; however the effect was reduced by higher treatment concentrations. All other results indicated that increasing the treatment duration or concentration resulted in very similar effects. The reduction in increase of water contact angle was most apparent for the most extreme treatments. The water contact angle measurement requires an intact surface, however at the highest treatment concentrations and durations the skin layer was almost entirely removed. So this anomalous result may be a product of the inability to take a surface measurement when there is no surface.

5.4 Conclusions

Sodium hydroxide treatment with concentrations in the range 0.01 to 0.2 mol dm^{-3} and over the durations of 10 – 30 min resulted in significant changes to the surface of the membranes. These concentrations allow ease of use in the laboratory without undue hazards from concentrated solutions and practical durations for treatments. In agreement with literature alkaline treatment results in increased degradation over similar acidic treatment, and alkaline treatment more specifically targets the surface of the membrane.

The similarities in the increase in cell adhesion over a range of pore sizes coupled with the correlation between cell adhesion and pore size above a critical pore size shows the significance of both nano- and micro-scale surface features for these membrane structures. However the number of factors influencing cell adhesion and proliferation require that it is difficult to predict the response of cells to a particular surface and treatment combination.

Water contact angles suggest an increase in surface hydrophilicity with treatment; provided there remains a surface to test. In agreement with many reports in the literature increased lactide content in the membrane acts to slow hydrolysis of PLGA. In agreement with literature the study suggests that the reaction is first order with respect to sodium hydroxide and second order overall; suggesting it is also first order to PLGA, however as the sodium hydroxide is the limiting reagent this is difficult to prove.

CHAPTER SIX - SURFACE TREATMENT OF HOLLOW FIBRES

Modification of hollow fibre membranes to improve wetting, cell adhesion and hydraulic permeation

6.1 Introduction

An investigation into the effects of using acid and alkali solutions to selectively remove the surface of flat sheet membranes was described in Chapter Five. In this chapter similar treatments are used to treat hollow fibre membranes; identifying any specific aspects arising from the tubular form of the membrane and the skin layer on both sides of the membrane.

Both the inside and the outside of the hollow fibres are similar to the upper surface of the flat sheets (Figure 6.1). A skin layer is supported above a region of finger-like pores that are perpendicular to the membrane surface. The hollow fibres also have a lumen of the scale where surface tension may prevent the admission of the aqueous solution. The only significant difference between the two membranes in the thickness of the skin-layer, on the hollow fibres the skin layer is approximately 8 – 10 μm thick whereas the skin layer on the flat sheets is only in the region 1 – 2 μm.

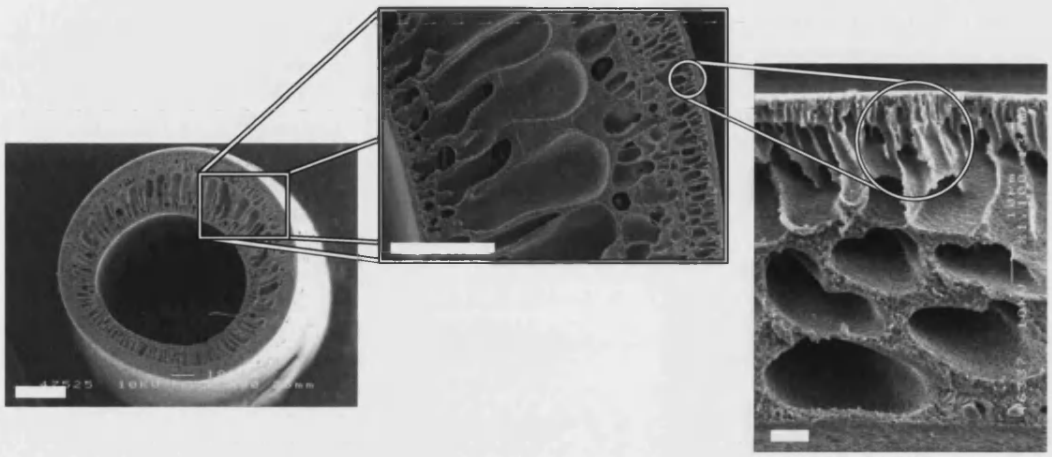

Figure 6.1 Electron micrographs of membrane cross-sections.

***Left**: Hollow fibre membrane cross-section, scale bar 200 μm. **Middle:** Section of hollow fibre membrane cross-section at higher magnification, scale bar 100 μm. **Right:** Flat sheet membrane cross-section, scale bar 10 μm. The skin-layer on the surface of the membranes and the finger-like pores perpendicular to the surface are similar on both membrane forms; as highlighted by the linked circles which are of equivalent size on the two images (diameter ~ 30 μm).*

Considering the bioreactor as a whole, the hollow fibres have to support cells growing on their exterior while allowing the passage of nutrients through the fibre wall, without filtering out essential ingredients. The bioreactor offers the potential to treat the surface of the fibres *in situ* preventing the need to handle the fibres following treatment. This will not only reduce any potential damage to the fibres by handling once their protective skin-layer is removed. It also means that any potential contamination is reduced; any bacteria on the surface of the membranes are likely to be destroyed by the surface treatment agent (either a strong acid or a strong alkali) prior to sterilization.

6.1.1 Methodology

The conclusions of Chapter Five suggested that the sodium hydroxide treatment offered the greatest potential of the treatments tested as a surface treatment agent for PLGA membranes. However, the cell adhesion study showed the relevance of the nano- or micro-scale features on cell adhesion to the membranes is not completely understood.

Therefore in this chapter hollow fibres have been treated with both sodium hydroxide and hydrochloric acid which offer examples of treatments with very different magnitudes of effect. No difference was found to result from different acids or different alkalis so the fibres are only tested with one acid and one alkali.

The hydraulic permeation of the flat sheet membranes were not tested, this was because the entire membrane was not considered to be sufficiently similar to the hollow fibres to make a useful comparison. This is an important characteristic of the hollow fibre membranes that will be affected by the surface treatment so the hydraulic permeation of the membrane is also tested in this chapter. The hydrophilicity of the scaffold is likely to affect both its hydraulic permeation and the ability of cells to adhere to the scaffold. The fibres do not provide a flat surface suitable for testing the water contact angle, consequently the hydrophilicity of the fibres was determined by testing the water absorption.

It is important to anticipate the degradation rate of the scaffold in order to match it to the growth of the nascent tissue. The viscosity average molecular weight of the fibres is compared before and after treatment with sodium hydroxide and with the raw polymer used to make the fibres in order to evaluate any loss in half-life following treatment with sodium hydroxide or the fibre preparation process.

Cell attachment studies were not carried out on the hollow fibre membranes as there is no reason to believe there would be a different response compared to the flat sheets. The purpose of this study is to improve the aspects of the membrane relating to mass transfer through the membrane.

6.2 Results

6.2.1 Acid and alkali treatment of hollow fibres

6.2.1.1 Surface morphology

SEM images of the surface of the hollow fibres treated with acid and alkaline solutions show a similar response to that of the treated flat sheets (Figure 6.2 to Figure 6.6). The fibres all show rows of pores aligned along the length of the fibre on both the interior and exterior surfaces. This may be an effect of the extrusion process during their

formation. There is no significant difference between the distance between pores in adjacent rows and pores in the same row with the mean inter-pore distance 0.7 ± 0.3 μm for pores in the same row and 0.7 ± 0.3 μm for pores in adjacent rows (mean ± S.D., n = 10). There is also no significant difference between the inter-pore distance on the hollow fibres and the flat sheets with the inter-pore distance for the flat sheets 0.8 ± 0.4 μm (mean ± S.D., n = 10).

As with the flat sheet membranes the effect of the hydroxide on the membranes far exceeds the effects of the acid, which show very little change from the control. The pore size and porosity of the membranes treated with sodium hydroxide is seen to increase with increasing treatment concentration and duration as was found with the flat sheet membranes. The fibres consistently show increased changes to the exterior of the fibre over the interior; this is particular apparent on the membranes treated with sodium hydroxide where the changes to the membrane are much more severe. There is much more variation shown on the interior surfaces; in some a similar level of change is found as the relevant exterior, however some show little change from the control. This effect may be due to surface tension preventing the treatment solution from entering the fibre lumen in some of the samples.

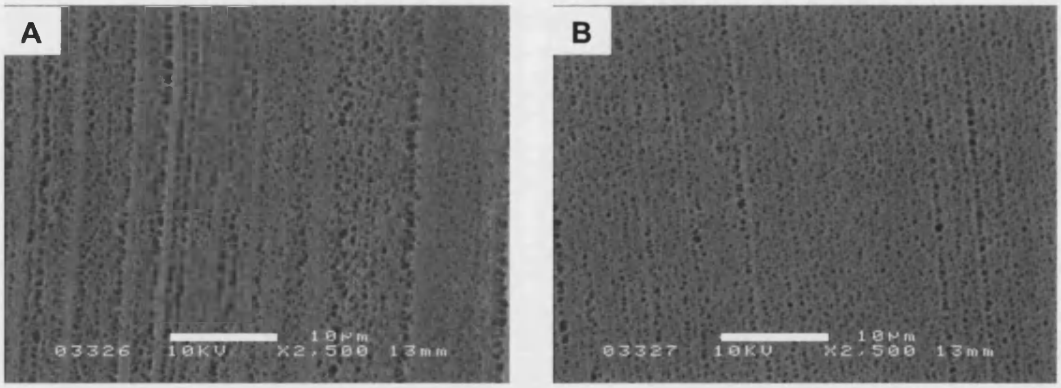

Figure 6.2 Electron micrographs of the surfaces of untreated hollow fibres.

*A: interior surface. **B**: exterior surface. Scale bar 10 µm. Both surfaces of the hollow fibres look similar. In contrast to the flat sheet surfaces the pores on these surfaces appear to be aligned along the length of the fibre.*

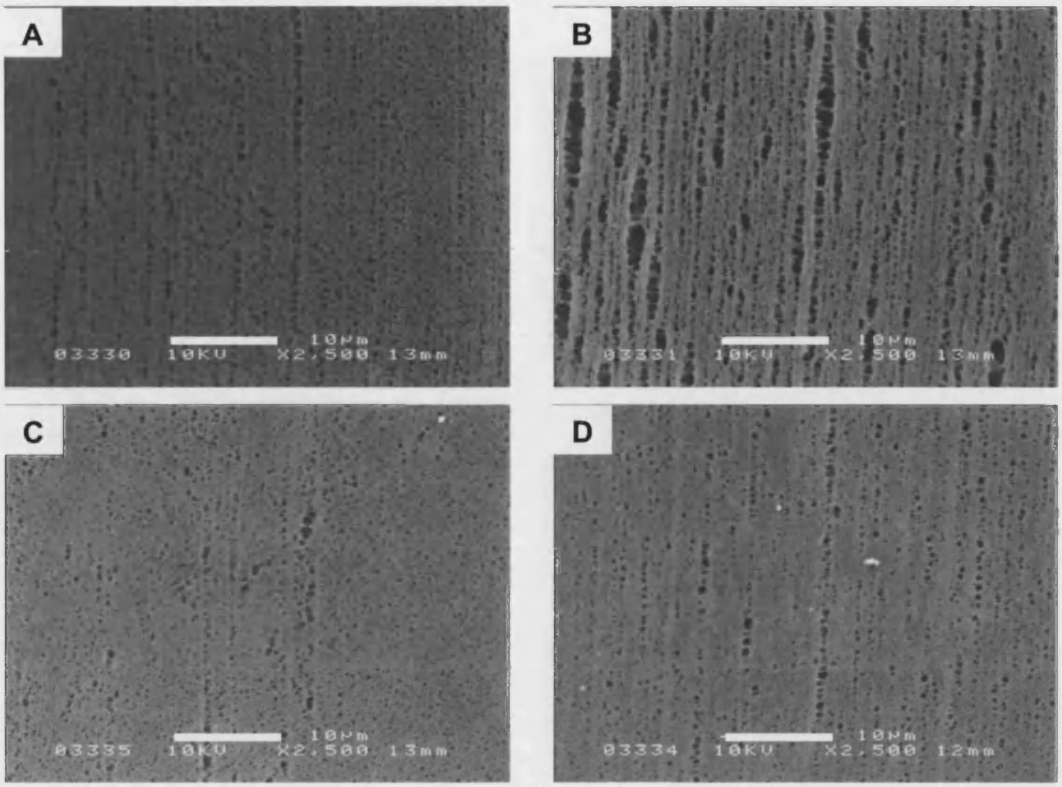

Figure 6.3 Electron micrographs of surfaces of hollow fibre membranes treated with 0.1 mol dm^{-3} HCl for 15 min (A and B) or 30 min (C and D).

A and C *show the interior of the fibres,* ***B and D*** *show the exterior of the fibres. Scale bar 10 μm. Little change is seen over the control fibres.*

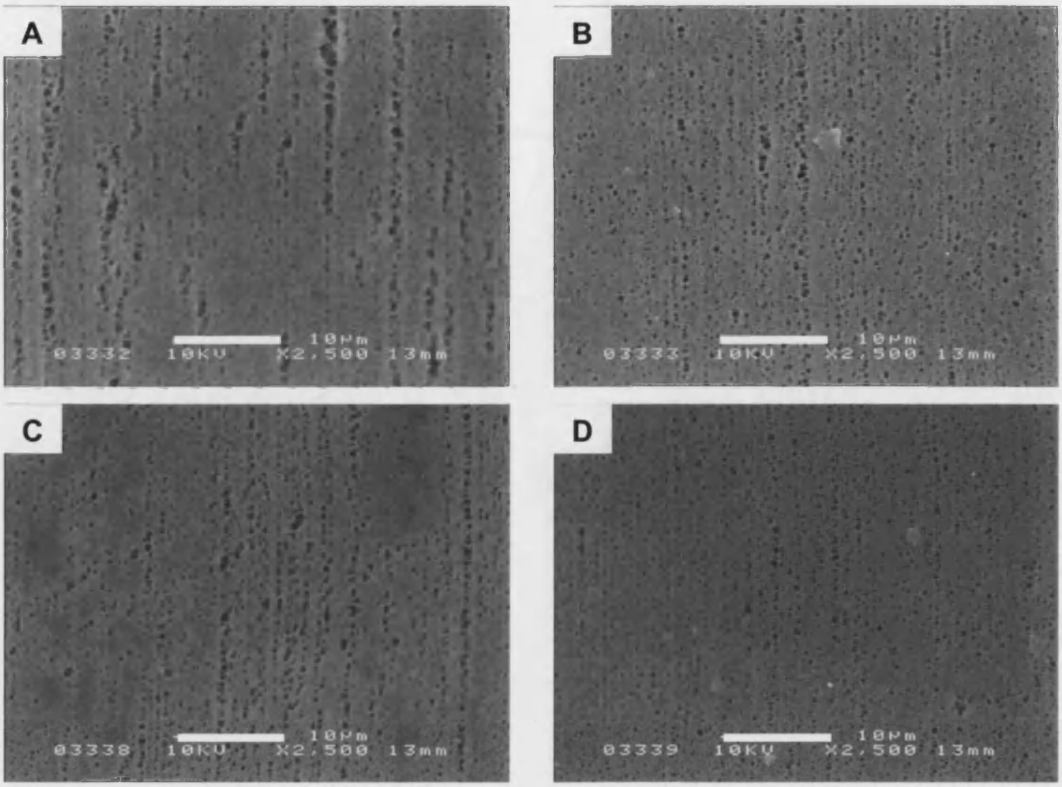

Figure 6.4 electron micrograph of surfaces of hollow fibre membranes treated with 0.2 mol dm^{-3} HCl for 15 min (A and B) or 30 min (C and D).

A and C *show the interior of the fibres,* ***B and D*** *show the exterior of the fibres. Scale bar 10 μm. Little change is seen over the control fibres or the fibres treated with 0.1 mol dm^{-3} HCl solution.*

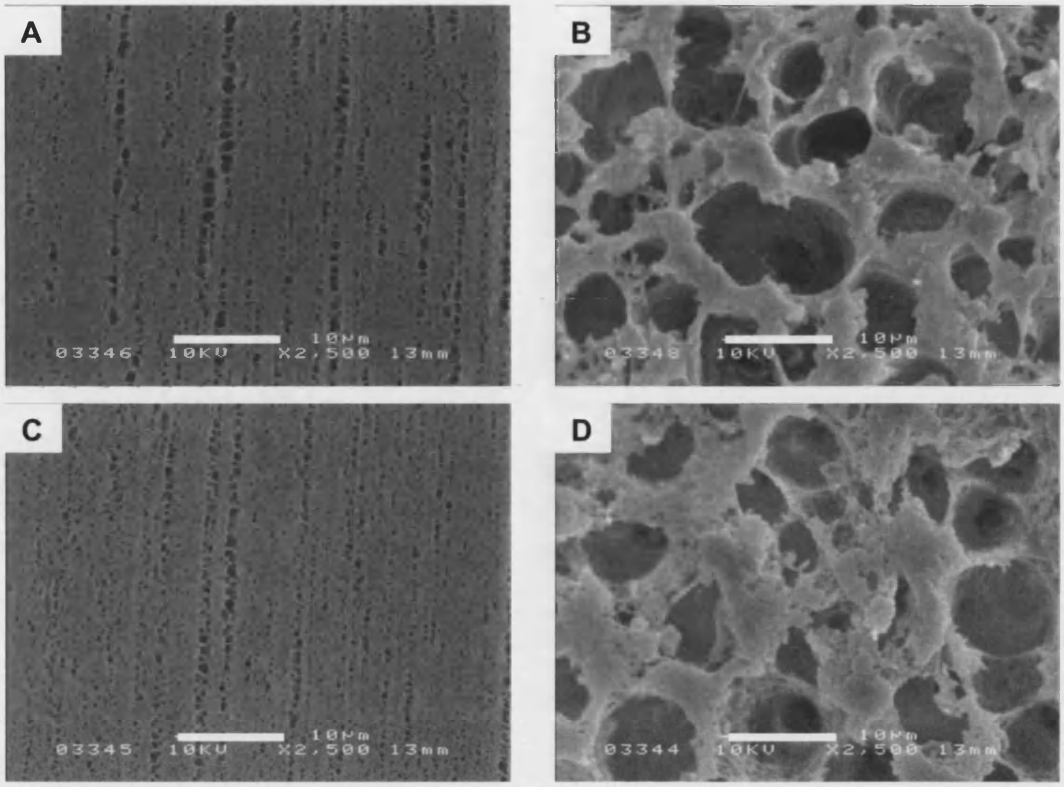

Figure 6.5 Electron micrograph of surfaces of hollow fibre membranes treated with 0.1 mol dm^{-3} NaOH for 15 min (A and B) or 30 min (C and D).

A and C *show the interior of the fibres,* ***B and D*** *show the exterior of the fibres. Scale bar 10 μm. A marked difference is seen on the exterior of the fibres with a much larger and more irregular pore structure visible. Little change has occurred to the interior of the scaffolds.*

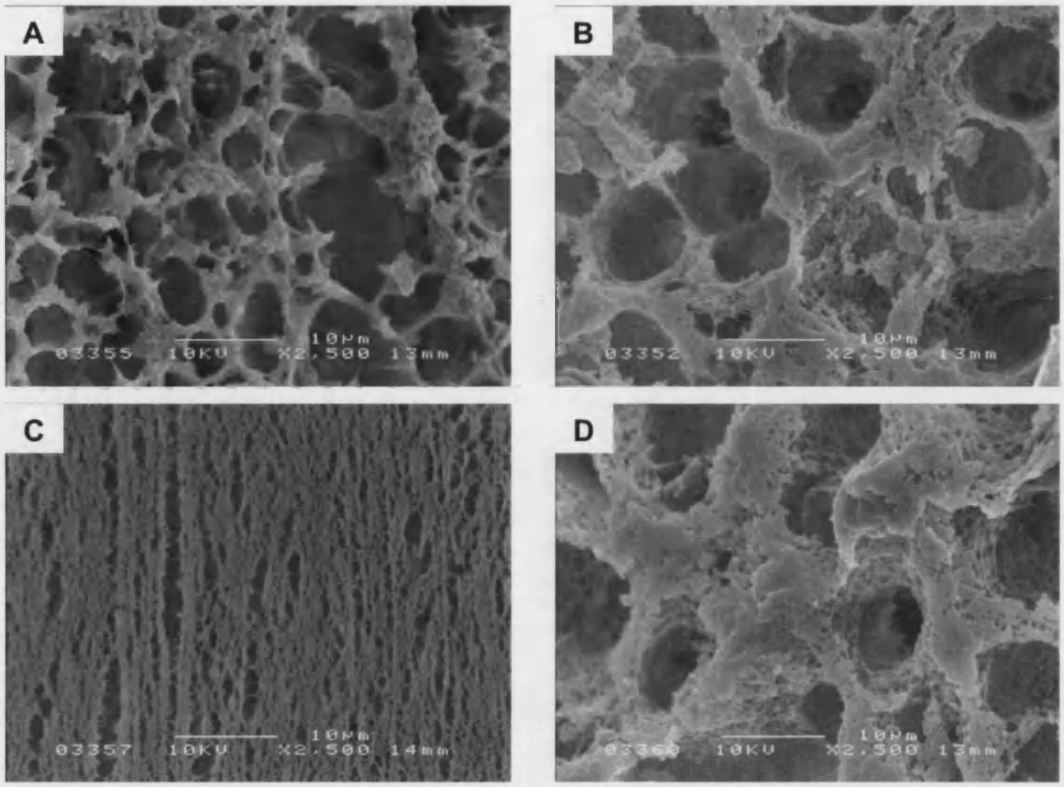

Figure 6.6 Electron micrograph of surfaces of hollow fibre membranes treated with 0.2 mol dm^{-3} NaOH for 15 min (A and B) or 30 min (C and D).

A and C *show the interior of the fibres,* ***B and D*** *show the exterior of the fibres. Scale bar 10 μm. As with the samples treated with 0.1 mol dm^{-3} NaOH solution a large difference is seen on the exterior of the fibres in comparison with the control. Here the shorter treatment duration has also resulted in a change to the interior surface, however no change is observed with the longer treatment duration.*

6.2.1.2 Pore size and porosity

Figure 6.7 shows the quantitative data from the image analysis of the SEM pictures (effective pore diameter is the diameter of a circle of the same area as the pore). Here, as with the flat sheets, the sodium hydroxide treatment is shown to result in a bigger difference in pore size than the hydrochloric acid treatment. Also the difference in the effects on the inside and the outside of the hollow fibres is highlighted; the results shown indicate that only the 0.2 mol dm^{-3}, 15 min sodium hydroxide sample exhibited much change from the control.

There is little difference in the pore sizes of the interior and exterior of the untreated fibres. Following treatment the exterior of the fibres show large pores and a larger range of pore sizes over the interior.

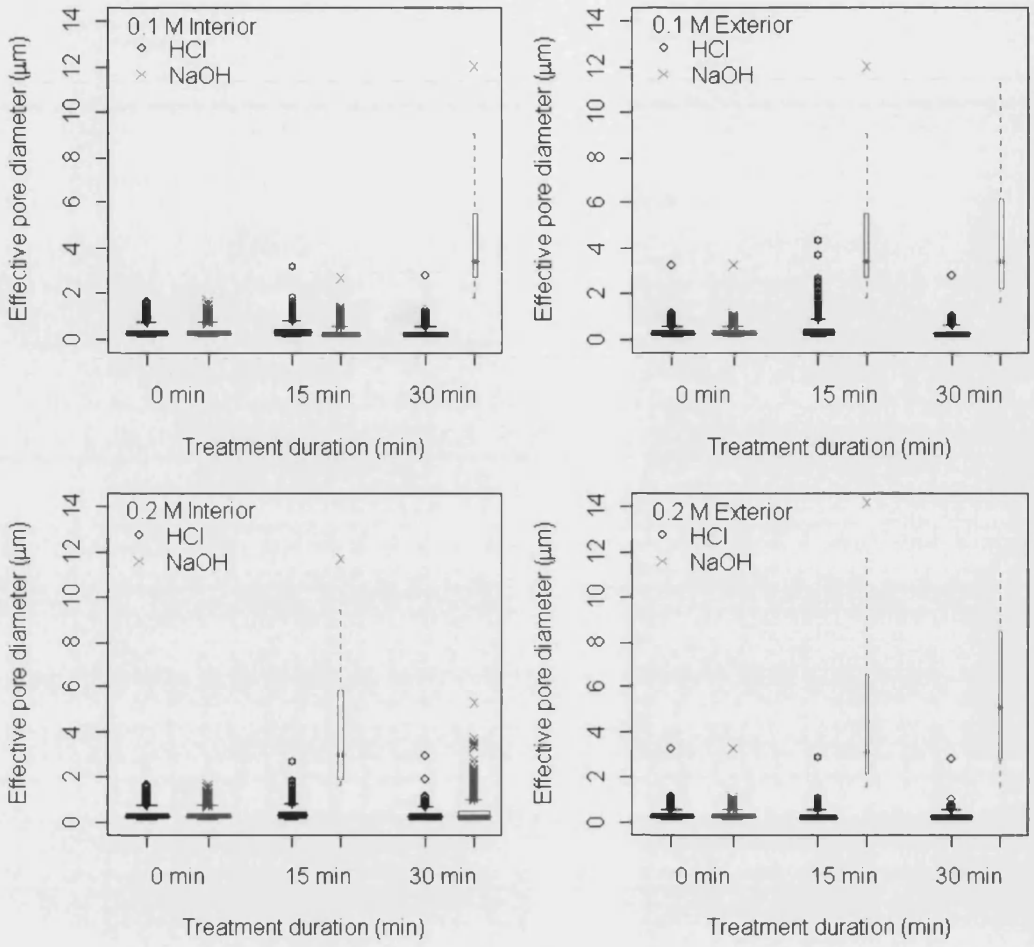

Figure 6.7 Series of box and whisker plots showing the effective pore diameter of hollow fibres following treatment.

*Pore diameters of the interior (**left hand column**) and exterior (**right hand column**) of hollow fibres treated for a range of durations with 0.1 mol dm^{-3} (**top row**) and 0.2 mol dm^{-3} (**bottom row**) sodium hydroxide (**gray**) and hydrochloric acid (**black**) solutions. Boxes show the inter-quartile range, the thick bar shows the median; whiskers show minima and maxima. Outliers (data more than 1.5 times the inter-quartile range above or below the quartiles) are shown as points. The width of the boxes is proportional to the square root of the number of pores.*

Figure 6.8 shows the geometric mean pore size (refer to Section 5.2.1.2) against the duration and concentration of treatment for both the interior and the exterior surfaces of the fibres. Only the exterior surface treated with sodium hydroxide showed a statistically significant correlation with treatment duration (as shown by the plane), treatment concentration was not found to correlate with pore size for any of the treated surfaces.

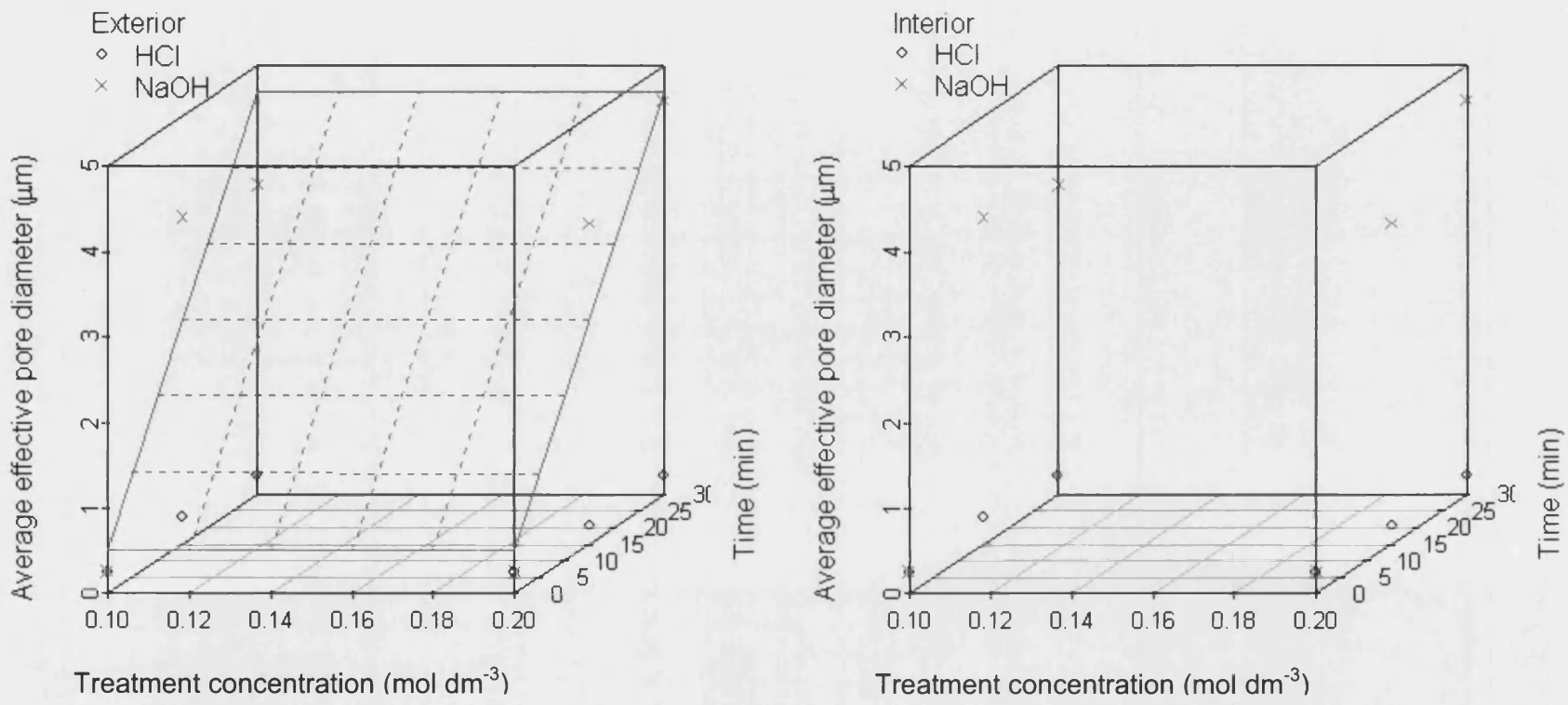

Figure 6.8 Three-dimensional scatter plots showing the relationship between average effective pore diameter and treatment concentration and duration.

*Pore diameter against concentration and duration of treatment for the exterior (**left**) and interior (**right**) of the hollow fibre membranes. The trend plane shown for the exterior is the significant ($p < 0.001$) interaction between treatment type and duration for the sodium hydroxide treated samples. No other significant effects were found by multiple regression. Points represent single data points.*

The porosity results mirror the pore size data with a very similar pattern to the graphs presented above.

6.2.1.3 Hydrophilicity

Figure 6.9 shows the results of a water absorption following treatment for 15 min in 0.1 mol dm^{-3} solutions. In addition to treatment with acid and alkali solutions the samples were also treated with ethanol and water. Ethanol is known to act as a hydrophilic agent and so is a useful comparison, however the effects of ethanol on the structure of the fibre (as documented in Chapter Four) make it an unsuitable treatment. The samples treated with water were to check whether any additional absorption was due to increased duration in an aqueous environment to absorb water. The only significant difference was found with the sodium hydroxide sample, suggesting the increased porosity and hydrophilicity, as indicated by the results given above and in Chapter Five for pore size and water contact angle, increase the intrusion of water into the membrane.

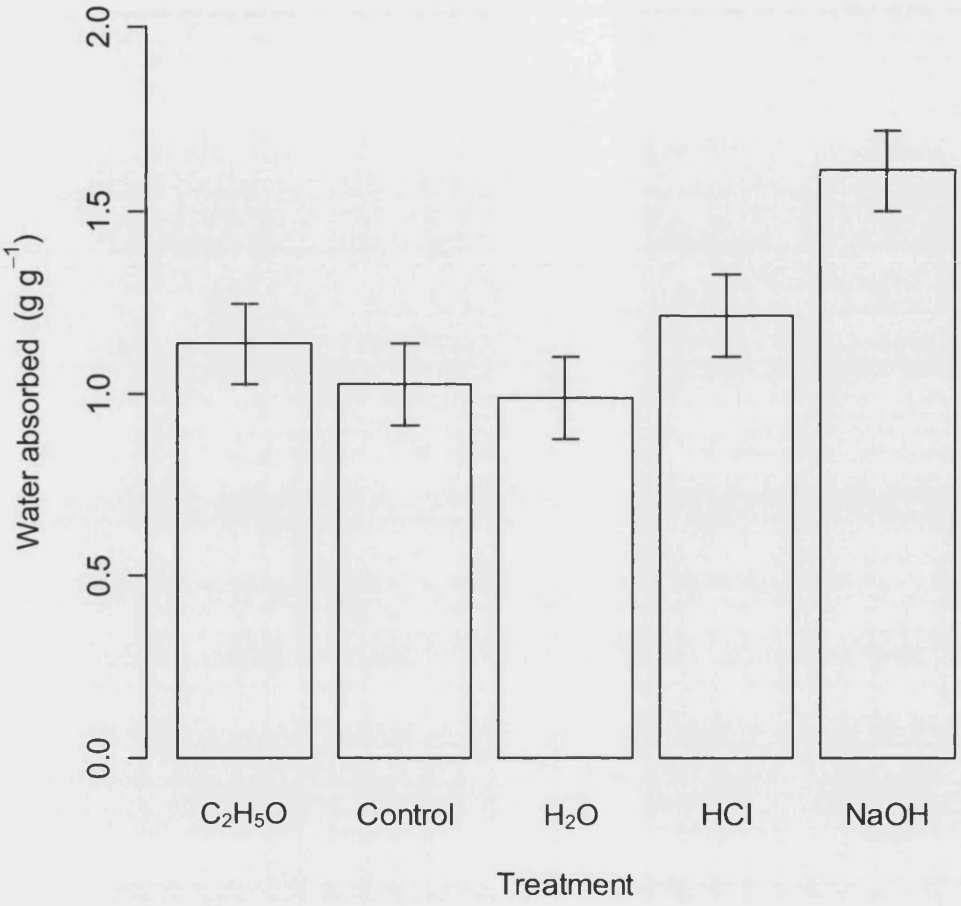

Figure 6.9 Bar chart showing the mass of water absorbed during a 48 h soaking period in distilled water by 50:50 PLGA hollow fibres following treatments of different 0.1 mol dm^{-3} solutions for 15 min.

Values are standardized to the initial mass of polymer (g water per g initial polymer mass) and presented as mean ± least significant difference; n = 6. Overlapping error bars indicate no significant difference; non-overlapping error bars indicate significant difference.

Table 6.1 Details of contrast significance.

Tukey's honest significant difference test.

Contrast	p	Significance
Control-H_2O	9.99E-01	
C_2H_5OH-H_2O	8.03E-01	
HCl-H_2O	4.65E-01	
NaOH-H_2O	7.87E-04	**
C_2H_5OH-Control	9.17E-01	
HCl-Control	6.27E-01	
NaOH-Control	1.54E-03	*
HCl-C_2H_5OH	9.78E-01	
NaOH-C_2H_5OH	1.21E-02	.
NaOH-HCl	4.52E-02	.

Significance codes: * = 0.0001, ** = 0.001, * = 0.01, . = 0.05**

6.2.1.4 Hydraulic permeability

Untreated fibres and fibres treated with hydrochloric acid were found to result in no hydraulic permeation. A period where no permeation occurred was followed by a sudden increase in apparent permeate collected; the use of a dye revealed this to be a result of a single fibre failure. However it is interesting to note: apart from usually a single pin-hole or fracture type fibre failure the fibre appearance changed very little over 3 or 4 days in the hollow fibre bioreactor (HFB) with both lumen and ablumen charged with water.

The sodium hydroxide treated samples behaved very differently. The fibres were treated and then soaked in distilled water (3 changes) to remove any remaining sodium hydroxide, they were then placed in the HFB rig and the ablumen charged with water. The pump passing water through the lumen was started. Within 30 min small air bubbles could be seen on the surface of the fibre. It is likely these bubbles resulted from water flowing into the fibre wall from the higher pressure lumen, displacing the residual air to the lower pressure ablumen.

Following a period of fibre wetting, where the bubbles were seen to appear and then stop forming as the fibre became fully wet, hydraulic permeation measurements were taken over a range of trans-membrane pressures. The details of which are presented in Figure 6.10. Multiple regression found there was no significant difference between samples treated for 15 or 30 min or different samples of the same treatment. A significant quadratic correlation between trans-membrane pressure difference and hydraulic permeation was identified. The equation of the line is given in Equation 6.1 (estimate ± standard error).

$$\dot{m}_w = (-3.74 \pm 10.7) \times 10^{-5} + (9.89 \pm 1.85) \times 10^{-8} P^2 \qquad \textbf{Equation 6.1}$$

$\dot{m}_w$ = Mass flow rate of water ($L^{-2}MT^{-1}$; kg s^{-1} m^{-2})

P = Trans-membrane pressure difference ($L^{-1}MT^{-2}$; Pa)

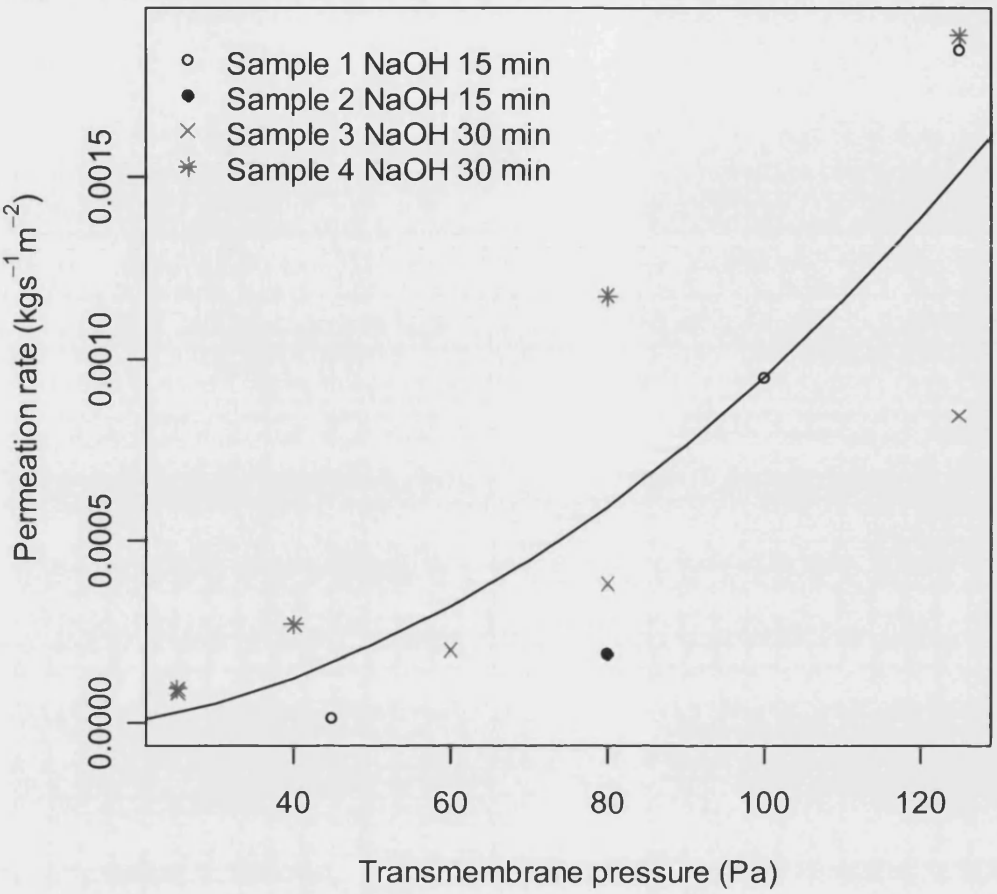

Figure 6.10 Scatter plot showing rate of water permeation through hollow fibre membranes. *Membranes were treated with 0.2 mol dm^{-3} sodium hydroxide for 30 min or 15 min. Samples 1 and 2 represent different samples where varying trans-membrane pressures were achieved by a combination of changing pump rpm and throttling flow with a needle valve. Points represent single data values, the significant correlation is shown by a* ***solid line.***

In the case of the treated fibres it was noticed after two or three days of continual hydraulic permeation the fibres became very distorted; as shown by the difference between Figure 6.11 and Figure 6.12. Initially the fibres are predominantly aligned and lying close to one another. After a period of permeation, the fibres were found to become distorted with regions with 90° bends and fibres swollen to more than twice their original diameter. Adjacent fibres were also found to fuse together. SEM images (Figure 6.13) revealed the changes to the fibre wall following a period of permeation. Initially distinct fibre walls became fused together in a homogenous structure, where no

difference could be found at the fused region and the finger-like pore structures were found to be more irregular. The overall structure appeared less porous.

Another effect pertinent to the treated fibres in the bioreactor was discovered when the fibres were treated *in situ*. When the fibres were rinsed, following treatment, and left in water in preparation for hydraulic permeation testing the treated fibres would snap. This was seen repeatedly for treated fibres but never for the wetting process of untreated fibres. This suggests the effect was in some way due to the sodium hydroxide treatment. If the fibres were treated, rinsed and dried, prior to potting into the bioreactor this problem was not encountered.

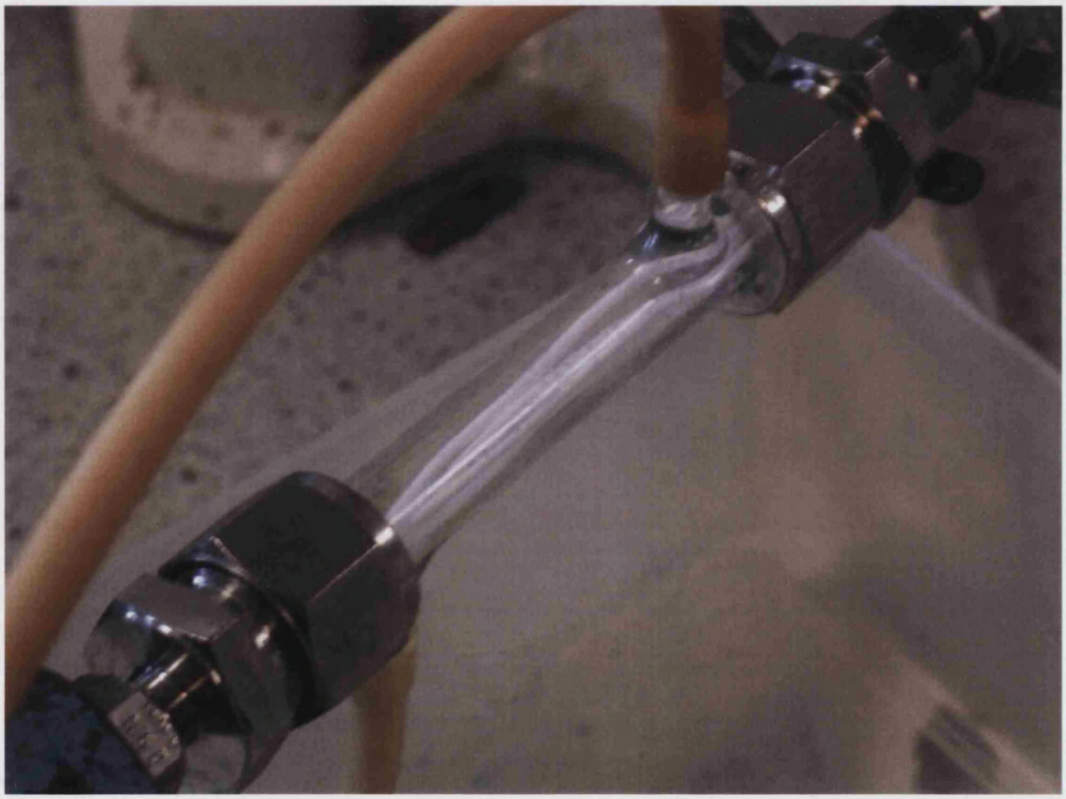

Figure 6.11 New fibres.

Photograph of bioreactor rig before permeation has started. Fibres are aligned in a bundle at the centre of the bioreactor. Bioreactor is 10 cm long.

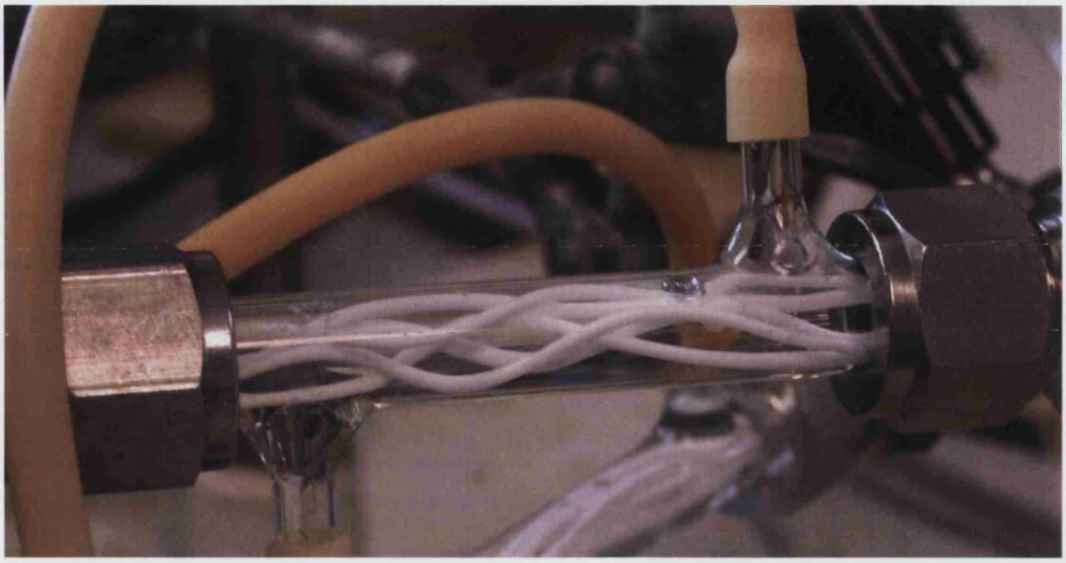

Figure 6.12 Distorted fibres.

Photograph of bioreactor rig after permeation. Fibres have become distorted showing increased curvature and swelling. Bioreactor is 10 cm long

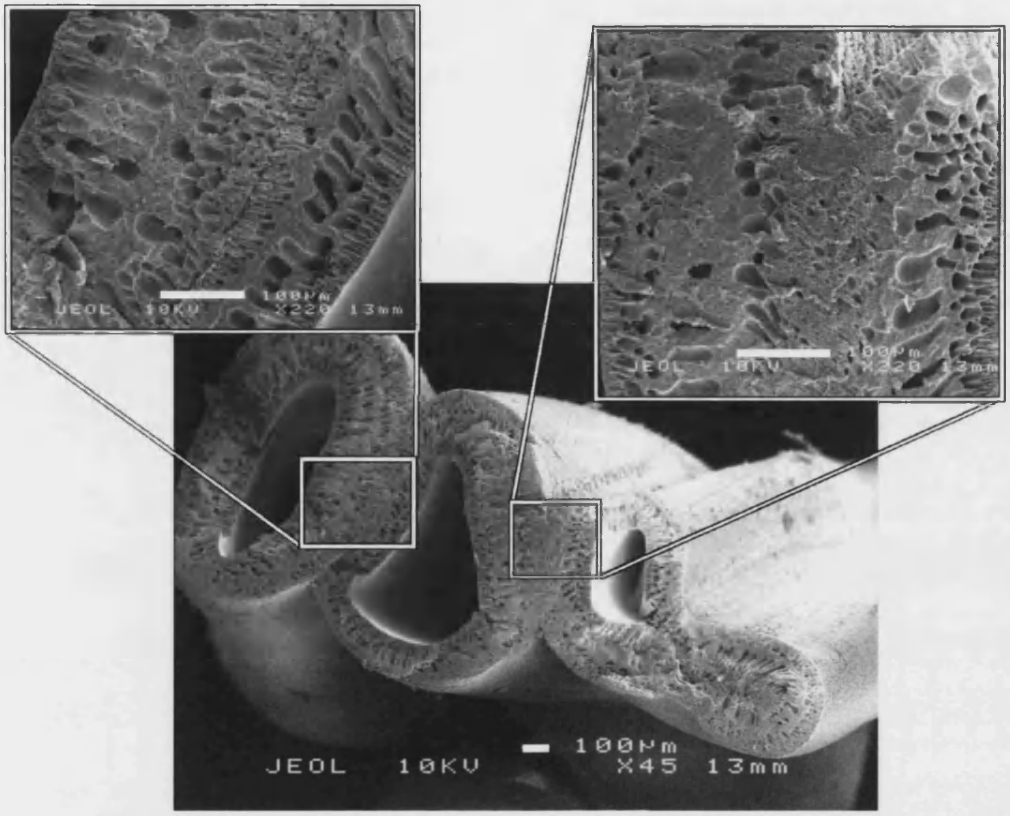

Figure 6.13 Electron micrograph of hollow fibres after hydraulic permeation.

Showing regions were adjacent fibres have fused together making one fibre wall indistinguishable form the next. Scale bar is 100 μm.

6.2.1.5 Viscosity average molecular weight

Low concentration solutions were made from the raw polymer, hollow fibres, flat sheets and sodium hydroxide treated hollow fibres in order to test the intrinsic viscosity of the polymer initially, after formation into membranes and following treatment. The viscosity of the low concentration solutions showed small deviations from Newtonian behaviour but these were deemed to be within the tolerances of the experiment. An average viscosity over a range of shear stresses was used for comparison with the solution concentration in order to determine the intrinsic viscosity.

The viscosity-concentration data was analysed with ANCOVA and revealed no significant difference between the different samples. This suggests that there is no significant loss in molecular weight during these processing stages and the surface treatment has successfully resulted in surface erosion rather than bulk degradation.

A significant exponential correlation was found between the concentration of the solution and the viscosity. The data and the correlation are shown in Figure 6.14 and the equation of the correlation is given in Equation 6.2 (estimate ± standard error).

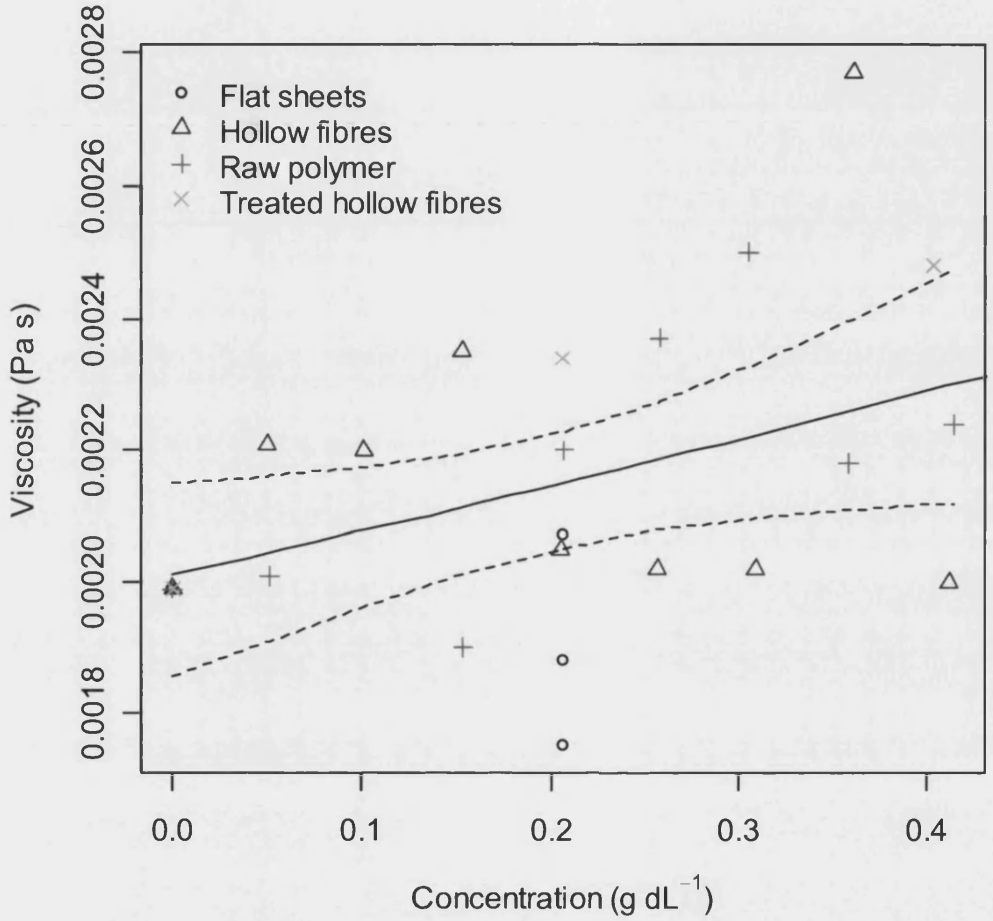

Figure 6.14 Scatter plot showing viscosity against concentration relationship for low concentration solutions from different polymer forms.

Low concentration solutions were made by re-dissolving the scaffold in NMP. Points represent single data values and the exponential regression line is presented as a ***solid line,*** *the* ***dashed lines*** *show the 95% confidence interval. The data shows a large degree of variance but no significant difference between the sample types.*

$$\mu = (2.0 \pm 2.8) \times 10^{-3} e^{(0.33 \pm 0.15)C} \qquad \textbf{Equation 6.2}$$

μ = Viscosity ($L^{-1}MT^{-1}$; Pa s)

C = Solution concentration ($L^{-3}M$; g dL^{-1})

The equation fits the form of the model proposed by Thomas and Thomas (1960) (Equation 6.3) for the variation of viscosity with concentration for higher polymers.

$$\mu = \mu_s e^{[\mu]c} \qquad \textbf{Equation 6.3}$$

μ_s = Solvent viscosity ($L^{-1}MT^{-1}$)

$[\mu]$ = Intrinsic viscosity (L^2M^{-1})

From this it can be seen that the experimental data is in good agreement with the viscosity of the solvent (μ_{NMP} = 2.01 × 10^{-3} Pa s, Sigma-Aldrich 2004). From the correlation the intrinsic viscosity of the polymer is found to be 0.33 ± 0.15 dL g^{-1} (estimate ± standard error).

The effect of the treatment on the degradation properties of the scaffold was monitored by a two week degradation study under cell culture conditions. Figure 6.15 shows the mass of the scaffolds following the degradation period as a percentage of the initial scaffold mass. There was a small difference between the sodium hydroxide treated sample and the control, suggesting the sodium hydroxide treatment underwent a slightly increased rate of degradation. However was only just on the border of what would be considered statistically significant. This could well be explained by the increase in diffusion of water into the scaffold due to the increased porosity.

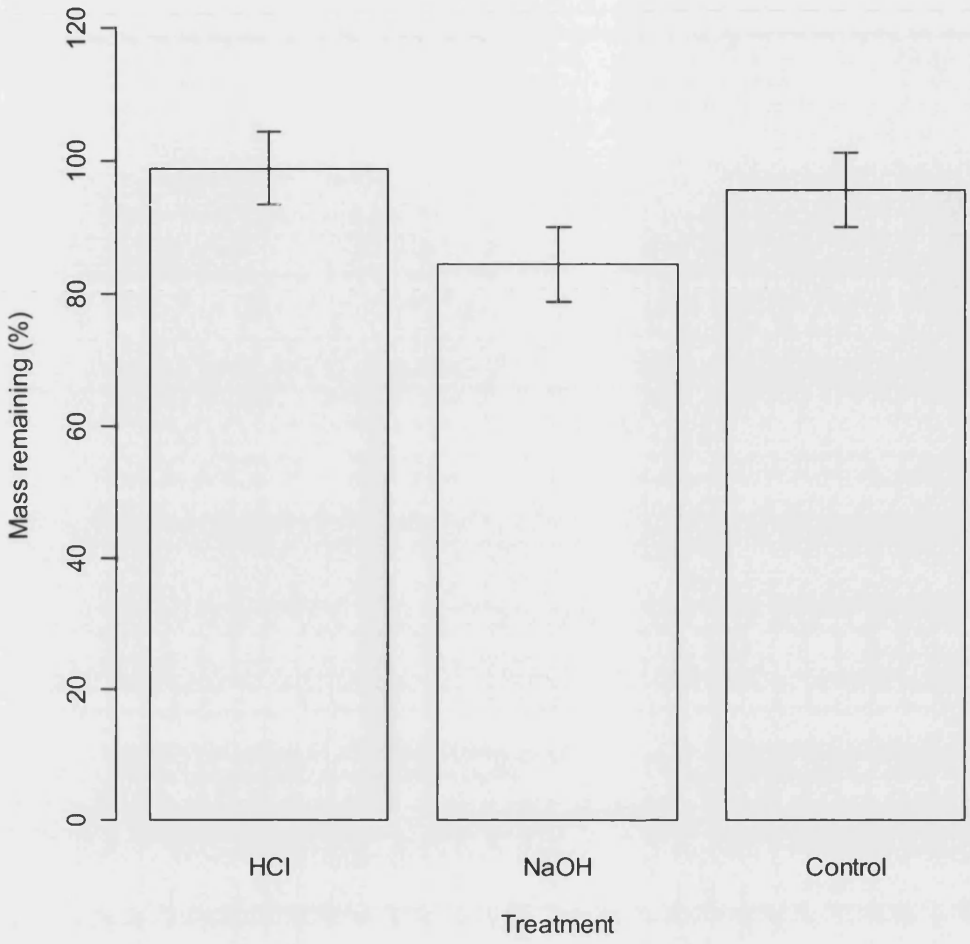

Figure 6.15 Bar chart showing the difference in mass of treated scaffolds degraded for 2 weeks under cell culture conditions.

Hollow fibres and flat sheets scaffolds were tested; the form of the scaffold was not found to significantly affect the mass of the remaining scaffold. The least significant difference error bars all overlap showing there is no significant difference between the control and the treated samples (mean ± lsd; n=6).

6.2.2 Summary of results with comparisons to Chapter Five

Table 6.2 Summary of results from surface treatment of both flat sheets and hollow fibres.

↗ = *significant proportional trend.* ↘ = *significant inversely proportional trend.* - = *No significant trend.* ***N/A*** = *Interaction not investigated.*

Parameter		***Permeation***	***Water adsorption***	***Cell attachment***	***Pore size***	***Porosity***	***Mass***	***Water contact angle***
Treatment type	NaOH KOH HCl $HClO_4$	NaOH: ↗ HCl: -	NaOH: ↗ HCl: - C_2H_5OH: - H_2O: -	NaOH: ↗ HCl: ↗ $HClO_4$: ↗ KOH: ↗	Alkali: ↗ Acid: -	Alkali: ↗ Acid: -	NaOH: ↘	NaOH: ↗
Conc. of treatment	0.2 0.15 0.1 0.05 0.01	0.1 mol dm^{-3}: - 0.2 mol dm^{-3}: ↗	N/A	↗ (logarithmic)	FS: ↗ HF: -	↗	N/A	↘ (result may be anomalous)
Duration of treatment	30 15 0	-	N/A	N/A (expected ↗ from pore size data)	↗	↗	↘	↗
Membrane composition	85:15 65:35 50:50	N/A	N/A	-	↘	N/A	N/A	↘
Membrane form	HF FS	N/A	N/A	N/A	-	-	N/A	N/A

6.3 Discussion

6.3.1 Structure of hollow fibre scaffolds

The hollow fibres exhibit a similar structure to the flat sheet membranes due to the similar processes involved in their manufacture. Figure 6.1 illustrated the similar structures of the two membranes; the only significant difference being the thickness of the skin layer which is up to five times thicker on the hollow fibre membranes. Another difference when the surfaces of the membranes are examined under the electron microscope is the arrangement of pores on the surfaces of the membranes, while the flat sheets exhibit an apparently random distributions of pores across the surface of the membranes in the hollow fibres the pores are arranged in parallel lines that are orientated along the length of the fibres. It is likely that these occur as a result of the extrusion process prior to phase-inversion precipitation. It is unlikely that this regular pore arrangement will have a significant effect on the use of the fibres in the bioreactor as the distance between rows of columns is not significantly different to the distance between pores in a single row; the mean inter-pore distance on both membrane types is very similar.

As polymer is extruded through the spinneret, to form hollow fibres, the solution is exposed to high shear rates as it flows past the walls and through the orifice of the spinneret; these can reach up to a maximum of about 5000 N m^{-2} (refer to Chapter 8, especially Figure 8.2). The theory in the literature suggests these high shear rates can cause the long polymer molecules to align, as the solution is then immediately immersed in the water bath; the polymer molecules remain in a highly aligned formation resulting in a dense skin layer which is likely to show an increased level of crystallization compared to the rest of the scaffold (Qin *et al.* 2001). The alignment of molecules on the surface of the hollow fibre will reduce the rate of diffusion of the non-solvent into the polymer solution during fabrication reducing precipitation and resulting in a larger skin layer and smaller pores. In contrast the flat sheets investigated in Chapter Five experience lower shear rates as the solution is spread across the glass plate. The shear stress caused by spreading the polymer solution into a flat sheet is in the region of 0.8 N m^{-2} (details in A.5); in addition there is a few seconds between the polymer being spread out on the glass plate and it being submerged in the water bath,

this gives the polymer molecules to relax into the lowest energy structure. In this experiment despite the huge difference in the value of the shear stress experienced by the polymer during membrane fabrication very little difference in pore size was observed; in fact the observed difference was in the other direction to that suggested by the literature (pores were larger for the hollow fibres) this difference was not found to be statistically significant. Table 6.3 summarizes the differences between the hollow fibre and flat sheet membranes.

Table 6.3 Summary of the similarities and differences between hollow fibres and flat sheets.
The tope surface of the flat sheets and the surfaces of the hollow fibres undergo similar conditions during manufacture and consequently share some characteristics.

Property	***Hollow fibres***	***Flat sheets***
Structure	Finger-like pores extending from inner and outer surface.	Finger-like pores extending from top surface with lower region exhibiting a random pore structure with larger void spaces.
Surface	Double skin (inside and outside).	Single skin (top).
Pore arrangement	Regular in lines aligned with length of fibre.	Randomly distributed.
Shear stress during formation	~ 5000 N m^{-2}	< 1 N m^{-1}
Molecular orientation	Aligned in skins due to high shear stresses.	No alignment due to low shears.
Membrane thickness	~ 300 μm	~ 250 μm
Skin thickness	~ 10 μm	~ 1 – 2 μm
Pore size	Inside ~ 0.25 μm outside ~ 0.25 μm	~ 0.23 μm (top)
Inter-pore distance	0.3 μm	0.4 μm

The exterior of the fibres show a similar pattern of change as was found with the flat sheets, when treated with acid and alkali solutions. The interior of the fibres shows a much more varied pattern of change with treatment. The degree of change of the interior pores appears to be unrelated to the degree of treatment (with increasing solution concentration and treatment duration and sodium hydroxide all leading to higher degrees of treatment; as revealed in Chapter Five) it can be hypothesized that the interior of the fibres is not consistently exposed or unexposed to the treatment solution due to restriction of access to the interior surface of the fibres by the treatment solution due to surface tension effects.

The purpose of increasing the porosity and pore size of the membrane is to achieve greater transfer of nutrients while still providing a suitable scaffold to support the cells. A narrow pore size range is required to maximize the pore size for mass transfer, while remaining under a pore size that would allow the ingress of cells into the fibre wall. A narrow pore size distribution will also help to reduce spatial variation in mass transfer through the membrane. The results show that all the sodium hydroxide treatments result in a large increase in the pore size distribution with the maximum pore size increasing by a factor of six or seven over the controls. However, the results show that this can be easily augmented through the use of lower durations.

The study on hollow fibres found no correlation between treatment concentration and pore size; a significant linear correlation was found for the same variables on the flat sheets. The treatment duration was found to increase the average effective pore diameter on the hollow fibres in the same way it had on the flat sheets. It is likely that the difference in effect with increasing concentration is due to the thicker skin layer on the hollow fibre membranes, it is possible over a different range of concentrations of treatment solution a similar correlation would be found.

While there is some degree of uniformity between effect of treatments on hollow fibres and flat sheets at the lower concentrations and durations of treatment this is found to be less proportional as treatments and concentrations increase. As the extent of the treatment effect increases the interior of the scaffold becomes revealed; showing the differences between the two structures.

6.3.2 Intrinsic viscosity

The intrinsic viscosity of the fibres before and after treatment was measured as an indicator for the type of degradation occurring to the scaffold. Intrinsic viscosity is a good indicator for molecular weight as longer polymer chains tend to increase the viscosity of a solution more than shorter polymer chains. The viscosity average molecular weight lies somewhere between the number average molecular weight and the weight average molecular weight but is typically closer to the weight average molecular weight.

The result of no significant difference in the intrinsic viscosity of the scaffold suggests no significant change in the molecular weight of the scaffold. This result is encouraging towards the use of a sodium hydroxide solution to selectively treat the surface of the membrane. If the membrane was undergoing bulk degradation a change would be expected in the overall molecular weight, which would have been picked up by a change in the intrinsic viscosity. Instead the result supports the hypothesis that the solution is only breaking down the molecules on the surface of the scaffold, as this is occurring the smaller chains become released from the scaffold resulting in no change to the overall molecular weight.

The Staudinger index is used to relate intrinsic viscosity to molecular weight. This is given by the Mark-Houwink equation (Equation 6.4).

$$[\mu] = K \times M_W{}^{\alpha} \qquad \textbf{Equation 6.4}$$

$[\mu]$ = Intrinsic viscosity ($L^{-1}MT^{-1}$)

K, α } Constants (specific to the solvent and temperature at which the intrinsic viscosity was determined) (-)

M_W = Molecular weight (-)

Mark-Houwink constants could not be found to relate intrinsic viscosity to molecular weight for this exact polymer solvent system (50:50 PLGA and NMP), however a range of data on similar systems is given in Figure 6.16.

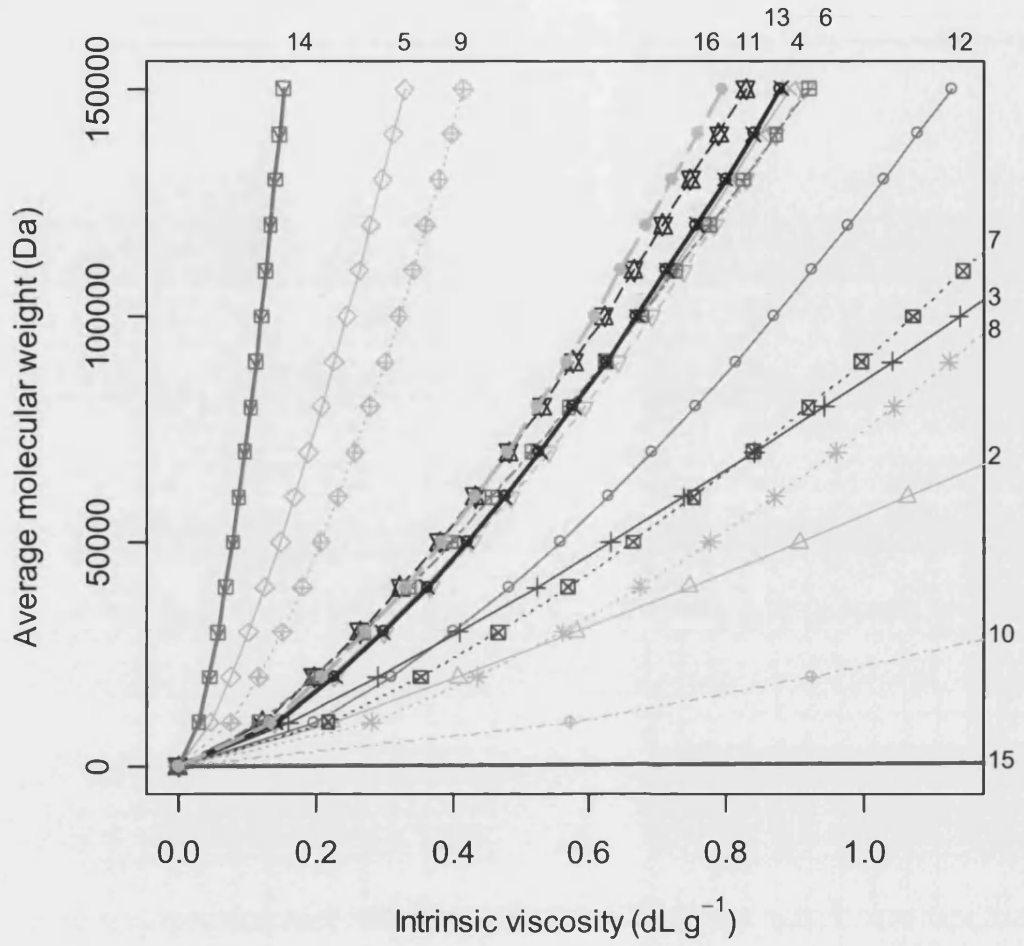

Figure 6.16 Chart showing the relationship between intrinsic viscosity and molecular weight for systems documented in the literature.

Numbers around the edge are used to identify the lines in Table 6.4 where the reference source and constants are given along with the solvent and type of PLGA. ***Thin solid lines:*** *PLA;* ***Short dashed lines:*** *85:15 PLGA;* ***Dotted lines:*** *75:25 PLGA;* ***Short-dash dot lines:*** *70:30 PLGA;* ***Long dashed lines:*** *65:35 PLGA;* ***Long-dash dot lines:*** *60:40 PLGA and* ***Thick solid lines:*** *50:50 PLGA. The solvents are:* ***Light grey****: -- hexafluoroisopropanol;* ***Grey:*** *-- dimethylformamide;* ***Dark grey:*** *-- tetrahydrofuran and* ***Black:*** *-- chloroform.*

Table 6.4 Details of lines on Figure 6.16

Due to similarity between lines, ID numbers are used to identify lines on the chart as well as lines. ***CF*** *= chloroform,* ***DMF*** *= dimethylformamide,* ***THF*** *= tetrahydrofuran,* ***HFIP*** *= hexafluoroisopropanol, * refer to Equation 6.4*

ID	Type	Ratio	Solv.	$K \times 10^4$ *	α *	Ref.	Av. MW
1○	PLA	-	THF	5.49	0.64	Schwarz and Epple 1999	Visc.
2△	PLA	-	CF	0.74	0.87	Schwarz and Epple 1999	Visc.
3+	PLA	-	DMF	0.64	0.85	Schwarz and Epple 1999	Visc.
4×	PLA	-	CF	2.39	0.69	Durect 2006	Weight
5◊	PLA	-	CF	0.55	0.73	Lu *et al.* 2000b	Weight
6▽	PLGA	85:15	CF	2.45	0.69	Durect 2006	Weight
7⊠	PLGA	75:25	DMF	3.80	0.69	Schwarz and Epple 1999	Visc.
8✳	PLGA	75:25	CF	8.5	0.63	Schwarz and Epple 1999	Visc.
9◈	PLGA	75:25	CF	2.28	0.63	Durect 2006	Weight
10⊕	PLGA	70:30	CF	9.96	0.69	Schwarz and Epple 1999	Visc.
11✡	PLGA	65:35	HFIP	1.75	0.71	Durect 2006	Weight
12⊞	PLGA	60:40	THF	1.07	0.76	Kenley *et al.* 1987	Unknown
13⊗	PLGA	50:50	HFIP	2.99	0.67	Durect 2006	Weight
14☒	PLGA	50:50	THF	1.07	0.61	Schwarz and Epple 1999	Visc.
15■	PLGA	50:50	DMF	50.5	0.88	Schwarz and Epple 1999	Visc.
16●	PLGA	Generic	CF	3.04	0.66	Biomaterials 2005	Weight

Figure 6.16 and Table 6.4 show the huge range in values for the coefficients in the Mark-Houwink equation. Part of this disparity is due to different molecular weights

being quoted; constants are given as coefficients of both viscosity and weight average molecular weights and it is not always specified to which molecular weight the constant refers. The difference between the two definitions of molecular weight is a characteristic of the polymer being tested meaning there is no easy way to compare the two.

The measured value of 0.33 ± 0.15 dL g^{-1} for the intrinsic viscosity of the polymer was well below the value of 0.77 dL g^{-1} reported by the manufacturer on the certificate of analysis (COA) for the polymer (Biomaterials 2006). The initial molecular weight of the polymer is reported to be 72.3 kDa on the manufacturer's COA. The molecular weight based on the measured intrinsic viscosity, according to Figure 6.16, could be any where in the range of 0 - >> 150 kDa. Despite considerable doubt remaining over the absolute values of the intrinsic viscosity and the molecular weight there is no evidence to suggest that the intrinsic viscosity and molecular weight changing as a result of the surface treatment. These findings are in agreement with Burkersroda *et al.* (2002) who reported that alkaline degradation was found to result in no reduction in molecular weight; indicating the prevalence of surface erosion.

If the scaffolds are undergoing surface erosion there is less potential for the treatment to result in detrimental increases in the rate of degradation of the scaffold under use that would be expected with a decrease in the bulk molecular weight. This is found to be true by the very little difference seen in the mass of scaffolds following a two period cell culture conditions.

6.3.3 Water absorption and permeation

The results from the water absorption study are very positive; the increased water absorption by the sample treated with sodium hydroxide suggests a significant increase in hydrophilicity of the surface. This could be due to the larger pore sizes allowing the water to pass into the scaffold. The degradation process occurring at the surface of the membrane would also expose a greater number of carboxyl and hydroxyl end groups which may act to increase the hydrophilicity of the membrane.

The effects following hydraulic permeation and treatment of the fibres *in situ* are a major cause of concern. No hydraulic permeation was possible with the untreated fibres

with increasing pressure or duration resulting in the fibres bursting. The treated fibres did allow water to permeate through the walls, however they were found to distort after only a short period in the hydraulic permeation rig. Attempts to treat the fibres *in situ* resulted in fibre breakages. If the fibres do not remain intact within the bioreactor the foundation of the bioreactor is destroyed. There are a number of possible explanations for this phenomenon. The simplest explanation is that the fibres contain small flaws that are not visible to the naked eye but result in the failure of the fibre under operation. In the situation of the untreated fibre in the hydraulic permeation test the permeant will find the path of least resistance, in a fibre punctuated with flaws these flaws will allow passage of the permeant ahead of the less permeable intact fibre. In the case of the fibre completely severing following treatment *in situ* the existing flaw in the fibre is further weakened by the treatment, elastic potential in the fibre which is held taught at either end results in the fibre breaking at the point of the flaw.

The presence of flaws existing in the fibres will have to be dealt with during the manufacture of the fibre. It has been observed that small bubbles in the polymer solution can result in holes in the fibre wall. While a degassing stage is incorporated in the preparation process in an effort to remove the possibility of holes forming in this way it is possible that it is not completely successful. In a scaled-up process this specific functionality could be incorporated into the system design to prevent the entrapment of gas into the polymer solution on passage through the spinneret.

6.4 Conclusions

There are three important findings in this chapter. These are all positive towards the use of sodium hydroxide as a surface treatment agent for PLGA hollow fibres for use in a bone tissue bioreactor. These are that the treatment results in an increase in water absorption suggesting increased hydrophilicity of the membrane, increased hydraulic permeation over a value of zero, and no significant loss of molecular weight as determined through intrinsic viscosity measurement.

The intrinsic viscosity measurement has given a good indication that the treatment does not result in a significant change to the molecular weight of the scaffold. This suggests

that other than the more open structure, which may increase the rate of degradation, the degradation profile of the scaffold *in vitro* or *in vivo* should not be unduly affected.

The treatment also successfully increased the absorption of water into, and permeation of water through, the walls of the membrane; however this was accompanied by distortion to the fibres. As no permeation was achieved with the untreated fibres it is unknown whether the distortion was a result of the water permeating through the fibres or particular to the fibres treated with alkaline solutions.

The only cause of concern is the fragility of the fibres in the bioreactor. This is thought to be related to the presence of small bubbles entrained in the polymer solution during spinning. Greater care to de-gas and prevent the entrapment of air into the polymer solution combined with careful examination of the fibres prior to use should reduce the potential of fibre failure.

7

CHAPTER SEVEN – EFFECT OF OPERATING ENVIRONMENT AND TIME ON POLYMER SCAFFOLDS

An investigation into influences of the operating environment and time on hollow fibre, flat sheet and spherical PLGA scaffolds

7.1 Introduction

Degradation of the polymer fibres is a key aspect of the hollow fibre bioreactor; as the fibres degrade the environment within the reactor will change.

In biomedical engineering the distinction between degradable and non-degradable materials is made dependant on whether degradation is taking place within the useful life of the device or substantially after the useful life has ended (Göpferich 1996). In tissue engineering it is important that degradation of the scaffold mirrors the growth of new tissue and therefore occurs during the useful life of the scaffold.

It is widely accepted that the predominant mechanism of degradation of PLGA is hydrolytic degradation, as shown in Figure 5.2. However there are reports suggesting that enzymatic degradation processes play varyingly important roles in the whole degradation process. Williams 1992 shows that in synthetic arteries made from poly(ether urethane) a more open porous structure allowed greater ingress of cells into the scaffold which increased degradation. This could also be due to the ability for autocatalytic degradation products to more easily diffuse out of a more porous structure as discussed below. However the author refers to his previous work, where carbon-14 was used to show significant enzyme activity in the *in vitro* degradation of polyester,

polyamide and polyurethane substrates, to suggest that the increased degradation is due to the presence of cells. Vert *et al.* (1992) suggest that while enzymatic processes are not directly responsible for degradation, hydrolysis is an equilibrium process, so if enzymes are involved in the removal of degradation products they will change the equilibrium and therefore the rate of hydrolysis. A further suggestion made by Williams (1992) is that inflammatory responses, such as activation of macrophages and phagocytosis, result in an increase in oxygen consumption, known as a respiratory burst, which releases a number of free radicals. Williams hypothesizes that while these species are only short lived, their continual generation at an implant surface may effect degradation. This effect is likely to be amplified by increased degradation leading to increased cellular response, which in turn will lead to increased degradation.

Even without the complication of cells the degradation process is not simply modelled. A number of groups have also shown the significance of autocatalysis on degradation processes (Deng and Uhrich 2002; Agrawal *et al.* 2000). High porosity structures exist for longer than those with lower initial porosities due to higher porosity allowing catalytic degradation products to be removed from the interior of the scaffold. Non-porous samples result in heterogeneous degradation due to increased degradation at the centre (Deng and Uhrich 2002). Placing scaffolds under flow has been shown to reduce degradation by removing catalytic degradation products (Agrawal *et al.* 2000). This however is somewhat contradictory to the suggestion made by Vert *et al.* (1992) that the removal of degradation products will tip the equilibrium of the process more in the direction of degradation.

As the polymer ages there are several effects that have been reported. Typically the term degradation refers to a chemical process resulting in the reduction of the average molecular weight. However, with time there will also be erosion which is a physical process whereby mass is lost from the sample by solubilization of polymer chains and their removal from the vicinity. The remaining polymer will swell as water is absorbed and crystallinity and lactic acid content will increase due to the removal of glycolic acid at a faster rate than lactic acid. Increased rates of degradation associated with glycolic acid over lactic acid are due to steric hindrance; the approach of the water molecule is hindered by the presence of the voluminous alkyl group (Göpferich 1996). The removal of glycolic acid has been reported to be as twice as fast as that of lactic acid from a

sample of 50:50 PLGA (Göpferich 1996). Increased crystallinity is in part due to increased degradation of amorphous regions and in part of the production of crystallized oligomers from the degradation of larger molecules (Göpferich 1996, Li *et al.* 1990c). 50:50 PLGA has a faster degradation rate than compounds containing any other ratio of lactic to glycolic acid; this is thought to be caused by its lower crystallinity allowing greater absorption of water into the structure.

It has also been shown that both the melting temperature and glass transition temperature of the polymer will change with degradation. The glass transition temperature has been shown by Deng and Uhrich (2002) and Wen and Tresco (2006) to reduce form a value around 50°C to below 37°C meaning that *in vivo* the polymer will change from glassy to amorphous structure as the glass transition temperature drops below that of body temperature. Mechanical properties of the scaffold will also change; mechanical stresses during degradation have also been shown to result in increased loss of breaking stress during degradation (Williams 1992).

Significant changes to the properties of the scaffold often are associated with the onset of erosion. Often little change is seen in the first few weeks as degradation will result in a loss of molecular weight but the overall integrity of the structure will remain. As erosion starts the removal of material from the scaffold, significant losses in mass and mechanical properties are observed. For ideal surface erosion, erosion rate is directly proportional to external surface area; for flat sheets where the external surface area remains constant so does the erosion rate. However Tamada and Langer (1993) showed two polymer disks (14 mm diameter), one twice the thickness of the other, completely eroded in the same time, suggesting it is the volume not the surface area which is significant for PLGA which is a characteristic sign of bulk erosion.

Kenley *et al.* (1987) hypothesizes that the reason there is no particular dependence on the solution pH is because the pH caused by the degradation is much lower than the difference in the pH of the test conditions, and therefore the pH of the solution is changed as soon as degradation begins. However a study by Lu *et al.* (2000a) found 50:50 PLGA foams degraded faster *in vivo* than *in vitro* which they put down to the limited removal of catalytic degradation products. They also found that differences in

porosity were more significant in the faster degrading 50:50 PLGA than in slower degrading 85:15 PLGA.

A significant finding by Kenely *et al.* (1987) validates the *in vitro* testing carried out by a number of groups. These workers found no significant difference between degrading samples *in vivo* or *in vitro* suggesting the *in vitro* response gives good indication of what will happen *in vivo*.

The most relevant study to this work was carried out by Wen and Tresco (2006) on 50:50 PLGA hollow fibres. Wen and Tresco degraded the fibres under static conditions in PBS, the fibres were reported to show no observable weight loss in the first two weeks, the fibres retained structural integrity until week 4 and by week 8 the fibres had completely disappeared. In contrast to non-porous pellets that were degraded in the same way, the fibres were found to degrade homogeneously.

7.1.1 Methodology

This chapter investigates the changes the scaffold will undergo during operation under culture conditions and how these can be influenced through use of different scaffold structures, lactide content and intrinsic viscosities to optimize the scaffold for cell growth and nutrient transfer. In order to make the conditions as similar to those in cell culture the membranes were sterilized, treated with foetal calf serum (a process used to increase cell adhesion) and placed in complete cell culture media in an incubator (for further details refer to Section 3.5). The fluid was replaced twice weekly as would be necessary for cell culture. Evidence of changes to the scaffold will therefore accumulate within in the flask between changes.

While the effects of scaffold internal structure (porosity) have previously been investigated in relation to degradation, the effects of external scaffold architecture and surface area have not been investigated. This investigation will also consider how the operating conditions will affect the properties of different shape scaffolds where the cell-scaffold construct cannot be considered to be on average homogeneous, and changes to the scaffold will affect both the support and the nutrient delivery to the cells.

7.2 Results

The physical properties of the scaffolds were measured before and after a two week culture period, and in the case of the volume of the scaffold, during the culture period. The two week duration was chosen as a compromise. The duration must be long enough to result in changes to the scaffold pertinent to its use as a bone tissue engineering scaffold, but not result in too extensive degradation that would make the measurement of the physical properties of the scaffold too difficult. When used as a tissue engineering scaffold the cells will be laying down their own scaffold matrix providing extra support as the polymer scaffold degrades. A preliminary study over a two week period indicated the scaffolds showed visual signs of degradation and were just becoming difficult to handle, suggesting a longer period would mean the scaffolds were very difficult to analyse.

Although it is likely the liquid containing the polymer will also change as a result of polymer degradation, for example in terms of pH, there are no results presented on changes to the liquid. The reasons for this are explained in Appendix B.2.2.

The changes to the physical properties of the polymers were evaluated in a number of situations. The influences of the properties of the polymers pertinent to changes occurring when exposed to operating conditions were evaluated through the use of different polymers, details of which are given in Table 7.1 (these can be related to details of the manufacturer in Table 3.1). The influence of the polymer type was evaluated concurrently with scaffold form; three scaffold forms offering a range of initial scaffold porosities and surface area to volume ratios were analysed, these were hollow fibre membranes flat sheet membranes, and spherical particles. These samples were all held in cell culture conditions; submerged in complete cell culture media and incubated at 37 °C and 5% CO_2. A single polymer type (PS5050) was used to investigate the effect of environmental conditions such as temperature (20 °C or 37 °C) and fluid (cell media or water) on the sample, all three scaffold forms were evaluated. To investigate the effects of flow and cells on the polymer only a single polymer type (PS5050) and only hollow fibres were investigated.

The results are presented divided into sections based on the physical properties evaluated. Within each section the three different investigations: polymer and scaffold influences, environmental conditions, and effects unique to the hollow fibre bioreactor are dealt with in turn.

Table 7.1 Details of initial properties of polymers and scaffold used in study.

ID = identification code, L= lactide content, IV = intrinsic viscosity, MW = molecular weight, COA = cert. of analysis, test = test result, μ = viscosity of sol. Conc = concentration of sol. OD = outer diameter, ID = inner diameter, YM = Young's modulus, HF = Hollow fibre, FS = flat sheet, S = sphere. (Mean ± S.D, where applicable)

ID	L (%)	IV (dL g^{-1}) COA (test)	MW (kDa) COA (test)	μ (Pas)	Conc (%)	Fibre (mm) OD	Fibre (mm) ID	Porosity (%)	Mass (mg)	Volume x 10^8 (m^3)	YM (GPa)	Pore diameter (μm)
RG503	51	0.42 (0.38)	(56)	1.0	26.2	1.4	0.8	HF: 70 ± 4 FS:81±0.6 S: 79 ± 4	HF: 14 ± 1 FS: 32 ± 1.4 S: 28 ± 3.5	HF: 3.3 ± 0.1 FS: 11.8±0.9 S: 1 ± 0.1	3.5 ± 1.3	HF Interior: 0.45 HF Exterior:0.44 FS: 0.44
RG504	51	0.56 (0.32)	(55)	1.4	23.7	1.4	0.8	HF: 38±23 FS:78 ± 2 S: 65 ± 2	HF: 13 ± 0.5 FS: 9 ± 4.4 S: 23 ± 2.3	HF: 1.6 ± 0.5 FS: 9.3 ± 1.1 S: 0.5 ± 0.1	1.75 ± 0.7	HF Interior: 0.46 HF Exterior:0.43 FS: 0.48
PS5050	54	0.72 (0.41)	17-22 (67)	1.2	23.6	1.3	0.8	HF: 51±13 FS: 86 ± 2 S: 71 ± 2	HF: 12 ± 3 FS: 17 ± 6.7 S: 27 ± 0.6	HF: 1.7 ± 0.5 FS: 8.9 ± 2.6 S: 0.7 ± 0	6.5 ± 6.8	HF Interior: 0.49 HF Exterior:0.44 FS: 0.46
LS5050	53	0.67	(148)	0.6	20.0	1.4	0.7	HF: 68±12 FS: 83 ± 2 S: 64 ± 5	HF: 9 ± 0.5 FS: 20 ± 4.7 S: 32 ± 0	HF: 2.1 ± 0.6 FS: 8.9 ± 2.1 S: 0.7 ± 0.1	4.5 ± 1.6	HF Interior: 0.46 HF Exterior:0.47 FS: 0.51
D7525	76	1.12 (0.41)	(171)	1.2	20.0	1.4	0.8	HF: 48±13 FS: 89 ± 2 S: 81 ± 1	HF: 10 ± 0.5 FS: 11 ± 0.6 S: 21 ± 1.5	HF: 1.5 ± 0.3 FS: 7.4 ± 0.8 S: 0.8 ± 0.1	5.5 ± 5.6	
D5050	52	0.68 (0.16)	(125)	1.3	16.2	1.3	0.7	HF: 70 ± 5 FS: 88 ± 1 S: 86 ± 3	HF: 12 ± 0.5 FS: 17 ± 2 S: 21 ± 0.6	HF: 2.8 ± 0.6 FS: 10 ± 0.2 S: 1.2 ± 0	1.7 ± 0	HF Interior: 0.54 HF Exterior:0.22 FS: 0.5
RG755	75	0.8 (0.27)		0.7	20.0	1.3	0.7	HF: 44 ± 4 FS: 84 ± 1 S: 80 ± 4	HF: 11 ± 0.5 FS: 21 ± 3.6 S: 22 ± 3.5	HF: 1.3 ± 0.2 FS: 9.5 ± 1.2 S: 0.8 ± 0	3.8 ± 0.8	HF Interior: 0.49 HF Exterior:0.24 FS: 0.46
RG756	75	0.77 (0.38)	72.3 (76)	1.2	19.5	1.3	0.7	HF: 60±13 FS: 82 ± 1 S: 82 ± 2	HF: 10 ± 0.5 FS: 18 ± 1.7 S: 21 ± 0.6	HF: 1.9 ± 1 FS: 7.4 ± 1 S: 0.9 ± 0.1	3.9 ± 0.9	HF Interior: 0.49 HF Exterior:0.44 FS: 0.54

7.2.1 Mass change

The polymer scaffolds exhibited a small mass loss over two weeks' incubation under culture conditions. The mean mass loss was 6.3% (of the original mass) with a standard deviation of 13.6% ($n = 74$).

Initial examination of the data indicated the mass change of the two lactide contents is different. Both membrane compositions show increasing mass remaining with increased initial porosity. However for the 50:50 L:G membranes the mass remaining very slightly increases with increasing intrinsic viscosity, whereas the 75:25 L:G ratio membranes showed a marked decrease in mass remaining with increase in intrinsic viscosity. Three of the 75:25 L:G samples incurred an increase in mass up to 140% of the initial value. These anomalous results all came from a single polymer-scaffold combination, and while a similar increase was seen in all three samples of that particular combination, in terms of a degradation study these results are deemed to be anomalous. It is likely that some aspect of the polymer-scaffold combination is acting to either attract material out of the media, which would remain adding mass to the sample after drying, or the drying process was not rigorous enough for this sample despite performing adequately for all the other samples. However if these results are removed from the data set the correlation between mass loss and explanatory variables is vastly simplified. In this instance only the initial porosity of the scaffold is found to influence the mass loss of the polymer. The new data set and significant linear correlation is presented in Figure 7.1 and Equation 7.1 (mean ± standard error).

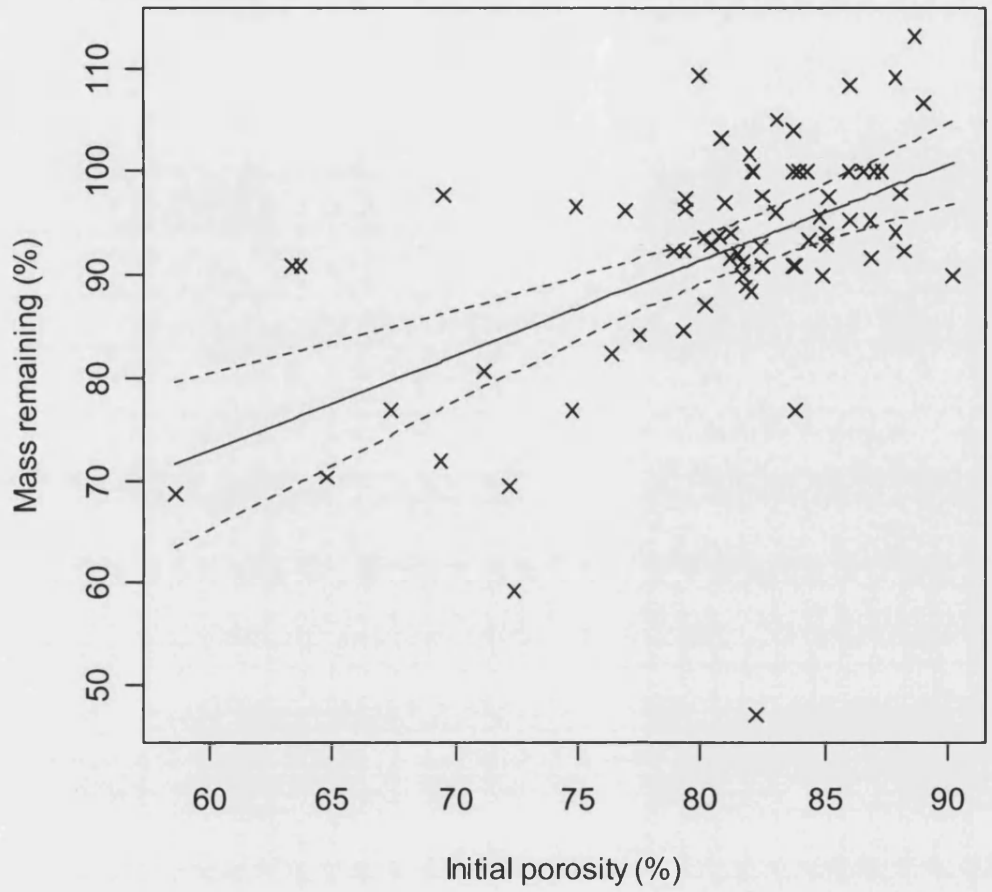

Figure 7.1 Scatter plot showing the relationship between initial porosity of scaffold and mass loss. *When three potentially erroneous results are removed from the data set (for final masses approximately 140% of the initial mass) the correlation for mass loss is simplified to initial porosity of the scaffold. Points represent single data points; the significant linear correlation (solid line) and 95% confidence interval (dashed line) are shown.*

$$m = 17.2 \pm 14.2 + (9.3 \pm 1.8) \times 10^{-1} P$$ **Equation 7.1**

m = Percentage mass remaining (-; %)

P = Percentage initial porosity of scaffold (-; %)

It is also noted a number of other scaffolds exhibit a small increase over their initial mass, however these are found to be within in the tolerance of the experiment and not exhibiting undue influence over the correlation.

The mass changes of the scaffolds were also evaluated in four different conditions, namely: water at 20°C, water at 37°C, media at 20°C, and media at 37°C. No significant differences were found between the mass losses of the samples in different conditions.

Effects specific to the unique environment within the bioreactor were also investigated. Different flow regimes, including flow in the ablumen only, lumen only, counter-current flow in the lumen and ablumen and static flow were all investigated with and without cells. The exception being that static flow was not investigated in the presence of cells as cells would require the media to be changed over the two week test period which would deviate from the required static conditions. The results are shown in Figure 7.2, no significant difference was found for the mass remaining of the scaffolds for the different conditions within the reactor.

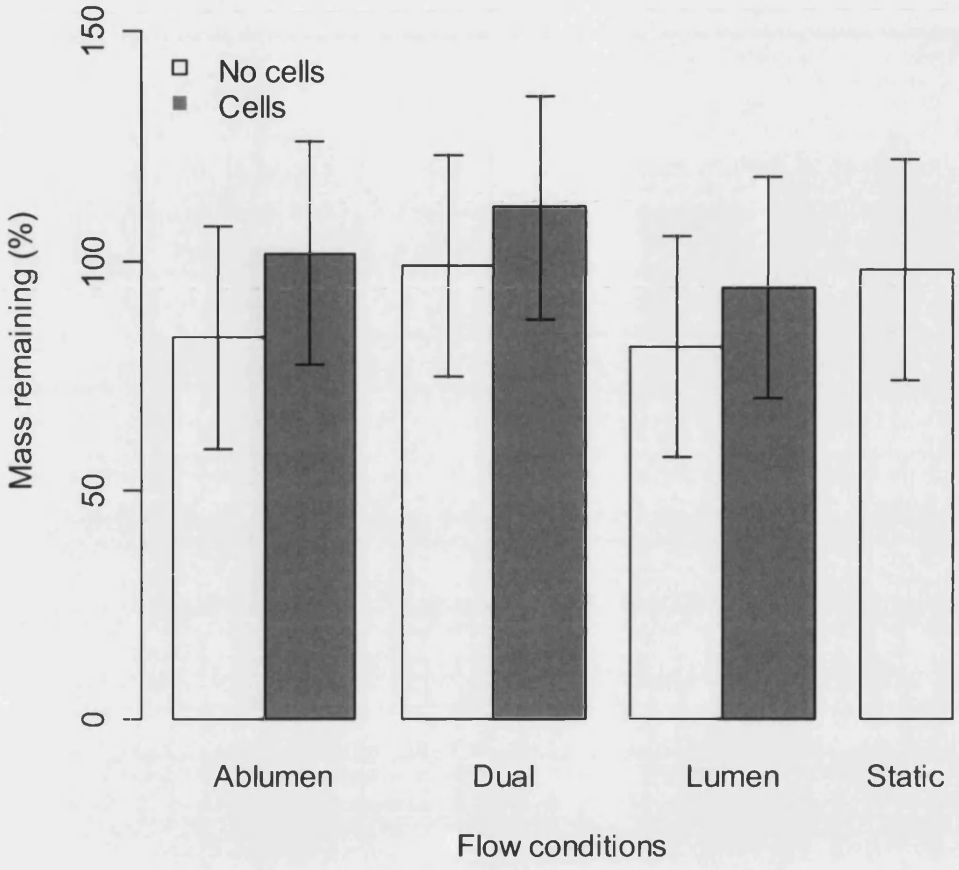

Figure 7.2 Bar plot showing the relationship between flow regimes within the bioreactor and the presence or absence of cells on the change in mass of hollow fibre scaffolds over a two week culture period.

There is no significant difference (lsd error bars overlap) in the mass remaining of the scaffolds for samples under different flow regimes, with or without cells (mean ± lsd; n = 3). ***Ablumen:*** *relates to abluminal flow only,* ***Dual:*** *relates to counter-current luminal and abluminal flow,* ***Lumen*** *relates to luminal flow only,* ***Static:*** *relates to no flow in the bioreactor, this condition was not tested with cells due to the requirement to supply cells with fresh media to maintain growth. Flow rates were all 20 cm^3min^{-1}; bioreactors were incubated at 37°C and at 5% CO_2. Samples were analysed per unit length to allow for different lengths of fibre recovered from the bioreactor where they were glued in place.*

7.2.2 Volume change

The change in volume of the scaffolds was investigated, both as a function of time during the experiment and as a function of scaffold characteristics at the end point of the experiment. Figure 7.3 shows the change in cross-sectional area of the scaffold with

time; the cross-sectional area was used as an indicator for volume to allow measurement without disturbing the samples.

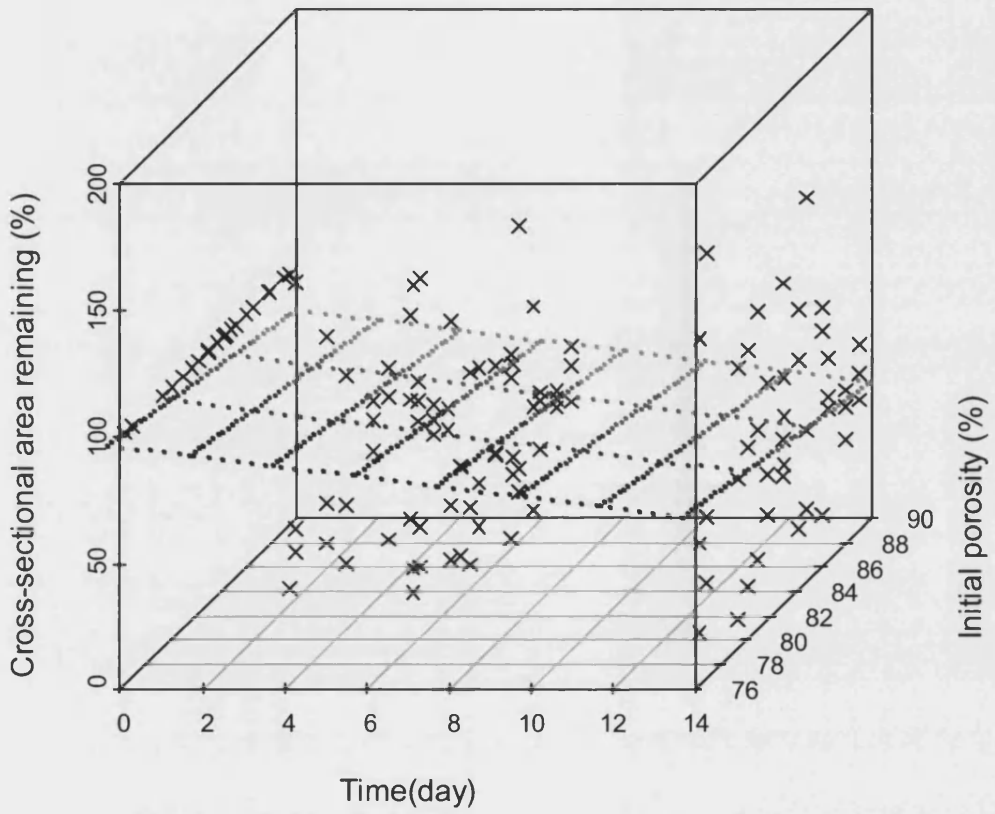

Figure 7.3 Three-dimensional scatter plot showing the change in cross-sectional area of PLGA scaffolds over a two week culture period.

Hollow fibre, flat sheet and spherical scaffolds were kept in complete cell culture medium in an incubator (37°C, 5% CO_2) for two weeks. The initial porosity of the scaffold was found to affect the cross-sectional area loss with time. The form of the scaffold (flat sheet, hollow fibre, and sphere), surface area to volume ratio, intrinsic viscosity and lactide content of the polymer were not found to affect the rate of cross-sectional area change with time. The significant trend is shown by the ***plane,*** *with the darkness of the points marking the plane reducing with increasing initial porosity.*

The significant correlation plane for change in cross-sectional area against time and initial porosity is given in Equation 7.2 (estimates ± standard error). The cross-sectional area was found to give a good correlation with the volume of the scaffold

when both values were measured at the end-point of the study. The graph showing the relationship between cross-sectional area and volume for the three different scaffold forms is given in B.2 in Appendix B.

$$A = (198.4 \pm 52.2) - (2.0 \pm 0.4)t - (1.3 \pm 0.6)P \qquad \textbf{Equation 7.2}$$

A = Percentage cross-sectional area remaining (-; %)

t = Time (T; day)

P = Percentage initial porosity of scaffold (-; %)

The scaffolds show a large degree of variation (Figure 7.3) in cross-sectional area, however overall the trend shows decreasing cross-sectional area with time and initial scaffold porosity.

The volume of the scaffolds at the end of the two week culture period, as a percentage of the initial value, was found to correlate with the lactide content, the surface area to volume ratio, the intrinsic viscosity and the initial porosity of the scaffold. There were also complex interactions between the explanatory variables. Figure 7.4 shows the graphical representation of the data and the correlation.

The results show the volume remaining decreasing with initial porosity for all but the highest surface area to volume ratios. The samples with higher lactide content show a bigger change with initial porosity than the 50:50 L:G ratio polymers. With the exception of the low and medium surface area to volume ratios for the 50:50 samples the volume remaining increases with increasing polymer intrinsic viscosity.

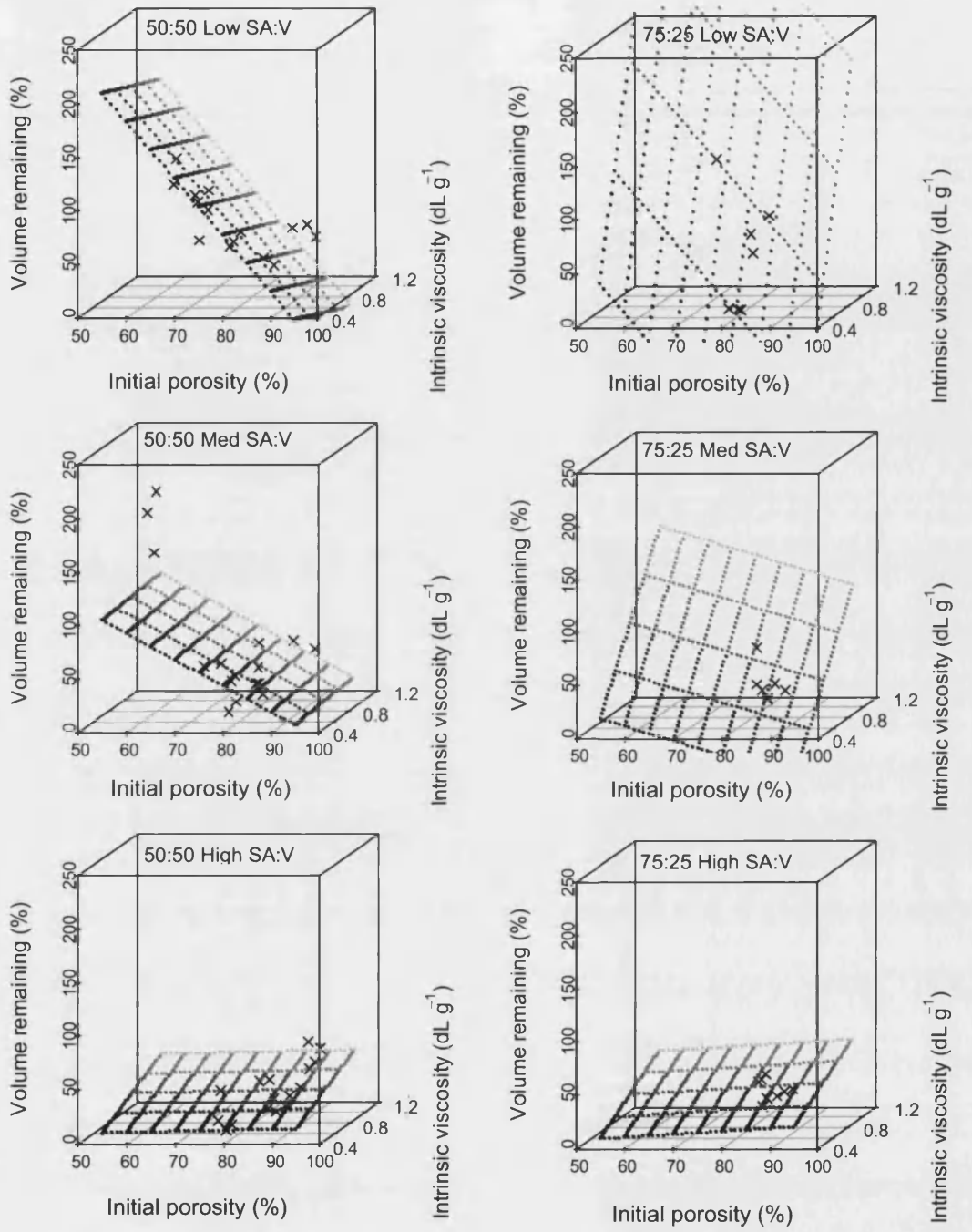

Figure 7.4 Series of three-dimensional scatter plots showing volume of scaffold remaining following a two week period under culture conditions.

Hollow fibre, flat sheet and spherical scaffolds were kept in cell culture medium in an incubator (37°C, 5% CO_2) for two weeks. ***Right-hand column:*** *50:50 L:G ratio polymers,* ***Left-hand column:*** *75:25 L:G ratio polymers,* ***Top row:*** *Low surface area to volume ratio,* ***Middle row:*** *Medium surface area to volume ratio,* ***Bottom row:*** *High surface area to volume ratio. Scaffolds were divided into three groups of surface area to volume ratio independently of scaffold shape. Surface area to volume ratio, lactide content, initial porosity and intrinsic viscosity were all found to significantly affect polymer shrinkage; the correlation is shown by the* ***plane*** *darker points represent lower values of intrinsic viscosity.*

The equation of the regression plane is presented in Equation 7.3.

$$v = 1.7\times10^{3} - 20M - 1.7\times10^{-1} r_{sa:v} + 1.4\times10^{3}[\mu] - 7.0P + 1.9\times10^{-3} Mr_{sa:v} + 27M[\mu] + 1.4\times10^{-1} r_{sa:v}[\mu] + 7.1\times10^{-4} r_{sa:v}P - 2.6\times10^{-3} Mr_{sa:v}[\mu] \quad \textbf{Equation 7.3}$$

v = Percentage volume remaining (-; %)

M = Percentage lactide content of polymer (-; %)

$r_{sa:v}$ = Surface area to volume ratio (L^{-1}; m^{-1})

$[\mu]$ = Intrinsic viscosity (L^3M^{-1}; dL g^{-1})

P = Percentage initial porosity of scaffold (-; %)

Table 7.2 gives details of the regression correlation that was applied to the data from the volume loss under culture conditions experiment. The first column identifies which parameter the value relates to; with the 5 individual factors that influence the degradation presented in the top half of the table. Further down the table the interactions between variables that are found to be statistically significant are presented. The value of the estimate of the coefficient for each parameter and the standard error of the estimate are presented in columns two and three. The *p* value and significance code are presented in the two right-hand columns on the table. These indicate the significance of the correlation, a low *p* value, as highlighted by higher numbers of stars, indicates a large significance. For example in the above table the three stars in the *Porosity* row indicate that the initial porosity of the membrane is more influential on the volume loss of the membrane than the initial viscosity (IV) which only has one star in its row.

Table 7.2 Regression correlation for the volume loss of PLGA scaffolds in media at 37 °C.
Values of the coefficients from the regression correlation for the response of the percentage volume remaining of PLGA membranes over a two week period in complete cell culture media under incubation conditions (37°C, 5% CO2). Membrane porosity (Porosity; %), lactide content (Lactide; %), intrinsic viscosity (IV; dL g^{-1}) and surface area to volume ratio (SA/V; m^{-1}) all influence the degradation of the polymer membrane.

	Estimate	Std. Error	P	Sig.
Intercept	1.7×10^{3}	3.6×10^{2}	2.41×10^{-5}	***
Lactide	-2.0×10^{1}	6.9	6.27×10^{-3}	*
SA/V	-1.7×10^{-1}	4.5×10^{-2}	4.59×10^{-4}	**
IV	1.4×10^{3}	5.2×10^{2}	9.84×10^{-3}	*
Porosity	-7.0	9.4×10^{-1}	4.76×10^{-10}	***
Lactide:SA/V	1.9×10^{-3}	0.0	3.63×10^{-2}	.
Lactide:IV	2.7×10^{1}	9.9	9.76×10^{-3}	*
SA/V:IV	1.38×10^{-1}	6.7×10^{-2}	4.45×10^{-2}	.
SA/V:Porosity	7.1×10^{-4}	2.1×10^{-4}	1.17×10^{-3}	*
Lactide:SA/V:IV	-2.6×10^{-3}	1.3×10^{-3}	4.89×10^{-2}	.

Significance codes: * = 0.0001, ** = 0.001, * = 0.01, .= 0.05**

Figure 7.5 graphically presents the significance of the different variables influencing the change in volume of the scaffold under culture conditions. The tree diagram illustrates the information presented in Table 7.2. The long branches at the top of the diagram show that initial porosity is the main factor determining the volume remaining in the scaffold. The short branches at the bottom of the right-hand side of the diagram show that surface area to volume ratio also influence the volume remaining of the scaffold but these are only influential when there is a high initial porosity and a low volume remaining in the scaffold. The numbers at the end of the branches give the mean value for percentage volume remaining for each group.

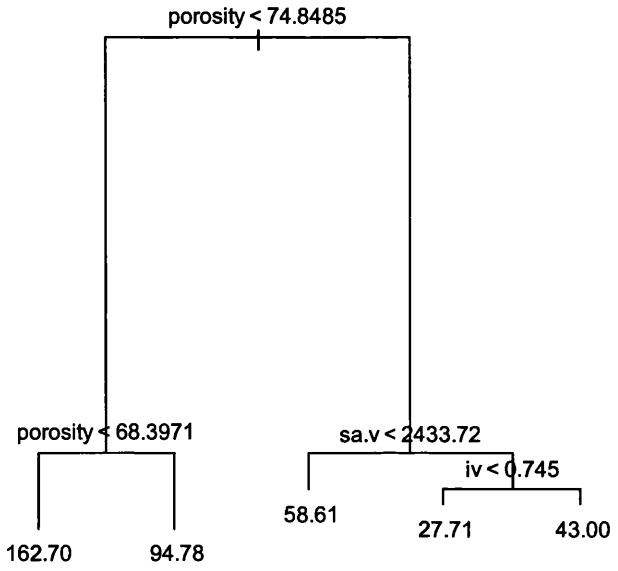

Figure 7.5 Tree diagram showing the significant interactions between independent variables correlating with the volume loss of PLGA under culture conditions.

Hollow fibre, flat sheet and spherical scaffolds were kept in complete cell culture medium in an incubator (37 °C, 5% CO_2) for two weeks. The length of the branches indicates the level of significance; the number at the end of the branch indicates the mean value for that group. Initial porosity has the greatest influence over the volume loss, polymers with high initial porosity show increased volume loss. Porosity refers to initial scaffold bulk porosity, sa.v refers to the initial scaffold surface area to volume ratio and iv refers to the initial scaffold intrinsic viscosity.

The volume of the scaffold at the end of the culture period was found to be affected by the culture conditions. Samples were held under conditions of 20°C and 37°C in both media and water. The samples maintained at the higher temperature of 37°C were found to result in less of the original volume of the scaffold remaining at the end of the degradation period. The fluid the scaffolds were placed in was also found to influence the volume of the scaffold. Scaffolds kept in complete cell culture media were found to result in a greater volume loss that those kept in water. The scaffolds tested in different conditions all had the same intrinsic viscosity and lactide content. As with the study above the initial porosity and surface to volume ratio of the scaffold were found to influence the volume loss in addition to the effects of the different conditions. The combinations of these effects are presented graphically in Figure 7.6.

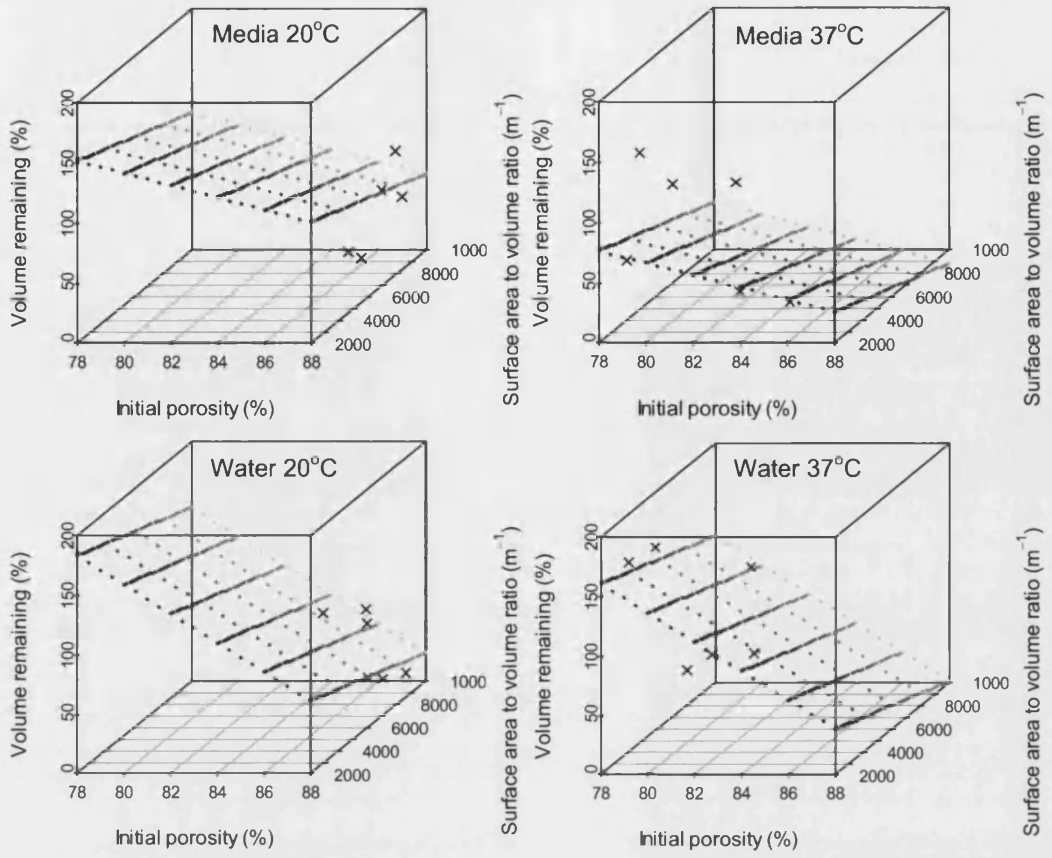

Figure 7.6 Series of three-dimensional scatter plots showing the relationship between culture conditions, initial scaffold porosity, surface area to volume ratio and change in volume of scaffold of flat sheet and hollow fibre scaffolds undergoing culture like conditions for two weeks.

Left hand column: *Scaffolds maintained at 20°C,* ***Right hand column:*** *Scaffolds maintained at 37°C.* ***Top row:*** *Scaffolds placed in complete cell culture medium,* ***Bottom row:*** *Scaffolds placed in distilled water. Flat sheet and hollow fibre scaffolds were placed in different conditions for a two week period. Changes to the scaffold mass, volume and porosity were measured. Culture fluid (cell culture media or water), temperature, initial scaffold porosity and initial surface area to volume ratio were all found to significantly correlate with the volume remaining in the scaffolds. Individual data points and the regression* ***planes*** *are shown, with darker points on the plane representing lower values of surface area to volume ratio.*

The correlation is presented for the two different liquid conditions in Equation 7.4 and Equation 7.5 for media and water respectively, further details of the regression correlation and standard errors are given in Appendix C.1.1.

Media: $v = 6.4\times10^{2} - 4.4T - 4.7\times10^{3} r_{sa:v} - 5.1P$ **Equation 7.4**

Water: $v = 1.2\times10^{3} - 1.3T - 4.7\times10^{3} r_{sa:v} - 12.0P$ **Equation 7.5**

v = Percentage volume remaining (-; %)

T = Temperature (Θ; °C)

$r_{sa:v}$ = Surface area to volume ratio (L^{-1}; m^{-1})

P = Percentage initial porosity of scaffold (-; %)

The volume change for scaffold within the bioreactor environment, with different flow conditions and in the presence or absence of cells, resulted in no significant changes to the volume of the scaffold remaining at the end of the study. Figure 7.7 shows the data presented as a bar plot illustrating the mean values and the least significant difference. The error bars of all the samples overlap indicating there is no significant difference between samples. Neither the flow, nor the presence of cells influences the way the volume of the polymer scaffold changes.

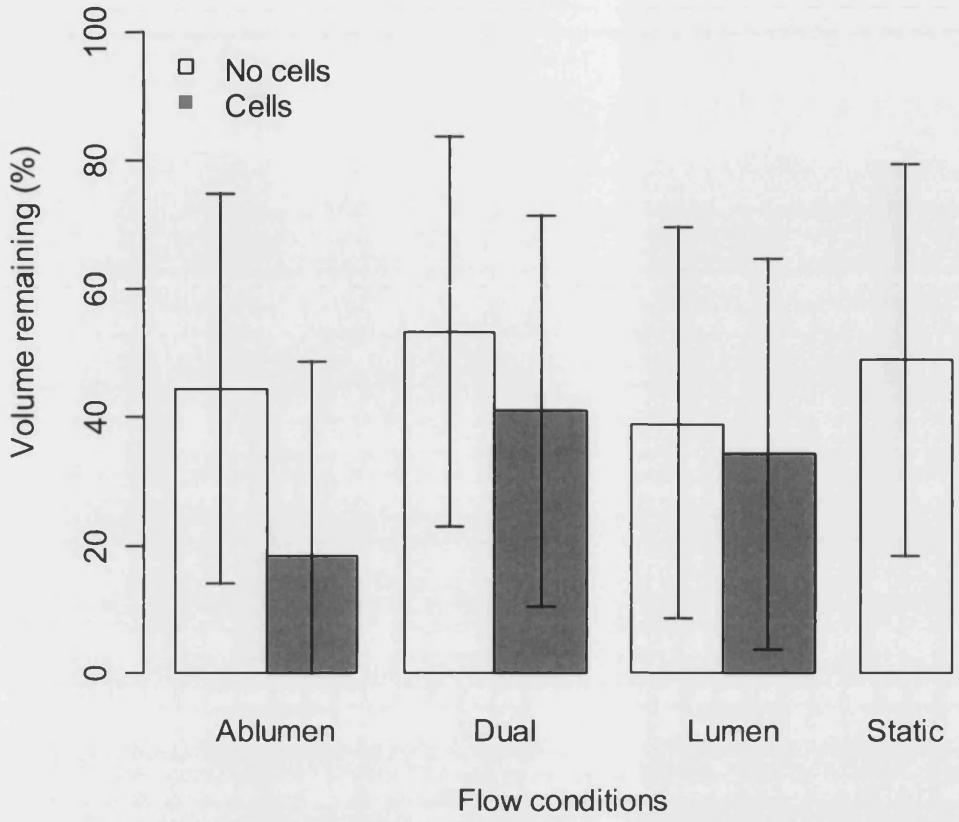

Figure 7.7 Bar plot showing the relationship between flow conditions within the bioreactor and the presence or absence of cells on the change in volume of hollow fibre scaffolds over a two week culture period.

There is no significant difference in the volume remaining of the scaffolds for samples cultured in the bioreactor under different flow regimes, with or without cells (mean ± lsd; n = 3). ***Ablumen:*** *relates to abluminal flow only,* ***Dual:*** *relates to counter-current luminal and abluminal flow,* ***Lumen*** *relates to luminal flow only,* ***Static:*** *relates to no flow in the bioreactor, this condition was not tested with cells due to the requirement to supply cells with fresh media to maintain growth. Flow rates were all 20 cm^3min^{-1}; bioreactors were incubated at 37°C and at 5% CO_2. Samples were analysed per unit length to allow for different lengths of fibre recovered from the bioreactor where they were glued in place.*

7.2.3 Porosity change

The porosity of the scaffolds was found to follow a similar response to the volume of the scaffolds with the porosity decreasing over the two week period. The scaffold surface area to volume ratio, initial porosity, and intrinsic viscosity were all found to correlate with the change in porosity. The data is presented in Figure 7.8 with the significant correlations shown by the plane; the equation for the plane is given in

Equation 7.6. The porosity data shows a large degree of variation; overall the trend shows a decrease in porosity following the culture period. However at the lower values of intrinsic viscosity this is less well defined, with samples with a high surface area to volume ratio and a low intrinsic viscosity showing an increase in porosity over the degradation period. Further details of the regression correlation are given in Appendix C.1.2.

$$P_r = 4.9\times10^{2} - 2.1\times10^{-1} r_{sa:v} - 4.6P + 1.8\times10^{-1} r_{sa:v}[\mu] + 2.3\times10^{-3} r_{sa:v} P - 2.0\times10^{-3} r_{sa:v} P[\mu] \quad \textbf{Equation 7.6}$$

P_r = Percentage volume remaining (-; %)

$r_{sa:v}$ = Surface area to volume ratio (L^{-1}; m^{-1})

$[\mu]$ = Intrinsic viscosity (L^3M^{-1}; dL g^{-1})

P = Percentage initial porosity of scaffold (-; %)

Figure 7.8 Three-dimensional scatter plots showing the porosity remaining after 2 weeks incubation in complete media of PLGA flat sheet, hollow fibre and spherical scaffolds.

Left: *Low surface area to volume ratio,* ***Middle:*** *medium surface area to volume ratio,* ***Right:*** *High surface area to volume ratio. Scaffolds were divided into three groups of surface area to volume ratio independently of scaffold shape. Surface area to volume ratio, initial porosity and intrinsic viscosity were all found to significantly affect polymer porosity change with complex interactions; the correlation is shown by* ***dotted lines****, darker points represent lower values of intrinsic viscosity.*

Figure 7.9 shows the results of a study into the effect of conditions on the porosity change of hollow fibre, flat sheet and spherical polymer scaffolds over a two week period. The trend planes shown in the figure are described by Equation 7.7 and Equation 7.8 for media and water respectively.

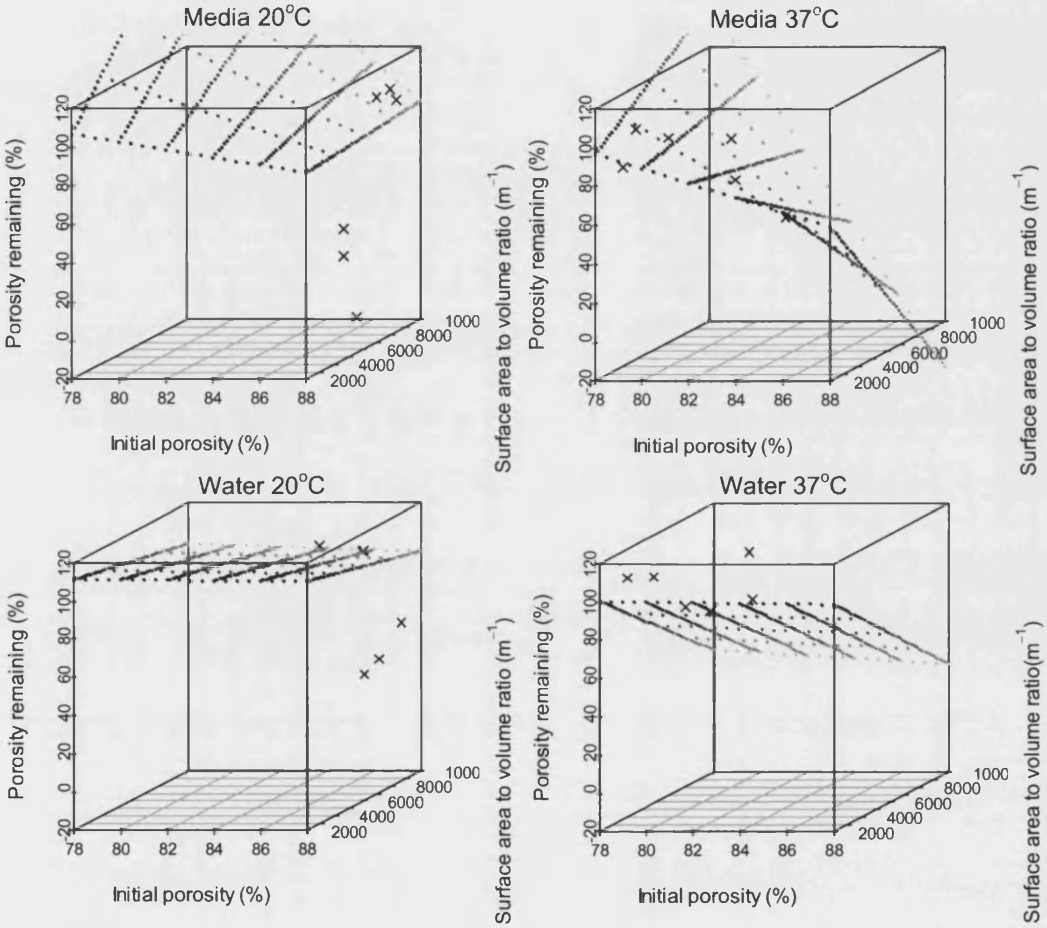

Figure 7.9 Series of three-dimensional scatter plots showing the relationship between conditions, initial scaffold porosity, surface area to volume ratio and change in scaffold porosity of flat sheet and hollow fibre scaffolds undergoing culture like conditions for two weeks.

Left hand column: *Scaffolds maintained at 20°C,* ***Right hand column:*** *Scaffolds maintained at 37°C* ***Top row:*** *Scaffolds placed in complete cell culture medium,* ***Bottom row:*** *Scaffolds placed in distilled water. Flat sheet and hollow fibre scaffolds were placed in different conditions for a two week period. Changes to the scaffold mass, volume and porosity were measured. Culture fluid (cell culture media or water), temperature, initial scaffold porosity and initial surface area to volume ratio were all found to significantly correlate with the porosity remaining in the scaffolds. Individual data points and the regression planes are shown.*

Media:
$$P_r = 85.3 \pm 9.0 + (1.7 \pm 0.3) \times 10^{-2} r_{sa.v} + (3.6 \pm 1.5) \times 10^{-3} r_{sa.v} T - (5.0 \pm 1.8) \times 10^{-5} r_{sa.v} T P_i$$ **Equation 7.7**

Water:
$$P_r = 114.3 \pm 12.2 + (5.3 \pm 3.1) \times 10^{-3} r_{sa.v} - (1.7 \times 10^{-1} \pm 1.8 \times 10^{-3}) r_{sa.v} T - (1.9 \times 10^{-1} \pm 2.1 \times 10^{-5}) r_{sa.v} T P_i$$ **Equation 7.8**

P_r = Percentage of initial porosity of scaffold remaining (-; %)

$r_{sa:v}$ = Surface area to volume ratio (L^{-1}; m^{-1})

T = Temperature (Θ; °C)

P_i = Percentage initial porosity of scaffold (-; %)

The results show the porosity of the scaffold decreases more for the conditions most similar to those required for cell culture. The temperature of 37°C shows lower values of porosity than 20°C, similarly the samples kept in media show lower values of porosity than those kept in water. Again the change in porosity correlated with the initial porosity and surface area to volume ratio of the scaffold.

The flow conditions required for the operation of the hollow fibre bioreactor and the presence of cells within the bioreactor were not found to significantly affect the porosity of the polymer. The data for the porosity change of the scaffold under different flow regimes with and without cells is shown in Figure 7.10.

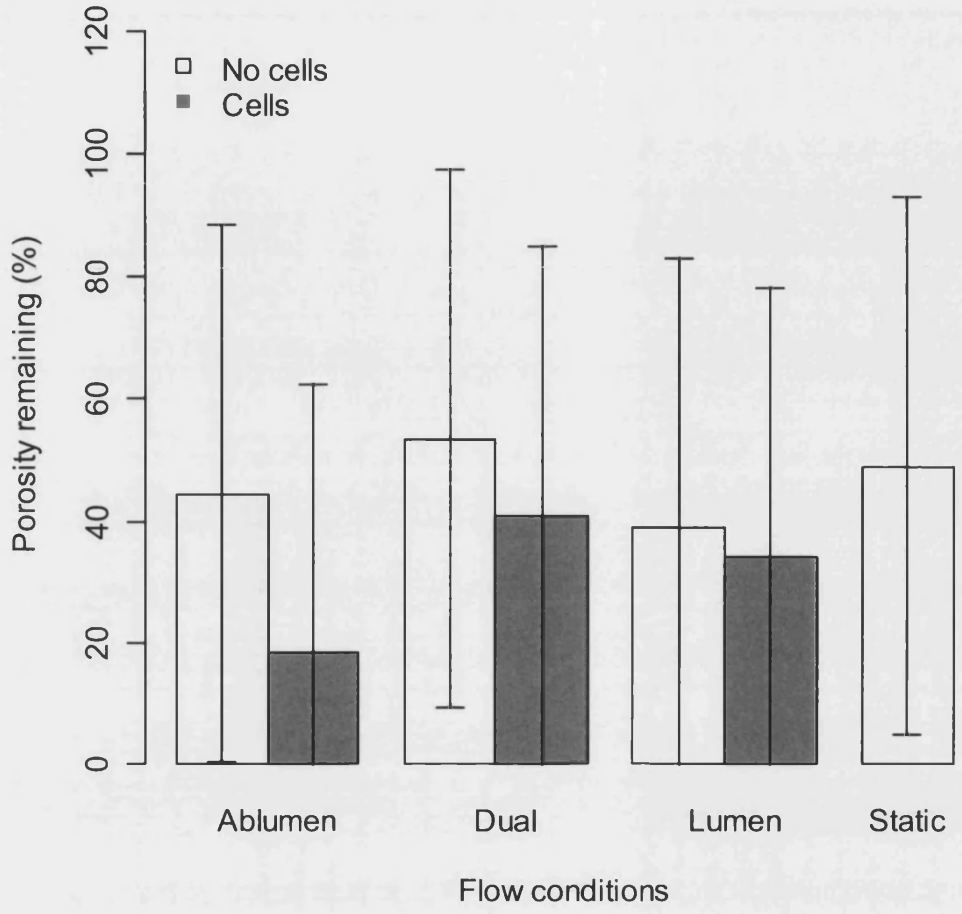

Figure 7.10 Bar plot showing the relationship between flow regimes within the bioreactor and the presence or absence of cells on the change in porosity of hollow fibre scaffolds over a two week culture period.

There is no significant difference in the porosity remaining of the scaffolds for samples under different flow regimes, with or without cells (mean ± lsd; n = 3). ***Ablumen:*** *relates to abluminal flow only,* ***Dual:*** *relates to counter-current luminal and abluminal flow,* ***Lumen*** *relates to luminal flow only,* ***Static:*** *relates to no flow in the bioreactor, this condition was not tested with cells due to the requirement to supply cells with fresh media to maintain growth. Flow rates were all 20 cm^3min^{-1}, bioreactors were incubated at 37 °C and at 5% CO_2. Samples were analysed per unit length to allow for different lengths of fibre recovered from the bioreactor where they were glued in place.*

7.2.4 Mechanical property changes

The change in mechanical properties of the scaffolds was monitored by the Young's modulus of the fibres. The Young's modulus of the fibres was found to change over a two week culture period. For samples under cell culture conditions (media and 37°C)

the change in Young's modulus was found to correlate with the lactide content of the polymer and the intrinsic viscosity of the polymer. The data is presented in Figure 7.11; including the trend line, the equation of which is given in Equation 7.9, further details of the regression correlation are given in Appendix C.1.3.

$$E = 6.6 - 0.45T + 0.85TM + 60T[\mu] - 1.1TM[\mu] \qquad \textbf{Equation 7.9}$$

E = Young's modulus ($LM^{-1}T^{-2}$; MPa)

t = Time (T; day)

M = Percentage lactide content of polymer (-; %)

$[\mu]$ = Intrinsic viscosity (L^3M^{-1}; dL g^{-1})

The effect of the conditions on the Young's modulus of the fibres was also tested. Figure 7.12 shows the change in Young's modulus for samples in different conditions. ANOVA revealed no significant difference between the samples held in media or water at 20°C or 37°C and the control sample, however there was no loss in explanatory power of the correlation (as determined by ANOVA) when all the cultured samples were grouped together. This test revealed there was a significant difference between the treated samples and the control, but no significant difference between the individual treated samples. This suggests that while the two week period resulted in a reduction in Young's modulus for all of the samples the differentconditions did not affect this change in Young's modulus.

The Young's modulus of samples cultured within the bioreactor under different flow regimes and both in the presence and absence of cells was also monitored. No significant difference was found between samples under luminal, abluminal, and dual flow or static conditions, with or without cells and the control sample. In this case the no relevant grouping of samples lead to significant differences. Suggesting that the change in Young's modulus associated with the static cultures of different polymers is reduced in the bioreactor under flow conditions.

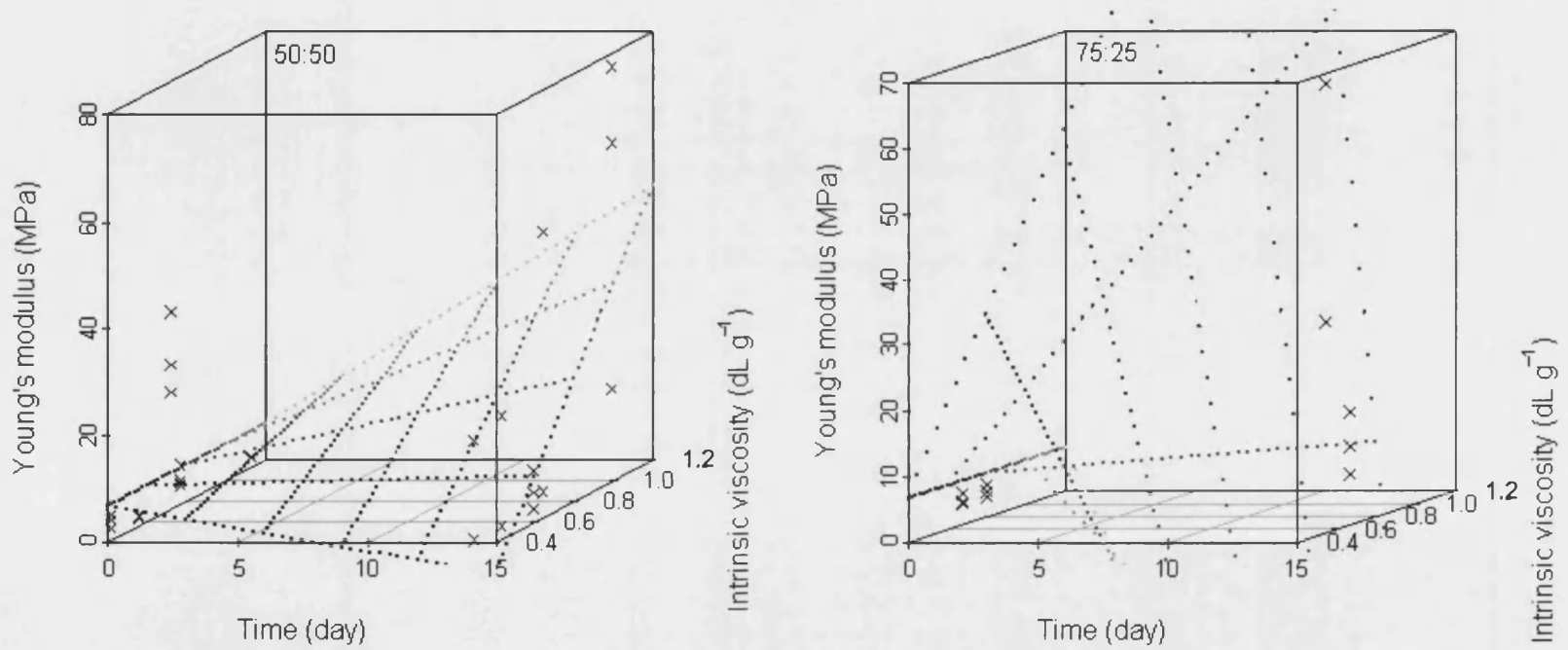

Figure 7.11 Three-dimensional scatter plots showing the change in Young's modulus of the scaffolds against time and intrinsic viscosity for 50:50 and 75:25 L:G polymer ratios.

Left: *50:50 L:G polymer ratio,* ***Right:*** *High 75:25 L:G polymer ratio. Scaffolds were degraded in cell culture conditions for two weeks. Their Young's modulus was determined before and after the degradation period. Points of the graph represent single samples; the* ***plane*** *illustrates the significant relationship between Young's modulus, time (before and after degradation) and the lactide content of the polymer. Darker points on the plane represent lower values of intrinsic viscosity.*

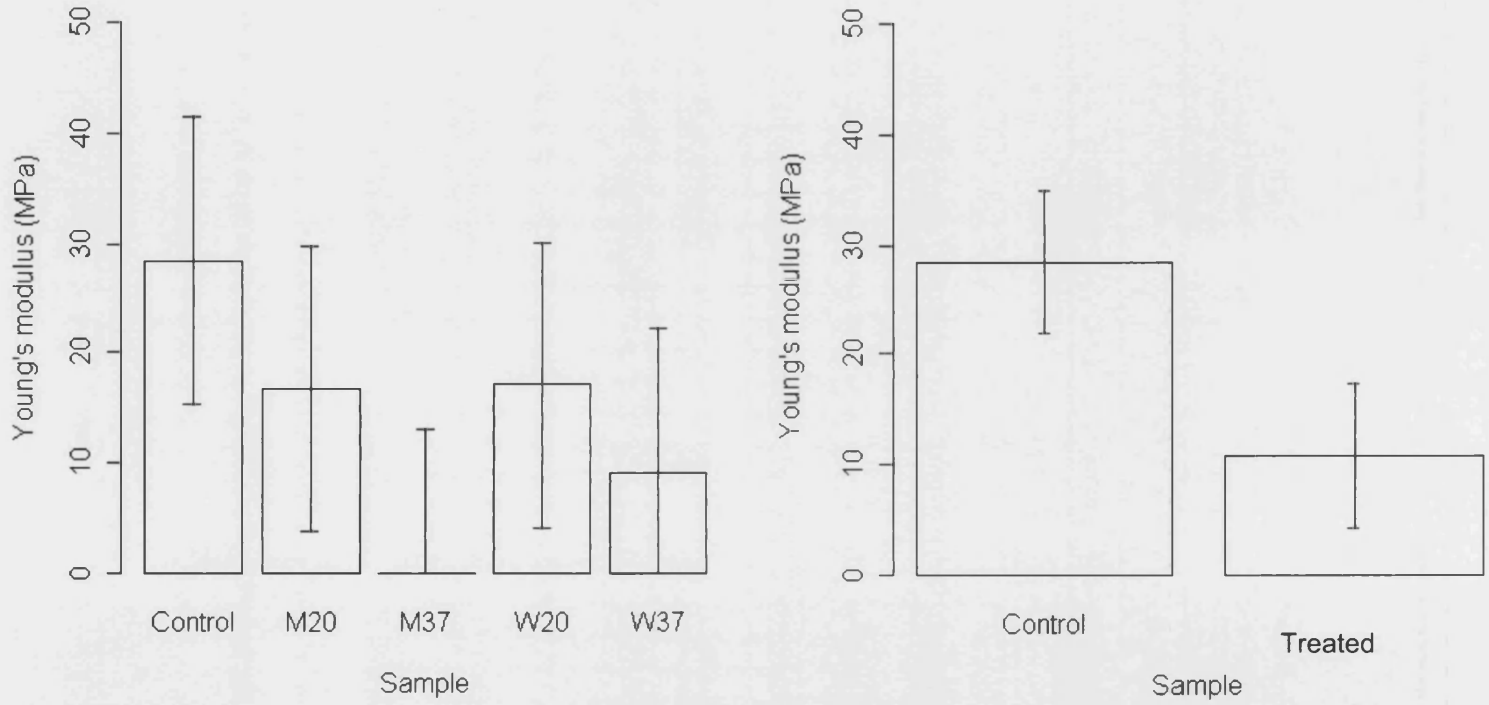

Figure 7.12 Bar plots showing change in Young's modulus of the samples following culture in different conditions.

Left: *There is no significant difference between the control sample and the samples cultured in different conditions (**M20:** Media and 20°C, **M37:** media and 37°C, **W20:** water and 20 °C, **W37:** Water and 37°C), (mean ±lsd. N=3).* ***Right:*** *When the samples held under different conditions are grouped into "Treated" samples there is a significant loss of Young's modulus compared to the control. There is no loss in explanatory power of this correlation compared to the more complicated comparison, as determined by ANOVA (mean ± lsd; control n = 3, degraded n=12). Overlapping least significant difference error bars indicate no significant difference; non-overlapping error bars indicate a significant difference between samples.*

7.2.5 Pore size changes

The surface average effective pore diameter of the scaffolds before and after culture was evaluated from electron micrographs of the scaffold surfaces. The effective pore diameter is calculated from the pore area assuming circular pores. The geometric mean is used as an average value for comparison; refer to Section 5.2.1.2 for justification. The influence of polymer type on change in pore size is presented in Figure 7.13 (details of the polymers in Table 7.3), the average effective pore diameter on both hollow fibre interior and exterior surfaces and the top surface of the flat sheets membranes was found to decrease after a two week culture period. The polymer type and intrinsic viscosity and lactide content along with scaffold form and surface location were not found to affect the average effective pore diameter. By grouping the samples into before and after culture it was possible to determine a significant decrease in the average effective pore diameter which is presented in Figure 7.14.

Table 7.3 Key to alphabetical sample labelling in Figure 7.13.
L:G *is the ratio of lactic acid to glycolic acid in the polymer.*

Label	*Intrinsic Viscosity (dL g^{-1})*	*L:G (%)*
A	1.12	50:50
B	0.77	50:50
C	0.72	50:50
D	0.42	50:50
E	0.56	50:50
F	0.68	75:25
G	0.80	75:25

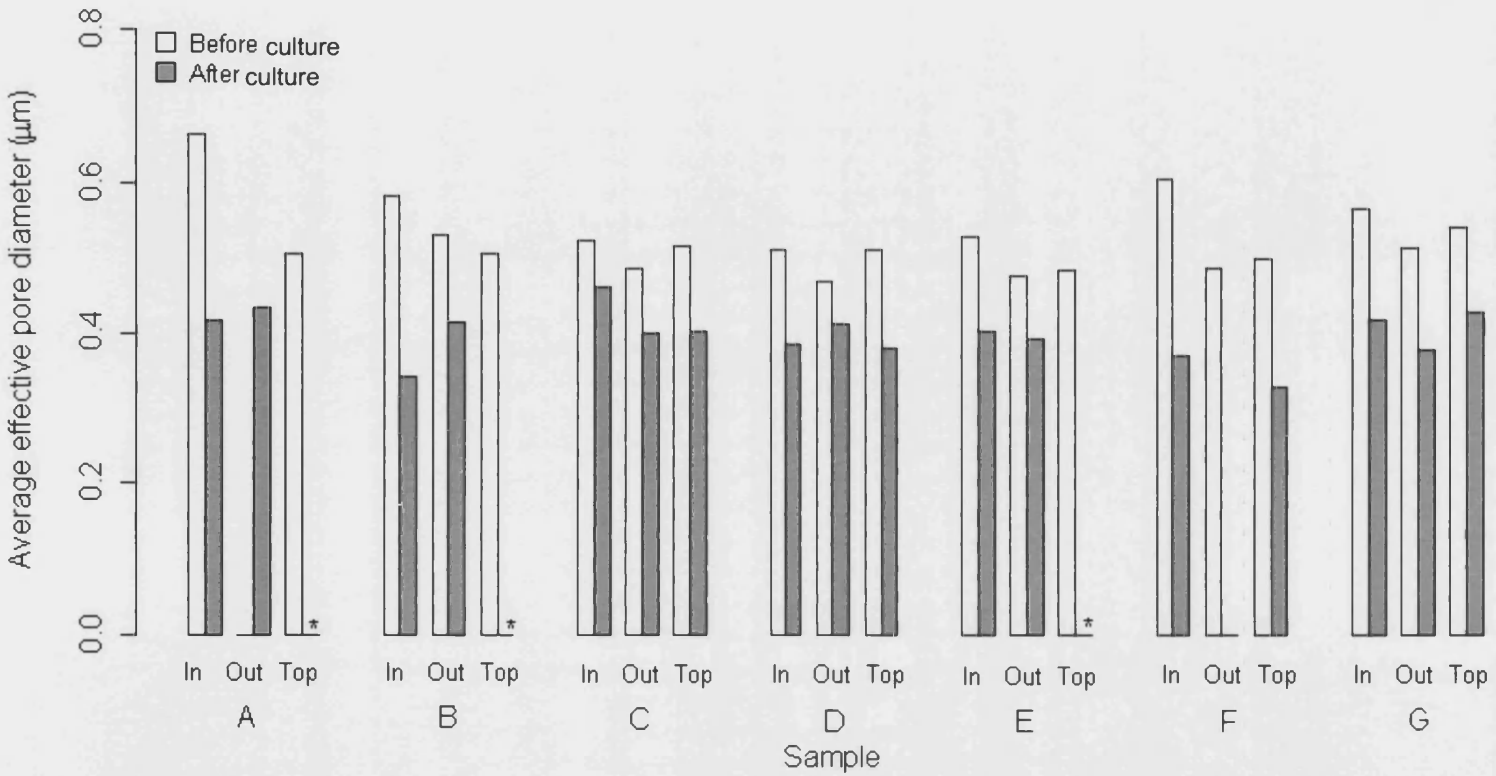

Figure 7.13 Bar plots showing change in average effective pore diameter of interior and exterior surfaces of hollow fibres and the top surface of flat sheet membranes before and after culture.

*Samples were cultured for two weeks in cell culture conditions (media and 37 °C. 5% CO_2). **In** refers to the interior surface of hollow fibres. **Out** refers to the exterior surface of hollow fibres. **Top** refers to the upper surface of flat sheet membranes. Average pore diameter was determined by image analysis of electron micrographs. Single images of an area of the membrane surface 1823 μm^2. Polymer characteristics for the alphabetically coded samples are given in Table 7.3. * denotes a sample which was not analysed.*

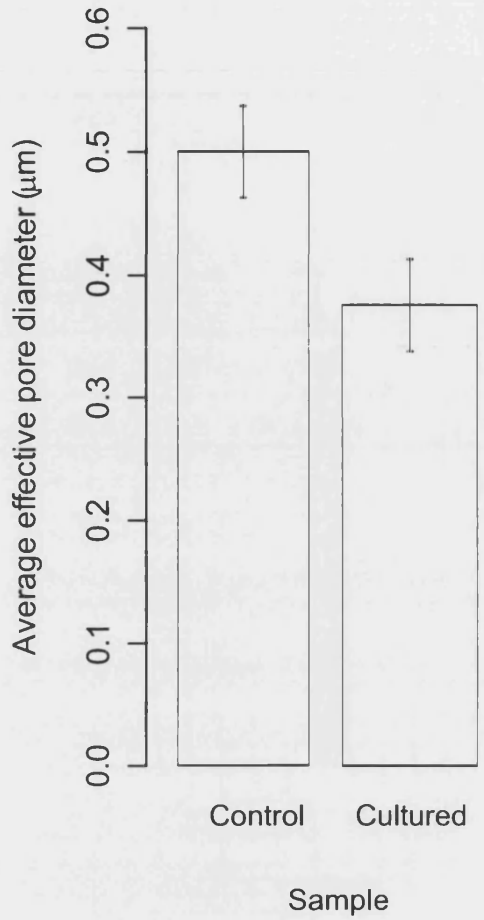

Figure 7.14 Bar plot showing the change in average effective pore diameter on the hollow fibre and flat sheet membrane surfaces before and after culture.

The cultured polymers showed a significantly lower average effective pore diameter following a two week period under culture conditions (immersed in media and incubated at 37 °C and 5% CO_2). No explanatory power of the correlation was lost by grouping results from different locations (interior and exterior of hollow fibre membranes and the top of flat sheet membranes) and different polymer lactide content and intrinsic viscosity (mean ± lsd; n=21). Non-overlapping least significant difference error bars indicate a significant difference between the samples.

The effect of flow conditions and the presence of cells within the hollow fibre bioreactor were also tested for their influence on the pore size of the membranes. The samples were potted into the hollow fibre bioreactor and set up with either dual flow (luminal and abluminal flow) or abluminal flow alone. Half the bioreactors were seeded with cells, half were not. The pore sizes on the surfaces of the membranes were all found to increase over the control membranes. The type of flow and presence of cells was not found to significantly influence the pore size on either the interior or the exterior of the membranes. Table 7.4 presents the mean values for the pore sizes on the different samples and locations.

Table 7.4 Average effective pore diameter for interior and exterior surfaces of hollow fibre membranes before and after a two week period under culture conditions.

Hollow fibre scaffolds were potted into the hollow fibre bioreactor and subjected to either abluminal or both luminal and albuminal flow with and without cells. Conditions were suitable for cell culture, namely in complete media and incubated at 37°C and 5% CO_2, flows were all 20 cm^3min^{-1}, pore diameters were determined by image analysis of an electron micrograph of 1823 μm^2 of membrane. The type of flow (abluminal or dual) and presence of cells were not found to influence the average effective pore diameter. The average effective pore diameter was found to increase over the control following the two week period under culture conditions. Single samples were analyzed to determine control pore sizes, three samples were analyzed for each of the surfaces of four different conditions (mean ± standard error).

Sample	Average effective pore diameter (μm)	
	Interior	Exterior
Control	0.54 ± 0.04	0.47 ± 0.04
Degraded	0.69 ± 0.04	0.63 ± 0.02

7.2.6 Summary of Results

Table 7.5 Summary of results from effect of operating environment and time on polymer scaffold studies.

A summary of the results from the study; general trends are given however complex interactions mean there are always exceptions. The trends shown illustrate the effect the parameter has on the property of the scaffold at the end of a two week culture period. ↗ = significant proportional trend. ↘ = significant inversely proportional trend. - = No significant trend. N/A = Interaction not investigated. Abbreviations: 50:50, 75:25 = L:G ratio of polymer, IP = Initial porosity, SA:V = surface area to volume ratio, FS = flat sheet, HF = hollow fibre, S = sphere, N = no flow, D = dual flow, A = albuminal flow only, CA = cells and abluminal flow, CD = cells and dual flow.

Parameter	Mass remaining (%)	Volume remaining (%)	Porosity remaining (%)	Young's modulus (GPa)	Pore diameter (μm)
Intrinsic viscosity	-	↗	↗	50:50: ↗ 75:25: ↘	-
Lactide content	-	Low SA:V: ↗ High SA:V: ↘	-	Low IV: ↗ High IV: ↘	-
In. porosity	↗	↘	↗	N/A	N/A
Surface area to vol. ratio	-	50:50: ↗ 75:25: ↘	-	N/A	N/A
Time	N/A	FS: ↘ HF: - S: ↗	N/A	50:50 low IV: ↘ 50:50 high IV: ↗ 75:25 low IV: ↗ 75:25 high IV: ↘	In bioreactor: ↗ Other: ↘
Form	-	S < HF < FS	-	N/A	-
Fluid	-	Water < Media	Water < Media	-	N/A
Temperature	-	↘	↘	-	N/A
Cells (Y/N)	-	↘	↗	-	-
Flow	-	N < D < A	N < D < A	-	-
Cells and flow	-	CA<CD, A, D	CA<CD, A, D	-	-

7.3 Discussion

The responses of the physical characteristics of polymer scaffolds in a culture environment were evaluated in order to assess the suitability of the scaffolds for use in a bone tissue engineering hollow fibre bioreactor.

The topic of degradation of PLGA is widely addressed in the literature. However it is noted that the degradation of PLGA is very specific to the structure of the PLGA scaffold and environment. Typically degradation studies focus on chemical changes to the polymer with molecular weight change commonly used as a defining criterion for degradation. The form of the hollow fibre scaffolds and their unique use as both a supporting scaffold and a nutrient delivery network in the bioreactor means that changes to the physical properties such as mass, volume, porosity, Young's modulus and surface pore diameter will give a greater indication to their suitability for use in the bioreactor than loss of molecular weight. The scaffold also undergoes changes when it enters a cell culture environment as the scaffold becomes wet and the temperature is raised. These changes have been considered concurrently the changes due to degradation of the scaffold in an aqueous environment.

This study found that the mass, volume and porosity of the scaffolds were all reduced at the end of two weeks' culture in a variety of conditions. Characteristics specific to the polymer, the scaffold form and the environmental conditions all affected the final state of the polymer; high-lighting the need to test the specific combinations of a polymer, scaffold, and bioreactor system before making assumptions about the profile of changes occurring to the polymer.

The polymer samples showed a decrease in mass over the two week period under culture conditions. Other degradation studies (Agrawal *et al.* 2000; Li *et al.* 1990a) have suggested that the mass of PLGA scaffolds are fairly constant over the first few weeks in degradation conditions, showing a massive decrease in mass after that. In a study by Lu *et al.* (2000a) it was found that PLGA foams showed constant mass up to week 7 followed by a linear reduction in mass with time after that point. However a study by Li *et al.* (1990b) found that PLGA scaffolds degraded in phosphate buffered saline had lost 95% of their original mass in under four weeks. This was in contrast to

samples degraded in water where the mass loss was less than 1% of their original mass. These findings indicate that there is a wide range of behaviours followed by degrading PLGA scaffolds and an average mass loss of 6%, as was determined by this study, is well within this range.

The majority of samples exhibit a loss of volume during the culture period, and this is reflected in a significant statistical correlation. However the samples with low lactide content (50:50) low surface area to volume ratio and low initial porosity showed some swelling also occurred. These may be a result of different rates of degradation and therefore different rates of transition through the stages of degradation. For degradation to occur first the water has to diffuse into the polymer scaffold, which may cause swelling, only then, when it is in good contact with the polymer surface can hydrolysis of the ester link and solubilization of short chain oligomers occur.

The volume of the scaffold was found to decrease with time when placed in cell culture conditions. The volume was the only property of the fibre that was monitored continuously throughout the culture period, because this was the only property that could be evaluated without disturbing the samples. The volume was found to decrease linearly with time.

Overall the results show the percentage volume remaining is lower for high initial porosities, and higher for higher surface area to volume ratios, higher lactide contents, and higher intrinsic viscosities.

In contrast to many studies where the compressive strength of the scaffold is evaluated, because of the nature of the hollow fibres, tensile rather than compressive strength was evaluated as an indicator of changes to the scaffold properties. The fibres showed a change in the value of Young's modulus before and after the culture period, when evaluated as a function of polymer and scaffold properties only the intrinsic viscosity and lactide content of the polymers were found to affect the Young's modulus.

The following discussions address how the individual parameters studied affected the polymer.

7.3.1 Initial porosity

The initial porosity was found to have a large influence over the extent of changes occurring in a two week period in conditions relevant to cell culture.

Initial porosity was found to be the only independent variable that significantly correlated with the mass loss of the scaffolds. This is in agreement with Agrawal *et al.* 2000 who found that mass remaining was higher for high porosity scaffolds than lower porosity scaffolds. Wu and Ding (2005) also relate initial scaffold porosity to degradation, showing increased molecular weight loss with reduced initial porosities. This is likely to be accompanied by a reduction in polymer mass; lower molecular weight chains are more easily solubilized at the scaffold surface resulting in a transfer of material from the scaffold to the solution.

It is likely that the results of this study correlating increased mass loss with reduced initial porosity of the scaffold may be explained by processes of autocatalysis. Lower scaffold porosity reduces the removal of autocatalytic degradation products that can build up within the scaffolds. This means degradation rates will be elevated in low porosity scaffolds.

The initial porosity of the scaffold was also found to be a significant explanatory factor for the volume change. The volume decrease was increased with higher initial scaffold porosities. This is in contrast to the mass loss which was higher for lower scaffold porosities. However considering it is most likely that the volume loss is associated with loss of void volume rather than polymer volume this contrast is not unexpected; the more void volume to start with the more void volume to lose.

7.3.2 Surface area to volume ratio

The surface area to volume ratio and its effects on degradation is not as well studied as the effects of polymer characteristics on degradation. However a large surface area would be expected to provide good mass transfer of water into the polymer scaffold, which would be expected to increase the rate of degradation.

While the correlation presented in the results section suggests the initial porosity of the scaffold is the most likely explanatory variable for the mass loss of the scaffold, if the

surface area to volume ratio is evaluated as the only explanatory variable for mass loss, it also showed good correlation with the mass loss of the scaffolds (refer to Appendix B.2.3). In this case the surface area to volume ratio compares the superficial external area of the scaffold to its bulk volume; not taking into account the porosity of the scaffolds. However, when the surface area to volume ratio was evaluated alongside initial porosity, lactide content, and intrinsic viscosity it was not found to add significant explanatory power to the correlation. The surface area to volume ratio is found to show a significant linear correlation with the initial porosity (refer to Appendix B.2.4), despite the surface area to volume ratio only considering the superficial external area (not the surface area associated with pores). Therefore while it is the initial porosity of the scaffold that appears to be the most significant explanatory factor according to the statistical correlation the surface area to volume ratio may also be influential.

Higher the surface area to volume ratios were found to result in reduced volume loss. This contrasts the hypothesis that a high surface area efficiently brings the polymer and water together causing increased rates of degradation, however the efficient mass transfer of water into the scaffold may also result in increased swelling which would lead to a higher final scaffold volume.

7.3.3 Culture conditions

The liquid the scaffold was submerged in, media or water, was not found to influence the mass loss of the scaffold. Similarly the temperature was also not found to influence the mass remaining of the polymer after two weeks. This result was unexpected, as previously mentioned Li *et al.* (1990b) found a massive difference, 95% to less than 1% mass loss when comparing samples degraded in phosphate buffered saline to water. In this study the comparison was between complete cell culture media (a buffered solution) and water. This they explain as due to the higher solubility of carboxyl-terminated oligomers in buffer over water. In this study the other components of the media may act to reduce the solubility of the shorter chain polymer molecules, reducing the disparity between the media and water degraded samples. In addition the smaller mass loss overall due to the shorter time period would also reduce the difference. The liquid was changed regularly to mimic the conditions of batch-fed cell culture; this would eliminate the potential for acidic degradation products to build up within the un-buffered water system which could potentially catalyse further degradation. The

temperature difference of 20°C to 37°C was also anticipated to increase degradation, as shown by Dunne *et al.* (2000) through improved diffusion of water into the polymer and improved solubilization of short chain oligomers at higher temperatures as well as an Arrhenius temperature dependence of the rate of reaction. However the results show there was no significant change in the mass loss by the scaffolds under different conditions. This may be because the temperature change was not large enough and the mass loss not great enough for any temperature dependency to be separated from the variance of the experiment.

In contrast to the mass of the cultured scaffolds the volume remaining was significantly dependent on the conditions of culture; increased temperature resulted in less volume of the scaffold, samples cultured in media also had less residual volume that those cultured in water. The environmental conditions were only investigated for one polymer type; however, all three different scaffold forms were investigated. In this case increased surface area to volume ratio was found to result in decreased residual volume of scaffold. The change in volume of the scaffold attributed to the surface area to volume ratio is only small, but this change increases with the scaffolds cultured at the higher temperatures. As the increased temperature did not affect the residual mass of the scaffolds it is likely that the increased temperature resulted in a contraction of the scaffold volume rather than a removal of material. It is likely that as the polymer was brought closer to its glass transition temperature the polymer molecules were free to re-align within the scaffold, reducing the void space.

Evaluating the influence of culture conditions on the Young's modulus revealed a decrease in Young's modulus following the culture period (fibres tested were all 50:50 L:G ratios) but no significant difference between fibres degraded in media or water or at the two different temperatures (20°C and 37°C).

7.3.4 Flow in the bioreactor

Agrawal *et al.* (2000) report increased mass loss by degradation under static conditions compared to flow conditions. In this study the flow was not found to significantly alter the mass loss of the polymers.

While it may be hypothesised that flow through the bioreactor would aid the removal of autocatalytic degradation products from the vicinity of the degrading polymer, it is possible that because of the unique arrangement of the hollow fibre bioreactor this does not occur. In most other situations the scaffold is perfused with media, however in the case of the hollow fibre bioreactor it would be possible to have flow within the lumen or ablumen of the fibres, or both, while not passing media through the walls of the bioreactor. Therefore the effects of autocatalysis may be prevented at the surfaces of the fibres but any accumulation of autocatalytic degradation products within the wall of the fibre would not be affected.

The scaffolds cultured under flow conditions showed no significant difference in volume remaining to the scaffolds cultured without flow. This suggests that the pressures and pressure drops associated with the flow in the bioreactor are not sufficient to cause a collapse of the fibre wall which would be revealed by a reduction of the remaining volume under flow conditions.

The average effective pore diameter for the surfaces of the membranes were found to decrease following the culture period with the exception of the samples cultured within the bioreactor under flow conditions. This decrease may be associated with the volume loss of the scaffolds, as the scaffold shrinks the polymer volume stays constant meaning the pore diameter is reduced. The increased pore sizes associated with culture under flow conditions may result from the good mass transfer properties offered by the hollow fibre bioreactor. The flow past the fibres would rapidly remove any solubilized material from the vicinity. It is likely that material is eroded from the interior walls of the pores resulting in a larger pore diameter.

7.3.5 Polymer intrinsic viscosity

The intrinsic viscosity varies proportionally with the molecular weight of a scaffold (Equation 6.4), higher molecular weight scaffolds require more bonds to be broken to release short enough chains to be solubilized. This study found that the volume remaining increased with higher polymer intrinsic viscosity but the porosity remaining decreased. Further discussion about comparisons between changes to the volume and porosity of the scaffolds is given in Section 7.3.7.

The intrinsic viscosity of the polymers was not found to influence the mass loss by the polymers. This may be because of the low mass loss recorded over the two week culture period. It is likely that a longer study may find the intrinsic viscosity of the polymer does affect the mass loss.

The change in Young's modulus with intrinsic viscosity following culture for the 50:50 and 75:25 L:G ratio polymers differed. Initially the fibres exhibited the same Young's modulus with no difference with lactide content or polymer intrinsic viscosity. After two weeks' culture both the lactide content and the polymer intrinsic viscosity were found to influence the Young's modulus of the polymer. After two weeks' culture the lower lactide content polymers showed increased Young's modulus with increased intrinsic viscosity, while the higher lactide content polymers showed decreased Young's modulus with increased intrinsic viscosity. The range of variation encompassed both decreases and increases in Young's modulus over the initial value. This variation in Young's modulus at the end of the culture period with lactide content of the polymer is further discussed in Section 7.3.6.

7.3.6 Lactide content of polymer

It is widely accepted that higher glycolide content, and consequently lower lactide content polymers show increased degradation compared to higher lactide content polymers (Göpferich 1996). This would suggest if any the 50:50 ratio polymers would be further on in the degradation process than the 75:25 ratio polymers. It has been hypothesised that this is due to increased crystallinity and steric hindrance preventing the water molecules from coming into contact with the ester bond (Göpferich 1996).

The change in Young's modulus for the 50:50 and 75:25 L:G ratios were very different, the 50:50 scaffolds showed an increase in Young's modulus with intrinsic viscosity following the culture period. However the 75:25 scaffolds showed an increase in Young's modulus with intrinsic viscosity at the end of the culture period. Both these changes were found to be statistically significant by least squares regression.

Wu and Ding (2004) describe a characteristic behaviour of degrading PLGA and PLA scaffolds comprising of four stages based on compressive testing of porous scaffolds. Scaffolds exhibit a slight loss of elastic modulus on wetting, elastic modulus then

increases before reaching a plateau; this is followed by a rapid loss of elastic modulus for PLGA scaffolds while PLA scaffolds maintain their elevated elastic modulus. Comparing the results of this study with those of Wu and Ding (2004) suggests that while the 50:50 ratio scaffolds have undergone sufficient degradation to reach a fragile state associated with a loss of Young's modulus the 75:25 ratio scaffolds are experiencing the increase in mechanical properties described by the Wu and Ding as occurring during the early stages of degradation. The increase in mechanical properties initially exhibited by the scaffolds is attributed to the loss in volume of the scaffolds (Zhang and Ma 2001 cited by Wu and Ding 2004). The Young's modulus is calculated as a function of the cross-sectional area of the sample. If the volume of the sample is decreased by a loss in void space but no change to the polymer the calculated value for Young's modulus will be higher. The 75:25 samples in this study show an increased loss of volume compared to the 50:50 samples, which is decreased with increasing intrinsic viscosity, this pattern mirrors the variation in Young's modulus, with 75:25 samples showing higher Young's modulus which decreases with intrinsic viscosity.

7.3.7 Porosity change and changes to the scaffold structure

The porosity of the scaffolds was not found to be linearly correlated with the volume as might be expected. There are a number of relationships between the porosity change and volume change of porous scaffolds that may characterise the type of changes the scaffold structure is undergoing these are described in Table 7.6 and Table 7.7.

Table 7.6 Possible mechanisms of changes to porous scaffolds under culture conditions and defining relationships between loss of volume and loss of porosity.

Name	*Description*
Surface erosion	Scaffolds lose material from their outer edge decreasing in overall volume while keeping the porosity constant.
Shrinkage	The scaffolds contract but do not lose material, both the volume and the porosity will decrease.
Bulk erosion	Scaffolds lose material from all over the scaffold meaning the volume stays constant, or shows a small decrease, while the porosity increases.
Autocatalytic	Scaffolds lose material from the centre meaning the volume stays constant and the porosity increases.
Combined effects	The scaffold shows some of all the above effects, the scaffolds undergo some shrinkage to reduce the volume and the porosity, some material is lost through autocatalytic and bulk erosion meaning the porosity does not fall as low as it would from shrinkage alone.

Table 7.7 Different mechanisms of changes to porous scaffolds under culture conditions have different characteristic appearances and porosity and volume loss relationships.

Shrink. *= shrinkage,* ***Auto-cat.*** *= auto-catalytic,* ***Comb. effects*** *= combined effects,* P_i *= initial porosity,* P_f *= final porosity,* v_i *= initial volume,* v_f *= final volume,* P_R *= Porosity remaining,* v_R *= volume remaining,* ***R'nship*** *= relationship between porosity remaining and volume remaining. Mechanisms of degradation are defined in List 7.1. The diagrams show a pictorial representation of a cross-section of scaffold, diagrams are drawn smaller to represent a change in volume and darker colours represent denser scaffolds, white areas within the scaffold represent regions where autocatalysis has caused a large localised loss of material.*

	Initial	***Surface erosion***	***Shrink.***	***Bulk erosion***	***Auto-cat.***	***Comb. effects***
Porosity	P_i	$P_f = P_i$	$P_f << P_i$	$P_f > P_i$	$P_f > P_i$	$P_f > P_i$
Volume	v_i	$v_f << v_i$	$v_f << v_i$	$v_f < v_i$	$v_f < v_i$	$v_f < v_i$
R'nship	-	$P_R \propto v_R$	$P_R < \propto v_R$	$P_R > \propto v_R$	$P_R > \propto v_R$	$P_R > \propto v_R$
Spherical	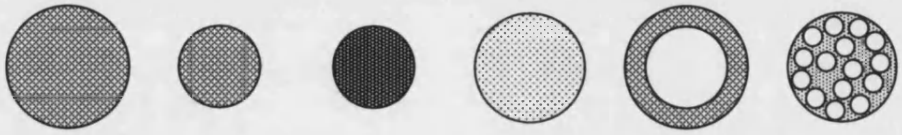					
Flat sheet	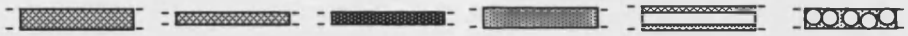					
Hollow fibres						

In order to determine the relationship between the volume change and the porosity change of the scaffold the following equations (Equation 7.10 to Equation 7.16) show a derivation of a linear model between the porosity remaining and volume remaining of the scaffolds.

Defining the percentage volume remaining:

$$v = \frac{v_f}{v_i} \times 100 \qquad \textbf{Equation 7.10}$$

v = Percentage volume remaining (-)

v_f = Final volume of scaffold (L^3)

v_i = Initial volume of scaffold (L^3)

The percentage porosity remaining:

$$P_r = \frac{P_f}{P_i} \times 100$$ **Equation 7.11**

P_r = Percentage porosity remaining (-)

P_f = Final porosity of scaffold (%)

P_i = Initial porosity of scaffold (%)

And the composition of the polymer in terms of void volume and polymer volume:

$$v_i = a_i + b_i \qquad v_f = a_f + b_f$$ **Equation 7.12**

a_i = Initial volume of void space (L^3)

a_f = Final volume of void space (L^3)

b_i = Initial volume of polymer (L^3)

b_f = Final volume of polymer (L^3)

The porosities of the scaffold at the beginning and the end of the culture period may be defined:

$$P_i = \frac{a_i}{v_i} \qquad P_f = \frac{a_f}{v_f}$$ **Equation 7.13**

Substituting these into Equation 7.11 give:

$$P_r = \frac{\frac{a_f}{v_f}}{\frac{a_i}{v_i}} = \frac{a_f}{v_f}\frac{v_i}{a_i} = \frac{a_i}{a_f}\frac{1}{v}$$ **Equation 7.14**

Assuming the volume of the polymer is negligible; the mass change of the scaffolds is much smaller than the volume change (~ 6% for mass compared to ~ 40% for volume).

$$b_i = b_f = b \qquad \textbf{Equation 7.15}$$

b = Volume of polymer (L^3)

Using Equation 7.10 and Equation 7.13 results in an expression for the remaining porosity of the scaffolds as a function of the remaining volume of the scaffolds:

$$P_r = \frac{v_i - b}{(v \times v_i) - b} \qquad \textbf{Equation 7.16}$$

The initial volume of the polymer and the scaffolds are known and therefore the porosity loss of the scaffolds (P_r) may be predicted from the volume loss of the scaffolds (v). Both the predicted values and experimental values of the porosity remaining plotted against volume remaining are shown in Figure 7.7. The graph shows the experimental values of porosity remain above those calculated. The trend line for the experimental results lies more than 20% above the calculated line in some places.

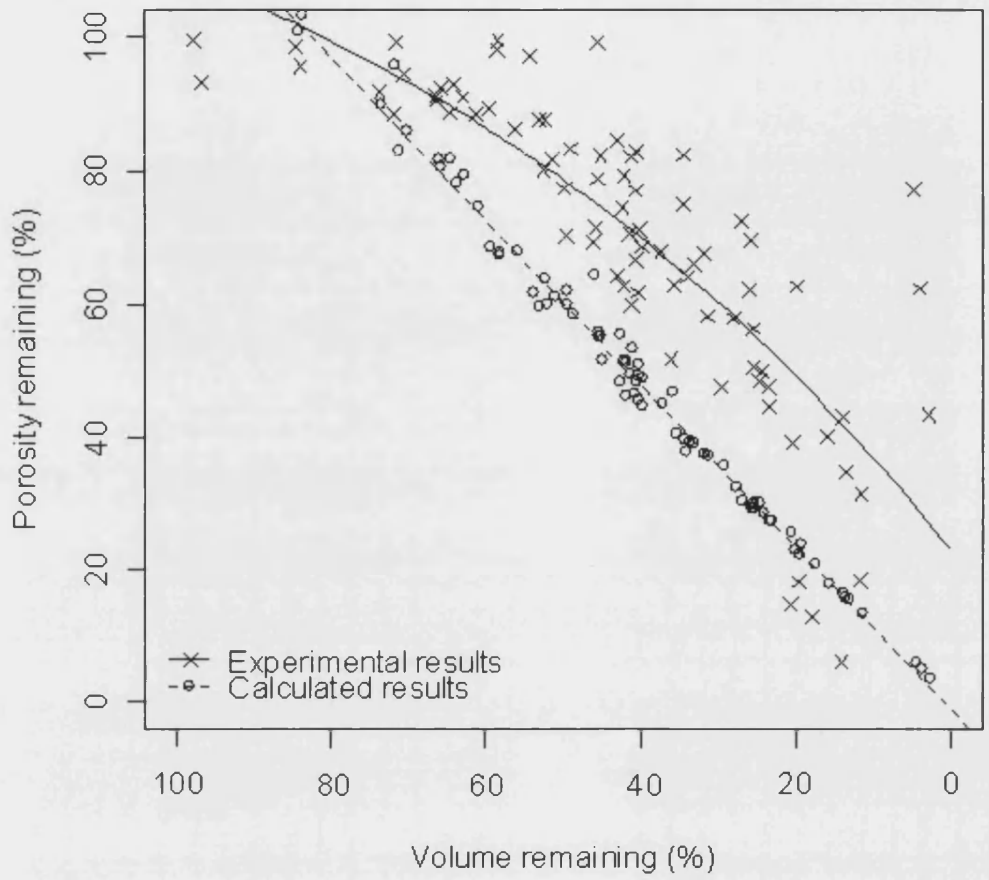

Figure 7.15 Scatter plot showing the relationship between residual volume and residual porosity of scaffolds following two weeks degradation.

Data was collected from all the culture studies, individual data points are shown with the statistically significant asymptotic trend line. Details of how the calculated results were generated are given in text and Equation 7.16.

The results show there is some decrease in porosity, ruling out the possibility of surface erosion being the single method of degradation, the porosity does not decrease as much as would be expected if shrinkage was the sole cause of the changes seen in the scaffold. This leaves the possibility of bulk erosion, autocatalytic degradation and combined effects. All three of these possibilities result in the same porosity and volume relationships; electron micrograph images can help to differentiate between the three options. These are shown in Figure 7.16; the spherical scaffold shows a large void appearing in the centre of the scaffold following a two week degradation period under

culture conditions. The degraded hollow fibre scaffold shows a slightly smaller diameter than the non-degraded sample, the pores in the fibre wall appear larger but are still well distributed through the scaffold.

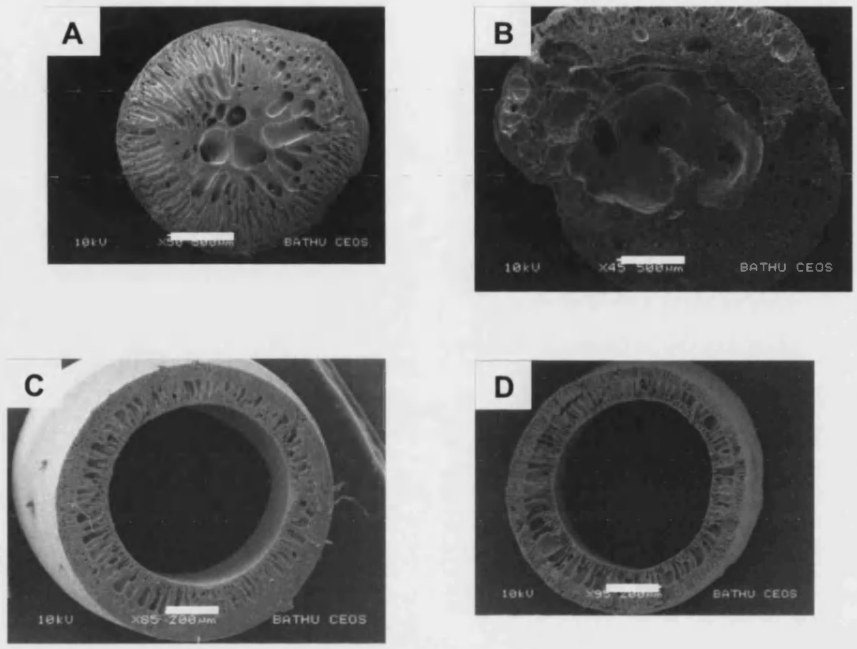

Figure 7.16 Electron micrographs of 50:50 PLGA scaffold cross sections before and after degradation.

A and B: *Spherical scaffolds, scale bar 500 μm,* ***C and D:*** *Hollow fibre scaffolds, scale bar 200 μm.* ***A and C:*** *Scaffolds before degradation,* ***B and D:*** *Scaffolds after two weeks under culture conditions. NB. The spherical particles are made from two different polymer types but this is a good representation of the characteristic structure of the spheres before and after culture. The hollow fibres are both the same type of polymer. The scale bar is the same length for the pictures of the same scaffold types. The spherical scaffold initially shows a highly porous structure with finger-like pores perpendicular to the surface of the scaffold, with a more heterogeneous region in the interior showing larger voids. After culture the interior of the scaffold shows a large void region characteristic of auto-catalytic degradation. The hollow fibre initially shows finger like pores perpendicular to the fibre walls, the degraded fibre shows a slightly smaller diameter and larger pores, the pores are still homogenously distributed around the fibre wall.*

Comparisons between the changes to the porosity and volume of the scaffold combined with electron micrograph images of the scaffold cross-sections reveal there are different mechanisms going on in the different scaffold shapes. The spherical particles appear to be under-going auto-catalytic degradation; build up of acidic degradation products in the scaffold interior that can't diffuse out leads to a faster rate of degradation in the interior of the scaffold, resulting in a large void area. This phenomenon has been observed in microspheres that are effectively the same structure just on a much smaller scale (Badri Viswanathan *et al.* 2001 and Park 1994), the spherical particles used in this study were approximately 1.5 mm (≡ 1500 μm) in diameter, an order of magnitude larger than microspheres that are typically ~ 100 - 200 μm in diameter. The microspheres observed to be undergoing autocatalytic degradation by Badri Viswanathan *et al.* (2001) were P(DL)LA, and similar PLGA microspheres degraded far more homogeneously, however the work by Park (1994) showed PLGA microspheres undergoing autocatalytic degradation, it has also been shown elsewhere (Grizzi *et al.* 1995) that heterogenic degradation is more common in larger scaffolds, quoting an estimated value of 200 – 300 μm as the scaffold size below which degradation would be homogeneous and above which degradation would be heterogeneous. So by that definition the spheres used in this study would definitely be expected to show autocatalytic degradation profiles.

Work by Park (1994) and Fu *et al.* (2000) confirmed that the appearance of a central void during degradation was a result of localised autocatalytic degradation. Park correlated the appearance of a central void with an expansion of the molecular weight range indicating that while degradation was occurring to shorten the molecular weight of the polymer, some of the polymer remained at the initial value of molecular weight, suggesting regions of degraded and un-degraded polymer. Fu *et al.* provided visual evidence of an acidic region associated with the void during degradation, confirming the theory that the release of acidic degradation products is responsible for the accelerated degradation in the region.

Autocatalytic degradation has also been shown to occur in thin films of PLGA (Lichun Lu 1999) resulting in void regions within the membrane.

The degradation of hollow fibre membranes has not been discussed in the literature as their use in the field of tissue engineering is relatively novel. It may be hypothesised that the membrane would undergo similar degradation to flat sheet membranes, as the membrane structure is very similar and may be considered to be a flat sheet wrapped round into the form of a fibre. The relationship between the porosity change and the volume change for the hollow fibre membranes followed the same pattern as the flat sheet and spherical scaffolds in this study, however the cross sectional electron micrograph (Figure 7.16) shows a more homogeneous structure than that of the spherical particle. The diameter of the fibre is slightly less than the initial image showing some shrinkage has occurred, however rather than one central void the porosity of the fibre has more homogeneously increased. The finger-like pores that the membrane develops during formation have increased in size but the basic structure has remained very similar. It is likely that the finger-like pores provide sinks for aqueous media to diffuse into the scaffold during degradation, in a similar role to when they act as sinks for the non-solvent and then solvent during membrane formation. Degradation of the polymer on the exterior of these pores occurs, reducing the pH of the media in the pore, this in turn catalyses further degradation. Where a more random porous network leads to the formation of a single large void in the scaffold centre the large poorly connected finger-like pores form lots of smaller voids. It is anticipated that this is mode of degradation is distinct from both typical autocatalytic behaviour and homogeneous bulk degradation. It is likely that a review of the molecular weight of the polymer would result in a broader molecular weight range than the initial scaffold but not to the same extent as with autocatalytic scaffolds.

7.4 Conclusions

This study has investigated the effects of PLGA properties such as lactide content and intrinsic viscosity, alongside scaffold properties such as initial porosity and surface area to volume ratio and the effects of different degradation conditions on the scaffolds.

The initial porosity of the scaffold was found to be the most influential factor in determining the extent of changes to the polymer and a lot of the results may be explained through a loss of the void space. However the characteristics of the polymer

such as lactide content and intrinsic viscosity may be used to tailor the change profile to meet specific requirements.

The conditions under which the scaffold is cultured are found to influence the changes to the polymer with those more closely matching *in vivo* conditions resulting in increased change. While it is not possible to adjust the conditions used for cell culture, understanding how these influence the polymer allows the correct decisions to be made when selecting polymers for specific applications.

The unique structure of the hollow fibre membranes has meant that a combination of autocatalytic degradation and homogenous degradation occurs in this scaffold form. An evaluation of the changes to the volume and porosity of the scaffolds was carried out. Spherical particles were found to be undergoing autocatalytic effects resulting in a single central void space developing within the scaffold. The hollow fibres were found to have a similar relationship between porosity and volume decrease with degradation; however the cross-sectional images suggested that rather than a single central void the initial interior architecture of the scaffold caused many smaller voids to develop. The internal pore structure allows small regions of auto catalysed degradation to occur but prevents the development of large macro voids that are more common with a more irregular interconnected porous structure.

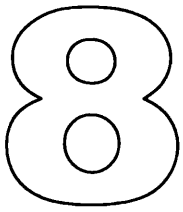

CHAPTER EIGHT - SPINNING OPERATION AND SPINNERET DESIGN

Considerations relating to the design and operation of the spinning rig

8.1 Introduction

The process of forming flat sheet or hollow fibre membranes through immersion-precipitation phase-inversion has been used for a long time. Despite numerous studies into its optimization the process remains somewhere between a science and an art. The reason for this is the level of complexity of the system; this process may initially seam simple – the extrusion of a polymer solution into a water bath – however the number processes governing the solidification of the polymer solution into a fibre make the precise control of the process difficult. This chapter aims to optimize the use of this process to manufacture PLGA hollow fibres for the bone tissue bioreactor through an extensive review of the literature and experimental investigations.

8.1.1 Mechanism of membrane structure formation

It is known that PLGA flat sheet and hollow fibre membranes suitable for tissue engineering may be cast by phase-inversion from polymer in solution with 1-methyl-2-pyrrolidinone (NMP) upon immersion in a water bath (Ellis 2005). In the PLGA:NMP:water system high miscibility between NMP (solvent) and water (non-solvent), and low polymer concentrations (~20% w/w) result in very rapid diffusion of solvent out of the polymer solution (Brodbeck *et al.* 1999). If the rate of diffusion of solvent out of the top layer is rapid this layer coagulates and restricts further diffusion by both solvent and non-solvent. The skin-layer thickness will increase until the

diffusion of the solvent out of the casting solution has led to sufficient coagulation to prevent further rapid diffusion (Young and Chen 1995). The skin layer resists mass transfer leading to a reduction in the gradient of the ratio of diffusivity of solvent to non-solvent, perpendicular to the surface, in the region below the skin layer. Due to the similar rates of diffusion across the sub-layer this layer develops a homogenous structure. At this point the structure of the sub-layer is dependant on the diffusion of non-solvent through the polymer skin. As the non-solvent diffuses through the skin layer the composition of the mixture crosses the binodal boundary line shown on the ternary phase diagram (Figure 8.1) and the solution becomes thermodynamically unstable and the nucleus of a pore is formed (Figure 8.2) (Young and Chen 1995). The nascent pore grows by the non-solvent continuing to diffuse into the pore providing a sink for the solvent to diffuse into and coagulation occurs at the perimeter of the pore. As the solvent diffuses out of the casting solution and into the pore the surrounding casting solution will become enriched in polymer leading to solidification, and this will prevent the pore from further growth. Finger-like pores perpendicular to the surface of the membrane are a result of solvent and non-solvent rapidly and consecutively diffusing into a nascent pore before solidification takes place (Young and Chen 1995).

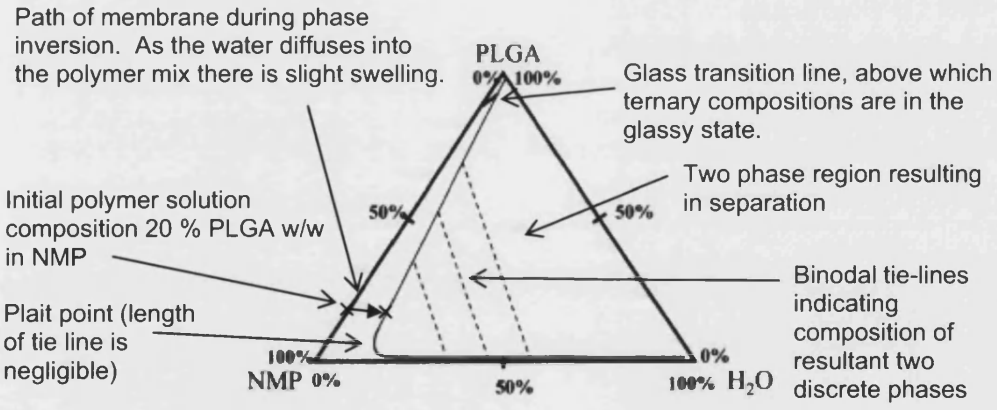

Figure 8.1 Phase diagram for PLGA, NMP and water .

Adapted from Brodbeck et al. 1999, tertiary diagram showing phase boundaries for the tertiary system PLGA, water, NMP. During casting the 20% solution of PLGA in NMP moves away from the NMP corner towards the H_2O corner, crossing the two phase boundary resulting in precipitation of the polymer.

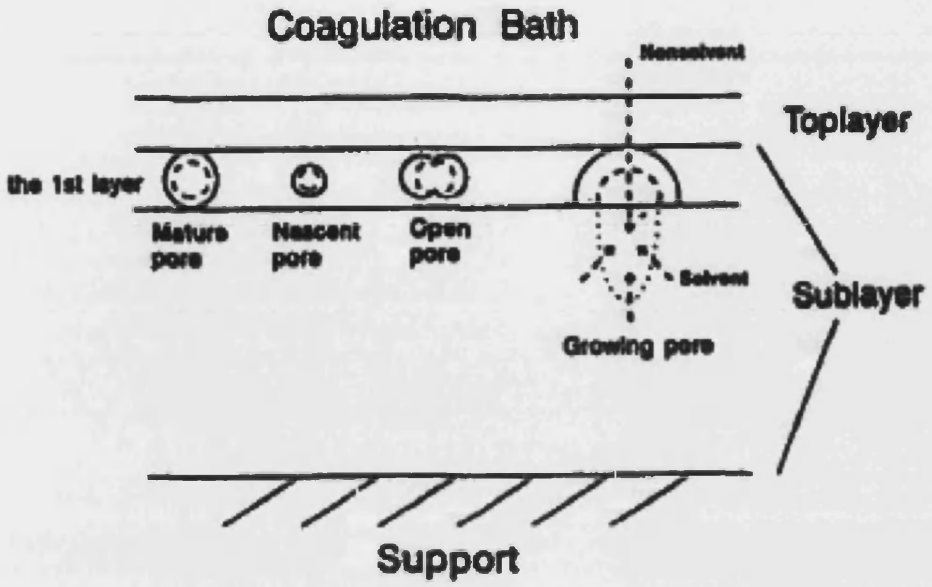

Figure 8.2 Schematic representation of pore formation in immersion-precipitation phase-inversion (Young and Chen 1995).

As the non-solvent diffuses into the solvent the tertiary mix becomes unstable causing a nascent pore to form. This pore then acts as a sink for both non-solvent and solvent, causing the pore to grow deeper into the membrane. Eventually enough polymer will have precipitated around the pore to prevent further growth of the pore.

The polymer precipitate continues to absorb water and can swell to almost double its original volume leading to large void fractions.

The presence of the finger-like pores, while reducing resistance to mass transfer, have also been reported to increase the distortion and occurrence of pin hole fractures in the fibres (Cabasso *et al.* 1977). For this reason in the field of gas separations efforts are made to reduce the formation of finger-like voids to improve the performance of the membranes.

The hollow fibres are the most critical component of the bioreactor. They must:

1. Support the cells,
2. Allow the transfer of nutrients through the fibre wall,
3. Degrade in a timely and predictable manner.

The properties of the fibres required to fulfil these criteria are all influenced by the production process.

8.1.2 Spinneret design

The design of the spinneret will influence the properties of the fibre; however the flexibility of the spinning process is such that even the dimensions of the fibre are not fixed by the geometry of the spinneret alone. Depending on the fluid dynamics of the solutions passing through the spinneret the polymer extrusion may swell as it exits through the orifice (Walczak 2002). Depending on the tertiary system the fibre may swell or shrink as residual solvent is removed by soaking and then as the fibre dries.

Spinneret design is a complex process. The internal geometry of the spinneret must be designed to provide the correct flow profile for the polymer. Differences to the shear stresses and flow of the polymer can lead to differences in the resultant fibre structure (Chung and Hu 1997a). Additionally the precise machining required to make a spinneret is very costly, therefore often compromises must be made in order to keep the costs at an acceptable level. Spinnerets may be utilised for the manufacture of more than one type of fibre with different requirements meaning specificity of spinneret to application is lost in favour of flexibility. The material the spinneret is made from is also important; the spinneret must be able to withstand the pressure required to pass a viscous solution through a small orifice. The material must be compatible with the solvents used in both the polymer solution and subsequent cleaning; any erosion of the surface could lead to undesired movement within the spinneret. It is important that the spinneret must be practical to use, including being able to thoroughly clean and validate as such. Any parts that come apart should allow adjustment to ensure the concentricity of the two orifices when put back together.

The consequence of the complexity of spinneret design means that almost all the research on hollow fibres reported in the literature is about fibres made on unique spinnerets; the design of which is often not clearly presented. This reduces the comparisons that may be made between reports in the literature and increases the need for independent study on the spinneret and polymer system in question.

8.1.3 Operating parameters

The effect of varying the operating parameters on the fibres can be divided into two categories; those affecting the macroscopic properties of the fibres (dimensions, ID/OD, shape), and those affecting the microscopic properties of the fibres (pore size,

permeability). The former has been well summarized in a table by McKelvey *et al.* (1997) and is shown in Figure 8.3. The latter is well discussed in the literature and a review is given below.

Processing Parameters	Macroscopic Properties: OD	ID	Diameter Variance, DV	Non-concentric bores, NCB	Irregular bores, IB	Ovality, OV	Fiber breaks, FB
Spinneret Design, SD 	Second order to DR.	Second order to Q_b.		Verify concentricity of D_1, D_2, D_3. Can require new SD to improve dope flow asymmetry.			SD often limits maximum Q_d due to dope elasticity and excessive pressure drop across spinneret.
Dope extrusion rate, Q_d	OD decreases as Q_d decreases when take-up vel. held constant.						FB increase as Q_d increases when DR is held constant due to dope elasticity.
Draw ratio, DR $\frac{V_f}{V}$	OD decreases as DR increases.	ID is controlled by Q_b onve OD is established using DR and Q_d.	Highly dope specific, DV often decreases as DR decreases.		Second order to SC, IB tend to decrease as DR decreases.	Second order to location of SLG, OV tends to decrease as DR increases since decreasing OD increases VK.	Typically, FB decrease as DR decreases since tensile stress tends to be reduced.
Gap height, GH			DV dependent on GH but highly dope specific.		Second order to SC.	Second order to VK in quench bath.	FB dependent on GH but highly dope specific.
Bore fluid extrusion rate, Q_b	Second order to DR.	ID decreases as Q_b decreases.				Second order to location of SLG, however, OV tends to decreases as Q_b increases since increasing OD/ID increases VK.	
Solvent concentration in bore fluid, SC					IB decrease as SC increases.	OV tends to decrease as SC decreases since SC is coupled to VK.	Low SC can increase FB.
Vitrification kinetics, VK	Fiber shrinkage is second order to DR.	Second order to Q_b.	Highly dope specific, DV tends to decrease as VK increases.		IB decrease as VK at fiber ID decrease.	OV decreases as VK increases.	Highly dope specific, decreasing VK often allows increased DR without FB.
Spin line guides, SLG			Minimize fluctuations in tensile force.			OV decrease as residence time in quench bath before contacting first SLG increases.	Decrease FB in or after the quench bath by decreasing SLG friction.

Figure 8.3 Summary of the parameters controlling the macroscopic features of the fibres, adapted from Mc Kelvey *et al.* (1997).

The macroscopic features of the fibres may be controlled by controlling the processing parameters during spinning. Some of these may be varied easily such as flow rates and gap height, however the bore diameters are fixed by the spinneret.

The microscopic properties of the fibre, which will influence its performance in all three of its roles within the bioreactor, are controlled by two key factors:

1. Diffusion rates of non-solvent and solvent into and out of the polymer solution;
2. Shear rates in the spinneret which act to align polymer molecules.

A review of the literature allows the following table (Table 8.1) to be generated for operating parameters influencing the microscopic properties of the fibres.

Table 8.1 A review of literature on the effects changing operating parameters during spinning has on the fibre structure.

Processes utilising spinning technology for the production of hollow fibres are widely published, however the process is still not well understood and spans the boundary between art and science. Factor 1 relates to the parameter being controlled by the diffusion rates of the solvent and non-solvent. Factor 2 relates to the parameter being controlled by the shear stresses within the spinneret. ***MWCO*** *is molecular weight cut off,* ***DMSO*** *is dimethyl sulfoxide,* ***DMF*** *is dimethylformamide,* ***THF*** *is tetrahydrofuran*

Operating Parameter	***Factor 1 or 2***	***Influence***	***Notes***	***Ref***
Solvent	1	Different solvents can result in membranes with different MWCO. Eg.50:50 PLGA with: DMSO – 70 kDa, DMF – 80 kDa, THF – 100kDa	The choice of solvent also has a number of other influences on the polymer structure and may ultimately impact on the biocompatibility of the fibres. In this case the solvent chosen has been fixed as NMP based on work by Ellis and Chaudhuri 2005.	Wen and Tresco 2006; Ellis 2005
Water flow rate	2	Increasing water flow rate reduced MWCO.	This is probably attributed to increasing shear stresses, however it is also likely that it would reduce boundary layer concentration profiles by increasing mixing in the bore fluid.	Wen and Tresco 2006
Polymer flow rate	2	Increased polymer flow rate reduces MWCO.	Increasing polymer flow rate increases shear stresses within the reactor, this is thought to align the polymer molecules which allows for tighter packing on molecules on the surface and the formation of a dense skin. This prevents the movement of molecules allowing the passage of permeant molecules	Wen and Tresco 2006; Chung and Hu 1997a
Air gap	2	* See text below	* See text below	* See text below
Temperature	1 and 2	Increase MWCO	Temperature will act in two ways, firstly it will reduce the viscosity of the spinning dope, reducing the shear stresses within the spinneret; secondly it will increase the diffusion coefficients of the solvent and non-solvent.	Wen and Tresco 2006

Continued

Table 8.1 Continued

Operating Parameter	*Factor 1 or 2*	*Influence*	*Notes*	*Ref*
Porogen	-	Adding a porogen will increase porosity and increase MWCO	The presence of a porogen changes the mechanism by which the pores are produced. The porogen would then have to be eliminated from the fibre, addition further processing stages.	Wen and Tresco 2006
Polymer concentration	1 and 2	Increasing polymer concentration will increase MWCO	Increasing polymer concentration will increase solution viscosity which will increase shear stresses in the spinneret. It will also change the driving forces for the diffusion of solvent and non solvent. As more space will be taken up by polymer there will be reduced porosity.	Wen and Tresco 2006
Bore fluid composition	1	Presence of solvent in bore fluid increases the distance between adjacent pores*. It also reduces the finger-like pore structures below the surface and reduces the thickness of the skin layer.	(*This information is from the formation of flat sheets.) In this reference the formation of pores is described as a result of osmotic shock from a large currant of solvent into the non-solvent; by loading the non-solvent with solvent the concentration difference is reduced, reducing the flow of solvent out of the scaffold, and reducing the number of pores. The presence of finger-like pores perpendicular to the surface are also reduced by the presence of solvent in the quench fluid. The presence of solvent in the bore fluid also reduces the initial rate of coagulation, thereby reducing the change in rate of coagulation over the initial stages that results in a skin layer.	Cohen Addad *et al.* 1995 Cabasso *et al.* 1977; Chung and Hu 1997a

* There are many opinions on the effects of the presence of an air-gap in the spinning process. There are examples of an increased air gap both increasing and decreasing the permeance of the membranes. This may be due to a number of factors which have opposing influences and the significance of these different factors may come in to play at different points for different systems. Table 8.2 gives a summary of these arguments.

The presence or absence of an air gap and its subsequent effect on the nascent fibre is a widely argued point. Contradictory arguments for an air gap leading to increased or decreased fibre permeance are presented in Table 8.2.

Table 8.2 Influence of the air gap on fibres formed by the spinning process.

Summary of arguments for the air gap during spinning to increase or decrease skin pore size and

Air gap increases pore size/permeance	***Air gap decreases pore size/permeance***
The air gap increases longitudinal stress which may act to pull apart adjacent polymer chains or adjacent phase separated regions (Chung and Hu 1997b).	The air gap increases longitudinal stress which may act to orientate polymer chains allowing tighter packing (Chung and Hu 1997b).
Shear stresses in the spinneret align polymer molecules, which are frozen in this densely packed arrangement on immediate contact with the water bath (Qin *et al.* 2000, Qin *et al.* 2001).	In the solvent the polymer chains are relaxed, on sudden precipitation on contact with the water bath they contract leaving more free space. In the air gap the contact with moisture is slower allowing polymer chains to relax into their new shape with complex short range interactions and reduced free volume (Chung and Hu 1997b).
Decreasing the air gap decreased the molecular weight cut off (experimental data; Wen and Tresco 2006).	Air gap reduces permeations by generating fibres with a more defect free skin due to the low initial rates of solvent removal (Qin *et al.* 2001).

8.1.4 Methodology

The reports given in the literature on the affects of operating parameters on the macro and microscopic properties of the fibres vary. This makes the decision making process for the optimization of hollow fibres for use in a bone tissue engineering hollow fibre bioreactor harder. The following study is designed to monitor the effects of polymer and operating conditions on the fibres. Different polymer compositions and intrinsic viscosities are studied alongside varying operating conditions. The experiment is conducted within the limitations of an existing spinning rig, as previously mentioned the precision engineering required for the manufacture of spinnerets is extremely costly, and therefore the cost prohibits the use of a variety of spinneret configurations. However due to the particular sensitivity of this study to the fibre manufacturing procedure some adaptations were made to the operation of the spinning rig. Method B (Section 3.3.1.3) was employed for the method of extrusion of the polymer, affording greater control over the flow rates of both the polymer and water as well as minimising polymer wastage, which becomes increasingly significant when multiple batches of

fibres are required. In addition to adapting the feed of the polymer and the water, small changes were made to the spinneret to improve fibre concentricity and reduce the potential for the water to leak inside the spinneret causing the polymer to precipitate and block the orifice.

8.2 Results

The results are divided into sections reviewing the contributions to the final form of the fibre from the spinneret and operating conditions and the polymer solution. Details of the polymers used are given in Table 3.1. Where a unique polymer is not identified the results are given as an average for all the polymers tested. Where an average value is presented there was no statistically significant reason for differences between the polymers. All membranes studied in this Chapter were hollow fibres.

8.2.1 The spinneret and spinning conditions

Diameters of fibres extruded through the spinneret are presented in Table 8.3; no indication of significant die swell is occurring with the maximum fibre diameter only 13% larger than the diameter of the orifice. There was no significant difference between the different polymers tested. Details and a diagram of the spinneret are given in Section 3.3.1.3.

Table 8.3 Inner and outer diameters of the spinneret and fibres.

Measurements were taken from all the different polymers spun with the spinneret (n = 8).

	Inner diameter (mm)	*Outer diameter (mm)*
Spinneret	0.65	1.30
Mean fibre diameter (± s.d.)	0.78 ± 0.07	1.36 ± 0.06
Min. fibre diameter	0.70	1.30
Max. fibre diameter	0.90	1.47

Figure 8.4 shows that the absence of die swell in fibres extruded through the spinneret is typical of the flow rates and orifice diameters used. Solid fibres were extruded through a range of nozzle sizes appropriate to the spinneret. The range of nozzle sizes, flow rates tested with a PLGA:NMP:water system showed no signs of die swell. This experiment did not take into account the shape of the spinneret; the fibres were extruded

through a single circular orifice and the nozzle approaching the orifice was tapered. However the results suggest the spinneret is behaving typically for the orifice size and polymer flow rates.

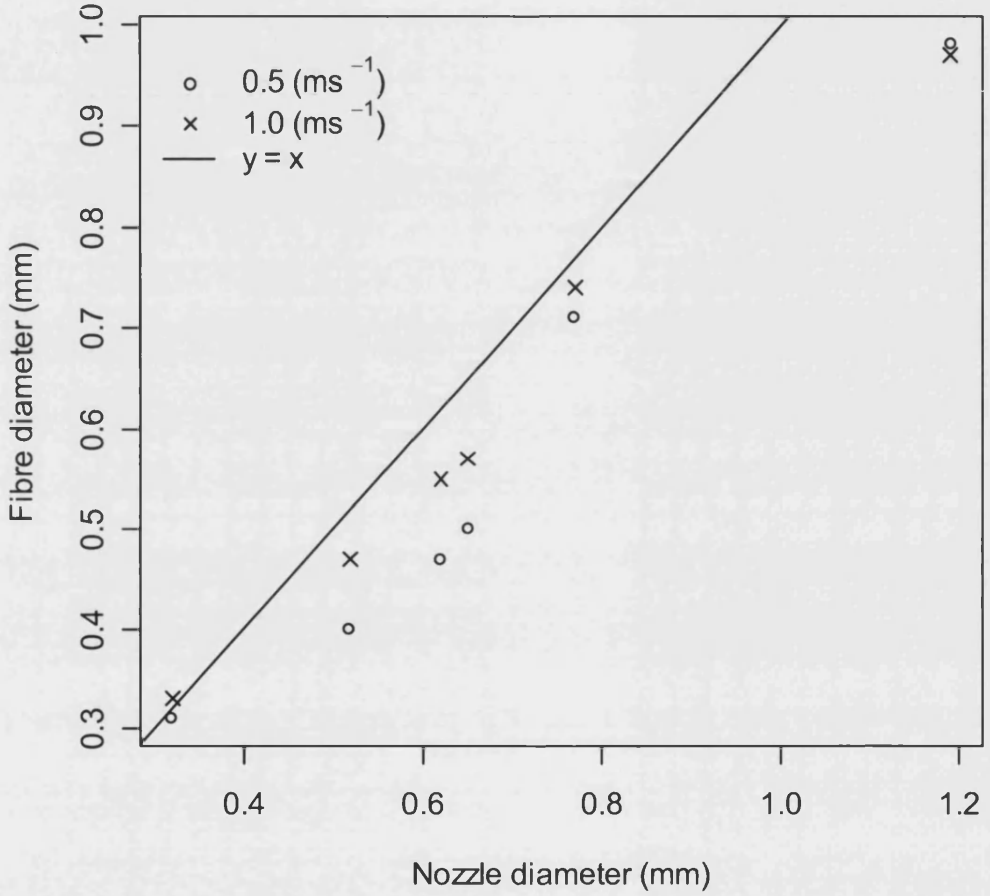

Figure 8.4 Chart showing die swell characteristics of polymer solution extruded through nozzles of varying diameter at different flow rates.

Solid fibres extruded through nozzles of a similar size to the spinneret at speeds relevant to the spinning process showed no indication of the die swell phenomena. The diameters of the resultant dry fibres were typically just below the size of the nozzle through which they had been extruded.

Table 8.4 details the operating parameters used when spinning; values calculated to aid the characterisation of the flow through the spinneret are also presented. Details of the calculations used to obtain these values are given in Appendix A.5. These details are further discussed in Section 8.3.3.2 and are used to make assumptions about the flow profile though the spinneret.

Table 8.4 Spinning parameters.

The operating conditions and physical parameters with the spinning rig included calculated values for reference.

Parameter		Value	Unit	Notes	Ref
Orifice inner radius	R_1	3.25×10^{-4}	m		
Orifice outer radius	R_2	5.00×10^{-4}	m		
OD/ID ratio	R_2/R_1	1.54		Should be around 2	McKelvey *et al.* 1997
Annulus length	L	3.00×10^{-3}	m		
Annulus area	A	4.54×10^{-7}	m^2		
Take up rate	u	1.33×10^{-1}	$m\ s^{-1}$	No drawing (stretching of the fibre during collection)	
Polymer volumetric flow rate	Q	6.05×10^{-8}	$m^3\ s^{-1}$	Range used 170 – 220 $cm^{-3}h^{-1}$ (≈ 10 cm s^{-1} linear velocity)	
Water volumetric flow rate	Q_w	6.05×10^{-8}	$m^3\ s^{-1}$	Range used 170 – 220 $cm^{-3}h^{-1}$ (≈ 10 cm s^{-1} linear velocity)	
Air gap		0	m	Range used 0 – 0.1 m	
Concentration of NMP in bore fluid		0	%	Range used 0 – 75%	
Temperature of water bath		14	°C	Ambient	
Viscosity of polymer	μ	1.00	$kg\ m^{-1}\ s^{-1}$	Ideally between 1-10	Ellis 2005
PLGA density	r_{PLGA}	1.39×10^3	$kg\ m^{-3}$		MSDS
NMP density	r_{NMP}	1.03×10^3	$kg\ m^{-3}$		MSDS
Solution composition	C	2.20×10^{-1}	w/w	Range used 15-25% (w/w)	
Solution density	r	1.11×10^3	$kg\ m^{-3}$		
Hydraulic mean diameter	d_h	3.50×10^{-4}	m		Coulson *et al.* 1999
Reynolds number	Re	5.18×10^{-2}		=> Laminar flow. Should be around 0.5	Coulson *et al.* 1999, Shilton 1997
Friction factor	f	2.13×10^2		Due to low Re, friction factor is independent of roughness	Coulson *et al.* 1999
Pressure drop per unit length	dl/dz	1.92×10^{-8}	$kg\ s^{-2}$	In annulus	Coulson *et al.* 1999
Acceleration due to gravity	g	9.81	$m\ s^{-1}$		Perry *et al.* 1997

8.2.2 Diffusion of water into an element of polymer solution

Figure 8.22 shows the results of a study into the propagation of the coagulation front into an element of a fibre using a purpose designed chamber (details of which can be found in the materials and methods section 3.6.2.2). The experimental result and significant polynomial correlation is presented. The pattern of the experimental data is a factor of the accuracy of the experiment. Measurements of the position of the coagulation front were made from a series of photographs; the resolution meant that the measurements were only accurate to 100 μm.

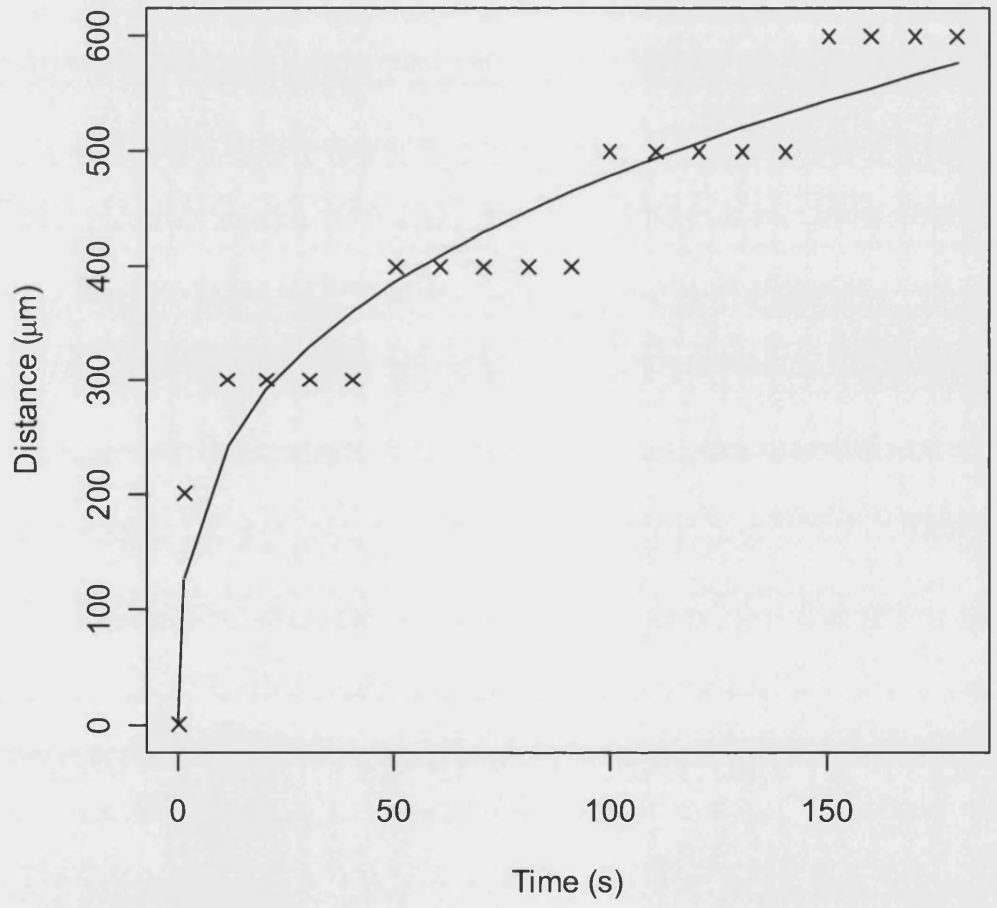

Figure 8.5 Chart showing the diffusion profile of water into a droplet of polymer.
*Both the experimental results (shown as **crosses**) and the statistically significant polynomial regression line (shown as a **solid line**) the polymer tested was D7525.*

Polynomial regression resulted in a statistically significant polynomial correlation between the position of the coagulation front and time. The line is shown in Figure 8.5 and the equation given by Equation 8.1 (mean estimate ± standard error).

$$d_t = (112.4 \pm 17.0)t^{(0.31 \pm 0.03)} \qquad \textbf{Equation 8.1}$$

d_t = Distance into polymer of coagulation front at time = t (L)

t = Time (T)

8.2.3 Polymer solution

A range of polymer lactide contents and intrinsic viscosities were tested for influence on the fibre properties. A range of suppliers were used to generate a suitable range of polymers. It was noted the polymer appearance varied considerably in both colour and form. The colour of the polymer was recorded from a photograph. The values of the red green and blue channels were combined into a single grey-scale value to give a numerical value for the colour of the polymer. No correlation was observed between the numerical value for the colour of the polymer and any contamination with trace elements as reported in the certificates of analysis, lactide content or intrinsic viscosity. A communication to one of the manufacturers revealed the colour variation of the polymer was to do with the temperature of the polymerization and would bear no influence on the properties of the polymer (Bryant 2006).

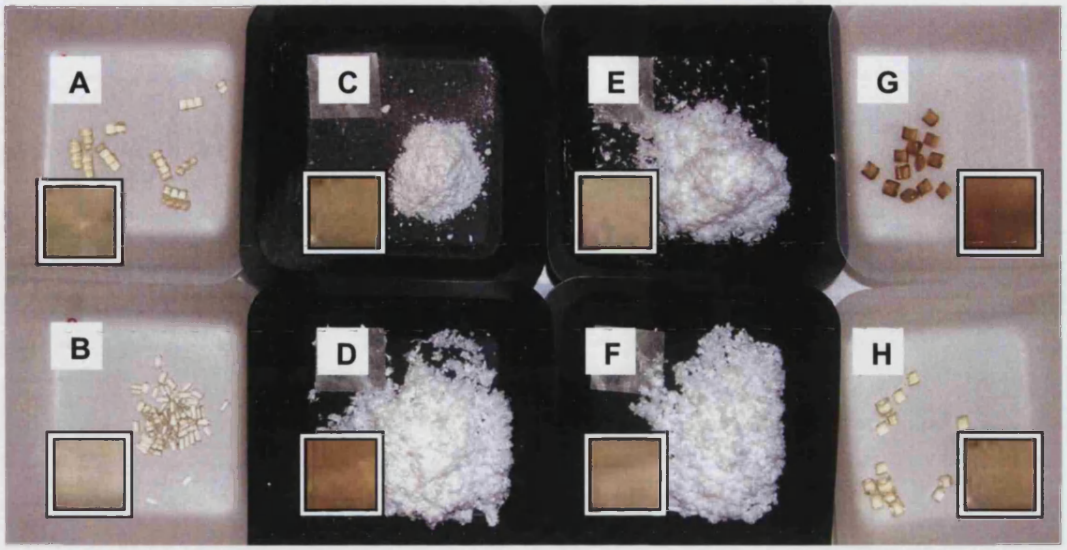

Figure 8.6 Photograph showing the varied appearance of the polymer raw materials.
The same mass of each polymer is shown, polymer varied in colour from white to brown, with forms of pellets, bulky powders and crystalline powders. Even different batches of the polymers with the same specifications from the same manufacturers were observed to vary in appearance. Insets show the colour of solutions of the polymers in NMP; the colour of the raw polymer is not always a good indicator of the colour of solution. ***A*** *= LS5050,* ***B*** *= PS5050,* ***C*** *= RG503,* ***D*** *= RG504,* ***E*** *= RG755,* ***F*** *= RG756,* ***G*** *= D5050,* ***H*** *= D 7525. Details of the polymer properties are given in Table 3.1 (Background colours were chosen to improve the contrast with the polymer and hold no significance).*

In improve the consistency of the fibres the viscosities of the polymer solutions used for spinning were controlled to within a narrow band by altering the composition of the solution. Figure 8.7 shows the relationship between concentration and viscosity for each of the polymer solutions. Also shown is the optimum range chosen for spinning. Ellis (2005) reports that a viscosity of 1 – 10 Pa s is required for the solution viscosity to be sufficiently low to flow through the spinneret while sufficiently high that the extruded annulus may hold its shape during the precipitation process. The low end of this range was chosen as the viscosity must be adjusted be changing the concentration of the polymer solution, it is likely a lower polymer concentration will result in a higher porosity of the resulting fibre. It was found that the lower end of this band could be extended to as low as 0.7 Pa s without any detrimental effects on the fibre. The lowest intrinsic viscosity polymer required a solution concentration of nearly 45% w/w to achieve a viscosity high enough for spinning; however the solution was found to be

unable to hold itself together in the form of a fibre. The polymer fragmented and appeared granular when it was extruded into the water bath.

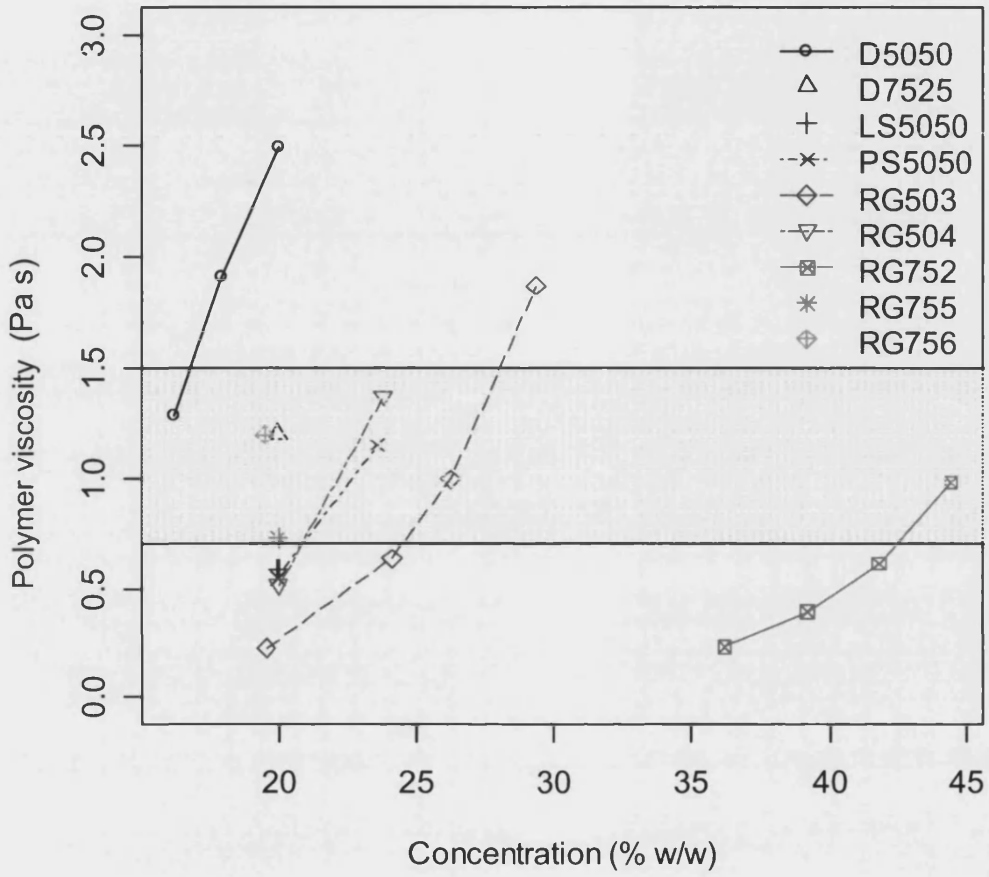

Figure 8.7 Relationship between concentration and viscosity for the different polymers.
Polymer solution viscosities were adjusted by altering the concentration of the solution to ensure the viscosity was optimized for spinning. Details of the polymers are given in Table 3.1. All polymer solutions were tested at 20°C. ***Shaded region*** *shows optimal spinning conditions.* ***Connecting lines*** *are presented to highlight the trend for individual polymers, they are for display purposes only and have no physical meaning. The lowest intrinsic viscosity polymer (RG752S) was found to be unsuitable for spinning even with a viscosity within the required range.*

8.2.3.1 Pore size and porosity

The pore size and surface porosity of the scaffolds were evaluated through image analysis of electron micrographs. Effective pore diameters were calculated from the pore area assuming circular pores. The geometric mean was used as an average value

for comparison (refer to Section 5.2.1.2). The bulk porosity was evaluated from the mass and density of the polymer and the bulk volume of the scaffold.

The influence of the concentration of the spinning solution on the bulk porosity of the resultant fibre is presented in Figure 8.8. Different polymers were used to create solutions of different concentration that were of suitable viscosity for spinning. Details of the polymers are given in Table 3.1.

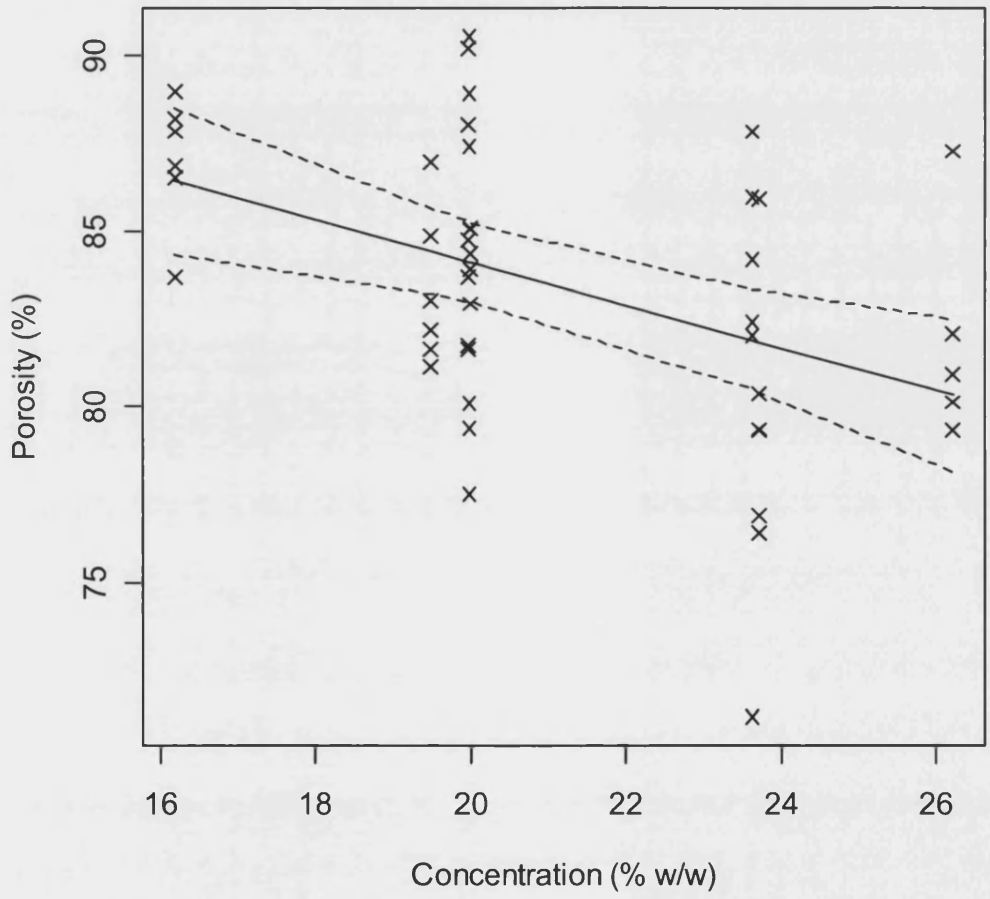

Figure 8.8 Scatter plot showing the influence of the concentration of the polymer solution on the hollow fibre membrane porosity.

A significant ($p < 0.005$) linear correlation is found and shown along with the 95% confidence interval.

$$p = (93.4 \pm 5.9) - (0.5 \pm 0.3)C \qquad \textbf{Equation 8.2}$$

p = Porosity (%)

C = Concentration of solution (% w/w) (-)

The influence of the operating conditions during spinning on the surface pore size and surface porosity of the fibres were also investigated. The air gap and the water bath temperature were found to influence the internal pore diameter, however the concentration of NMP in the bore fluid was not found to influence internal pore diameter. This data is presented in Figure 8.9 and Figure 8.10 with details of the significant trend lines in Equation 8.3 and Equation 8.4. Increasing the air gap resulted in a decrease in the average effective interior pore size, as did increasing the water bath temperature.

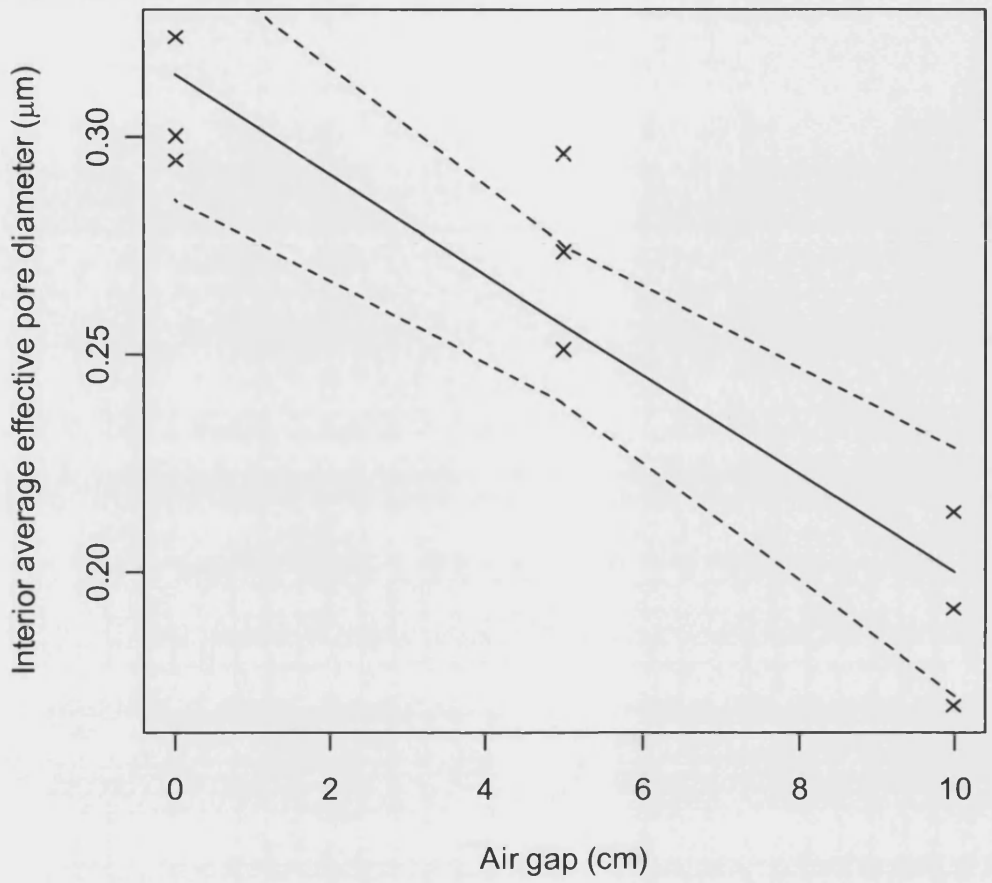

Figure 8.9 Scatter plot showing effect of air gap on interior average effective pore diameter.

A significant correlation is found between the interior average effective pore diameter and the air gap, all data is from the D7525 polymer. No correlation is found between the pore diameter and the bore fluid composition, or the temperature of the water bath.

$$\bar{d}_{ei} = (3.1 \pm 0.1) \times 10^{-1} - (1.1 \pm 0.2) \times 10^{-2} G \qquad \textbf{Equation 8.3}$$

$\bar{d}_{ei}$ = Interior average effective pore diameter (L)

G = Air gap (L)

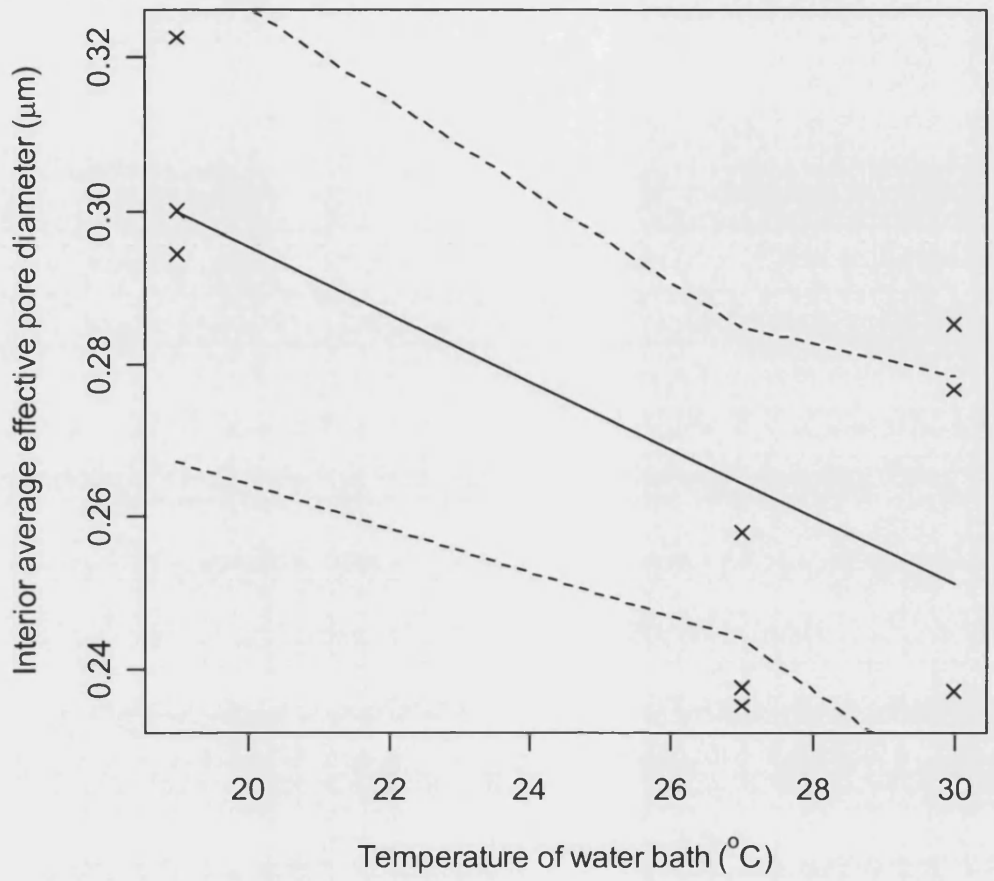

Figure 8.10 Scatter plot showing effect of water bath temperature on interior average effective pore diameter.

A significant correlation is found between the interior average effective pore diameter and the external water bath temperature. All data is presented for the D7525 polymer No correlation is found between the internal pore diameter and the bore fluid composition, or the temperature of the water bath and the external pore diameter.

$$\bar{d}_{ei} = (3.8 \pm 0.5) \times 10^{-1} - (4.4 \pm 1.8) \times 10^{-3} T \qquad \textbf{Equation 8.4}$$

$\bar{d}_{ei}$ = Interior average effective pore diameter (L)

T = Temperature of water bath (Θ)

The external pores size was found to be influenced only by the concentration of the NMP in the bore fluid and not by the temperature of the water bath or the air gap.

Increasing the concentration of NMP in the bore fluid was also found to result in a decrease in pore size on the exterior of the membranes. The data is presented in Figure 8.11 with the equation for the significant trend plane given in Equation 8.5.

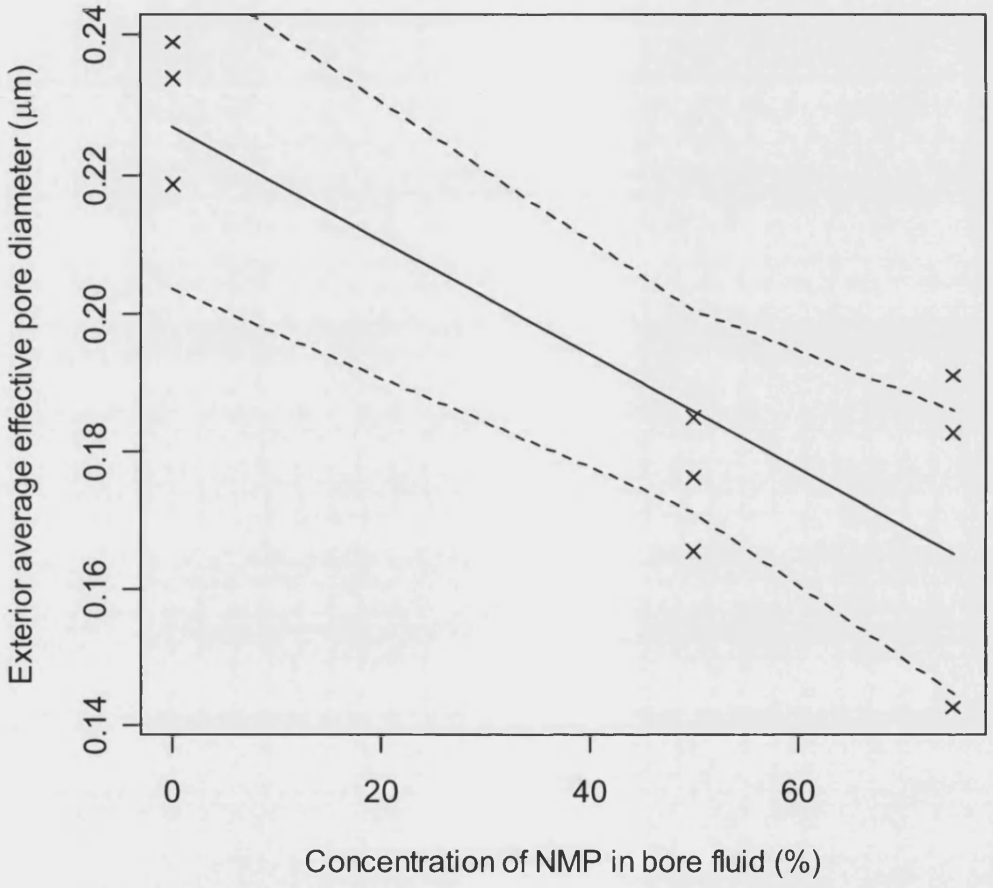

Figure 8.11 Scatter plot showing effect of concentration of NMP in bore fluid on exterior average effective pore diameter.

A significant correlation is found between the exterior average effective pore diameter and the concentration of NMP in the bore fluid. All data is presented for the D7525 polymer. No correlation is found between the pore diameter and the temperature of the water bath or the air gap.

$$\bar{d}_{ee} = (2.2 \pm 0.1) \times 10^{-1} - (8.2 \pm 1.9) \times 10^{-4} B \qquad \textbf{Equation 8.5}$$

$\bar{d}_{ee}$ = Exterior average effective pore diameter (L)

B = NMP concentration in bore fluid (%) (-)

The polymer and water flow rates were not found to affect the surface pore size on either the interior or the exterior of the fibre, however the surface porosity of the interior of the fibre was found to be influenced by water and polymer flow rates. Data for the interior and exterior surface porosity against both polymer flow rate and water flow rate is presented in Figure 8.12 with a trend line showing the significant correlation for the interior surface porosity, no significant correlation was found for the exterior surface porosity. Decreasing the polymer flow rate and increasing the water flow rate was found to increase the interior surface porosity, the equation for the trend plane is given in Equation 8.6.

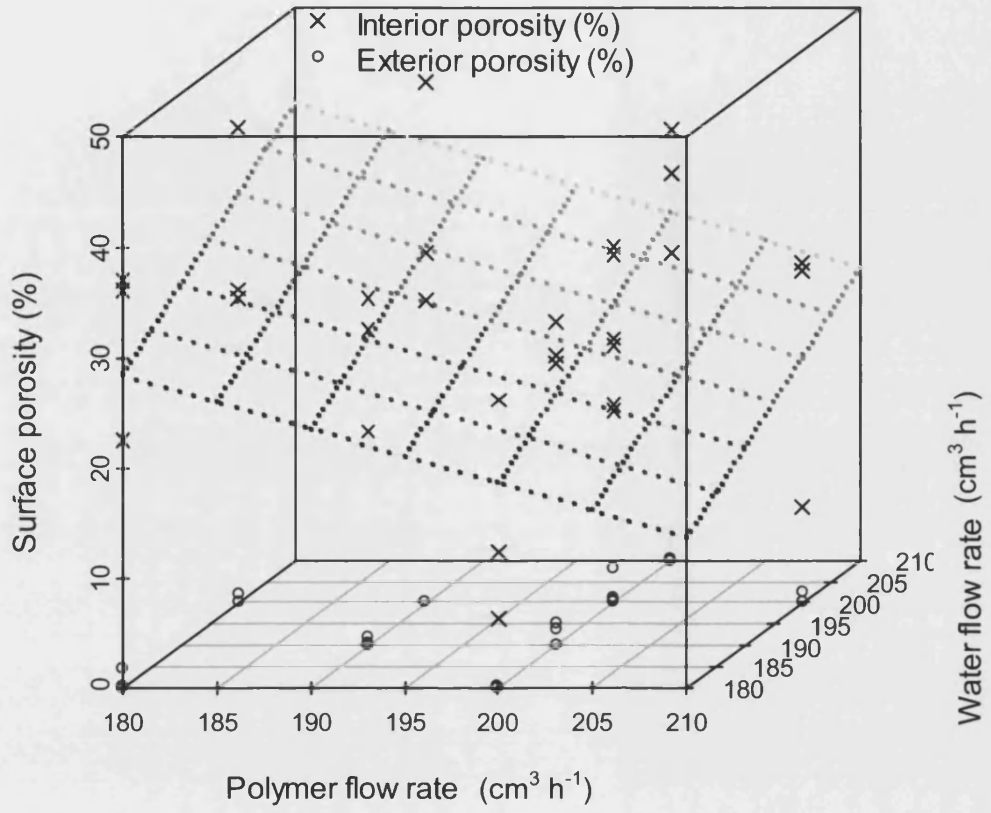

Figure 8.12 Three-dimensional scatter plot showing effect of polymer and water flow rates on membrane surface porosity.

*A significant correlation is found between the internal surface porosity and polymer and water flow rates, as shown by the plane (**dotted lines**). No correlation is found between the external porosity and polymer and water flow rates. Typically the exterior surface of the membrane exhibits much lower surface porosity. Points on the plane darken with decreasing values of water flow rate.*

$$p = 39.9 \pm 37.6 - (4.9 \pm 1.6) \times 10^{-1} v_p + (4.3 \pm 1.6) \times 10^{-1} v_w \qquad \textbf{Equation 8.6}$$

p = Porosity (%) (-)

v_p = Volumetric flow rate of polymer (L^3T^{-1})

v_w = Volumetric flow rate of water (L^3T^{-1})

The porosity and pore size of the membranes is very closely related, suggesting an increase in porosity is a result of an increase in pore size rather than pore number. Figure 8.13 presents data from the interior and exterior of fibres, no significant difference in the correlation between pore size and surface porosity was found between the interior and the exterior of the fibres. This correlation is presented in Equation 8.7.

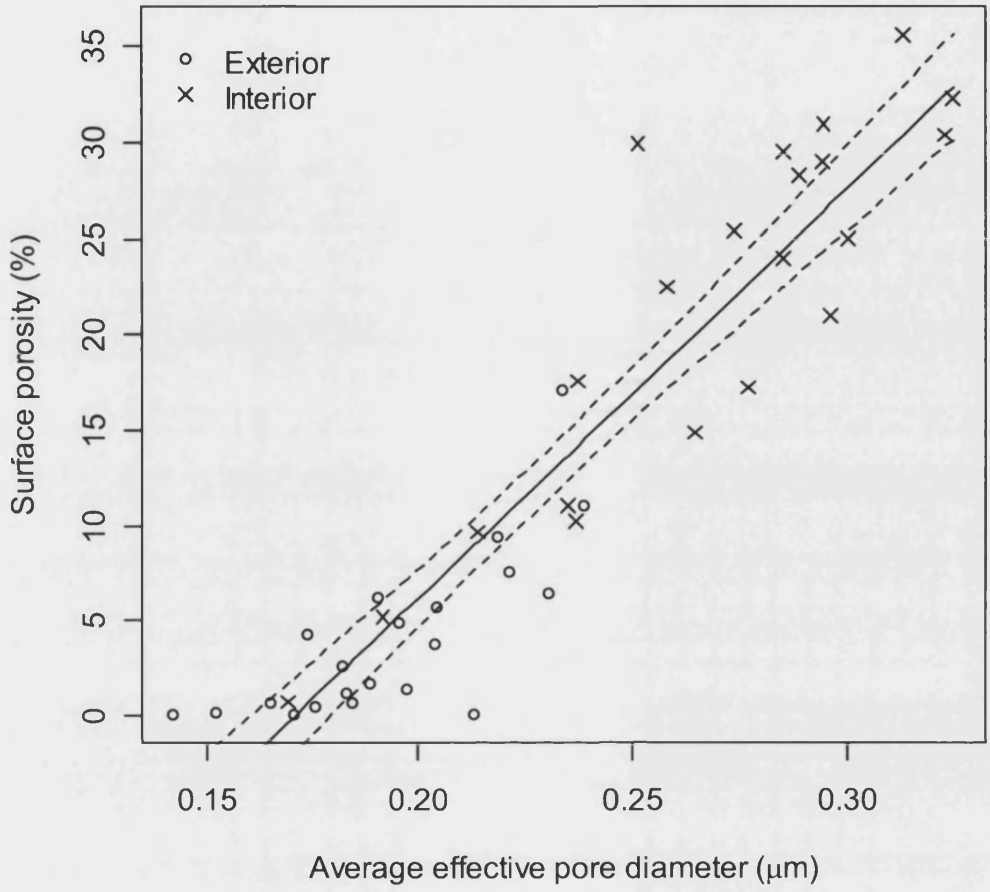

Figure 8.13 Scatter plot showing the correlation between pore size and porosity for hollow fibre membranes.

A significant correlation is found between the porosity and pore diameter on both the interior and exterior of the hollow fibre membranes across all the polymer types.

$$P = (214.4 \pm 12.9)\bar{d}_e - 36.7 \pm 3.0 \qquad \textbf{Equation 8.7}$$

P = Surface porosity (%) (-)

$\bar{d}_e$ = Average effective pore diameter (L)

The average effective pore diameters on both surfaces of the hollow fibre membranes were compared to that of the upper surfaces of flat sheets membranes. No significant difference was found between the three values by ANOVA. The interior of the hollow

fibres showed the larges average pore size followed by the upper surface of the flat sheets with the exterior surfaces of the hollow fibres exhibiting the smallest pore sizes as is shown in Figure 8.14.

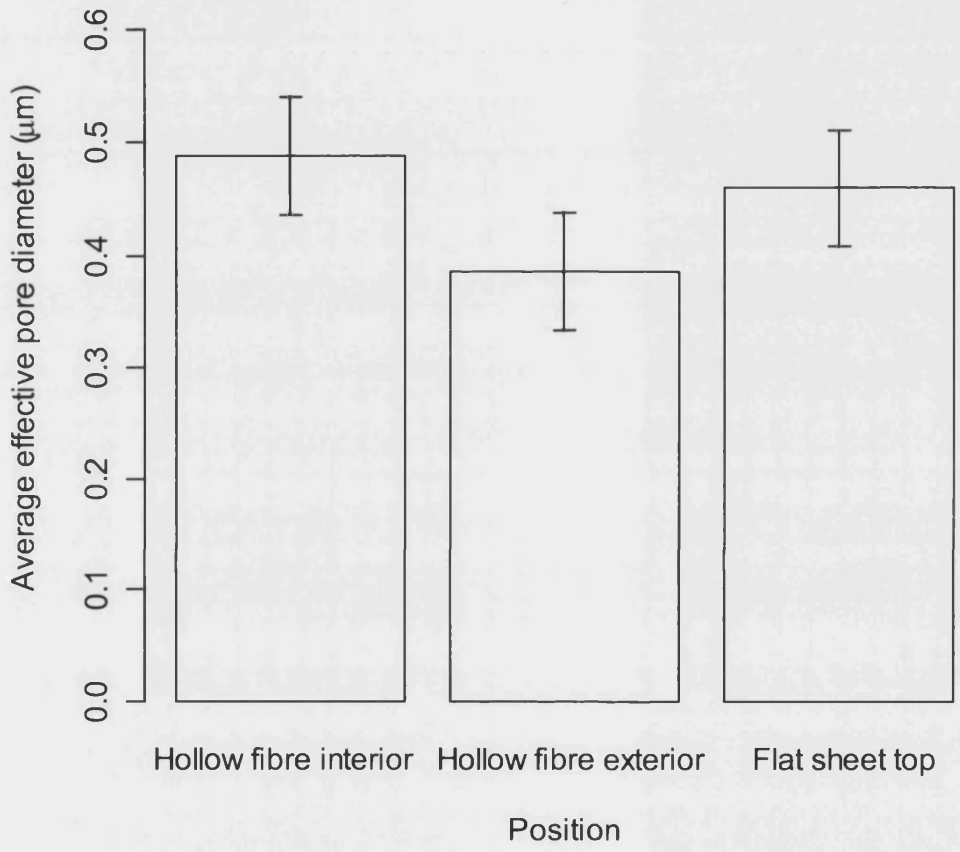

Figure 8.14 Average effective pore diameter on different membrane locations.

A significant difference was found between the average pore diameter on the interior and exterior of the fibres. The average pore size on the top surface of the flat sheets was in between the values for the hollow fibres with no significant difference between the flat sheets and the interior or exterior of the fibre measurements were taken across all the different polymer types and no other significant explanatory variable was found (mean ± lsd; n=8).

8.2.3.2 Shape

Two fibre shape factors were defined to quantitatively assess the influence of the operating parameters on the fibre shape. The fibre concentricity factor is defined by Equation 8.8 and is a quantitative summary of the concentricity of the fibre, or how symmetrically the lumen is placed within the fibre outer profile.

$$R = \frac{t_{min}}{t_{max}}$$ **Equation 8.8**

R = Fibre concentricity factor (-)

t_{min} = Minimum fibre wall thickness (L)

t_{max} = Maximum fibre wall thickness (L)

The fibre structure factor, as described by Equation 8.9, defines the length of the interior ring of finger like pores. This value is anticipated to be influenced by the relative rates of diffusion into the interior of the fibre wall and the exterior of the fibre wall.

$$\alpha = \frac{t_p}{t} \times 100$$ **Equation 8.9**

α = Fibre structure factor (-)

t_p = Length of finger-like pores (L)

t = Fibre wall thickness (L)

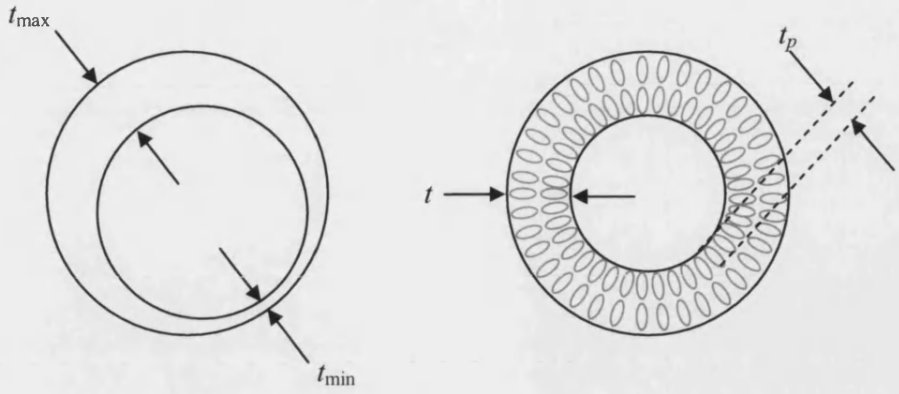

Concentricity factor, $R = \frac{t_{min}}{t_{max}}$ Fibre structure factor, $\alpha = \frac{t_p}{t} \times 100$

Figure 8.15 Diagram illustrating factors relating to fibre structure.

Concentricity factor quantitatively measures the concentricity or symmetry of the fibre by comparing the thinnest wall thickness to the thickest wall thickness, this value would be 1 for a completely concentric fibre. The fibre structure factor quantifies the variation in the wall structure of the fibre by comparing what percentage of the fibre wall is made up of finger-like pores radiating into the fibre wall from the lumen of the fibre. As the formation of finger like pres are controlled by diffusion of the solvent and non-solvent, this value helps to identify the differences between the exterior of the fibre and the interior during phase inversion. The value would be expected to be 50% if the conditions for phase inversion where exactly the same for the interior and exterior of the fibre.

Both the fibre concentricity factor and fibre structure factor appeared to decrease with an increase in concentration of NMP in the bore fluid (Figure 8.16 and Figure 8.17). The low number of samples at the higher levels of bore fluid concentration requires that these results are considered cautiously. Operation of the spinning process was found to be harder with high levels of NMP in the bore fluid, fibres were observed to be much softer as the precipitation process was slowed down. This meant these fibres were more susceptible to damage as they were fed through the water tanks and collected in the final water tank. Additionally the environmental aspects of increased solvent usage meant that further experiments with increased solvent concentrations in the bore fluid were not carried out; preliminary data analysis revealed there were not going to be significant improvements through the use of solvent in the bore fluid.

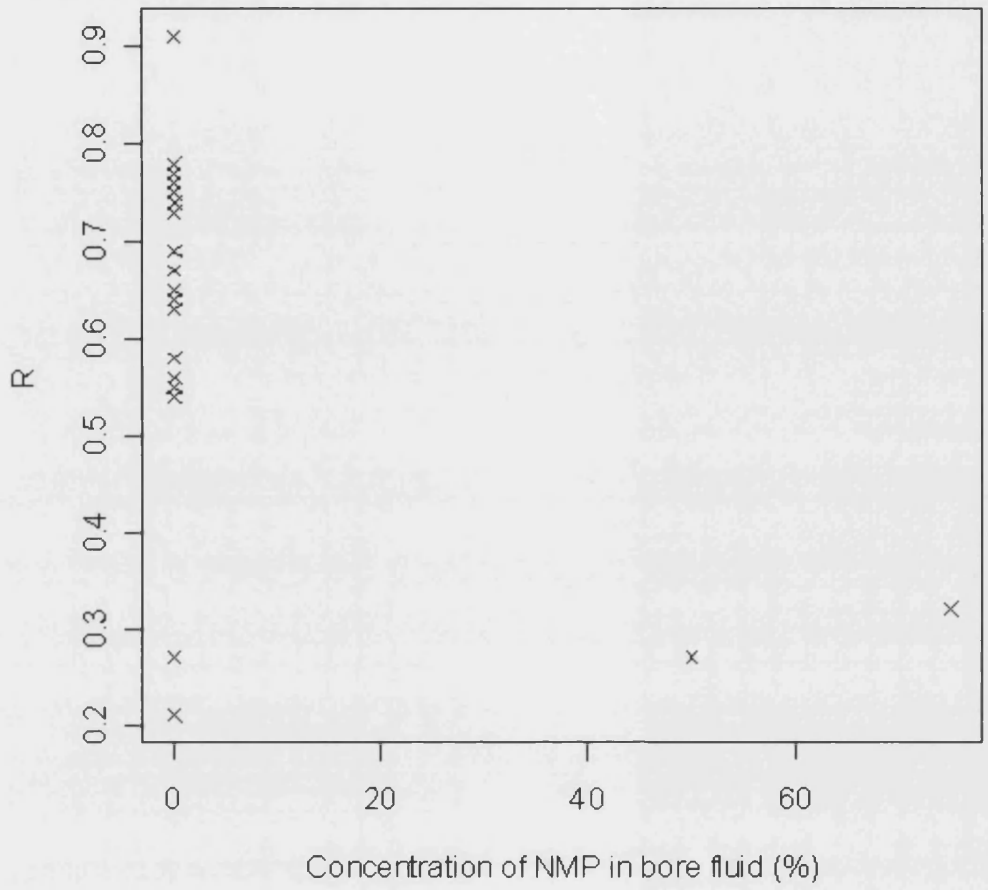

Figure 8.16 Scatter plot showing effect of bore fluid composition on the concentricity of the fibre.
The concentricity factor of the fibre (the fibre wall thickness at its thinnest point divided by the fibre wall thickness at the thickest point) appears to decrease with the NMP concentration in the bore fluid used when spinning.

It may be seen from Figure 8.16 above that the average fibre concentricity value for fibres spun with no air gap (as is the normal practice for this type of fibre) is around 0.6, meaning the thinnest part of the fibre wall is considerably smaller than the thickest. This is well below the ideal fibre concentricity factor of one, which would result for a completely concentric fibre. Observations of the spinning process suggest that this is due to lack of concentricity in the spinneret. Positioning the needle centrally in the spinneret requires a great deal of experience and patience; great care must then be taken to ensure the needle is not knocked off centre when attaching the polymer and water feed lines and positioning the spinneret above the water bath. It is anticipated that further improvements can not be made to this part of the process without the use of a new spinneret.

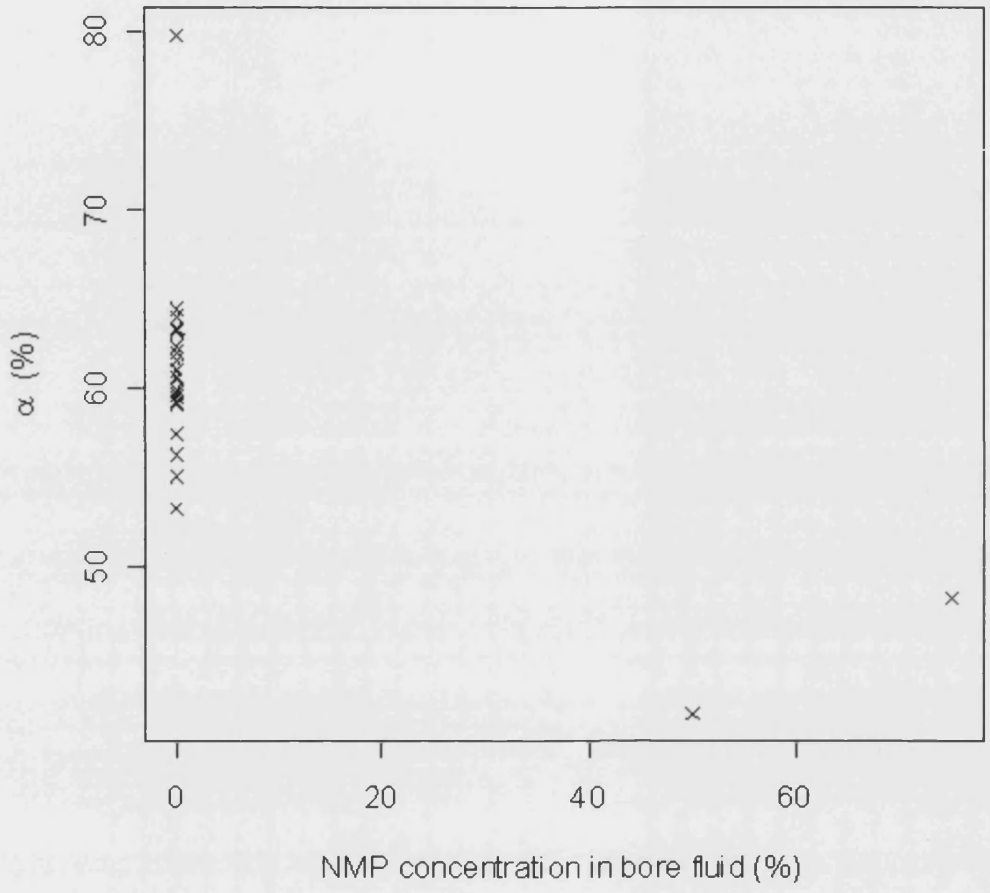

Figure 8.17 Scatter plot showing effect of bore fluid composition on the fibre structure.
The structure of the fibre wall in terms of percentage of the fibre wall made up by the inner ring of finger-like pores α*, appears to decrease with the percentage NMP in the bore fluid. The air gap, temperature of the water bath, and flow rates of polymer and water were not found to influence the fibre structure.*

The polymer and water flow rates, air gap when spinning and water bath temperature were not found to influence the two quantitative fibre structure values.

8.3 Discussion

8.3.1 Polymer solution

Controlling the viscosity of the spinning solution allows the flow profile of the solution as it passes through the spinneret to be fixed, allowing fibres with consistent properties to be produced. The viscosity of the solution depends on the concentration of the polymer, the polymer intrinsic viscosity and the solvent used. In this work the solvent used is NMP which was shown to be suitable for spinning PLGA hollow fibres by Ellis (2005). The relationship between solution viscosity, concentration and intrinsic viscosity is only well understood at very low concentration solutions. Correlations have been developed relating the solution viscosity, concentration and intrinsic viscosity by assuming a solution so dilute that each polymer molecule may be considered independently, with no interactions from other molecules (Thomas and Thomas 1960). As the concentration of the solution increases this assumption no longer holds true and hydrodynamic interactions between polymer molecules and different parts of the same molecule must be considered. This topic extends beyond the scope of this work, however is considered theoretically by Freed and Edwards (1974). The concentrations appropriate for spinning are well above those covered by Thomas and Thomas's model of dilute polymer solutions, however the form of the model (Equation 8.10) combined with the exponential appearance of the graph plotting solution viscosity against concentration for the different polymer types (Figure 8.7), as well as the physical impossibility of a solution viscosity of below zero suggests an exponential relationship between solution viscosity, concentration and intrinsic viscosity.

$$\mu = \mu_s e^{[\mu]C} \qquad \textbf{Equation 8.10}$$

μ = Solution viscosity ($L^{-1}MT^{-1}$)

μ_s = Solvent viscosity ($L^{-1}MT^{-1}$)

$[\mu]$ = Intrinsic viscosity (L^2M^{-1})

C = Solution concentration ($L^{-3}M$; g dL^{-1})

An exponential statistical correlation was developed for the experimental results. The anomalous behaviour of the lowest intrinsic viscosity polymer (RG752), which could

not be formed into a porous scaffold through immersion precipitation phase inversion, was reflected in the quantitative results. The results from this polymer were found to unduly influence the correlation, leading to a poor fit across the rest of the data. If this polymer was removed an exponential correlation relating solution viscosity, concentration and intrinsic viscosity could be developed. This correlation is presented in Figure 8.18 with the equation of the plane given by Equation 8.11. The correlation is also presented in a two-dimensional plot to show the goodness of fit for the majority of the polymers and the extent of the anomaly with the polymer RG752 in Figure 8.19. The units used in the charts are presented in Pa s for viscosity and g dL^{-1} for concentration based on common usage. These archaic units are related in a non-dimensionally balanced empirical equation (Equation 8.11) to offer consistency.

No distinction is made between the different lactide ratios in the correlation. The interactions governing the viscosity of higher polymer molecules in solution are typically based around the physical size and shape of the molecules (Freed and Edwards 1974) meaning no difference is anticipated between the two very similar polymer chains. Statistical analysis of the experimental data suggested no significant difference in the polymer viscosity and concentration relationship between the two polymer compositions studied.

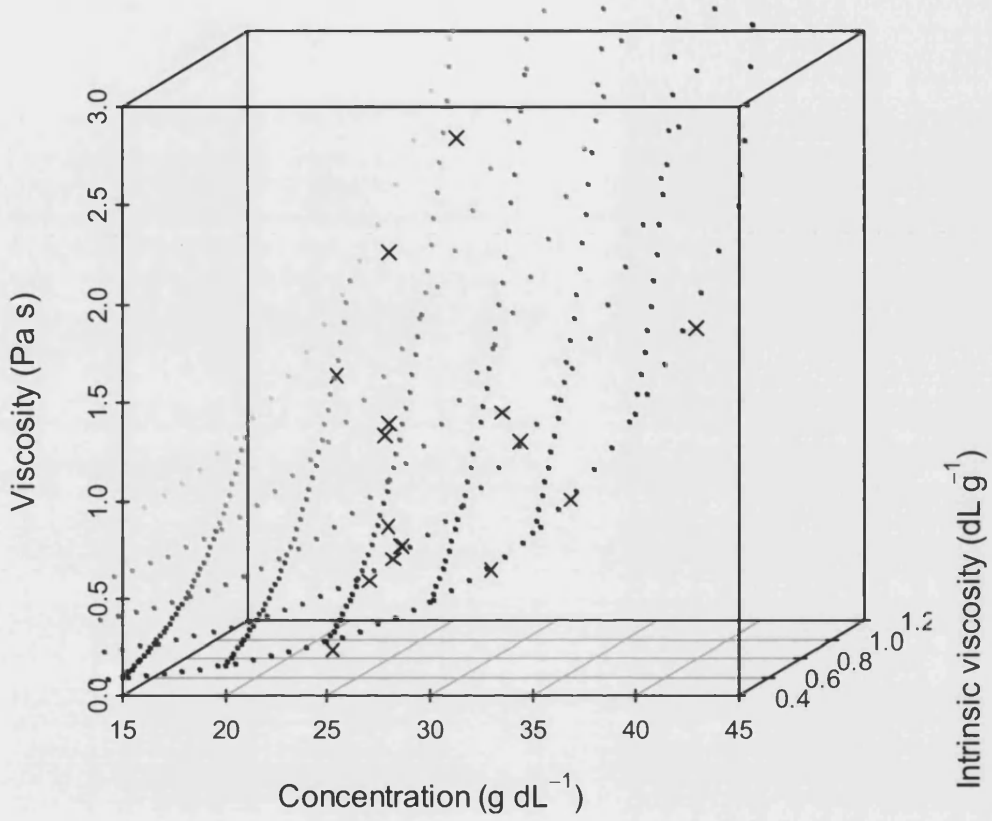

Figure 8.18 3D Three-dimensional plot illustrating the variation in concentration and both intrinsic and solution viscosity of the polymer solutions in NMP.

A significant exponential relationship is found between solution viscosity and both solution concentration and polymer intrinsic viscosity. The points illustrating the exponential relationship darken with decreasing intrinsic viscosity.

$$\mu = 5.4 \times 10^{-3} e^{0.11C+3.0[\mu]} \qquad \textbf{Equation 8.11}$$

μ = Viscosity ($L^{-1}MT^{-1}$; Pa s)

C = Concentration of solution (ML^{-3}; g dL^{-1})

$[\mu]$ = Intrinsic viscosity ($L^{3}M^{-1}$; dL g^{-1})

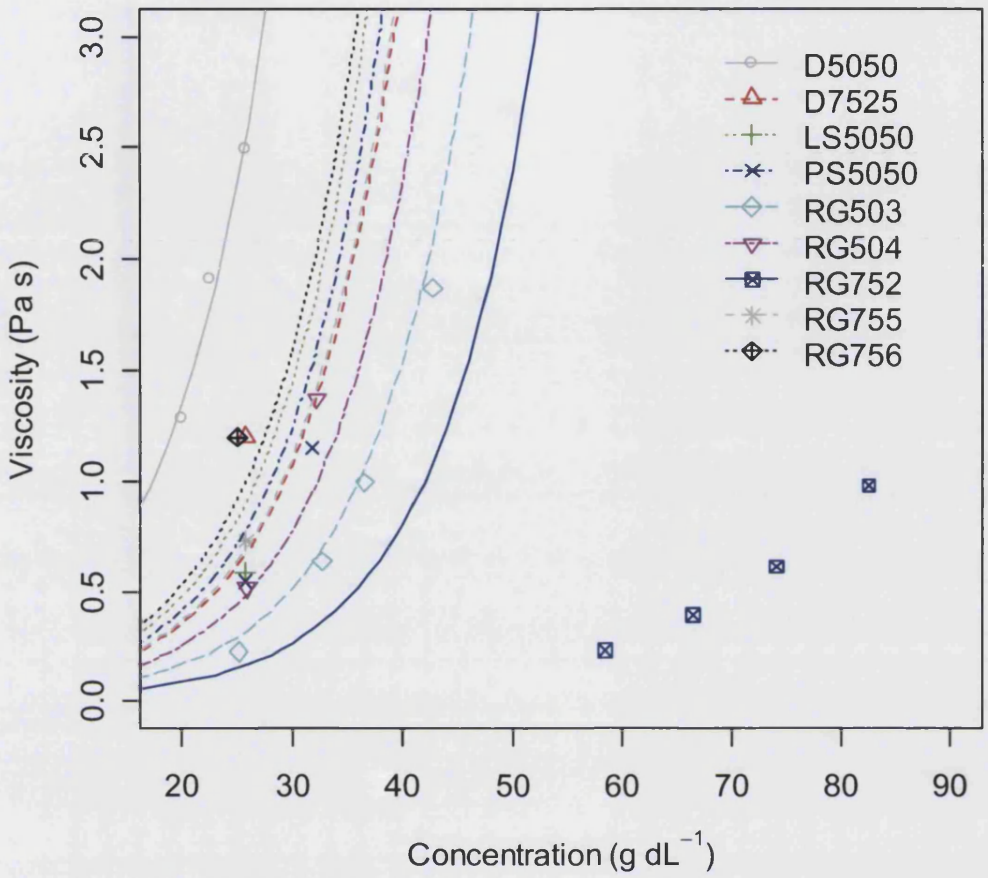

Figure 8.19 Scatter plot illustrating the variation in solution viscosity with concentration for different intrinsic viscosity polymers in NMP.

*The statistical exponential correlation appears to fit the experimental results well with the exception of the RG752 polymer (**dark blue solid line and crossed box points**) with the lowest intrinsic viscosity of those tested.*

The above correlation (Equation 8.11) is a useful tool for predicting the concentration of the solution required for spinning for a PLGA polymer based on its intrinsic viscosity. The measurements were taken at 20°C; deviations from this temperature will change the relationship between polymer solution concentration and viscosity. While it is still advisable to test each polymer solution before spinning as precise control of the viscosity can lead to improved spinning performance, the above formula can save lengthy trial and error adjustments of solutions to achieve the desired viscosity. Additionally as may be seen in the example of the polymer RG752 an anomalous

viscosity result may be an indication of a problem with the polymer which should be investigated prior to the initiation of the spinning process which is costly in both time and polymer requirements.

Wide varieties in the performances of polymers from different batches of the same source, or different sources of polymer were observed in this study. Polymer raw material colour and form were found to vary independently of variation in performance. This suggests a great deal of care is required when sourcing polymers. Polymers range in price from around £2.5 g^{-1} to more than £30 g^{-1} with no apparent correlation between quality and price. It is possible that some of the disagreements found in the literature, as discussed in the introduction from this chapter, result from comparisons of work involving polymers from different sources that, although not formally recognized, differ vastly from one another. Until a supply of reliable, consistent good quality polymer may be identified the results from this study suggest the need to sample polymers extensively to fully characterise their behaviour, both physically and chemically, before undertaking lengthy experimental work. This will not only improve consistency within in one study but will also improve the comparisons that may be made with other work by giving the reader the ability to make informed opinions of the cause of a difference or similarity.

The previous discussion has focussed on the ability to match the viscosity of the polymer solution to a suitable value for spinning by altering the concentration of the solution. However this is not without consequence. Increasing the concentration of the polymer solution reduces the porosity of the fibres. The porosity of the fibres is likely to have further implications on the performance of the bioreactor. Mass transfer through the fibres is likely to be higher through a fibre with increased porosity and the porosity is known to influence the degradation rate of the polymer (refer to Chapter Seven). This means a balance must be achieved between an intrinsic viscosity (which is determined by molecular weight) which offers an agreeable degradation time frame, a solution which is viscous enough to spin and a fibre porosity which performs adequately within the bioreactor. This is presented diagrammatically in Figure 8.22.

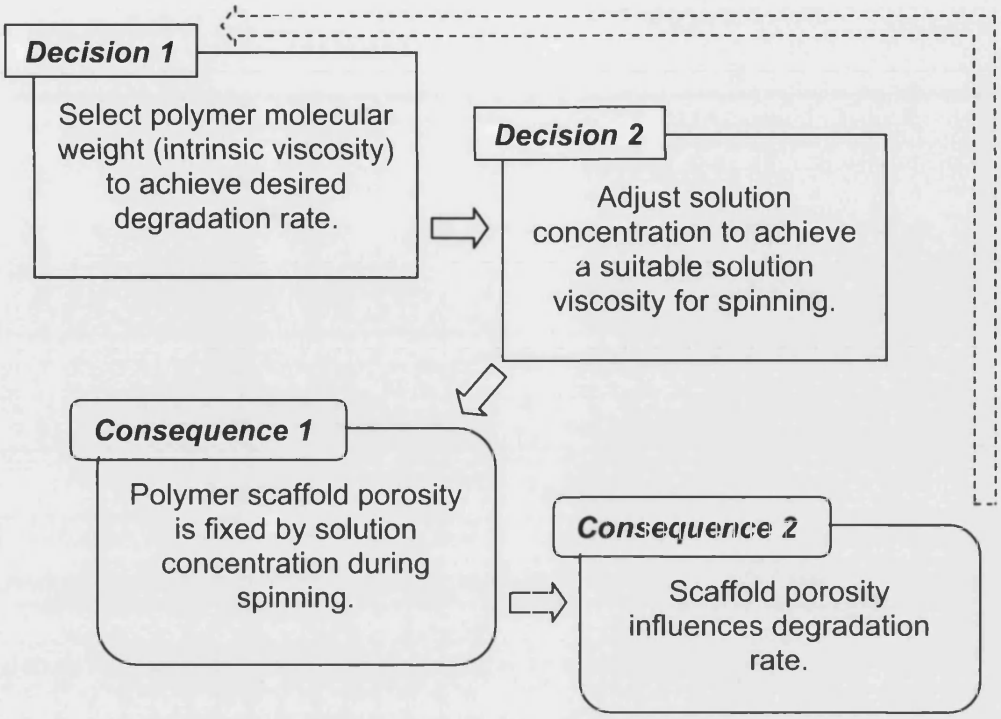

Figure 8.20 Flow diagram showing decisions and consequences in polymer selection.

The selection of polymer intrinsic viscosity (molecular weight) has many influences on the bioreactor. Consequently the selection of a polymer will be the result of an iterative process.

The formation of the fibre, the mass transfer and the degradation processes are all controlled by diffusion of water into and out of the polymer. In scaffold formation diffusion occurs between the polymer solution and the water bath, during mass transfer diffusion is occurring between the aqueous media and the porous scaffold, this is also occurring during degradation. If water cannot diffuse into the structure the interior will be protected from degradation, however if water can diffuse in, but the bulkier degradation products cannot diffuse out, autocatalysis will increase the degradation rate in the interior of the scaffold. Lower molecular weight polymers have lower intrinsic viscosities which require higher concentration solutions to spin. These will produce denser fibres, compounding the increased degradation of polymers with lower molecular weights.

8.3.2 Influence of operating conditions during spinning on fibre form

Altering the operating conditions during the spinning process allow some control over the features of the fibre. These will be discussed in the following section.

8.3.2.1 Pore size and porosity

The results show the internal pore diameter was influenced by the air gap during spinning and the external water bath temperature. The external pore diameter was influenced by bore fluid composition.

Chung and Hu (1997b) and Qin *et al.* (2001) both suggest that pore diameter will decrease with increase in air gap, their arguments are presented in the right-hand column of Table 8.2, where the hypotheses that the air gap increases longitudinal stress to orientate the polymer chains leading to tighter packing, polymer chains relax due to slow initial rates of solvent removal during the air gap leading to tighter packing, and slower solvent removal resulting in a more defect free skin are proposed. However this is, of course, in contrast to the arguments presented in the left-hand column of Table 8.2, where the case is made for an air gap increasing the membrane pore size. Where the same longitudinal stresses that are proposed as aligning the polymer molecules leading to denser packing are proposed to pull apart the polymer chains, shear stresses within the spinneret are also proposed to lead to densely packed aligned polymer molecules. It is likely however that all these arguments are proposed for the external pore size, where the presence of an air gap means that instead of coming directly into contact with water the polymer solution is initially in contact with air. However for the interior of the membrane the polymer comes directly into contact with water whether or not there is an air gap, the water is extruded simultaneously with the polymer. This would suggest that less difference would be expected with or without an air gap for the interior pore size that the exterior pore size. However this was not found to be the case for the experimental results. The subject of shear stresses in the spinneret and any potential influence on the surface pore size are further discussed in Section 8.3.3 below.

The influence of the bore fluid concentration on the external but not the internal pore size was unexpected. The fluid is influencing the size of pores on the opposite side of the membrane to the one which it is in contact with. Similarly the temperature of the

external water bath influences the internal pore diameter but not the external pore diameter; in these tests the temperature of the bore fluid remained constant.

Chung and Kafchinski (1997) investigated the influence of external water bath temperature on a different system for polyamide fibres, finding that an increased temperature lead to a change in fibre structure with a move away from the finger-like pores towards a more homogenous structure, which is attributed to the higher solubility and diffusivity at increased temperatures. No change in structure was observed with increased temperature on the fibres in this study, however as well as an increased interior pore size the Young's modulus was also found to increase with water bath temperature.

It is possible that the causes behind the increased interior pore size with increased water bath temperature and increased exterior pore size with increased NMP concentration in the bore fluid are both related to the diffusion of the water into the fibre. If the increased concentration of NMP in the bore fluid decreases diffusion of NMP out of the fibre in the lumen this may be compensated for by an increase in diffusion of NMP out of the exterior of the fibre leading to an increase in pore diameter on that surface. Similarly if increased water bath temperature increases diffusion of water into the membrane at the expense of the counter-diffusion of NMP out of the membrane exterior surface the rate of diffusion of NMP into the lumen may increase. Increased diffusion of NMP out of the membrane may lead to increased pore sizes, while a delayed precipitation does not significantly reduce pore diameters. However it is possible other mechanisms are responsible for the results of pore size at increased water bath temperatures. As well as increasing rates of diffusion increased temperature also increases solubility, this may delay the precipitation of PLGA. If this occurs, the normal nascent pores which develop, and will ultimately become the characteristic finger-like pores, will not provide a sink for the solvent, again reducing solvent removal from the solution at the outer edge of the fibre.

While the surface pore size of the membranes were not found to be affected by the polymer or water flow rates the porosity of the interior of the membrane was found to decrease with increased polymer flow rate and increase with water flow rate. Considering the relative speed of the water against the polymer this change amounts to

the same thing, the velocity of the water is greater than the velocity of the polymer. As the trend was not mirrored in the pore size, the increase in porosity must be a result of a greater number of pores on the interior surface with increased water velocity over polymer velocity. Increasing the differential between the speeds of the polymer and water flow will decrease the thickness of any boundary layer existing in the water adjacent to the polymer; this will mean that NMP is quickly moved away from the polymer surface.

8.3.2.2 Fibre structure

Two factors were defined to quantitatively assess any changes to the fibre structure with operating conditions. The fibre concentricity was defined by the fibre wall thickness at its minimum divided by its maximum, and the fibre structure factor was defined as the distance of the membrane thickness taken up by the finger-like pores divided by the total membrane thickness. Only the bore fluid composition was found to result in a statistically significant correlation with either of these factors. Increasing the concentration of NMP in the bore fluid was found to decrease both factors, leading to decreased concentricity and decreased length of finger-like pores. As the finger-like pores measured were those on the inner half of the membrane wall this finding is consistent with reduced diffusion through the inner wall of the fibre. The presence of finger-like pores is associated with the rapid diffusion of water into the membrane as is discussed in the introduction to this chapter.

If the fibres are to perform well in the bioreactor they must provide as homogenous environment as possible for the cells. Lack of concentricity in the fibre may lead to weakness that result in the fibre failing, spatially variable mass transfer properties and premature degradation of the fibres.

8.3.3 Spinneret and polymer precipitation

8.3.3.1 Shear stress

A lot of discussion on the subject of shear stresses and the spinning of hollow fibres is reported in the literature (Chung and Hu 1997b; Shilton 1997; Chung *et al.* 1998; Chung *et al.* 1999; Chung *et al.* 2000; Qin *et al.* 2000; Qin *et al.* 2001; and Wen and Tresco 2006). The primary effect attributed to shear stresses is the alignment of polymer molecules which leads to dense packing, if these are then instantly frozen into the

polymer, in the case of wet spinning with no air gap, they result in small pore diameters. However it is often proposed that a small air gap, sometimes as little as 1 cm, allows the polymer time to relax before entering the water bath leading to larger pore sizes. If the air gap is increased too far this is again responsible for increasing longitudinal stress in the nascent fibre, this time either due to gravity or a take up rate faster than the polymer flow rate, depending on the mode of spinning. Here a theoretical examination of the process is presented in an attempt to identify the significance of shear stress within the spinneret on the pore size of the fibre.

Graphical representations of the shear stress and velocity profiles of the polymer and water passing through the spinneret are illustrated in Figure 8.21; the calculations used to model the polymer flow profiles are based on work by Shilton (1997) and are given in Appendix A.6. From these profiles it is possible to see the maximum shear the polymer solution undergoes is on the interior fibre wall with a maximum value of approximately 5000 N m^{-2}. The calculations have been performed on the typical operating conditions and physical configuration of the spinneret used for this work. Details are presented in Table 8.4.

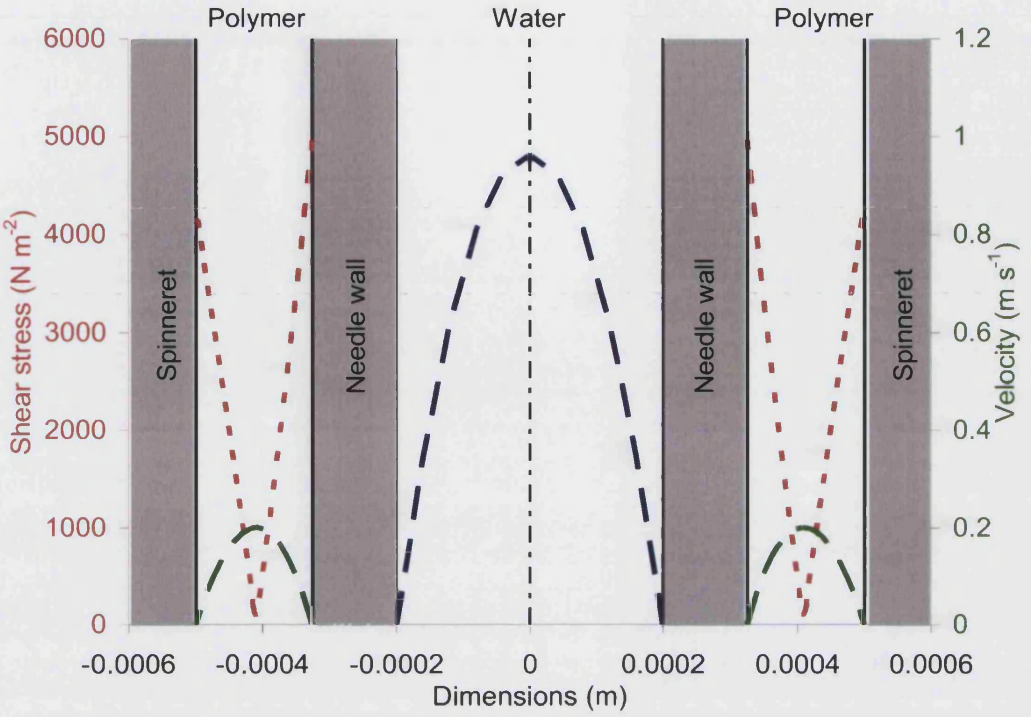

Figure 8.21 Chart illustrating shear stress and velocity profiles through the spinneret.
Shaded areas *represent spinneret hardware,* ***Red line*** *shows shear stress profile,* ***Blue and green lines*** *show water and polymer velocity profiles respectively. Based on equations given by Shilton (1997), details in appendix A.5. This model assumes the length of the annulus is such that normal laminar flow is obtained after passing through sudden contraction. The shear stress and velocity profiles are calculated on the average values of the polymer solution composition and polymer and water flow rates used in this study.*

Whether the shear stresses are still influencing the packing of the polymer molecules by the time precipitation occurs depends on both the relaxation time of the polymer and the diffusion rate of the water into the polymer solution.

There are two predominant theories on the relaxation time of polymer molecules. These are the Rouse model (Rouse 1953) and the Zimm model (Zimm 1956). Both of these models relate to dilute polymer systems of less that 1 g dL^{-1}. This is clearly a major difference between the values of more than 20 g dL^{-1} used for the spinning solutions. Further work has been carried out on the relaxation of polymers since the 1950's and is reported in the literature (Shiwa 1993 is one example), however the effects of polymer molecular weight, polydispersity index, rate of stress and frictional factors all make the

prediction of the polymer relaxation time extremely difficult. However by considering the dynamics of the diffusion of water into the fibre and the rate at which the polymer coagulation moves from the perimeter of the polymer solution into the centre it may be possible to define a critical time period, which if the polymer relaxation time falls within will effect different parts of the scaffold structure.

8.3.3.2 Diffusion of water into polymer solution

Cohen *et al.* (1979) propose that for ternary polymer:solvent:non-solvent systems where diffusion coefficients depend on the composition alone the diffusion layer thickness, described as a region between the zone with a concentration gradient and the zone unaffected by diffusion to and from the water bath, is directly proportional to $t^{1/2}$. The model by Cohen *et al.* involves complex differential equations and an extensive knowledge of the polymer:solvent:non-solvent interactions. While the data required for the accurate modelling of the system is not available, the generalized summary of the model that the coagulation front will move into the polymer solution at a rate proportional to $t^{1/2}$, where t is time. It should be noted that although this model is widely cited in literature it is generally to offer the opinion that the basis for the model is correct, however a number of critical assumptions are questioned. While these references go on to further elaborate on the model they also require a far more extensive knowledge of the system than is available, and offer no argument to reject the general proportionality trend. The inclusion of a constant of proportionality, k, into Cohen and co.'s model gives Equation 8.12 which predicts the thickness of the diffusion layer at a certain time (t).

$$d_t = k \times t^{0.5} \qquad \textbf{Equation 8.12}$$

d_t = Distance into polymer of coagulation front at time = t (L)

t = Time (T)

k = Constant of proportionality ($LT^{-1/2}$)

Figure 8.5 presented the experimental results of the progression of the diffusion front into an element of a solid fibre. These are presented again in Figure 8.22 along with the statistical correlation as previously defined in the results section and the empirical

correlation proposed by Cohen *et al.* The constant of proportionality, k, was determined by least squares regression to be 47.1 ± 1.4 μm $s^{-1/2}$ giving Equation 8.13.

$$d_t = 47.1 \times t^{0.5} \qquad \textbf{Equation 8.13}$$

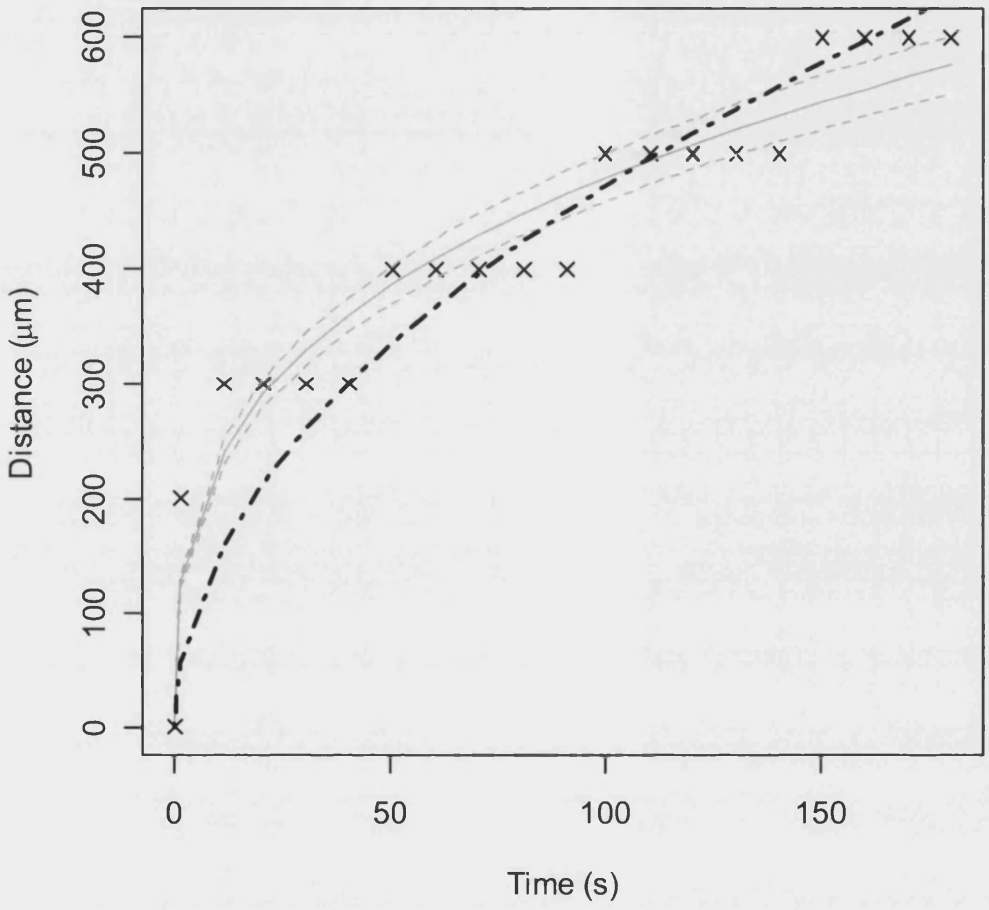

Figure 8.22 Chart showing the diffusion profile of water into an element of fibre, comparison of experimental data and correlation.

*Both the experimental results (shown as **crosses**) and the statistical correlation (**solid line**) along with 95% confidence interval (**dashed line**) are shown alongside the model proposed by Cohen et al. 1979 (**bold dash dot dashed line**).*

Based on the appearance of Figure 8.22 the model proposed by Cohen *et al.* (1979) does not exactly fit the data, or even lie within the 95% confidence interval of the trend line estimated through statistical analysis. However the model does give an acceptable

correlation with the data over the range of the experimental results ($R^2 = 0.91$, compared to $R^2 = 0.94$ for the statistical correlation).

From the literature it appears that Cohen and co workers' correlation is an acceptable approximation of the diffusion of water into the fibre; from this a number of calculations may be made. According to the correlation water will have diffused into the centre of the fibre within 30 s. This helps to predict the time required for the fibre to harden; until the water has diffused through the fibre the polymer structure may be damaged by handling. The proportionality constant for this correlation is based on the experimental results of the polymer solution changing from translucent to opaque, so while enough water may have diffused in to the fibre centre, (note in a hollow fibre this is the centre of the wall, not the centre of the fibre) it is likely that at this stage the polymer will not be completely precipitated and further time will be required for residual solvent to diffuse out of the fibre vicinity.

The structure of the fibre is known to be controlled by rates of diffusion, as described in the introduction to this chapter, a skin layer on the edge of the fibre is a result of initial rapid diffusion rates; this is then responsible for reducing the rates of diffusion for layers below the skin layer. The hollow fibres have been observed to have a skin layer approximately 10 μm. According to the diffusion correlation this skin layer is formed within 10 s of the polymer entering the water. This is a very generous estimate and actual value is likely to be well below this; at very low values of t the correlation does not fit the data very well. Therefore it is likely that the skin layer will form in less than 10 s.

Referring back to the discussion of the influence of shear stresses on the membrane pore size, it is likely that any influence of the shear stress on the membrane will be confined to this layer, as this is the layer that will experience the highest shear stresses and have the least time to relax before coagulating.

Whether the air gap provides a critical period in which the shear stresses induced in the polymer solution may relax before the polymer precipitates on contact with water or whether the gravitational longitudinal stresses the nascent fibre experiences in this air gap result in greater influences on the fibre structure is again very hard to determine

theoretically. In this study the air gap was found to influence the pore size on the interior membrane, decreasing the pore size with increased air gap. The largest air gap used in this study was 10 cm with the smallest being 0 cm, or no air gap. If the residence time of the fibre in the air gap is calculated from the velocity of the polymer extruded from the spinneret alone, which we will soon see to be incorrect, the residence time will be approximately 1 s (refer to polymer velocity in Table 8.4). However as the polymer is extruded there will be a number of forces acting on the polymer, Ziabicki and co workers (cited by Walczak 2002) defined the forces acting on a solid fibre filament in this region as those presented in Equation 8.14 for balanced flow.

$$F_e + F_g = F_r + F_i + F_s + F_a \qquad \textbf{Equation 8.14}$$

F_e = External forces (LMT^{-2})
F_g = Gravitational forces (LMT^{-2})
F_r = Rheological forces (LMT^{-2})
F_i = Inertial forces (LMT^{-2})
F_s = Surface forces (interfacial tension) (LMT^{-2})
F_a = Aerodynamic forces (LMT^{-2})

External forces relate to those from the process such as drawing, in this case the take up rate is balanced to the fibre production rate so there should be no external forces. Gravitational forces will act on the polymer whether there is an air gap or not, however the inertial forces, surface forces, aerodynamic forces and even rheological forces will differ depending on whether there is an air gap or the polymer is extruded directly into the water bath. Compounding the relative differences between the polymer solution and air or water is the fact that in the air gap solvent evaporation will begin to cause the polymer to precipitate and in the water bath rapid diffusion of solvent and non-solvent will cause the polymer to precipitate. This makes modelling the formation of the fibre at this point very difficult, even the prediction of the time the polymer takes to pass through the air gap cannot be resolved theoretically without experimentally determined factors.

Despite the lack of precise modelling of the influences of the forces one may assume the following. Assuming negligible evaporation of solvent in the air gap, based on the low volatility of the solvent used (NMP), there will be negligible density change in the polymer solution. In a balanced system the mass of polymer solution entering the air gap must equal the mass of polymer solution leaving the air gap. As the density is not changing the volumetric flow rate entering must also equal the volumetric flow rate leaving the air gap. No significant difference was found in the diameters of the fibres spun with or without the air gap suggesting the cross-sectional area of the fibre remains constant over the air gap. This implies that as well as the mass flow rate and volumetric flow rate the velocity of the polymer may be considered constant over this air gap. If this is the case the residence time of the polymer in the air gap can be calculated from the polymer extrusion rate and is approximately equal to one second.

From the arguments presented above a timeline may be drawn to indicate the significance of a polymer relaxation time within different time boundaries (Figure 8.23)

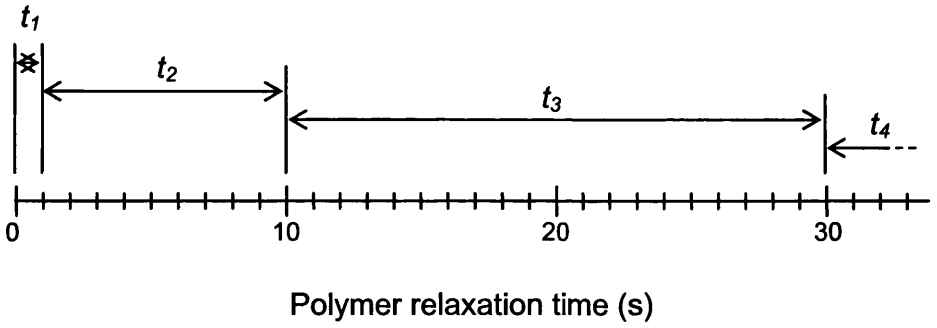

Figure 8.23 Time line showing significance of different polymer relaxation times.
If the polymer relaxation time falls within different time bands it will influence the polymer in different ways. t_1 *- A relaxation time of less than one second will allow the polymer to relax in the air gap, meaning polymer orientation will be influenced by the presence of an air gap.* t_2 *- A polymer relaxation time of 1 – 9 s will mean the polymer does not have time to relax in the air gap and the presence of an air gap will not significantly affect the polymer orientation, however only the skin layer will have precipitated in this time, confining the orientated polymer molecules to the skin layer.* t_3 *- A polymer relaxation time of 10 - 30 s will mean some but not the entire polymer scaffold is made up of aligned polymer molecules.* t_4 *- A polymer relaxation time of more than 30 seconds will mean that all of the scaffold structure contains some degree of aligned polymer molecules as the polymer will have started to coagulate the entire polymer matrix before the polymer has fully relaxed.*

While it may be hypothesised that the presence or absence of an air gap would be more influential on the exterior pore size that the interior, which comes directly into contact with water in either process, this is shown experimentally not to be the case. This situation may result from similar processes that mean the concentration of solvent in the bore fluid influence the exterior but no the interior pore sizes and the exterior water bath temperature influences the interior pore size but not the exterior. The fibre wall is thin enough that changes in the concentration of solvent, polymer and non-solvent on the outside wall of the fibre are close enough to influence the diffusion profiles on the inside of the fibre wall.

Chung *et al.* (1999) suggest a resolution to the issue of increased or decreased pore sizes in relation to the air gap and shear stresses within the spinneret. In their work on the subject the propose that medium stresses in the air gap result in molecular orientation and denser packing leading to tighter pores, where as higher stresses can act to pull apart the molecules leading to more void space and larger pores. If this theory holds true for the system investigated in this study the results of a decrease in pore size with increase in air gap suggest that the air gap of 10 cm induces medium stresses in the fibre.

Comparing the pore sizes on the interior and exterior of the hollow fibre with the pore sizes on the upper surface of flat sheets suggests that it is not shear stresses or longitudinal stresses that are responsible for governing pore sizes in this system. The shear stresses on the hollow fibre surfaces are approximately equal and in the region of 5000 N m^{-2}, whereas the shear stresses on the flat sheets resulting from spreading the polymer solution onto the glass support are in the region of 1 N m^{-2}. The flat sheet is then placed into the water bath, but the delay between spreading the polymer on the glass sheet and placing the polymer in the water bath is likely to be several seconds, giving the polymer a relaxation period similar to an air gap with out inducing any other stresses, due to gravity *et cetera.* However no significant difference was found between the pore sizes on the hollow fibres and the flat sheets, with the average pore diameter of the flat sheets lying between the average interior pore diameter and the average exterior pore diameter for the hollow fibres. This suggests that the shear stresses induced in the spinneret and the longitudinal stresses induced in the air gap are negligible compared to other factors when considering the pore size of the membranes.

8.3.3.3 Die swell

The spinneret geometry plays an important role in defining the macroscopic features of the fibre such as internal and external diameters. However it is known that under certain flow regimes the polymer may swell as it is extruded through a small orifice. This phenomenon is known as die swell and is difficult to predict. Die swell is dependant on the flow profile through the spinneret which may be affected by the solution viscosity, flow rate and geometry and surface roughness of the spinneret. The results of this study suggest that the flow regime and spinneret geometry used do not undergo any swelling phenomenon. The lack of die swell in the fibres extruded from orifices of relevant size to the spinneret may be due to: the low pressure extrusion of the polymer solution; laminar flow through the spinneret with very low Reynolds number; and the low pressure drops over the spinneret (Table 8.4).

8.3.3.4 Improved spinneret design

This study required that a number of fibres were produced from different polymer solutions that were as similar to one another in all other aspects as possible. This highlighted inconsistencies in the spinning process. The control of the flow of water and polymer in to the spinneret was improved through the use of highly accurate syringe pumps. However the spinneret itself was also found to introduce undesired variability in the fibres. Figure 8.24 shows a potential spinneret design that includes a number of features to improve usability. The main body of the spinneret is designed around a hexagonal piece; this allows the spinneret to be grasped by tools more easily. Three hex keys on the top allow adjustment of the position of the needle within the outer orifice addressing a major area of inconsistency in the fibres which is the lack of concentricity of fibre. The use of commercially available needles allows that this piece may be replaced if it becomes worn or blocked. It also offers the potential to vary the size of the fibres produced through the spinneret while minimising the custom hardware required. Smooth flat surfaces in the polymer reservoir should minimise the time taken to clean the spinneret.

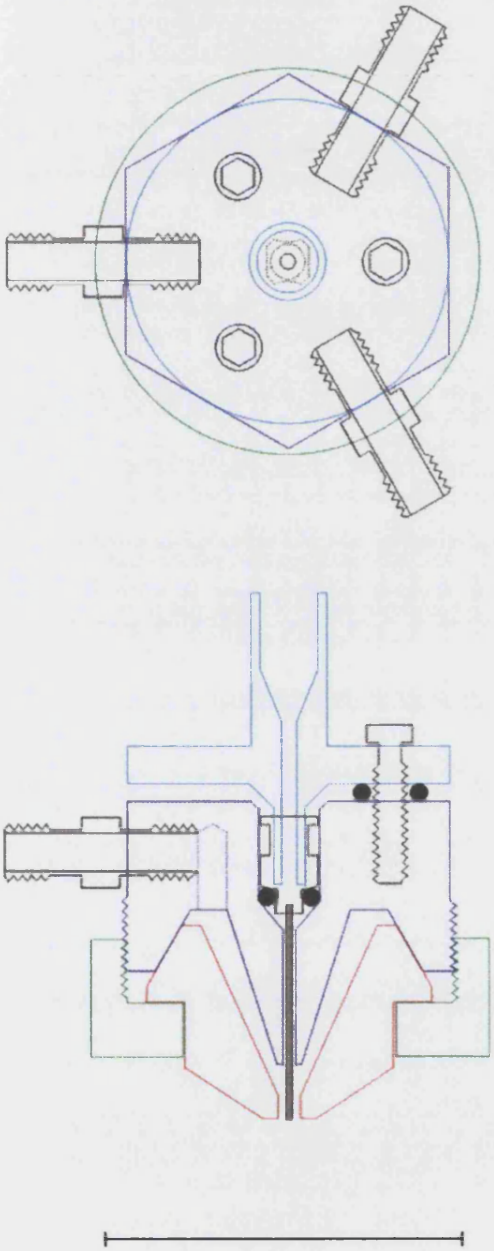

Figure 8.24 Diagram of new spinneret design. ***Top****: Plan view from above,* ***Bottom:*** *cross sectional view from the side,* ***scale bar*** *is 5 cm.* ***Black components*** *represent parts that meet the specification of commercially available components.* ***Coloured components*** *represent pieces that would require machining from a suitable material that is compatible with the solvent and offers low manufacturing costs, while giving the spinneret a useful lifespan free from deformation.* ***Blue*** *represents the top of the spinneret; the upper part is a tube, onto which a standard ferrule fitting may be attached. This part is attached to the spinneret body by three radially positioned hex screws. The lower part fits into a commercially available needle, the use of which allows cheap and easy replacement in the event of blockage or damage. A washer below the needle provides a seal to prevent water entering the polymer chamber. The use of thick washers around the hex screws provide a pivot that allows the concentricity of the needle in the outer orifice to be adjusted by tightening the hex screws independently.* ***Purple*** *represents the main body of the orifice. Three polymer connections are available through standard ¼" pipe fittings. Cones are used both at the needle socket and for connection to the lower part of the spinneret to help the components fit together concentrically. The body of the spinneret has a hexagonal profile; this is to allow the use of tools to separate the components should the spinneret become jammed together. The* ***Orange*** *component is the base of the spinneret containing the orifice through which the fibre will be extruded. Different versions of this piece offer the potential for orifices with different outer diameters, coupled with the use of different gauge commercial needles affords the spinneret the potential to spin different size fibres with minimal additional hardware requirements. The* ***green*** *piece is used to hold the lower part o f the spinneret to the body of the spinneret.*

8.4 Conclusions

This Chapter considers the process by which the fibres for the hollow fibre bioreactor are formed and the raw materials used to form them. Both the process and the raw materials have been found to introduce undesired variability in the performance on the hollow fibre bioreactors.

An empirical correlation has been proposed as a tool for determining the required concentration of solution for spinning from the polymer intrinsic viscosity. The viscosity of the solution is found to increase exponentially with both solution concentration and intrinsic viscosity.

The influence of the operating conditions such as relative polymer and water flow rates, solvent concentration in the bore, air gap and water bath temperature have been investigated. The system is not found to be influenced by the process of die swell, meaning the diameter of the orifice is a good indicator of the diameter of the resultant fibre. The use of solvent in the bore was found to influence the external pore diameter at the expense of fibre concentricity and finger-like pores. Combining this with the environmental aspects of increased solvent usage and the ability to augment the external pore diameter through other measures meant the use of solvent in the bore fluid of this system was not recommended.

The shear stress and velocity profile inside the spinneret was modelled but the experimental results of similar pore sizes on flat sheets, where shear stresses are minimal, and hollow fibres, that undergo large shear stresses, suggest that the shear stresses are not responsible for governing the surface pore sizes in this system.

The propagation of the coagulation front into the polymer was found to follow a relationship proportional to the square-root of time.

A potential spinneret design is presented to improve fibre consistency and ease of operation during the spinning process.

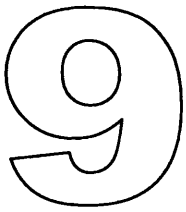

CHAPTER NINE – CONCLUSIONS AND FUTURE WORK

9.1 Introduction

This work has been carried out with the intention of developing the hollow fibre bioreactor for bone tissue engineering proposed by Ellis (2005). Specifically the hollow fibres were targeted as a critical component of the bioreactor that had yet to be specifically optimized for their new role. The investigative work completed has provided a greater understanding of the properties of the hollow fibres and how these may be suited to the hollow fibre bioreactor, as well as an evaluation of the performance.

9.2 Conclusions of the experimental investigations

The sterilization study described in Chapter Four shows the significance of the effects of sterilization on PLGA scaffolds. The use of ethanol, a commonly used disinfection agent, that is reported as suitable for use on PLGA scaffolds (Holy *et al.* 2001) was found to be inappropriate for use with the PLGA hollow fibres. Antibiotic treatment was found to provide a convenient, effective method with which to sanitize PLGA hollow fibres for use as a tissue-engineering scaffold with out adversely affecting the scaffold structure.

Chapters Five and Six investigate the potential to conveniently alter the surface pore size and porosity of flat sheet and hollow fibre scaffolds respectively. Sodium hydroxide treatment with concentrations in the range 0.01 to 0.2 mol dm^{-3} and over the durations of 10 – 30 min resulted in significant changes to the surface of the membranes. These concentrations allow ease of use in the laboratory without undue hazards from concentrated solutions and practical durations for treatments. Surface

modification was found to increase cell adhesion over the untreated membrane surfaces. All the treated surfaces showed increased cell adhesion, with increased cell attachment correlating with pore size for the large increases in pore size achieved through sodium hydroxide treatment. Increased hydrophilicity was observed for the sodium hydroxide treated samples (as indicated by water absorption). The treated fibres allowed water to permeate through the fibre wall which was not found to occur for the untreated fibres. The treatment was not found to influence the intrinsic viscosity of the polymer suggesting the mechanism is truly surface erosion (and not bulk degradation). This provides good evidence to suppose the effect of surface treatment on degradation is limited to the effects of a more open structure allowing greater contact with water and increased hydrophilicity. It is unlikely that these effects can be separated from the improved performance in permeation and cell adhesion tests; suggesting the effect of surface treatment on degradation is minimized.

A correlation is proposed to link mass loss by the polymer to both the order of the reaction and the exact mechanism by which the surface treatment agent affects the surface of the membrane. By the principle of parsimony a first order reaction with respect to sodium hydroxide is accepted. A correlation with the material lost from the surface of the membrane suggests that the mechanism of pore size increase is that a thin layer of material is removed from the surface of the membrane; exposing pores already present in the polymer.

Chapter Seven investigated the effects of PLGA properties alongside scaffold properties and the effects of different conditions on the scaffolds under an operating environment for two weeks. The initial porosity of the scaffold was found to be the most influential factor in determining the extent of change to the polymer. However the characteristics of the polymer such as lactide content and intrinsic viscosity may be used to tailor the change profile to meet specific requirements.

An evaluation of changes to the volume and porosity of the scaffolds has lead to the conclusion that the unique structure of the hollow fibre membranes results in a combination of autocatalytic degradation and homogenous degradation. The internal pore structure allows small regions of auto catalysed degradation to occur but prevents

the development of large macro voids that are more common with a more irregular interconnected porous structure.

Chapter Eight considers the process by which the fibres for the hollow fibre bioreactor are formed and the raw materials used to form them. An empirical correlation is proposed as a tool for determining the required concentration of solution required from spinning form the polymer intrinsic viscosity. Evaluation of the shear stress profiles within the spinneret and comparisons to flat sheet membranes produced with minimal shear suggest that shear stresses are not responsible for governing the surface pore sizes in this system. The propagation of the coagulation front into the polymer was found to follow a relationship proportional to the square-root of time. A potential spinneret design is presented to improve fibre consistency and ease of operation during the spinning process.

9.3 Future work

The investigations carried out for this thesis represent a step forward in the development of a hollow fibre bioreactor for use in bone tissue engineering. However there is still further work required to bring this process closer to clinical significance. The future work required is divided into two sections: that which may be carried out in the short term and that which is more distant from the work of this thesis and will take longer to achieve. These are detailed in the next two sections (9.3.1 and 9.3.2) and are illustrated in Figure 9.1.

Short term work

- **Fibres**
  - Degradation in numbers and configurations relevant to bioreactor
  - Degradation in tandem with cell proliferation
- **Cells**
  - Longer term cell culture in the bioreactor
  - Differentiation and migration

- **Bioreactor**
  - Fibre arrangement
    - Number of fibres
    - Spacing
    - Fibre layout
  - Flow
    - Flow conditions
    - Flow rates
- **Polymer**
  - Characterization

Longer term work

- **Fibres**
  - Size of fibres

- **Cells**
  - Cell source
  - Cell proliferation and migration
- **Bioreactor**
  - Sterilization
  - Culture to the point of tissue-like cell densities

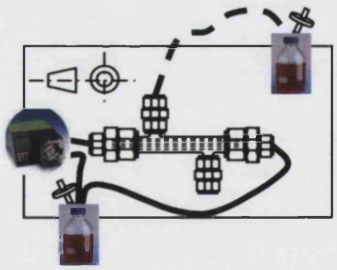

- **Polymer**
  - Reliable source of PLGA
  - Molecular weight

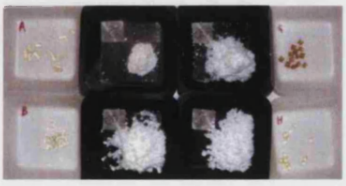

Figure 9.1 Outline of future work.

*General topics for short term (**left column**) and longer term (**right column**) work are identified.*

9.3.1 Short term work

In the short term further work must be carried out to bring the findings of this thesis together into the bioreactor. For example, the degradation of the hollow fibres has been shown to be unique compared to other scaffold forms, however when the fibres are arranged as a tightly packed bundle do they continue to degrade in a profile similar to that of a single hollow fibre? Or does the bundle act as a continuous scaffold (a scaffold made up of hollow fibres), within which the autocatalytic degradation products of one fibre increases the degradation rate of an adjacent fibre? Surface treatment with sodium hydroxide has been shown to improve the performance of the hollow fibres in the bioreactor over very short culture periods. However longer duration investigations must be carried out to discover if the increased porosity unduly increases degradation rates, or if cells are able to migrate into the large surface pores blocking the nutrient delivery network. The arrangement of fibres within the bioreactor is another issue that must be addressed along with the number of fibres and flow conditions within the bioreactor.

9.3.2 Longer term work

In the longer term work must be carried out on the bioreactor to bring the laboratory research closer to clinical application. Considerations must be given to scaling up the bioreactor both radially and axially and the implications this will have on the system. Will the longer fibre lengths have the appropriate mechanical properties to withstand the stresses they are under? Is the regular use of antibiotics a sufficiently stringent sterilization procedure for a construct that will be ultimately implanted into humans? Additionally is the routine use of antibiotics an ethically sustainable process or is this irresponsible in terms of antibiotic resistance? Minimal work has been carried out in this thesis on the cellular component of the tissue engineering construct. The ability of cells to adhere to the membranes was previously shown (Ellis 2005). This has been advanced to the stage where increased cell adhesion was achieved through surface modification, however these short term cultures, and simple cell counts are a significant area that needs addressing. The identification of cell source is another area that has not been addressed by this work. Consideration has been given to proliferating cells and encouraging them to form tissue. However it is likely that once a cell source is identified further customization of the bioreactor will be required. Stem cells offer huge potential in the field of regenerative medicine; however their use complicates both the

science of the bioreactor and the ethics. The osteosarcoma cell line used in this work is known to be easy to work with. This simplified the cell culture processes undertaken allowing work to be carried out quickly and simple evaluation of biocompatibility of the polymer surfaces to be made. Culture of other cell types, in particular stem cells, is more difficult. Adapting the system to support stem cells may require further adaptations to the surface of the fibres. In the body there are four types of bone cell, should representatives of each of these types be seeded into the reactor is guided differentiation required to generate a natural cell population.

The hollow fibres have been identified as crucial to the success of this type of bioreactor. The polymer raw material the fibres are made from has been identified as largely variable in quality. An important step forward in the development of this bioreactor and any other bioreactors encompassing PLGA scaffolds will come from the development of improved synthesis methods for PLGA. While laboratory investigations may move forward through the careful characterization of polymers and bulk ordering of single batches to ensure continuity of results this is not a suitable long term solution. Variations in quality and performance are not acceptable in the raw material of something that will be implanted into humans. Until unwanted variations of this form are eliminated the complex process of developing bioreactors for tissue engineering is unnecessarily disadvantaged.

REFERENCES

AGRAWAL, C. M., MCKINNEY, J. S., LANCTOT, D. and ATHANASIOU, K. A., 2000. Effects of fluid flow on the in vitro degradation kinetics of biodegradable scaffolds for tissue engineering. *Biomaterials,* 21 (23), 2443-52.

ATHANASIOU, K. A., NIEDERAUER, G. G. and AGRAWAL, C. M., 1996. Sterilisation, toxicity, biocompatibility and clinical applications of polylactic acid/ polyglycolic acid copolymers. *Biomaterials,* 17 (2), 93-102.

BADRI VISWANATHAN, N., PATIL, S. S., PANDIL, J. K., LELE, A. K., KULKAMI, M. G. and MASHELKAR, R. A., 2001. Morphological changes in degrading PLGA and P(DL)LA microspheres: implications for the design of controlled release systems. *Journal of Microencapsulation,* 18 (6), 783 - 800.

BERESFORD, J., *Maximum pore size to prevent cell migration into pores.* Email to M. J. ELLIS (M.J.Ellis@bath.ac.uk)

BILEZIKAN, J. P., RAISZ, L. G. and RODAN, G. A. 1996. Principles of Bone Biology, Academic Press: 1398.

BIOMATERIALS, L., 2005. *What is the correlation between Inherent Viscosity and Molecular Weight?* [online]. Available from: http://www.lakeshorebiomaterials.com/pdf/lakeshore-viscosity-weight.pdf [7 September 2006].

BIOMATERIALS, L. 2006. Certificate of Analysis: PLGA 5050 High IV. lot: LP-178.

BRODBECK, K. J., DESNOYER, J. R. and MCHUGH, A. J., 1999. Phase inversion dynamics of PLGA solutions related to drug delivery: Part II. The role of solution thermodynamics and bath-side mass transfer. *Journal of Controlled Release,* 62 (3), 333.

BRYANT, C., (cbryant@lakeshorebio.com), 21 Feb 2006. *PLGA.* Email to H. SHEARER (h.shearer@bath.ac.uk)

BURKERSRODA, F. V., SCHEDL, L. and GOPFERICH, A., 2002. Why degradable polymers undergo surface erosion or bulk erosion. *Biomaterials,* 23 (21), 4221.

CABASSO, I., KLEIN, E. and SMITH, J. K., 1977. Polysulfone hollow fibers. II. Morphology. *Journal of applied Polymer science,* 21 165-80.

CHRESAND, T. J., GILLIES, R. J. and DALE, B. E., 1988. Optimum fiber spacing in a hollow fiber bioreactor. *Biotechnology and Bioengineering,* 32 983-92.

CHUNG, T.-S. and HU, X. 1997a. Effect of Air-Gap Distance on the Morphology and Thermal Properties of Polyethersulfone Hollow Fibers. Journal of applied Polymer science, Wiley. 66 1067-77.

CHUNG, T.-S. and HU, X., 1997b. Effect of air-gap distance on the morphology and thermal properties of polyethersulfone hollow fibers. *Journal of applied Polymer science,* 66 (6), 1067-77.

CHUNG, T. S. and KAFCHINSKI, E. R., 1997. The effects of spinning conditions on asymmetric 6FDA/6FDAM polyimide hollow fibers for air separation. *Journal of applied Polymer science,* 65 (8), 1555.

CHUNG, T. S., QIN, J.-J. and GU, J., 2000. Effect of shear rate within the spinneret on morphology, separation performance and mechanical properties of ultrafiltration polyethersulfone hollow fibre membranes. *Chemical Engineering Science,* 55 (6), 1077-91.

CHUNG, T. S., TEOH, S. K., LAU, W. W. Y. and SRINIVASAN, M. P., 1998. Effect of shear stress within the spinneret on hollow fiber membrane morphology and separation performance. *Industrial and Engineering Chemistry Research,* 37 (10), 3930-8.

CHUNG, T. S., XU, Z. L. and LIN, W., 1999. Fundamental understanding of the effect of air-gap distance on the fabrication of hollow fiber membranes. *Journal of applied Polymer science,* 72 (3), 379-95.

COHEN ADDAD, J. P., ICARD, B. and PELLICIOLI, L., 1995. Skinned polymeric membranes. Approach to the mechanism of formation of surface holes. *Polymer International,* 38 299-303.

COHEN, C., TANNY, G. B. and PRAGER, S., 1979. Diffusion-controlled formation of porous structures in ternary polymer systems. *Journal of polymer science: Polymer Physics Edition,* 17 477-89.

COOMBES, A. G. A. and MEIKLE, M. C., 1994. Resorbable synthetic polymers as replacements for bone graft. *Clinical Materials,* 17 35-67.

COULSON, J. M., RICHARDSON, J. F., BACKHURST, J. R. and HARKER, J. H., 1999. *Coulson and Richardson's Chemical engineering Volume 1 Fluid flow, heat transfer and mass transfer.* 5. Oxford: Butterworth Heinemann.

CRACAUER, R. F., WALKER, R. D. and GRUENBURG, M. L., 1987. *Hollow fiber cell culture device and method of operation* U. S. P. A. T. OFFICE 088463.

CRAWLEY, M. J., 2005. *Statistics: An introduction using R.* Chippenham: John Wiley & Sons Ltd.

CROLL, T. I., O'CONNOR, A. J., STEVENS, G. W. and COOPER-WHITE, J. J., 2004. Controllable surface modification of poly(lactic-co-glycolic acid) (PLGA) by hydrolysis or aminolysis I: Physical, chemical, and theoretical aspects. *Biomacromolecules,* 5 (2), 463-73.

CURTIS, A. S. G., GADEGAARD, N., DALBY, M. J., RIEHLE, M. O., WILKINSON, C. D. W. and AITHCHISON, G., 2004. Cells react to nanoscale order and

symmetry in their surroundings. *IEEE Transactions on Nanobioscience,* 3 (1), 61-5.

DAVIES, J. E. and HOSSEINI, M. M., 2000. Histodynamics of endosseous wound healing. *In*: J. E. DAVIES, eds. *Bone Engineering*. Toronto: EM Squared Incorporeted, 1-14.

DENG, M. and UHRICH, K. E., 2002. Effects of in vitro degradation on properties of poly(DL- lactide-co-glycolide) pertinent to its biological performance. *Journal of Materials Science-Materials in Medicine,* 13 (11), 1091-6.

DUNNE, M., CORRIGAN, O. I. and RAMTOOLA, Z., 2000. Influence of particle size and dissolution conditions on the degradation properties of polylactide-co-glycolide particles. *Biomaterials,* 21 (16), 1659.

DURECT, 2006. *Inherent Viscosity vs. Molecular weight chart for 50/50DLPLGA* [online]. Available from: http://www.absorbables.com/charts.asp?page=5050 [06 September 2006].

ELLIS, M. J. 2005. Development of a novel hollow fibre membrane for use as a tissue engineered bone graft scaffold. Chemical Engineering. Bath, University of Bath. **Ph.D**.

ELLIS, M. J. and CHAUDHURI, J. B., 2005. Development of PLGA hollow fibre membranes for use as a tissue engineering scaffold. *To be published,*

FISCHBACH, C., TESSMAR, J., LUCKE, A., SCHNELL, E., SCHMEER, G., BLUNK, T. and GOPFERICH, A., 2001. Does UV irradiation affect polymer properties relevant to tissue engineering? *Surface Science,* 491 (3), 333-45.

FLOM, D. G. and ELVING, P. J., 1953. Application of high frequency oscillators. *Analytical Chemistry,* 25 (4), 541-9.

FOURNIER, R. L., 1999. *Basic transport phenomena in biomedical engineering*. First. Philadelphia: Taylor & Francis.

FREED, K. F. and EDWARDS, S. F., 1974. Polymer viscosity in concentrated solutions. *The Journal of Chemical Physics,* 61 (9), 3626-33.

FU, K., PACK, D. W., KLIBANOV, A. M. and LANGER, R., 2000. Visual evidence of acidic environment within degrading poly(lactic-co-glycolic acid) (PLGA) microspheres. *Pharmaceutical Research,* 17 (1), 100-6.

GÖPFERICH, A., 1996. Mechanisms of polymer degradation and erosion. *Biomaterials,* 17 103-14.

GRIZZI, I., GARREAU, H., LI, S. and VERT, M., 1995. Hydrolytic degradation of devices based on poly(-lactic acid) size-dependence. *Biomaterials,* 16 (4), 305.

HOLY, C. E., CHENG, C., DAVIES, J. E. and SHOICHET, M. S., 2001. Optimizing the sterilization of PLGA scaffolds for use in tissue engineering. *Biomaterials,* 22 (1), 25-31.

HUANG, Q., DAWSON, R. A., PEGG, D. E., KEARNEY, J. N. and MACNEIL, S., 2004. Use of peracetic acid to sterilize human donor skin for production of acellular dermal matrices for clinical use. *Wound Repair and Regeneration,* 12 (3), 276-87.

HUTMACHER, D. W., 2000. Scaffolds in tissue engineering bone and cartilage. *Biomaterials,* 21 (24), 2529-43.

JANSEN, E. J. P., SLADEK, R. E. J., BAHAR, H., YAFFE, A., GIJBELS, M. J., KUIJER, R., BULSTRA, S. K., GULDEMONDS, N. A., BINDERMAN, I. and KOOLE, L. H., 2005. Hydrophobicity as a design criterion for polymer scaffolds in bone tissue engineering. *Biomaterials,* 26 (21), 4423-31.

KARP, J. M., SHOICHET, M. S. and DAVIES, J. E., 2003. Bone formation on two-dimensional poly(DL-lactide-co-glycolide) (PLGA) films and three-dimensional PLGA tissue engineering scaffolds in vitro. *Journal of Biomedical Materials Research,* 64A 388-96.

KAY, S., THAPA, A., HABERSTROH, K. M. and WEBSTER, T. J., 2002. Nanostructured polymer/nanophase ceramic composites enhance osteoblast and chondrocyte adhesion. *Tissue Engineering,* 8 (5), 753-61.

KELLER, T. S., MAO, Z. and SPENGLER, D. M., 1990. Young's modulus, bending strength, and tissue physical properties of human compact bone. *Journal Of Orthopaedic Research,* 8 (4), 592-603.

KENLEY, R. A., LEE, M. O., MAHONEY, T. R. and SANDERS, L. M., 1987. Poly(lactide-co-glycolide) decomposition kinetics in vivo and in vitro. *Macromolecules,* 20 (10), 1398-2403.

KHANG, G., CHOEE, J.-H., RHEE, J. M. and LEE, H. B., 2002. Interaction of different types of cells on physicochemically treated poly(L-lactide-co-glycolide) surfaces. *Journal of applied Polymer science,* 85 1253-62.

KIRBY, A. J., 1972. Hydrolysis and formation of esters of organic acids. *In*: C. H. BAMFORD and C. F. H. TIPPER, eds. *Ester formation and hydrolysis, and related reactions.* London: Elsevier Publishing Company, 57-207.

KNAZEK, R. A., GULLINO, P. M., KOHLER, P. O. and DEDRICK, R. L., 1972. Cell culture on artificial capillaries: An approach to tissue growth in vitro. *Science,* 178 65-7.

KNAZEK, R. A., WU, Y.-W., AEBERSOLD, P. M. and ROSENBERG, S. A., 1990. Culture of human tumor infiltrating lymphocytes in hollow fiber bioreactors. *Journal of immunological Methods,* 127 29-37.

KUMAR, S., WITTMANN, C. and HEINZLE, E., 2004. Minibioreactors. *Biotechnology Letters,* 26 1-10.

LEE, S. J., CHOI, J. S., PARK, K. S., KHANG, G., LEE, Y. M. and LEE, H. B. H. B., 2004. Response of MG63 osteoblast-like cells onto polycarbonate membrane surfaces with different micropore sizes. *Biomaterials,* 25 (19), 4699.

LI, K., KONG, J. F., WANG, D. A. and TEO, W. K., 1999. Tailor-made asymmetric PVDF hollow fibers for soluble gas removal. *Aiche Journal,* 45 (6), 1211-9.

LI, S. M., GARREAU, H. and VERT, M., 1990a. Structure-property relationships in the case of the degradation of massive aliphatic poly-(alpha-hydroxy acids) in aqueous media, Part 1: Poly(DL-lactic acid). *Journal of Materials Science: Materials in Medicine,* 1 123-30.

LI, S. M., GARREAU, H. and VERT, M., 1990b. Structure-property relationships in the case of the degradation of massive aliphatic poly-(alpha-hydroxy acids) in aqueous media, Part 2: Degradation of lactide-glycolide copolymers: PLA37.5GA25 and PLA75GA25. *Journal of Materials Science: Materials in Medicine,* 1 131-9.

LI, S. M., GARREAU, H. and VERT, M., 1990c. Structure-property relationships in the case of the degradation of massive aliphatic poly-(alpha-hydroxy acids) in aqueous media, Part 3: Influence of the morphology of poly(L-lactic acid). *Journal of Materials Science: Materials in Medicine,* 1 198-206.

LICHUN LU, C. A. G. A. G. M., 1999. In vitro degradation of thin poly(DL-lactic-co-glycolic acid) films. *Journal of Biomedical Materials Research,* 46 (2), 236-44.

LIU, X. H. and MA, P. X., 2004. Polymeric scaffolds for bone tissue engineering. *Annals of Biomedical Engineering,* 32 (3), 477-86.

LU, L., PETER, S. J., LYMAN, M. D., LAI, H.-L., LEITE, S. M., TAMADA, J. A., UYAMA, S., VACANTI, J. P., LANGER, R. and MIKOS, A. G., 2000a. In vitro and in vivo degradation of porous poly(-lactic-co-glycolic acid) foams. *Biomaterials,* 21 (18), 1837.

LU, L., STAMATAS, G. N. and MIKOS, A. G., 2000b. Controlled release of transforming growth factor β1 from biodegradable polymer microparticles. *Journal of Biomedical Materials Research,* 50 (3), 440-51.

MAJESKA, J., 2001. Cell Biology of Bone. *In*: S. C. COWIN, eds. *Bone Mechanics Handbook.* Boca Raton: CRC Press, 2.1-2.24.

MCFETRIDGE, P. S. 2002. Tissue Engineering Small diameter Vascular Grafts. Department of Chemical Engineering. Bath, University of Bath. **Ph.D.**

MCKELVEY, S. A., CLAUSI, D. T. and J., K. W., 1997. A guide to establishing hollow fiber macroscopic properties for membrane applications. *Journal of Membrane science,* 124 223-32.

MIDDLETON, J. C. and TIPTON, A. J., 2000. Synthetic biodegradable polymers as orthopedic devices. *Biomaterials,* 21 2335-46.

ORTHOTEERS, 2001. *Bone growth* [online]. Available from: http://www.orthoteers.co.uk/Nrujp~ij33lm/Orthbone1.htm [19 April 2005].

PARK, T. G., 1994. Degradation of poly(DL-lactic acid) microspheres: Effect of molecular weight. *Journal of Controlled Release,* 30 (2), 161.

PERRY, R. H., GREEN, D. W. and MALONEY, J. O., Eds. (1997). Perry's Chemical Engineers' Handbook. Sydney, McGraw-Hill.

PIRET, J. M. and COONEY, C. L., 1990. Mammalian cell and protein distributions in ultrafiltration hollow fiber bioreactors. *Biotechnology and Bioengineering,* 36 (9), 902 - 10.

PLANCHAMP, C., VU, T. L., MAYER, J. M., REIST, M. and TESTA, B., 2003. Hepatocyte hollow-fibre bioreactors: design, set-up, validation and applications. *Journal Of Pharmacy And Pharmacology,* 55 (9), 1181-98.

QIN, J.-J., GU, J. and CHUNG, T.-S., 2001. Effect of wet and dry-jet wet spinning on the shear-induced orientation during the formation of ultrafiltration hollow fiber membranes. *Journal of Membrane science,* 182 (1-2), 57.

QIN, J.-J., WANG, R. and CHUNG, T.-S., 2000. Investigation of shear stress effect within a spinneret on flux, separation and thermomechanical properties of hollow fiber ultrafiltration membranes. *Journal of Membrane science,* 175 (2), 197.

R Development Core Team 2007. R: A language and environment for statistical computing. R Foundation for Statistical Computing, Vienna, Austria. http://www.R-project.org

Wright Cell Imaging Facility 1997-2006. ImageJ. National Institutes of Health, Maryland. http://rsb.info.nih.gov/ij/

RHO, J. Y., KUHN-SPEARING, L. and ZIOUPOS, P., 1998. Mechanical properties and the hierarchical structure of bone. *Medical Engineering & Physics,* 20 (2), 92-102.

ROSE, F. R. A. J., 2005. *Sterilization with antibiotics.* Email to J. B. CHAUDHURI (J.B.Chaudhuri@bath.ac.uk)

ROUSE, P. E. J., 1953. A theory of the linear viscoelastic properties of dilute solutions of coiling polymers. *The Journal of Chemical Physics,* 21 (7), 1272-80.

SCHWARZ, K. and EPPLE, M., 1999. A detailed characterization of polyglycolide prepared by solid-state polycondensation reaction. *Macromolecular Chemistry and Physics,* 200 (10), 2221-9.

SHILTON, S. J., 1997. Flow profile induced in spinneret during hollow fiber membrane spinning. *Journal of applied Polymer science,* 65 (7), 1359-62.

SHIWA, Y., 1993. Theory of polymer relaxation times in semidilute solutions. I: mode relaxation. *Physics,* 3 477-86.

SIGMA-ALDRICH 2004. Material Safety Data Sheet: 1-methyl-2-pyrrolidinone.

TAMADA, J. A. and LANGER, R., 1993. Erosion kinetics of hydrolytically degradable polymers. *Proceedings Of The National Academy Of Sciences Of The United States Of America,* 90 552-6.

THARAKAN, J. P. and CHAU, P. C., 1985. A radial flow hollow fiber bioreactor for the large-scale culture of mammalian cells. *Biotechnology and Bioengineering,* 28 329-42.

THARAKAN, J. P. and CHAU, P. C., 1986. Operation and pressure distribution of immobillized cell hollow fiber bioreactors. *Biotechnology and Bioengineering,* 28 1064-71.

THOMAS, D. K. and THOMAS, T. A. J., 1960. Viscosity-concentration relationships in solutions of high polymers. *Journal of applied Polymer science,* 3 (8), 129-31.

VERT, M., LI, S. M., SPENLEHAUER, G. and GUERIN, P., 1992. Bioresorbability and biocompatibility of aliphatic polyesters. *Journal of Materials Science-Materials in Medicine,* 3 (6), 432-46.

WALCZAK, Z. K., 2002. *Processes of fiber formation.* Oxford: Elsevier Science Ltd.

WEI, J. and RUSS, M. B., 1977. Convection and diffusion in tissues and tissue cultures. *Journal of Theoretical Biology,* 66 775-87.

WEN, X. and TRESCO, P. A., 2006. Fabrication and characterization of permeable degradable poly(DL-lactide-co-glycolide) (PLGA) hollow fiber phase inversion membranes for use as nerve tract guidance channels. *Biomaterials,* 27 3800-9.

WILLIAMS, D. F., 1992. Mechanisms of biodegradation of implantable polymers. *Clinical Materials,* 10 9-12.

WU, L. and DING, J., 2004. In vitro degradation of three-dimensional porous poly(-lactide-co-glycolide) scaffolds for tissue engineering. *Biomaterials,* 25 (27), 5821.

WU, L. and DING, J., 2005. Effects of porosity and pore size on in vitro degradation of three-dimensional porous poly(DL-lactide-co-glycolide) scaffolds for tissue engineering. *Journal Of Biomedical Materials Research Part A,* 75A (4), 767-77.

YASZEMSKI, M. J., PAYNE, R. G., HAYES, W. C., LANGER, R. and MIKOS, A. G., 1996. Evolution of bone transplantation: molecular, cellular and tissue strategies to engineer human bone. *Biomaterials,* 17 175-85.

YE, H., DAS, D. B., TRIFFITT, J. and CUI, Z. F., 2006. Modelling nutrient transport in hollow fibre membrane bioreactors for growing three-dimensional bone tissue. *Journal of Membrane science,* 272 169-78.

YOUNG, T.-H. and CHEN, L.-W., 1995. Pore formation mechanism of membranes from phase inversion process. *Desalination,* 103 (3), 233.

ZIMM, B. H., 1956. Dynamics of polymer molecules in dilute solution: Viscoelasticity, flow birefringence and dielectric loss. *The Journal of Chemical Physics,* 24 (2), 269.

ZINGER, O., ZHAO, G., SCHWARTZ, Z., SIMPSON, J., WIELAND, M., LANDOLT, D. and BOYAN, B., 2005. Differential regulation of osteoblasts by substrate microstructural features. *Biomaterials,* 26 (14), 1837-47.

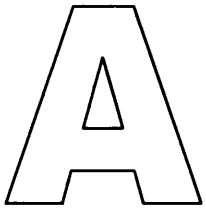

APPENDIX A - SAMPLE CALCULATIONS

A.1 Gas permeation calculations

Hollow fibre pore sizes were determined by measuring permeation of nitrogen gas through the walls of the hollow fibres. This is used to calculate pore size assuming Poiseuille flow through porous media. Below all equations used in the calculation are explained. Each sample was tested six times for each internal pressure. Internal pressures ranged form 1×10^2 kPa gauge to when the hollow fibre or potting resin gave way (control up to 5×10^2 kPa gauge, ethanol up to 9×10^2 kPa gauge, UV up to 4×10^2 kPa gauge, antibiotic up to 4×10^2 kPa gauge). Example calculations for the control fibre are given.

A.1.1 Membrane surface area

$$A = 2\pi rL \qquad \textbf{Equation A.1}$$

A = Membrane surface area (L^2)

r = Hollow fibre radius (3.13×10^{-4} m) (L)

L = Hollow fibre length (10^{-1} m) (L)

π = Pi (-)

$$2\times\pi\times3.13\times10^{-4}\times10^{-1} = 1.96\times10^{-4}\ \text{m}^2 \qquad \textbf{Equation A.2}$$

A.1.2 Mean pressure across fibre

$$P = \frac{P_{in} + P_{out}}{2} \qquad \textbf{Equation A.3}$$

P = Mean pressure across fibre ($L^{-1}MT^{-1}$)

P_{in} = Pressure inside fibre (2.01×10^5 Pa) ($L^{-1}MT^{-1}$)

P_{out} = Pressure outside fibre, atmospheric (1.01×10^5 Pa) ($L^{-1}MT^{-1}$)

$$\frac{2.01\times10^5 + 1.01\times10^5}{2} = 1.51\times10^5 \text{ Pa} \qquad \textbf{Equation A.4}$$

A.1.3 Mean gas flow rate

$$Q = \frac{V}{t} \qquad \textbf{Equation A.5}$$

Q = Volumetric gas flow rate (L^3T^{-1})

V = Volume of gas timed (4×10^{-5} m^3) (L^3)

t = Time taken (av. 9.36 s) (T)

$$\frac{4.00\times10^{-5}}{9.36} = 4.27\times10^{-6} \text{ m}^3\text{ s}^{-1} \qquad \textbf{Equation A.6}$$

To convert into mean *molar* gas flow rate:

$$N = \frac{QP_{out}}{RT} \qquad \textbf{Equation A.7}$$

N = Molar gas flow rate (NT^{-1})

R = Molar gas constant (8.31 J mol^{-1} k^{-1}) ($L^2MT^{-2}\Theta^{-1}N^{-1}$)
Perry *et al.* 1997

T = Temperature (313 K) (Θ)

$$\frac{4.27\times10^{-6}\times1.01\times10^5}{8.31\times313} = 1.77\times10^{-4} \text{ mol s}^{-1} \qquad \textbf{Equation A.8}$$

A.1.4 Gas permeation rate

$$J = \frac{N}{AP_{in}}$$ **Equation A.9**

J = Gas permeation rate ($L^{-1}M^{-1}TN$)

$$\frac{1.77\times10^{-4}}{1.96\times10^{-4}\times2.01\times10^{5}} = 9.00\times10^{-6}\ \text{mol s}^{-1}\ \text{Pa}^{-1}\ \text{m}^{-2}$$ **Equation A.10**

A.1.5 Data tables

Table A.1 Raw data for the control gas permeation sample.

Samples were timed six times and at 100 kPa intervals until either the fibre or the epoxy resin failed.

Internal Pressure (× 10^2 kPa gauge)	Time (s)					
1	9.33	9.36	9.36	9.38	9.37	9.37
2	4.31	4.37	4.31	4.354	4.41	4.42
3	2.65	2.72	2.81	2.65	2.59	2.67
4	1.78	1.77	1.73	1.78	1.82	1.77
5	1.31	1.27	1.29	1.19	1.23	1.17

Table A.2 Calculated data for the control gas permeation sample.

The permeability of the fibres were calculated and related to the trans-membrane pressure.

Internal Pressure (× 10^2 kPa gauge)	Absolute internal pressure (Pa)	Mean pressure across fibre (Pa)	Time (s)	Mean gas flow rate ($m^3\ s^{-1}$)	Mean molar gas flow rate (mol s^{-1})	Gas permeability (mol s^{-1} Pa^{-1} m^{-2})
1	2.01E+05	1.51E+05	9.36E+00	4.27E-06	1.77E-04	9.00E-06
2	3.01E+05	2.01E+05	4.36E+00	9.17E-06	3.79E-04	9.66E-06
3	4.01E+05	2.51E+05	2.68E+00	1.49E-05	6.17E-04	1.05E-05
4	5.01E+05	3.01E+05	1.78E+00	2.25E-05	9.32E-04	1.19E-05
5	6.01E+05	3.51E+05	1.24E+00	3.22E-05	1.33E-03	1.36E-05

A.1.6 Pore size

Mean pore diameter is determined from a plot of gas permeability against mean pressure across the fibre.

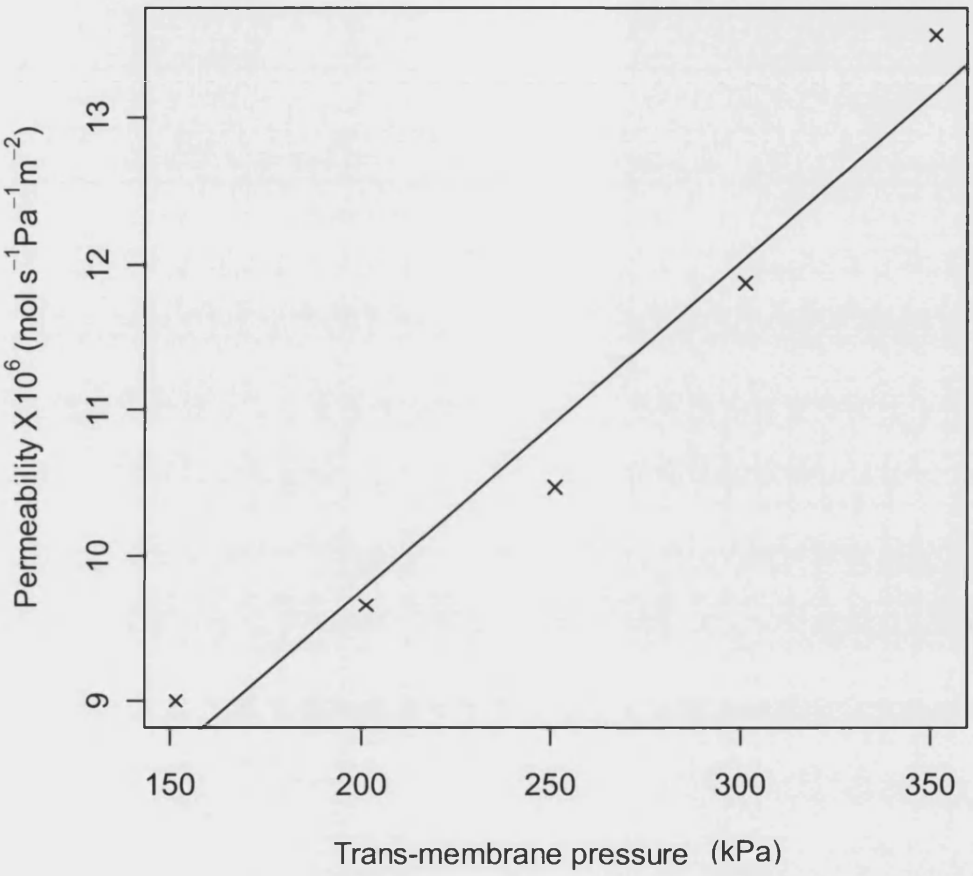

Figure A.1 Gas permeation against mean pressure.

Used to determine parameters required to calculate mean pore diameter.

$$r_p = \frac{16}{3}\left(\frac{P_0}{K_0}\right)\left(\frac{8RT}{\pi M}\right)^{0.5}\mu \quad \text{(Li } et\ al.\ \text{1999)}$$

Equation A.11

r_p = Mean pore diameter (L)

P_0 = Gradient of chart (2.26×10^{-11} mol s^{-1} Pa^{-2} m^{-2}) ($M^{-2}T^3N$)

K_0 = Intercept of chart (5.22×10^{-6} mol s^{-1} Pa^{-2} m^{-2}) ($L^{-1}M^{-1}TN$)

M = Gas molecular weight (2.8×10^{-2} $kgmol^{-1}$) (MN^{-1})

(Perry *et al.* 1997)

μ = Gas viscosity (1.78×10^{-5} Pa s) ($L^{-1}MT^{-1}$)

(Perry *et al.* 1997)

$$\frac{16}{3}\left(\frac{2.26\times10^{-11}}{5.22\times10^{-6}}\right)\left(\frac{8\times8.31\times313}{\pi\times2.8\times10^{-2}}\right)1.78\times10^{-5} = 1.94\times10^{-7}\,\text{m} = 0.19\,\mu\text{m}$$

Equation A.12

A.2 Water flux

Water flux measurements were taken for a range of inlet pressures from 1.2×10^5 Pa to 2.8×10^5 Pa. Inlet, outlet and permeate masses were collected over a timed period. Permeate mass was used to calculate the flux and inlet and outlet masses were used to determine error which was less than 0.1% of the inlet mass. Runs were repeated three times for accuracy and average mass and time values used in calculations. Inlet and outlet pressures were monitored and the permeate pressure was assumed to be atmospheric. Fluxes were plotted against average transmembrane pressure. Example calculations are given for the lowest inlet pressure of the control fibre.

A.2.1 Permeate flux

The permeate flux is calculated in mass per unit time and membrane area.

$$J = \frac{m_p}{tA}$$

Equation A.13

J = Permeate flux ($ML^{-2}T^{-1}$)

m_p = Mass of permeate collected (av. 6.0×10^{-4} kg) (M)

t = Time (av. 61.3 s) (T)

A = Membrane surface area (7.4×10^{-4} m^2) (L^2)

$$\frac{6.0\times10^{-4}}{61.3\times7.4\times10^{-4}} = 6.7\times10^{-2}\ \text{kg m}^{-2}\,\text{s}^{-1}$$

Equation A.14

A.3 Trans-membrane pressure difference

The transmembrane pressure difference is calculated as an average of the pressure drop across the membrane at the inlet and outlet.

$$\Delta P = \left(\frac{P_{inlet} + P_{outlet}}{2}\right) - P_{permeate}$$ **Equation A.15**

ΔP = Trans-membrane pressure difference ($L^{-1}MT^{-2}$)

P_{inlet} = Inlet pressure (2.2×10^5 Pa) ($L^{-1}MT^{-2}$)

P_{outlet} = Outlet pressure (1.3×10^5 Pa) ($L^{-1}MT^{-2}$)

$P_{permeate}$ = Permeate pressure (1.0×10^5 Pa) ($L^{-1}MT^{-2}$)

$$\left(\frac{2.2\times10^5 + 1.3\times10^5}{2}\right) - 1.0\times10^5 = 7.5\times10^4 \text{ Pa}$$ **Equation A.16**

A.4 Mechanical testing

Calculations used to calculate stress and strain at breaking point are detailed below with sample calculations from the control sample.

A.4.1 Fibre cross-sectional area

$$A = \pi\left(r_{out}^2 - r_{in}^2\right)$$ **Equation A.17**

A = Cross-sectional area (L^2)

r_{out} = Hollow fibre outer radius (7.0×10^{-4} m) (L)

r_{in} = Hollow fibre inner radius (lumen) (3.5×10^{-4} m) (L)

π = Pi (-)

$$\pi\left(7.0\times10^{-4} - 3.5\times10^{-4}\right) = 1.1\times10^{-3} \text{ m}^2$$ **Equation A.18**

A.4.2 Stress

$$\sigma = \frac{mg}{A}$$ **Equation A.19**

σ = Stress ($ML^{-1}T^{-2}$)

m = Mass of load at failure (3.16 kg) (M)

g = Acceleration due to gravity (9.81 m s^{-1}) (LT^{-1})
(Perry *et al.* 1997)

$$\frac{3.16\times10^{-1}\times9.81}{1.1\times10^{-3}} = 2.69 \times 10^{6}\ \text{N m}^{-2} \qquad \textbf{Equation A.20}$$

A.4.3 Strain

$$\varepsilon = \frac{l}{L} \qquad \textbf{Equation A.21}$$

ε = Strain (-)
l = Extension (5×10^{-4} m) (L)
L = Original length (5×10^{-3} m) (L)

$$\frac{5\times10^{-4}}{5\times10^{-3}} = 10^{-1} \qquad \textbf{Equation A.9.22}$$

A.4.4 Young's Modulus

$$E = \frac{\sigma}{\varepsilon} \qquad \textbf{Equation A.23}$$

E = Young's modulus ($ML^{-1}T^{-2}$)

$$\frac{2.69\times10^{6}}{10^{-1}} = 2.69\times10^{7}\ \text{N m}^{-2} \qquad \textbf{Equation A.24}$$

A.5 Calculations of fluid flow through the spinneret

Hydraulic mean diameter of flow through an annulus is given by Equation A.25.

$$d_h = 2(R_2 - R_1) \qquad \textbf{Equation A.25}$$

d_h = Hydraulic mean diameter (L)

R_1 = Inner radius (L)

R_2 = Outer radius (L)

Reynolds number is given by Equation A.26.

$$\mathrm{Re} = \frac{\rho u d_h}{\mu}$$ **Equation A.26**

Re = Reynolds number (-)

ρ = Density of fluid ($L^{-3}M$)

u = Velocity of fluid (LT^{-1})

d_h = Hydraulic mean diameter (L)

μ = Viscosity of solution ($L^{-1}MT^{-1}$)

At low Reynolds number friction factor is independent of roughness (Coulson *et al.* 1999) and is given by Equation A.27.

$$f = \frac{8}{\mathrm{Re}}$$ **Equation A.27**

f = Friction factor (-)

Re = Reynolds number (-)

Pressure drop per unit length in an annulus is given by Equation A.28.

$$-\frac{dP}{dl} = \frac{u}{\frac{1}{8\mu}\left(R_2^2 + R_1^2 - \frac{R_2^2 - R_1^2}{\ln\left(\frac{R_2}{R_1}\right)}\right)}$$ **Equation A.28**

$-\frac{dP}{dl}$ = Pressure drop per unit length (MT^{-2})

u = Velocity of fluid (LT^{-1})

μ = Viscosity of solution ($L^{-1}MT^{-1}$)

R_1 = Inner radius (L)

R_2 = Outer radius (L)

A.6 Shear stresses during scaffold preparation

A.6.1 Shear stresses in spinneret

The following equation is analytically derived by Shilton (1997) for Newtonian flow through a concentric annulus with boundary conditions as specified.

$$U_z = \frac{2Q}{\pi}\left(\frac{\left(\frac{\left(R_2^2 - R_1^2\right)\ln\left(\frac{R_2}{r}\right)}{\ln\left(\frac{R_2}{R_1}\right)}\right) - \left(R_2^2 - r^2\right)}{\left(\frac{\left(R_2^2 - R_1^2\right)^2}{\ln\left(\frac{R_2}{R_1}\right)}\right) - \left(R_2^4 - R_1^4\right)}\right) \qquad \textbf{Equation A.29}$$

U_Z = Velocity (LT^{-1})

Q = Volumetric flow rate (L^3T^{-1})

R_1 = Inner radius of spinneret (L)

R_2 = Outer radius of spinneret (L)

r = Radius (L)

$$\dot{\gamma} = \frac{8Q}{\pi}\left(\frac{1}{\frac{\left(R_2^2 - R_1^2\right)^2}{\ln\left(\frac{R_2}{R_1}\right)} - \left(R_2^4 - {}_1^4\right)}\right)\left(\frac{r}{2} + \frac{\left(R_2^2 - R_1^2\right)}{4r\ln\left(\frac{R_2}{R_1}\right)}\right) \qquad \textbf{Equation A.30}$$

$\dot{\gamma}$ = Shear rate (T^{-1})

Equation A.31

$$\tau = \mu\dot{\gamma}$$

τ = Shear stress ($ML^{-1}T^{-2}$)

μ = Viscosity ($ML^{-1}T^{-1}$)

A.6.2 Shear stresses in flat sheet formation

$$\tau = \frac{\mu U}{x}$$ **Equation A.32**

τ = Shear stress ($ML^{-1}T^{-2}$)

μ = Viscosity ($ML^{-1}T^{-1}$)

U = Velocity (LT^{-1})

x = Gap thickness (L)

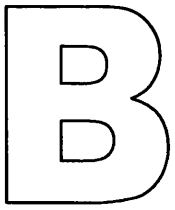

APPENDIX B - VALIDATION OF METHODS

B.1 Surface treatment of flat sheets

B.1.1 Mass loss

The mass of scaffolds prepared as normal and allowed to dry in ambient laboratory conditions was monitored before and after a 48 h freeze drying period. Any residual moisture content in the scaffolds that may affect mass measurements would be removed by freeze-drying. No significant difference was found between masses of the polymers before and after freeze-drying. Three different polymer compositions: 50:50, 65:35 and 85:15 L:G ratio PLGA, were tested, no differences were found between the different samples. This meant that freeze-drying the samples was not required before testing the samples in order to accurately quantify any mass loss of the scaffolds during subsequent experimentation.

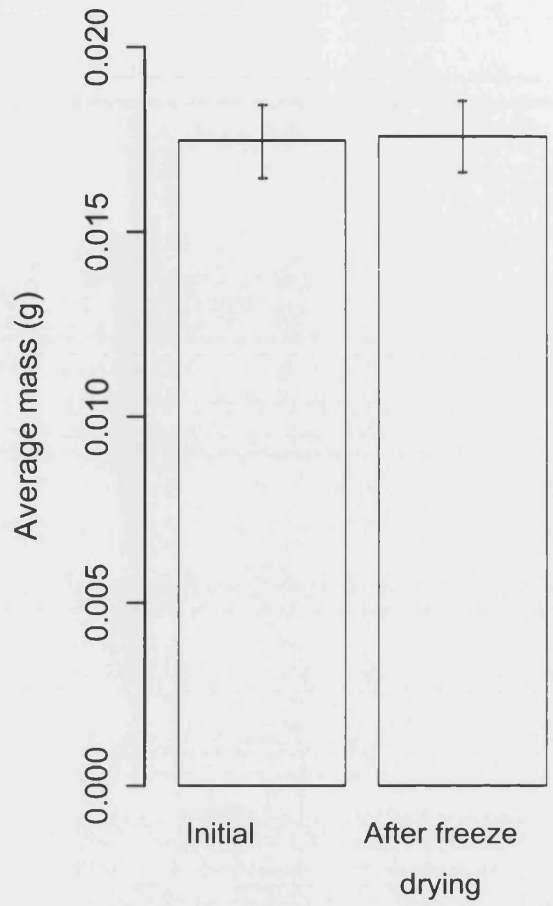

Figure B.1 Mass of polymer scaffolds before and after freeze drying.
Mass of 8 cm2 flat sheet (~ 250 μm thick) samples of various polymer compositions before and after freeze drying (mean ± lsd.; n = 10). No significant difference was found between the masses of 50:50, 65:35 and 85:15 polymer ratios (n = 2, 4, 4 respectively) before or after freeze drying. A paired Student's t-test revealed no significant difference in the initial and final mass of the samples.

B.2 Effect of operating environment and time study

B.2.1 Cross-sectional area and volume

The cross-sectional area of the scaffold is used as an indicator for the change in volume of the scaffold with time. Figure B.2 shows there is a good correlation between the cross-sectional area of the scaffolds and the volume of the scaffolds at the end point of the study (the only time point at which both measurements were taken). The three different forms show different correlations, however in all cases the relationship is proportional; suggesting the cross-sectional area gives a good indication of the volume of the scaffold when the volume cannot be measured directly without disturbing the study.

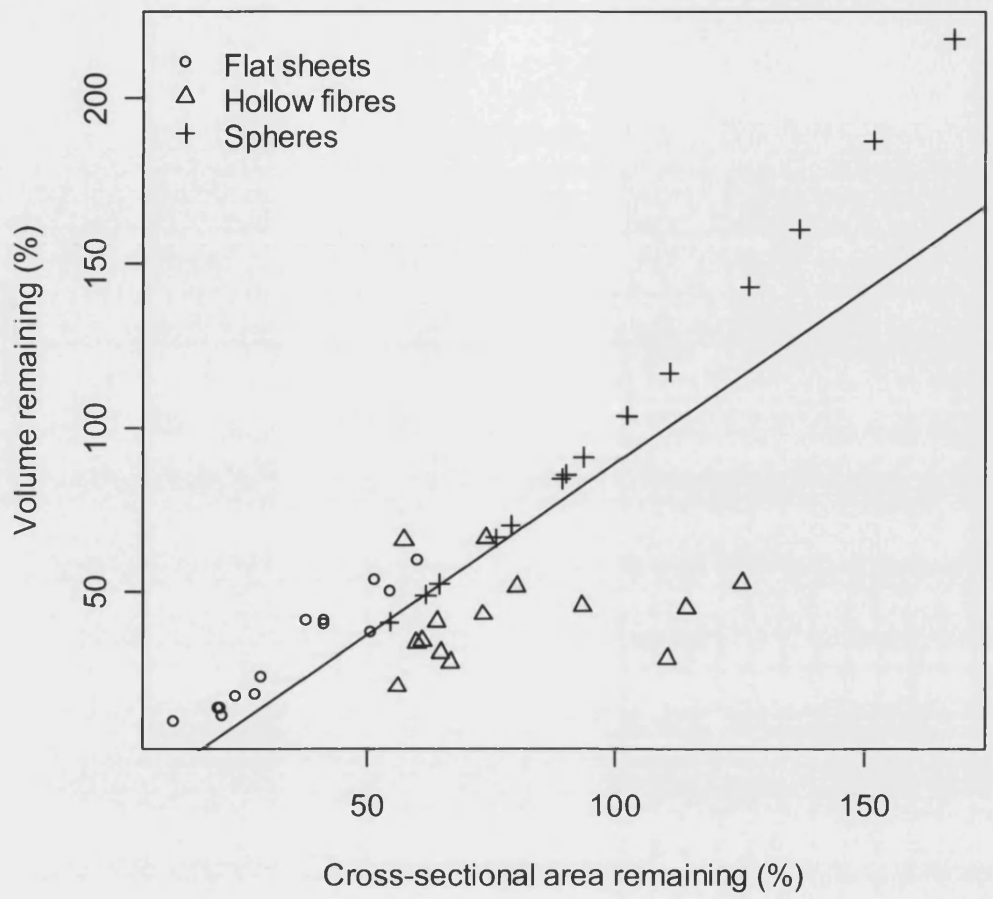

Figure B.2 Scatter plot of cross-sectional area remaining against volume remaining of three scaffold forms at end of two week culture period.

At the end of a two weeks under culture conditions the cross-sectional area of the scaffolds was determined from two-dimensional images of the scaffolds. The volume was determined by measuring the three-dimensions of the scaffold. A strong correlation is seen, meaning the cross-sectional area is a good indicator of the volume of the scaffold. The hollow fibres have their volume least well defined by their cross-sectional area as the two-dimensional image contains no information of the lumen of the fibre.

B.2.2 Changes to the liquid during culture of the polymer

The effect of operating environment and time experiment was operated as a closed system; with bi-weekly changes of media. The system is composed of three phases; the solid polymer, the liquid media and an air space. As the polymer degrades material will exchange between the solid and the liquid phase; meaning it should be possible to

measure either in order to monitor the changes to the polymer. However, it was found that no changes were observed in the composition of the fluid when monitored with a blood gas analyser and pH probe. This suggests that while the polymer is exchanging material with the liquid the liquid is exchanging material with the gas in the flask. This gas is in equilibrium, through a filter, with the gas in the incubator and is changed every time the flask is opened to take a sample or change the media. As the monitoring of the changes to the polymer gave useful results, further monitoring of the liquid was not carried out.

B.2.3 Surface area to volume ratio mass loss of scaffolds

Although the surface area to volume ratio did not appear to add significant explanatory power to the correlation of percentage mass remaining of polymer scaffolds after two weeks under culture conditions, alone the surface area to volume ratio did correlate with the mass remaining of the scaffolds.

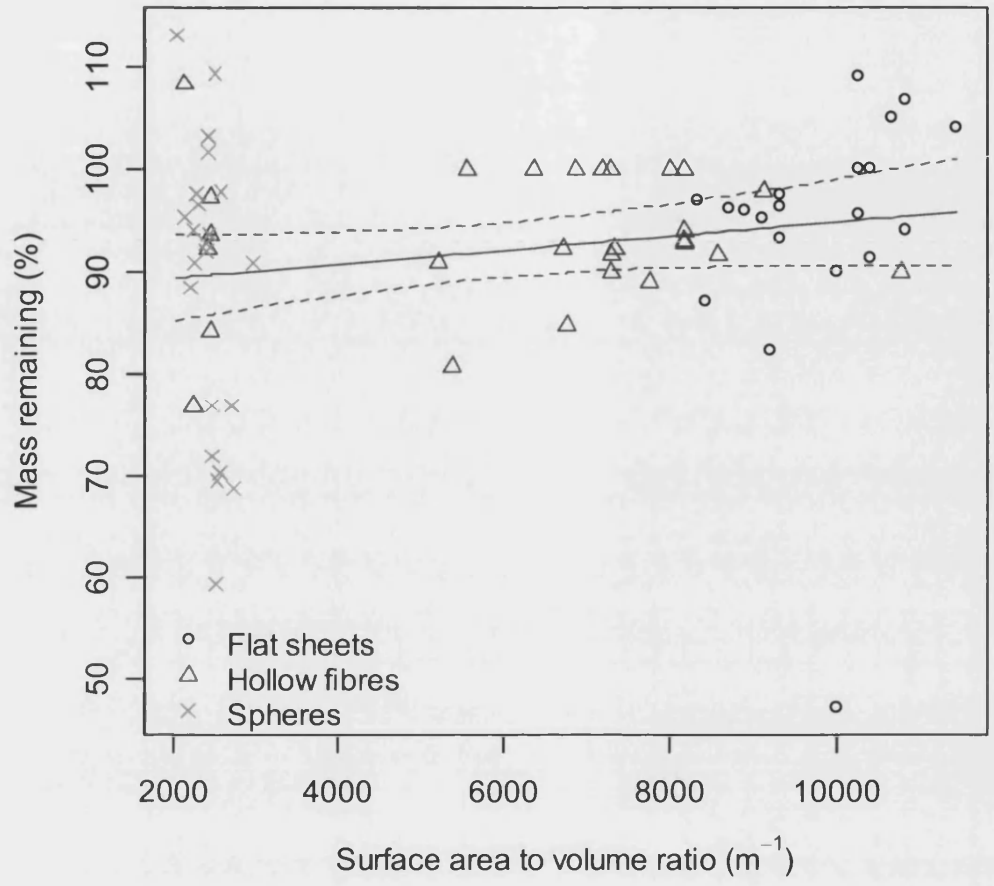

Figure B.3 Scatter plot of surface area to volume ratio against mass remaining of scaffolds after two weeks in culture conditions.

Points show individual data points made up of three scaffold forms: hollow fibres, flat sheets and spherical particles. The statistically significant linear correlation (solid line) and 95% confidence intervals (dashed line) are also shown.

B.2.4 Surface area to volume ratio and initial porosity of scaffolds

The surface area to volume ratio and initial scaffold porosity are both used as explanatory variables in understanding the changes to PLGA scaffolds under cell culture conditions. While considered independently it is important to note that there is a good correlation between the two values. The surface area to volume ratio only considers the superficial external surface area of the scaffold; otherwise this correlation would not be surprising. Figure B.4 shows the correlation between the two variables.

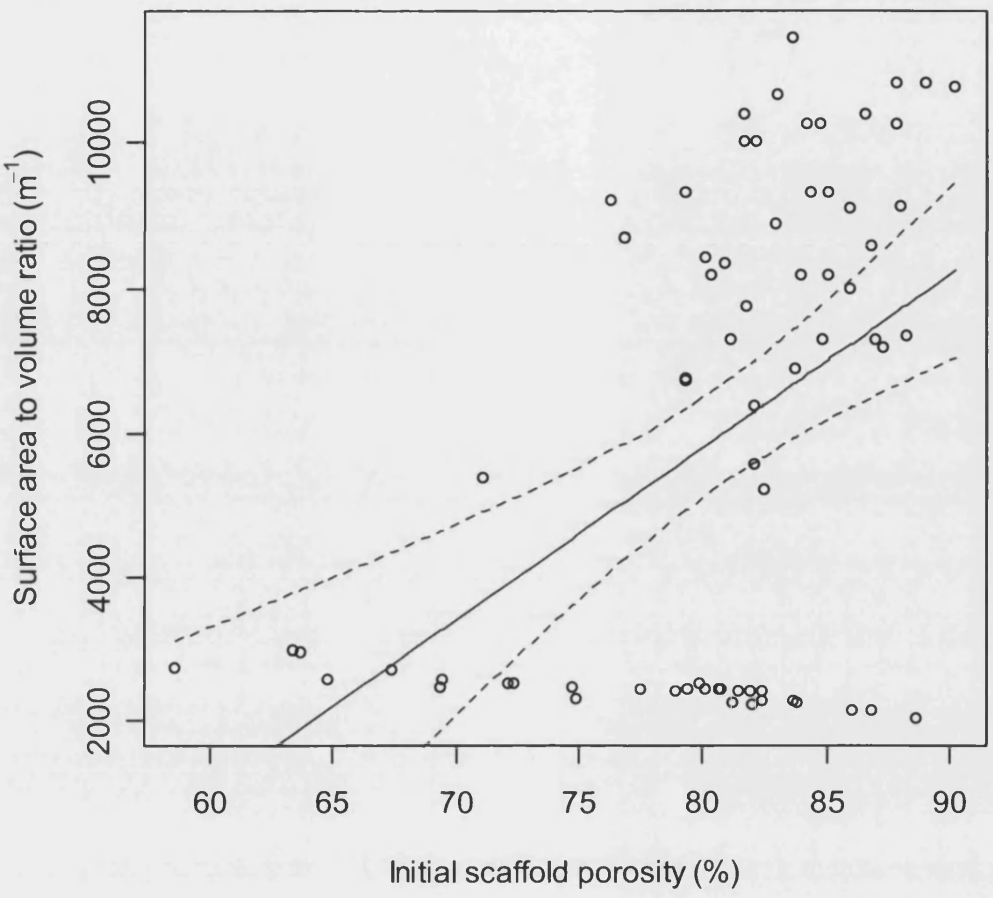

Figure B.4 Scatter plot of initial scaffold porosity against surface area to volume ratio of polymer scaffolds.

*Points show individual data points made up of three scaffold forms: hollow fibres, flat sheets and spherical particles. The statistically significant linear correlation (***solid line***) and 95% confidence intervals (***dashed line***) are also shown.*

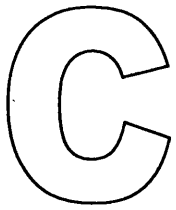

APPENDIX C – REGRESSION CORRELATIONS

C.1 Effect of operating environment and time

C.1.1 Volume change in different conditions

Table C.1 presents the regression correlation for the plane relating the percentage of the initial volume of the scaffold remaining after two weeks in conditions of either water or complete cell culture media at either 20°C or 37°C. The first column identifies the parameter, the second column gives the estimate of the coefficient; the coefficients are different for scaffolds cultured in water or media. The third column gives the standard error of the estimate. The *p* value is given in column four with lower *p* values indicating higher significance; this is highlighted by increasing numbers of stars in column five.

Table C.1 Regression correlation for the volume remaining of PLGA scaffolds in different conditions.

Values of the coefficients from the regression correlation for the response of the percentage volume remaining of PLGA membranes over a two week period in either complete cell media or distilled water at 20 °C or 37 °C. Temperature, fluid (media or water), surface area to volume ratio (SA/V; m^{-1}) and initial scaffold porosity (Porosity; %) all influence the degradation of the polymer membrane.

	Estimate	Std. Error	P	Sig.
Intercept (Media)	6.4×10^{2}	2.0×10^{2}	4.3×10^{-3}	*
Intercept (Water)	1.2×10^{3}	2.2×10^{2}	3.1×10^{-2}	.
Temperature (Media)	-4.4	6.5×10^{-1}	3.0×10^{-6}	***
Temperature (Water)	-1.3	9.3×10^{-1}	4.1×10^{-3}	*
SA/V	-4.7×10^{-3}	1.8×10^{-3}	1.9×10^{-2}	.
Porosity (Media)	-5.1	2.4	4.9×10^{-2}	.
Porosity (Water)	-1.2×10^{1}	2.7	1.6×10^{-2}	.

Significance codes: * = 0.0001, ** = 0.001, * = 0.01, .= 0.05**

C.1.2 Porosity change in cell culture conditions

Table C.2 shows the regression correlation for the porosity change of the scaffolds in cell culture conditions. The format of the table is explained in Section C.1.1.

Table C.2 Regression correlation for the porosity remaining of PLGA scaffolds following two weeks' culture.

Values of the coefficients from the regression correlation for the response of the percentage porosity remaining of PLGA membranes over a two week period in complete cell culture media under incubation conditions (37°C, 5% CO_2). Initial membrane porosity (Porosity; %), intrinsic viscosity (IV; dL g^{-1}) and surface area to volume ratio (SA/V; m^{-1}) all influence the degradation of the polymer membrane.

	Estimate	Std. Error	P	Sig.
Intercept	4.9×10^{2}	8.6×10^{1}	3.4×10^{-7}	***
SA/V	-2.1×10^{-1}	4.7×10^{-2}	4.2×10^{-5}	***
Porosity	-4.6	1.1	5.7×10^{-5}	***
SA/V:IV	1.8×10^{-1}	6.5×10^{-2}	6.7×10^{-3}	*
SA/V:Porosity	2.3×10^{-3}	5.6×10^{-4}	1.1×10^{-4}	**

SA/V:Porosity:IV	-2.0×10^{-3}	7.7×10^{-4}	9.7×10^{-3}	*

Significance codes: * = 0.0001, ** = 0.001, * = 0.01, .= 0.05**

C.1.3 Porosity change in cell culture conditions

Table C.3 shows the regression correlation for the porosity change of the scaffolds in cell culture conditions. The format of the table is explained in Section C.1.1.

Table C.3 Regression correlation for the Young's modulus of PLGA scaffolds before and after two weeks' culture.

Values of the coefficients from the regression correlation for the response of the Young's modulus of PLGA membranes over a two week period in complete cell culture media under incubation conditions (37°C, 5% CO_2). The Young's modulus is found to change with time (Time; day) (before and after the culture period), intrinsic viscosity (IV; dL g^{-1}) and lactide (Lactide; %) content of the polymer.

	Estimate	Std. Error	t	P	Sig.
Intercept	6.6	3.0	2.1	3.5×10^{-2}	.
Time	-4.5×10^{1}	1.2×10^{-1}	-3.7	7.2×10^{-4}	**
Time:Lactide	8.5×10^{-1}	2.4×10^{-1}	3.5	1.1×10^{-3}	*
Time:IV	6.0×10^{1}	1.6×10^{1}	3.7	7.3×10^{-4}	**
Time:Lactide:IV	-1.1	3.2×10^{-1}	-3.4	1.5×10^{-3}	*

Significance codes: * = 0.0001, ** = 0.001, * = 0.01, .= 0.05**